

**Predicting the outcomes  
of HIV Treatment Interruptions  
using Computational Modelling**

Andreas Hillmann

M.Sc.

A Dissertation submitted in partial fulfilment  
of the requirements for the award of

Doctor of Philosophy (Ph.D.)

to



Dublin City University  
School of Computing

Supervised by Prof. Martin Crane and Prof. Heather Ruskin

December 2020

## **Declaration**

I hereby certify that this material, which I now submit for assessment on the programme of study leading to the award of Doctor of Philosophy is entirely my own work, and that I have exercised reasonable care to ensure that the work is original, and does not to the best of my knowledge breach any law of copyright, and has not been taken from the work of others save and to the extent that such work has been cited and acknowledged within the text of my work.

Signed:        Andreas Hillmann

A handwritten signature in blue ink that reads "A. Hillmann". The signature is written in a cursive style with a long horizontal stroke at the end. Below the signature is a solid horizontal line.

ID No.:        54140757

Date:           10/12/2020

## Table of Contents

List of Abbreviations.....	viii
List of Figures .....	x
List of Tables.....	xxi
Abstract .....	xxii
Acknowledgements .....	xxiii
1 Introduction.....	1
1.1 Background.....	1
1.2 Availability of Data .....	2
1.3 Motivation for Modelling .....	3
1.4 Scope and Contribution .....	5
2 HIV Infection and Treatment.....	8
2.1 Introduction.....	8
2.2 HIV and AIDS .....	8
2.2.1 A Global Pandemic .....	8
2.2.2 Viral Transmission .....	9
2.2.3 HIV Infection .....	10
2.2.4 Viral Structure .....	13
2.2.5 Long-Term Implications.....	15
2.3 Antiretroviral Treatment.....	16
2.3.1 Drug Development .....	16
2.3.2 Principal Mechanisms .....	17
2.3.3 Treatment Regimen .....	19
2.4 Limitations of ART.....	20

2.4.1	Viral Reservoirs.....	20
2.4.2	Drug Pharmacology.....	21
2.4.3	Drug Resistance.....	21
2.5	Discontinuation of ART .....	22
2.5.1	Treatment Adherence .....	22
2.5.2	Structured Treatment Interruptions .....	23
2.6	Summary.....	25
3	Mathematical and Computational Models for HIV Infection .....	26
3.1	Introduction.....	26
3.1.1	Scale Considerations .....	26
3.1.2	Modelling Strategies.....	27
3.2	Top-Down Modelling .....	28
3.2.1	Model Forms .....	28
3.2.2	Application to HIV Progression .....	29
3.3	Bottom-Up Modelling .....	33
3.3.1	Attempts to Describe .....	33
3.3.2	Examples for HIV Progression.....	34
3.4	Modelling Treatment Interruptions.....	35
3.4.1	Commonly used Model Forms .....	35
3.4.2	Bottom-Up Approaches.....	37
3.4.3	Model Parameterisation.....	38
3.5	Summary.....	39
4	Methods for Bottom-Up Models.....	40
4.1	Introduction.....	40

4.2	Cellular Automata.....	40
4.2.1	Early Developments .....	40
4.2.2	Use in Immunology .....	42
4.2.3	Applications for HIV .....	43
4.3	Monte Carlo Simulation .....	45
4.3.1	Direct Monte Carlo.....	45
4.3.2	Inverse Monte Carlo .....	47
4.4	Implementation of Bottom-Up Models .....	50
4.4.1	Tool Options.....	50
4.4.2	Model Design .....	51
4.4.3	Computing Resources.....	52
4.4.4	Parallelisation Techniques.....	53
4.5	Summary.....	54
5	Two Models for Lymphatic Tissue Changes .....	55
5.1	Introduction.....	55
5.2	Biological Effects .....	55
5.2.1	Functions of Lymphatic Tissue .....	55
5.2.2	HIV Infection on Cellular Level .....	58
5.2.3	Implications for Lymphatic Tissue.....	60
5.2.4	Clinical Observations and Treatment .....	62
5.3	Stochastic Cellular Automata (SCA) Model .....	64
5.3.1	Surrounding Conditions .....	64
5.3.2	Model Rules .....	65
5.3.3	Parameter Sensitivity.....	69

5.4	CD4+ Motility (CM) Model .....	73
5.4.1	Model Overview .....	73
5.4.2	Model Setup and Rules.....	75
	Simulation Environment .....	75
	Tissue Collagenation Rules.....	77
	T-Cell Degradation Rules .....	79
5.4.3	Parameter Estimates .....	81
5.4.4	Simulation Setup .....	82
5.4.5	Simulation Results.....	84
5.5	Implementation Performance.....	89
5.5.1	Parallelisation Performance .....	89
5.5.2	Lattice Size .....	90
5.6	Summary .....	91
6	Effects of Treatment Interruptions on Lymphatic Tissue Structure .....	92
6.1	Introduction.....	92
6.2	Clinical Studies .....	92
6.3	Treatment Simulation .....	94
6.3.1	SCA Model Setup.....	94
6.3.2	Unstructured Interruptions .....	97
6.3.3	Structured Interruptions.....	99
6.4	Impact Assessment of STIs .....	101
6.4.1	SCA Model.....	101
	Experimental Setup.....	101
	Results.....	102
6.4.2	CM Model .....	110

6.5	Summary.....	112
7	Upscaling: iCTS Model Components and Inverse MC .....	113
7.1	Introduction.....	113
7.2	Data from Clinical Sources.....	113
7.2.1	Clinical Evidence .....	113
7.2.2	Clinical Trial Simulation .....	115
7.3	Mechanisms and Data.....	117
7.3.1	Observed and Hidden Data.....	117
7.3.2	Infection Progression.....	119
7.4	iCTS Model Components .....	122
7.4.1	Infection Progression Model .....	122
7.4.2	Medical Intervention Model.....	123
7.4.3	Therapy Removal Model.....	125
7.4.4	Risk Model .....	127
7.5	Inverse Monte Carlo Framework.....	129
7.5.1	Inputs and Outputs.....	129
7.5.2	Computational Model.....	131
7.6	Simulation and Results .....	133
7.6.1	Forward Simulation.....	133
7.6.2	Parameter Sensitivity.....	136
7.6.3	Comparison with Clinical Data .....	138
	Simulation Setup.....	138
	Results.....	138
7.6.4	Inverse Monte Carlo Simulations.....	140

Simulation Setup.....	140
Results for Simulated Data .....	140
Results for Clinical Data.....	144
7.7 Performance Optimisation .....	145
7.8 Summary.....	148
8 Conclusions and Further Work .....	150
8.1 Summary and Conclusions .....	150
8.2 Future Work.....	152
9 Bibliography.....	154
Appendix A The Human Immune System .....	A-1
A.1 Innate Immunity.....	A-2
A.2 Adaptive Immunity .....	A-4
A.2.1 Lymphatic System.....	A-6
A.2.2 Maturation of Immune Cells .....	A-8
A.2.3 Immune Activation.....	A-8
A.2.4 Immune Memory.....	A-10
Appendix B Antiretroviral Drug Regimen.....	B-1
Appendix C Alternative Model Formalisms .....	C-1
C.1 P-Systems .....	C-1
C.2 State Charts.....	C-2
C.3 Shape Space .....	C-3
C.4 Stochastic Simulations.....	C-4
C.5 Boolean Networks and Petri Nets.....	C-5
C.6 Cellular Potts .....	C-7
Appendix D The ZdSC Model .....	D-1

Appendix E	STI Studies in chronological order.....	E-1
Appendix F	SMART and LOTTI Comparison .....	F-1
Appendix G	Glossary .....	G-1
Appendix H	List of Publications .....	H-1

## List of Abbreviations

<b>ABM</b>	Agent Based Model
<b>AIDS</b>	Acquired Immunodeficiency Syndrome
<b>ART</b>	Antiretroviral Therapy
<b>CA</b>	Cellular Automata
<b>CD4</b>	Cluster of Differentiation 4
<b>CM</b>	CD4+ Motility
<b>C-S</b>	Celada-Seiden model
<b>CTS</b>	Clinical Trial Simulation
<b>DE</b>	Differential Equation
<b>DNA</b>	Deoxyribonucleic Acid
<b>FRCn</b>	Fibroblastic Reticular Cell network
<b>HAART</b>	Highly Active Antiretroviral Therapy
<b>HIV</b>	Human Immunodeficiency Virus
<b>LOTTI</b>	LOng Term Treatment Interruption study
<b>MC</b>	Monte Carlo
<b>M-H</b>	Metropolis-Hastings
<b>MPI</b>	Message Passing Interface
<b>NRTI</b>	Nucleoside Reverse Transcriptase Inhibitor
<b>ODE</b>	Ordinary Differential Equation

<b>PF</b>	Particle Filter
<b>PI</b>	Protease Inhibitor
<b>RNA</b>	Ribonucleic Acid
<b>SCA</b>	Stochastic Cellular Automata
<b>SMART</b>	Strategies for Management of Anti-Retroviral Therapy study
<b>STI</b>	Structured Treatment Interruption
<b>TI</b>	Treatment Interruption
<b>Treg</b>	Regulatory T-Cell
<b>ZdSC</b>	Zorzenon dos Santos and Coutinho model

## List of Figures

- Figure 2.1: **Stages of HIV infection.** Typical course of an untreated HIV infection over time (x-axis) as indicated by concentrations of CD4+ cells (blue) and virus particles (red) in peripheral blood along with infection stage (horizontal bars) and common symptoms (arrows)..... 11
- Figure 2.2: **Schematic of a Human Immunodeficiency Virus** (~100 nm diameter) with structural elements and proteins relevant for viral lifecycle. Diagram shows the env-Glycoprotein complex on the outer membrane which docks to receptors of CD4+ host cells and triggers fusion. The capsid (centre) containing double stranded viral RNA and Reverse Transcriptase proteins are then injected into host cells where transcription to DNA is started. .... 14
- Figure 2.3: **Effects of antiretroviral drug classes.** Figure shows schematic of viral budding, fusion with host cell, reverse transcription and formation of new virus. Targets of antiretroviral drug classes are shown in red. Each target addresses a key protein in the viral replication cycle. .... 18
- Figure 2.4: **Effect of CD4+ guided structured treatment interruptions on viral load and T-cell levels.** For CD4+ counts (blue) above 350 cells/ $\mu$ l, Antiretroviral Treatment (ART) is suspended followed by an increase of viral load (red) and decline of CD4+ count. ART is re-initiated at CD4+ counts below 250 cells/ $\mu$ l, thus allowing for a safety distance to critical CD4+ levels. .... 24
- Figure 4.1: **Different lattice types and neighbourhoods** (solid wireframes and shaded overlays). (a) left: Square lattice - von Neumann neighbourhood; right: hexagonal lattice; (b) left: Square lattice - Moore neighbourhood; right: Honeycomb lattice..... 41
- Figure 4.2: **Lattice segment of the ZdSC model** during simulated infection. Lattice sites may either assume a 'healthy' (red) or 'infected' (yellow/white)

state. Simulated infection depends on ‘infected’ sites in the neighbouring of ‘healthy’ sites. Image shows wave-like structures of alternating ‘infected’ and ‘healthy’ sites. These structures are propagating slowly, eventually covering the whole lattice.....45

Figure 4.3: **Approximation of pi using direct MC simulation.** Samples are placed at random on a unity square. Objective function determines whether samples are inside (red) or outside (black) a quarter circle with unity radius. The proportion of red samples approaches  $\pi/4$  for large sample sizes.....46

Figure 4.4: **Schematic of operation of the Metropolis-Hastings (M-H) algorithm.** The unknown Posterior distribution of parameter vector  $\theta$  can be approximated from some prior by a sequence of samples (grey dots w. arrows). Samples leading to lower scored than the previous sample may be rejected (dashed dots and arrows). (Lb -lower bound; Ub – upper bound)..49

Figure 4.5: **Schematic of operation of the particle filtering (PF) algorithm.** Random samples (yellow dots) are drawn in parameter space and weighted against their Likelihood of fitting the data. Weighted samples (blue dots) are then resampled where the number of samples corresponds with the respective weights.....49

Figure 5.1: **Topology of a subset of the murine FRCn reconstructed from microscopic imaging.** Scale bar in bottom left corner represents  $30\mu\text{m}$  ....57

Figure 5.2: **Effects of chronic infection on FRCs.** Prolonged exposure to inflammation signals lead to an increase in collagen around FRCs. Collagenation limits the exchange of cytokines, e.g. for  $\text{CD4}^+$  T-cells, leading to increased apoptosis.....58

Figure 5.3: **HIV induced alterations on lymphatic tissue structure.** Diagram shows typical composition of a lymph node with stromal cell types and zones for T- and B-cells. Enlarged portion (top left) illustrates the

structure of healthy lymphatic tissue. Image portion on bottom left indicates pathogenic alterations due to HIV infection.....59

Figure 5.4: **Distinct stages of lymphatic tissue collagenation.** Imaging of lymphatic tissue for (a) uninfected, (b) early, and (c) late stages HIV infection. Green-staining denotes functional tissue, red-staining represents non-functional collagen. ....61

Figure 5.5: **Cycle of HIV induced collagenation and decay of T-cell.** Mechanisms associated with HIV infection (highlighted red) drive a reaction cascade leading to T-cell death and collagen deposition in lymphatic tissue. ....62

Figure 5.6: **State change diagrams of model rules.** H: healthy CD4+ cell; HC: healthy CD4+ cell co-located with collagen; D: dead CD4+ cell (empty); C: empty site co-located with collagen. Transition probabilities and rules are described in the main text.....68

Figure 5.7: **Image of the lattice (SCA model).** Lattice configuration shows simulated lymphatic tissue in latent phase of HIV infection (300 time steps / weeks) with initially 1% of cells were collagenated. Colour coding: Green – healthy regions; Red, Orange – infected, collagenated; Black – dead cells. 68

Figure 5.8: **Simulation data from SCA model showing phases of HIV infection.** Simulated data for amounts of healthy (blue) and collagenated (red) cells in a simulated fraction of lymph tissue. Acute/ early phase occurs (3 to 25 weeks); pre-symptomatic phase - until proportion of healthy cells falls below 0.2 (grey line); after which the AIDS phase is entered and continues.....69

Figure 5.9: **Illustrative overview of sensitivity analysis of a selection of model parameters** reg, cyt, ap with treg (vertical axis). Color-coding represents Mean Square Error serving as a cost function. Diagram highlight complex interactions between the parameters. ....71

Figure 5.10: **Cost functions against proposed parameter value** (x-axis vs. y-axis). Results for  $t_{reg}$ ,  $a_p$ ,  $r_{reg}$  and  $c_{yt}$  (from top left to bottom right). Only the 1000 samples with lowest overall cost are shown to facilitate visualisation. ....72

Figure 5.11: **Response surface visualisation** of  $r_{reg}$  and  $a_p$  against cost function. Illustrative example shows significant distortion of surface (-see arrow) indicating possible transition (or critical) points. ....73

Figure 5.12: **Fundamental concepts of on-lattice collagenation model**. Left side: Solid arrows indicate neighbourhood effects. Originating from HEVs (black dots), collagen (solid grey boxes) spreads to adjacent non-collagenated / healthy sites (white boxes). Right side: Probability of CD4+ cells found present (grey shading/overlay) decreases quadratically with distance to HEVs, based on current assumptions of slow movement due to a random walk. In the event of more rapid T-cell dispersion (or influx from other sources) probabilities close to HEV regions would be relatively low, which corresponds to a more uniform distribution. ....75

Figure 5.13: **A (500 x 500) lattice section for lymphatic tissue showing spatially heterogenous probabilities of CD4+ cell presence**. Regions around HEVs (conduit entries for CD4+ cell movements; red) are associated with high probabilities, compared to non-HEV areas (blue).....80

Figure 5.14: **Result of 1000 inverse MC steps for the spatial model**. The X-axis denotes possible values for spatial collagenation parameter  $P_{INF}$  while the Y-axis corresponds to RMSE w.r.t. clinical data match. Marker colouring indicates value of corresponding ‘small world’ parameter  $P_s$ .....85

Figure 5.15: **Result of 1000 inverse MC steps for the random model**. The X-axis denotes possible values for random collagenation parameter  $P_{rand}$  while the Y-axis corresponds to RMSE w.r.t. clinical data match. Minimum RMSE value is obtained for  $P_{rand} \sim 0.0035$ . ....85

Figure 5.16: **Lattice snapshots of simulated collagen localisation** for spatial model (a) and random model (b), at simulation time step 100 (equivalent to ~2 years). Collagenation forms more distinct clusters (a) compared to (b). Colors indicate simulated collagen density (red – high; blue – low; white – none).....87

Figure 5.17: **Apoptosis rates per collagenated area (a) and log-log plot of profiles of collagen growth over time (b)** for the spatial model (thick blue line) and random model (thin red line). Y axis denotes ratio between the total reduction of CD4+ cells due to collagenation and total collagen accumulation. (Parameters. spatial model:  $P_{INF} = 0.035$ ,  $P_S = 0$ ; random model:  $P_{rand} = 0.0035$ , Y-scale in (a) truncated for visibility). .....88

Figure 5.18: **Comparison of run times**. Diagram shows averages of 24 parallel runs with different degrees of spatial parallelisation for 700 simulation steps with a 500 x 500 lattice. ....90

Figure 5.19: **Influence of square lattice size on inter-run variance** (250 runs respectively with 700 simulation steps each) by simulation step. Variance increase (red colour) occurs towards end of simulations due to incremental stochastic error (less pronounced for larger sizes). Overall variance is low for sample size chosen. ....91

Figure 6.1: **Effect of a structured treatment interruption period on model behaviour**. Continuous treatment initiated at time step 50 (arrow). Start of STI period (fixed cycle – 4 weeks on 4 weeks off) from step 400 to 600, followed by resumption of continuous treatment (c.t.). Enlarged portion of the graph shows the patterns of healthy cell decline, and damage spread in more detail. ....95

Figure 6.2: **Dependency of collagenation and CD4+ concentration**. Collagenation (blue line) and population of CD4+ cells (red line), grey rectangles superimposed on periods of treatment. Treatment starting at time

step 100 with 90% effectiveness. During treatment period, there is a 10% probability that treatment is left out for a week to simulate incomplete adherence which is visible as temporary decrease of CD4+ counts during treatment. Extended period (12 timesteps) of ‘drug holiday’ from time step 150.....97

**Figure 6.3: Effect of treatment adherence and initiation timing on increase of collagenation.** Different colours denote levels of collagen increase. Graph shows relative increase from time of treatment initiation. .98

**Figure 6.4: Effect of different treatment re-initiation thresholds on long term progression of collagenation.** Model simulation with CD4+ thresholds normalized to values before infection. Percent area covered by collagen evaluated after 520 timesteps (~ 10 years in real time). ‘preserved’: Treatment interruption regimen was applied immediately; ‘impaired’: TI regimen was applied after CD4 level reached 20%..... 100

**Figure 6.5: Interruptions affect FRC baseline.** Graphs shows FRC densities (Y-axis) before (blue) and after (red) treatment re-initiation for four subsequent interruption periods (X-axis). The respective interruption patterns were 50 weeks of no treatment followed by 50 weeks of treatment with perfect adherence..... 103

**Figure 6.6: Treatment adherence effect on FRC regeneration.** FRC levels (Y-axis) after multiple periods (X-axis) of occasional treatment, which was only applied in a proportion of weeks (see legend) The respective patterns were 50 weeks of occasional followed by 50 weeks of full treatment for each period..... 104

**Figure 6.7: Collagen build-up depends on adherence level.** Coloured bars indicate collagen coverage after multiple periods (X-axis) of occasional treatment, which was only applied in a proportion of weeks (see legend) and

after treatment interruption periods (X-axis) using the interruption pattern of 50 weeks of occasional followed by 50 weeks of full treatment..... 105

Figure 6.8: **Treatment initiation timing affects collagen build-up.** Shaded lines indicate different times of treatment initiation (0 – 240 weeks, see legend). Treatment interruption displayed takes place between weeks 500 to 505, visible as brief, rapid increase in collagen build-up. Treatment effectiveness was assumed to be 90% on average. .... 106

Figure 6.9: **Collagenation rates under treatment depend on treatment initiation timing.** Markers show rates of collagenation (Y-axis) after treatment initiation against time of treatment initiation (X-axis) after infection. Treatment effectiveness was assumed to be 90% on average.... 107

Figure 6.10: **Collagenation following interruptions depend on treatment initiation timing.** Markers denote total increase in collagenation (Y-axis) during the interruption period against time of treatment initiation (X-axis). Treatment interruption displayed takes place between weeks 500 to 505. Treatment effectiveness was assumed to be 90% on average. .... 108

Figure 6.11: **Collagenation patterns obtained by alteration of neighbourhood effects in comparison to tissue imaging.** Panels on left, centre-left and centre-right show simulation results obtained at time step of 250 weeks. Regions with red colours indicate collagen and healthy cells coloured green. Colour coding applies for simulated and stained tissue. Leveraging settings for effects of neighbourhood collagenation account for different collagenation patterns. Percentages indicate whether sites are collagenated at random (0% neighbourhood effects) or mainly due to neighbourhood effects (97%). Panel on right shows an image of FRC tissue during chronic phase of HIV infection showing curved line separating areas with different collagenation densities..... 109

Figure 6.12: **Contribution of modelled neighbourhood effects to total collagenation progression.** Model parameters were chosen that after 500 timesteps (weeks), 80% of the tissue matrix would be covered with collagen, resembling the terminal phase of infection. Legend shows proportion of neighbourhood effects vs random effects. In this context, 0% represents no collagenation due to neighbourhood effects (i.e. all collagenation caused by random effects). Values were chosen arbitrarily for illustration purposes and double logarithmic scale was chosen for better comparability. ....110

Figure 6.13: **Differences in collagenation increase following interruptions for spatial and random model.** Increase depends on amount of pre-existing collagenation for spatial (blue circles) and random model (orange squares). Markers denote total increase from baseline in collagenation (Y-axis) during subsequent interruption periods starting at specific time steps (X-axis) with respective duration of 50 time steps / weeks. ....111

Figure 7.1: **Example (cardiac drug) demonstrating drug efficacy through evidence-based and mechanistic reasoning.** Left diagram shows purely evidence-based approach by observing inputs and outputs and treating the system as a ‘black box’. Consideration of mechanisms (middle) enables improved system insight but bears risk of false results if not all relevant mechanisms are known. ....114

Figure 7.2: **Concept model for CTS studies** showing the three main steps and subtasks.....116

Figure 7.3: **Relationship diagram for a treatment interruption study.** Grey boxes denote data captured during the clinical study while ovals denote factors at least partially hidden e.g. replacement of lymphatic damage with something like immune damage where the former is not directly observable. ....118

Figure 7.4: **Histograms of CD4+ counts** for groups of HIV-uninfected (left) and infected (right) individuals. Increase in fatalities due to low CD4+ counts lead to asymmetric distribution shape for the HIV infected group. .... 120

Figure 7.5: **Distribution of time-to-AIDS in a patient cohort.** (a): Risk chart indicating proportion of patients with no HIV (at risk, y-axis) against time since seroconversion (years, x-axis); sample size  $n=125$ . (b): Histogram of relative incidence (y-axis) of CD4+ decline rates (cells/mm<sup>3</sup>/day, x-axis), pooled in 0.1 intervals until AIDS onset; and best fit with Weibull distribution..... 121

Figure 7.6: **Mortality rates of HIV-infected patients in relation to latest measurements of CD4+ counts.** Measurements from pooled clinical datasets, (*May et al., 2016; Palella et al., 2006*). Dashed line shows fit using a power-law function indicating asymptotic behaviour. .... 128

Figure 7.7: **Sample run of modelling framework using typical choices for parameter estimates.** Simulated treatment initiation occurs at timestep 250 with interruption at timestep 750 and subsequent re-initiation at timestep 1500 time steps (CD4+ count – T; Immune age - T<sub>c</sub>; each step is equivalent to one day in real time)..... 132

Figure 7.8: **Graphical representation of a Hidden Markov Model.** Circles denominate states (y – observed; x – hidden), arrows dependencies between states. .... 133

Figure 7.9: **Distribution of CD4+ T-cell counts at start of chronic phase of HIV infection.** Histogram height illustrates binned proportions of T-cell concentrations ( $n = 273$ ) obtained from the Amsterdam Cohort Studies on HIV / AIDS, (*Coutinho, 1998*). Red line shows fitted Normal distribution ( $\mu = 742, \sigma = 305$ ). .... 134

Figure 7.10: **Example of a simulated treatment interruption study.** The simulation starts with 2800 patients, treatment interruption occurs for CD4+

counts above 350 cells/mm<sup>3</sup> and (re-)initiation at CD4+ counts below 250 cells/mm<sup>3</sup>. (a) Distributions of CD4+ count at start (blue) and end (red) of study. (b) Distributions of Immune regeneration capabilities at start (green) and end (brown) of study. (c): Cumulative risk of adverse events study period. (d): Proportion of patients under treatment over study period. ....136

Figure 7.11: **Impact of non-patient specific parameters on total risk.** Heat map shows accumulated risk after 2500 simulation time steps (weeks) by colour in relation to different parameters selections. ....137

Figure 7.12: **Comparison of risk progression data** from SMART STI study (solid lines) - rates of death (orange) and opportunistic disease and death (green), with simulation data (dashed lines) for different initial choices of either intact (blue) or impaired (red) immune system function. Clinical data shows as more coarse-grained towards the end, (from censoring).....139

Figure 7.13: **Density of inverse MC samples** (as obtained with the Metropolis-Hastings algorithm) with respect to  $\mu$  (mean) and  $\sigma$  (sd) after 100k sampling steps on simulated risk progression data sets for (a) preserved/intact and (b) impaired immune functions. Shading is set to correlate with MC sample density. ....141

Figure 7.14: **Location of the respective 1000 MC samples with highest scores  $S$  in parameter space** ( $\mu$  -mean,  $\sigma$  -sd, x-axis truncated for visibility) for simulated datasets with immune function preserved/intact (a) and impaired (b). Colour gradient corresponds to negative  $S$  (= log score). ...143

Figure 7.15: **Location of the 1000 MC samples with highest score  $S$  for clinical data from SMART study** (points) in parameter space ( $\mu$  -mean,  $\sigma$  -sd). Colour gradient corresponds to negative  $S$  (= log score). Shaded areas show location of data for simulated data sets with immune function impaired (I) and intact/preserved (P).....144

Figure 7.16: **First 25 steps of inverse simulations of Particle Filter algorithm for different particle numbers** with progression of estimates of population parameters for two sets of simulated data (preserved / impaired).  
.....147

Figure A.1: **Cellular components of the immune system.** Figure shows differentiation paths from common multipotent stem cells, which propagate in the bone marrow. Myeloid (Greek ‘bone marrow’) precursor cells (left) form red blood cells and thrombocytes as well as cellular components of the innate immune system. Right path leads to lymphoid cells which need lymphoid organs for maturation and form the components of the adaptive immune system..... A-3

Figure A.2: **Lymphatic system (female) with principal organs.** Nodes and ducts forming the lymphatic network coloured green..... A-6

Figure A.3: **Schematic of a lymph node.** Lymph entering the node through afferent vessels flows slowly through the reticular network (enlarged portion), enabling lymphocyte contact with stromal cells before leaving the node through afferent vessels. .... A-7

Figure A.4: **Immune cell activation** and parts of the cellular immune response; B-cell response (top), macrophage activation (middle) and T-cell / CD8+ response (bottom). .... A-10

Figure C.1: **State space of a Boolean network** with  $N=4$  nodes and  $K=1$  links per node. .... C-5

Figure C.2: **Petri net with 4 nodes and 1 transition** shown before and after transitions ‘fires’.....C-7

Figure D.1: **Simulation of the HIV time-course using the ZdSC model** (50 runs averaged).. Time step on x-axis corresponds to 1 week in real time, y-axis represents absolute values of cell states described in legend for a 700 x 700 square lattice..... D-2

## List of Tables

Table 2.1: Antiretroviral drug classes and mechanisms of action.....	18
Table 3.1: Summary of model forms used in treatment interruption studies. .....	35
Table 5.1. Model parameter value selection for CD4+ cell and collagen build- up dynamics.....	69
Table 5.2: Parameter estimates for the spatial CA Tissue Model (from the literature). .....	81
Table 5.3: Estimates for $P_{inf}$ and $P_{rand}$ obtained by inverse MC simulations in relation to different infection progression speeds. Values denote averages and standard deviations of the 50 lowest scoring MC samples.....	86
Table 5.4: Specifications of the set up used for experiments with the SCA model.....	89
Table 6.1: Simulation parameters for treatment interruptions using the SCA model.....	94
Table 6.2: Experimental results for CD4+ guided structured treatment interruptions.....	99
Table 7.1: Parameter estimates for the CTS model.....	127
Table 7.2: Virtual study setup, (following basic parameters of SMART STI study) and characteristics of patient groups. ....	138
Table 7.3: Population parameters estimated from inverse simulations using the Particle Filter after 100 steps in comparison to the ‘real’ values used to prepare simulated data. Numbers in brackets denote standard deviations of particle values.....	146

# **Predicting the Outcomes of HIV Treatment Interruptions using Computational Modelling**

Andreas Hillmann

## **Abstract**

In the past 30 years, HIV infection made a transition from fatal to chronic disease due to the emergence of potent treatment largely suppressing viral replication. However, this medication must be administered life-long on a regular basis to maintain viral suppression and is not always well tolerated. Any interruption of treatment causes residual virus to be reactivated and infection to progress, where the underlying processes occurring and consequences for the immune system are still poorly understood. Nonetheless, treatment interruptions are common due to adherence issues or limited access to antiretroviral drugs. Early clinical studies, aiming at application of treatment interruptions in a structured way, gave contradictory results concerning patient safety, discouraging further trials. In-silico models potentially add to knowledge but a review of the Literature indicates most current models used for studying treatment interruptions (equation-based), neglect recent clinical findings of collagen formation in lymphatic tissue due to HIV and its crucial role in immune system stability and efficacy. The aim of this research is the construction and application of so-called ‘Bottom-Up’ models to allow improved assessment of these processes in relation to HIV treatment interruptions. In this regard, a novel computational model based on 2D Cellular Automata for lymphatic tissue depletion and associated damage to the immune system was developed. Hence, (i) using this model, the influence of spatial distribution of collagen formation on HIV infection progression speed was evaluated while discussing aspects of computational performance. Further, (ii) direct Monte Carlo simulations were employed to explore the accumulation of tissue impairment due to repeated treatment interruptions and consequences for long-term prognosis. Finally, (iii) an inverse Monte Carlo approach was used to reconstruct yet unknown characteristics of patient groups. This is based on sparse data from past clinical studies on treatment interruptions with the aim of explaining their contradictory results.

## Acknowledgements

An endeavour such as working on a research thesis would not be possible without individuals providing dedicated support. First, and foremost I want to thank my advisors Prof. Heather Ruskin and Prof. Martin Crane for providing prompt and overwhelmingly constructive feedback on my work and for their valuable guidance at any stage of this project. I am especially grateful that they kindled my interest in modelling during my master studies at DCU some years ago.

Also, I wish to express gratitude to Dr. Marija Bezbradica and the colleagues from Arc-Sym, namely Dr. Na Li, for enjoyable talks and exchange of experiences and ideas which let me feel part of the team despite being off campus most of the time.

I also want to thank my thesis examiners Prof. Anne Parle-McDermott and Prof. Ras Pandey for useful comments and invigorating discussions, which helped to further improve this work.

When doing part time research besides a job in industry, time allocation is always a challenge. Hence, I want to thank my colleagues and superiors for their understanding and for providing time flexibility when necessary.

Special thanks go to my parents who facilitated my entry into the world of academics many years ago and more recently helped with child-minding, along with my parents-in-law, securing me the ever-needed time for research work. My warmest thanks to my little son Jakob, who was born during the course of this work, for providing distraction and reminding me of the important things in life.

Lastly, to my wife Jana, who was a moving force to gain momentum for this project and, during its course, covered my back, especially when we became parents and provided some well-placed motivation more than once while having to endure me being 'into research' for extended times.

# **1 Introduction**

## **1.1 Background**

Almost four decades ago, a new type of lethal disease emerged rapidly among populations of homosexual males in the USA. This disease, termed Acquired Immunodeficiency Syndrome (AIDS), was associated with a variety of symptoms linked to immune system failure. Its cause, being subject of intensive research, was an infection with a yet unknown type of virus, termed Human Immunodeficiency Virus (HIV), (Barré-Sinoussi et al., 1983; Gallo et al., 1983). The virus was found to have unique capabilities not only by defeating the functions of the immune system but also by utilising them for its own replication and as a reservoir. At present time, HIV infection has grown to a major global health problem with approximately 38 million people infected with numbers still on the rise, mainly in resource-limited regions, (UNAIDS, 2019). Despite intensive research, neither a cure (removing the virus from the organism), nor an effective vaccine to prevent infection altogether appears within reach at the time of writing, (Fauci and Lane, 2020).

However, the increase in knowledge of the viral replication cycle enabled the development of specific drugs acting as inhibitors for key steps, (Arts and Hazuda, 2012). Unfortunately, these drugs quickly become ineffective if applied in monotherapy due to the high mutation rate of the virus, (Braithwaite et al., 2007). Combining different drug classes, however, led to a breakthrough, since it largely avoided the drug resistance problem. This treatment, termed combination Antiretroviral Therapy (cART), still forms the base of today's regimen, (Passaes and Sáez-Cirión, 2014). If applied properly, the virus becomes undetectable in the organisms with health and life expectancy greatly improved. To achieve such a state, drug combinations must be taken indefinitely according to a strict daily schedule, (WHO, 2013).

These requirements, however, cause considerable problems for the affected patients. Anti-HIV drugs frequently cause adverse side-effects due to drug interactions and toxicities, (Nansseu and Bigna, 2017), as well as triggering psychological stress, (Katz et al., 2013). These factors lead to treatments often being interrupted (voluntarily) for limited time spans, thus resulting in adherence issues, (Robbins et al., 2007). Situations where interruptions occur involuntarily due to a dearth of drugs, restricted access to therapy, (Mann et al., 2013), or social pressure (Murray et al., 2009), are a common and persistent issue.

As interruptions cause the drug concentrations in the organism being lowered, (Moreno-Gamez et al., 2015), the consequence is a reactivation of dormant virus. The so-called ‘latent viral reservoir’ is a key concern, as it is yet unreachable by treatment efforts. With very few exceptions, the consequence is a rapid increase in viral particle numbers, (Rothenberger et al., 2015). This immediate effect of treatment interruptions may result in serious implications for efficacy, making it necessary to treat with an alternative regimen, (Teklu and Yirdaw, 2017). Apart from this virological failure, less immediate effects, such as failure of the immune system to maintain an effective response, may follow treatment interruptions with detrimental effect to the immune system, (Imaz et al., 2013). The quantification of such effects, however, remains a challenge, hitherto assessed, in part, by clinical studies.

Further aspects of the viral lifecycle, mechanisms of treatment and interruptions will be covered in more detail in chapter 2.

## **1.2 Availability of Data**

To assess the physiological effects of treatment interruptions in a controlled clinical environment, *structured* treatment interruptions, following defined rules (Lau et al., 2019; Stecher et al., 2020), have been investigated. These

studies addressed questions of immune system boosting, reduction of overtreatment and relief of psychological stress. However, results regarding safety have been inconclusive to date, (Dubé et al., 2018). Hence, health authorities do not recommend treatment interruptions (AIDSinfo, 2019). Moreover, further direct clinical studies on structured treatment interruptions have been discouraged due to ethical reasons, (Hirschel and Flanigan, 2009), leaving the causes of inconclusive results of previous studies widely unknown. The resulting lack of sufficiently detailed and up to date clinical data impedes the assessment of treatment interruption impact on long-term prognosis of patients. Due to the ubiquity of treatment interruptions, therefore, any means of predicting failure or success without incurring patient harm would clearly be desirable.

### **1.3 Motivation for Modelling**

In the context of the limited availability of suitable data from clinical sources, modelling has proved to be a powerful *in-silico* tool for investigation of treatment interruptions and can give indicative outcomes of such interventions, (e.g. (Bajaria et al., 2004; Hernandez-Vargas, 2017)). Originally used to explain population dynamics (Berryman, 1992), the underlying concepts have been employed at various scales and for problems, including viral propagation within the host. Such mechanistic models, which consider known biological mechanisms, underpinning the clinical data observed have also been applied for several years to study immunology in general, (Castro et al., 2016), and HIV infection in the blood stream, (Ho et al., 1995; Perelson and Ribeiro, 2013).

However, model assumptions need to be carefully validated against available results from clinical trials or wet lab experiments to ensure that the model provides meaningful results. In contrast to population-based models, biological mechanisms at cellular or molecular level are in many cases not

completely known while obtaining the necessary data with sufficient precision is not feasible with available assay techniques. Hence, modelling in the context of HIV has long focused on few, well-known mechanisms, (Hillmann et al., 2017a), best represented by variants of a common set of model equations. While well-established in the modelling community, these variants provide a somewhat limited view of the complexities of HIV infection, which have been discovered in recent years, (Appay and Sauce, 2017).

Some newer clinical findings require rethinking established model structures in the context of HIV together with complementary alternative approaches, where suitable. Due to the complexity of the underlying biological system, however, definition of model entities and their interrelations is typically non-trivial. Also, limitations of available data from clinical or lab sources, as noted for the case of treatment interruptions, impede calibration and validation of the underlying model assumptions. This situation is exacerbated with increased model complexity, (Castiglione and Celada, 2015), affecting the informative value.

Further, the large body of clinical study data in existence for the case of treatment interruptions dates back several years to the point where further studies were discouraged on ethical grounds. Data obtained thus reflects knowledge on mechanisms of HIV infection only at the given time. However, more recent information on the nuanced biological mechanisms involved, may offer further elucidation of the sometimes-puzzling results of these earlier clinical studies.

Information gained from traditional models can be limited due to their more rigid assumptions, so that use of computational methods and novel models offer potential added value. Well-established computational formalisms allow for improved biological realism while maintaining a sufficiently simple, maintainable model structure.

## 1.4 Scope and Contribution

The body of my research addresses the following:

- (i) Modelling in the context of HIV treatment interruptions. Identification of limitations in regard to the physiological effects of infection progression.
- (ii) Proposing a model with improved biological realism while maintaining simple rules. (Utilises computational capabilities currently available through the university and notes further improvements.)
- (iii) The application of the model developed in the context of several scenarios of interrupted treatment.
- (iv) The assessment of the impact of model interruption scenarios with reference to past clinical study data on structured treatment interruptions. These data are sparse and incomplete with regard to current knowledge. Hence, statistical augmentation of these data to compensate for information lacking is proposed.

The thesis is structured in the following way to address the above issues, with initial chapters providing the groundwork for the models subsequently developed:

**Chapter 2** aims to provide an overview of the biological and medical foundations of HIV infection, treatment to date and difficulties for management, especially in the case of interruptions. The virus interacts with parts of the human immune system, itself highly complex, in manifold ways and shows emergent properties through interaction of a large number of components and different mechanisms. I therefore start with the description of major immune system elements and the related immune mechanisms. Further, I give an overview on how the HI virus *interferes* with the immune system, bypasses the immune defence and eventually leads to breakdown of

the system. State of the art treatment for HIV infection and a list of available drugs, classes and treatment regimen are discussed here, while this section also provides a basic view of the ways in which the drugs compromise the HIV lifecycle. Factors which impede treatment, (preventing a final cure for HIV infection to date,) such as drug resistance and viral reservoirs, are briefly reviewed. Finally, I give an overview of experiences with structured treatment interruptions (STIs). Possible reasons for treatment failures are listed and recent studies on treatment interruptions briefly summarised.

**Chapter 3** reviews the modelling literature for HIV infection and the special case of treatment interruptions (TIs). Emphasis is given to the modelling scale, which crucially affects outcomes of such studies. Relevant model techniques and related formalisms are briefly reviewed and their strengths and weaknesses for the HIV treatment interruption problem are highlighted. Further, gaps in these recent approaches are identified and suggestions are made how these may be overcome using bottom-up modelling techniques.

**Chapter 4** gives an overview of the methods, tools and algorithms used in this research. I briefly describe how these methods have evolved to the point, where newer developments are possible. Implementation and performance optimisation strategies of such methods in terms of practical computation are also covered briefly in order to provide the necessary mathematical and computational background for the work.

**Chapter 5** describes formulation of a model to provide improved description of the long-term prediction and effects of treatment interruptions. The model environment and rules are described in detail with relation to current knowledge on HIV pathology. Further, I conduct basic simulation experiments with the model and discuss outcomes regarding clinical study results.

**Chapter 6** subsequently applies the model developed in Chapter 5 to explore different interruptions strategies. Results on detrimental effects on the immune system are evaluated. From these, recommendations for optimal treatment interruption patterns are formulated.

**Chapter 7** addresses the issue of missing or incomplete clinical data in the context of treatment interruptions. I suggest a way to address this problem using a simulation-based approach by adapting common statistical concepts. The capabilities of the approach are then demonstrated by augmenting incomplete clinical results with additional relevant data, with a few examples to prove usability of the method.

**Chapter 8** summarises all findings and gives an outline of proposals on further research challenges and points to consider, highlighted during the course of this study.

## **2 HIV Infection and Treatment**

### **2.1 Introduction**

The following sections on the Human Immunodeficiency Virus (HIV) provide an overview on the history and current state of the HIV infection pandemic and the structure and mechanisms of action for this virus and infection progression. The history of treatment options, currently available drug classes and their mechanisms of actions and state of the art treatment regimen are considered, together with limitations of treatment strategy given the HIV's ability to evade eradication. Treatment interruptions are described in detail, including possible causes and effects on short and long-term progressions of disease. In the interest of conciseness, a detailed parametrisation discussion of the processes involved is deferred to Chapter 5.

### **2.2 HIV and AIDS**

#### **2.2.1 A Global Pandemic**

The first cases of a disease, termed AIDS (*Acquired Immunodeficiency Syndrome*), came to attention in the late 1970s in USA among homosexual males and intravenous drug users (Jaffe et al., 1983). The individuals concerned showed opportunistic infections, which were typified by a weakness of the immune system. The underlying cause, chronic infection with a new type of virus, termed *Human Immunodeficiency Virus type 1* (HIV-1) was discovered in 1983 (Barré-Sinoussi et al., 1983; Gallo et al., 1983). The virus was found to closely resemble another virus of the same type (*Simian Immunodeficiency Virus – SIV*), which causes similar symptoms in certain kinds of apes, (Chakrabarti et al., 1987). Genetic analysis of preserved tissue samples suggested SIV as an ancestor of HIV-1, where the former crossed the species barrier at the beginning of the 20<sup>th</sup> century, (Worobey et

al., 2008). HIV-1 is the most prevalent subtype both in Africa and the rest of the world. A much less prevalent subtype termed HIV-2 occurs predominantly in parts of West Africa, (Olesen et al., 2018). An infection with HIV-2 causes symptoms which are similar to HIV-1 infection, but the disease progresses more slowly and mortality rates for untreated infections are lower compared to those for HIV-1. It is currently believed that HIV-2 emerged from another subtype of SIV, also by crossing the species barrier, (Santiago et al., 2005). In the work presented here, reference to HIV is to HIV-1, since this makes up far more than 90% of worldwide infections to date, with increasing prevalence in relation to HIV-2, (Olesen et al., 2018).

### **2.2.2 Viral Transmission**

In contrast to other known viruses, HIV has the unique ability of evading the otherwise effective mechanisms of the human immune system (as well as sometimes using them to its advantage). A short summary of the basic components of the immune System and their normal function is given in Appendix A.

The way in which HIV progresses through the human body after infection is still mostly unknown. The main point of entry for HIV virions (virus particles) are the mucosal tissues<sup>1</sup> (e.g. vaginal, rectal). During passage through these barriers, the virus is assumed to infect dendritic cells<sup>2</sup> residing in these tissues in large numbers. It is suggested that around 80% of infections originate from *one single virus particle* passing the mucosal barriers, (McMichael et al., 2010). How the infection further progresses through the underlying epithelial<sup>3</sup> cells is not fully resolved, (Fackler et al., 2014).

---

<sup>1</sup> Layers of loose, constantly replenishing connectivity tissue covering the surface of body openings for protection from pathogens.

<sup>2</sup> Cells responsible for binding pathogens to be supplied to immune recognition.

<sup>3</sup> Tissue lining the surfaces of internal organs, but also the skin.

Infected cells are assumed to reach the lymphatic system from where the infection spreads into other lymphoid and other tissues, where the exact mechanism is also not known, (Fackler et al., 2014). Transmission of the virus has been found to be most effective if it occurs through direct cell contact, although cell-free infection is also occurring but is much less pernicious, (Agosto et al., 2015; Zhong et al., 2013). Susceptible T-helper cells of CD4+ type<sup>4</sup> reside in great numbers in lymph nodes with frequent contact to each other and move slowly through the lymphatic system. Therefore lymph nodes are considered as predominant anatomical compartments for viral propagation, (Pantaleo et al., 1993b). However, progression of the infection is determined by viral load as well as antagonistic CD4+ T-Lymphocyte levels in plasma obtained from peripheral blood<sup>5</sup>, (Mellors, 1997). Viral load levels in lymphoid tissue were found to correlate to blood plasma levels (Cavert et al., 1997), (where blood is easier to obtain for routine screening) although this equivalence has been questioned more recently, (Cohen, 2011).

### **2.2.3 HIV Infection**

An active infection is commonly characterised by concentration of specific biomarkers<sup>6</sup> in peripheral blood, e.g. inflammation enzymes, antibodies or viral components. Additionally, there are clinical conditions related to immune deficiency which are predominantly used to characterise the later stages of infection. These are commonly categorised into distinct stages of early HIV infection, (Fiebig et al., 2003).

Specifically, the timespan from the infection to the first biomarkers becoming visible is termed the *eclipse phase* which takes 11 days on average.

---

<sup>4</sup> Specific protein (,cluster of differentiation 4') on cell surface.

<sup>5</sup> Blood obtained from the circulation (excluding bone marrow or lymphatic system).

<sup>6</sup> Physiological quantity, which is used as an indicator for a certain biological state.

Subsequently, HIV RNA becomes detectable in blood using PCR<sup>7</sup> diagnostics (stage 1). After a further 5 days, HIV-specific antigen (p21) can be detected (stage 2) using immune assays. Virus RNA concentration in blood samples reaches its peak and after 5 more days, anti-HIV antibodies can be found in blood (stage 3), also termed *seroconversion*.

Subsequent to these initial stages, development of concentrations of virus particles in peripheral blood and T-helper cells show a characteristic course over time (see Figure 2.1), which is divided into three phases.

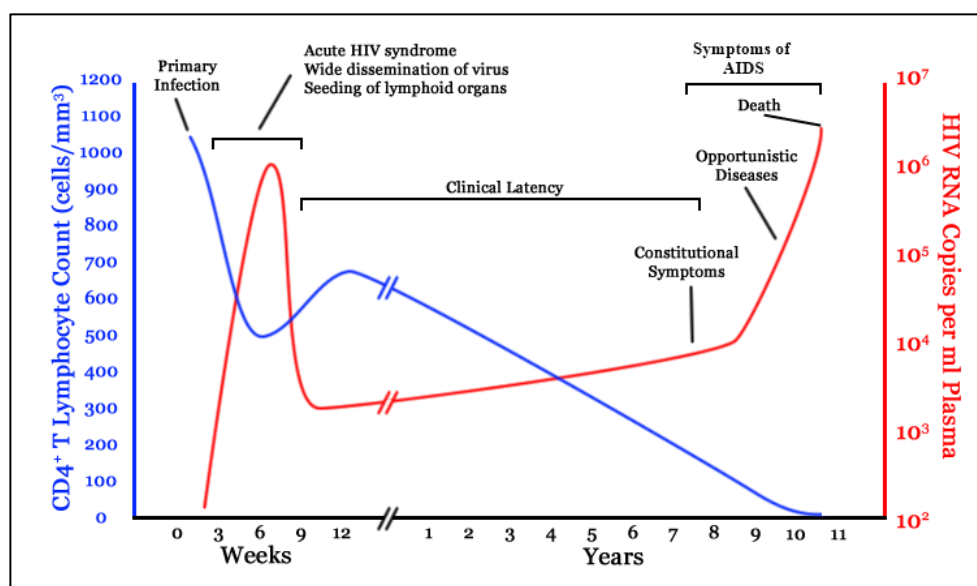


Figure 2.1: **Stages of HIV infection.** Typical course of an untreated HIV infection over time (x-axis) as indicated by concentrations of CD4+ cells (blue) and virus particles (red) in peripheral blood along with infection stage (horizontal bars) and common symptoms (arrows).

Image Source: Jurema Oliveira (2017) *File:Hiv-timecourse.png*, *Wikimedia Commons, the free media repository*. Available at: <https://commons.wikimedia.org/wiki/File:Hiv-timecourse.png> (Accessed: 6 March 2020). Use permitted under the Creative Commons Attribution License CC BY-SA (<http://creativecommons.org/licenses/by-sa/3.0/>)

<sup>7</sup> Polymerase Chain Reaction; a method to detect minute quantities of DNA and RNA by multiplication with the enzyme thermostable DNA polymerase.

During the following *primary phase* of infection, flu-like symptoms (e.g., swollen lymph nodes, joint and muscle pain, rashes, fatigue) do normally occur. Infection rates are initially high with doubling times of viral concentrations of under a day. This turnover rate appears to slow down subsequently, (Ribeiro et al., 2010), indicating partial immune control of the infection. However, genetic diversity of the viral population begins to increase. It is assumed that viral mutants, which are not yet recognised by the adaptive immune response, undergo a positive selection (*escape mutants*), (McMichael et al., 2010). The above is valid for the T-cell mediated immune response (see Appendix A for an explanation). The B-cell<sup>8</sup> response is usually more effective and provides long-term protection. For HIV infection, however, it has no marked impact, since the virus mutates too fast for the response to build up, (Moir and Fauci, 2009).

The concentration of virus decreases until it reaches an approximately stable level 3-6 months after infection, (Perelson and Ribeiro, 2013). This concentration is termed the *viral set point* and marks the beginning of the *chronic infection phase*. Considerable variability has been found for the viral set point between subjects. Clinical symptoms have usually passed by the start of the chronic phase; hence it is also termed the *asymptomatic phase*. This phase, however, is characterized by a persistent immune activation where the generation of CD4+ T-cells is permanently upregulated. This upregulation serves the purpose of improving immune response under normal conditions. Since CD4+ cells are the main target of HIV, however, it fuels infection. After a few years, the function of the immune system starts to decline, which leads to a severe clinical condition associated with immune deficiency, including skin tumours, ulcers, excessive weight loss and prolonged fever.

---

<sup>8</sup> Cellular component of the immune system responsible for (most effective) response related to immunoglobulin (antibodies).

The weakened immune defence also fosters infection in general (hence termed *opportunistic diseases*). The current suggestion is that overt AIDS disease emerges due to the depletion of naïve T-helper lymphocytes, (Doitsh et al., 2013), leading to terminal failure of the cellular immune system, which occurs approximately 10 years after infection, (Fauci et al., 1996), if not treated. However, despite the virus being able only to infect certain types of white blood cells (T-cells with CD4+ receptor), infection indirectly leads to damage of other parts of the immune system through systemic immune activation, (Zeng et al., 2012a).

#### **2.2.4 Viral Structure**

The structure of the virus has been researched extensively, (see (Seitz, 2016) for a comprehensive review). The diagram in Figure 2.2 highlights the key components of a viral particle.

The viral genome consists of two copies of single-stranded Ribonucleic Acid (RNA) which encode for nine genes in total (15 proteins). This genome is enclosed in a protein shell (capsid) and an envelope, to enable protection and fusion with the host cell. Moreover, proteins and glycoproteins, both fixed to the structure or in solution, are needed for the correct function of the virus. The genome, of course, provides the code for all building blocks to produce new functional viruses and the simple structure enables the generation of large amounts of functional virus particles, where the small diameter of ~100 nm is assumed to ease the passage through the mucosal barrier, (Dandekar, 2007).

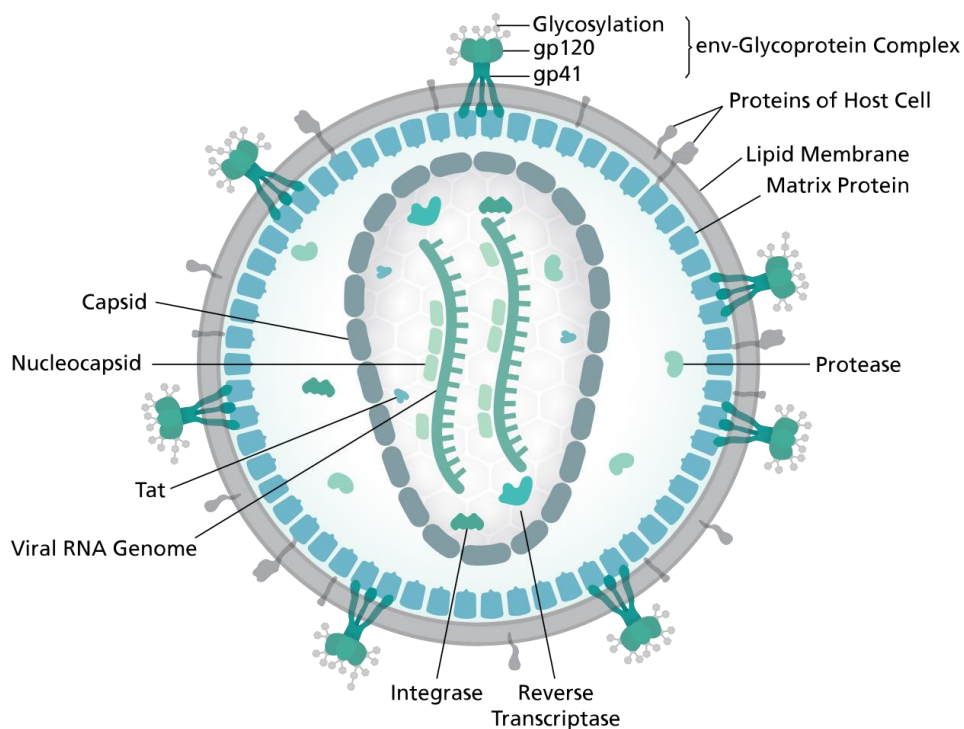


Figure 2.2: **Schematic of a Human Immunodeficiency Virus** (~100 nm diameter) with structural elements and proteins relevant for viral lifecycle. Diagram shows the env-Glycoprotein complex on the outer membrane which docks to receptors of CD4+ host cells and triggers fusion. The capsid (centre) containing double stranded viral RNA and Reverse Transcriptase proteins are then injected into host cells where transcription to DNA is started.

Image Source: Thomas Spletstoesser (www.scistyle.com) (2020) *File:HI-virion-structure en.svg., Wikimedia Commons, the free media repository.* Available at: [https://commons.wikimedia.org/wiki/File:HI-virion-structure\\_en.svg](https://commons.wikimedia.org/wiki/File:HI-virion-structure_en.svg) (Accessed: 6 March 2020). Use permitted under the Creative Commons Attribution License CC BY-SA (<https://creativecommons.org/licenses/by-sa/4.0>)

Normally, the genetic information of a cell encoded in the Deoxyribonucleic acid (DNA) in the cell core (or nucleus) is first *transcribed* into RNA which in turn is used to generate specific proteins (termed *translation*) which act as functional components of the cell. All known cell types and most viruses operate such that transcription is unidirectional from *DNA to RNA*. However, the key aspect of HIV and other *retroviruses* is the *reverse transcription of RNA to DNA*. This process, enabled by a specific protein (reverse transcriptase) supplied by the virus, leads to integration of the genetic information from the viral RNA into the DNA of the host cell. In

addition, the enzyme of reverse transcriptase lacks proofreading, which is crucial in the normal (forward) transcriptase process to reduce transcription errors. This lack is an advantage for HIV as the high frequency of transcription errors leads to rapid emergence of viral mutations (not recognised by the immune system). This fast accumulation of viral mutants effectively ‘outruns’ the capability of the immune system to adapt to new pathogens (see Appendix A.2) thus contributing to persistent infection.

Actively infected cells produce viral components in vast numbers leading to an eventual breakdown and death of the cell, approximately two days after its infection, (Ho et al., 1995). Due to the immune response and effective regeneration capabilities of CD4+ cells, losses are quickly replenished.

However, the more critical aspect of HIV is fostered by a key property of CD4+ cells. These cells may assume a ‘dormant’ state after contact with a pathogen such as a virus giving rise to a kind of *immune memory*. Normally, this would be reactivated when re-infection occurs, leading to an advantage for the immune response. However, in the case of HIV, T-cells may also assume this state after integration of the viral genome into their DNA, becoming ‘latently’ infected, remaining in an inactive state for months or even years before being reactivated and then starting to produce new virus. This *latent reservoir* forms one of the key barriers to complete eradication of the infection.

### **2.2.5 Long-Term Implications**

As stated above, the concentration of CD4+ cells in blood is a well-established marker for assessing infection progression, although the cause of the slow decline in cell numbers has yet to be completely resolved, (Appay and Sauce, 2017). However, it has been argued that the fast cycle of HIV-induced destruction and subsequent regeneration of CD4+ cells eventually lead to depletion of their source, (i.e. the bone marrow or thymus). An

alternative argument is that the elimination rate of such cells is slightly faster than their regeneration rate, leading to a slow decline in the cell pool. Another possible explanation involves the formation of immune memory, (McMichael et al., 2010). Due to the high mutation rate of HIV, the normal mechanism: ‘recognition of a foreign substance (antigen) and response’, has been found to be too slow to provide effective clearance, (Moir and Fauci, 2009), leading to accumulation of different *subspecies* (and memory T-cells which are specific to these) together with corresponding loss of naïve CD4+ cells, capable of responding to novel pathogens.

Other hypotheses attribute the acceleration of the normal ageing process of the immune system to viral activity, (Appay and Sauce, 2017). The parameterisation to quantify the above processes is discussed in Chapter 5.

## **2.3 Antiretroviral Treatment**

### **2.3.1 Drug Development**

Since the discovery of the virus, intensive research has been devoted to development of drugs to cure the infection and prevent AIDS, (Broder, 2010; Günthard et al., 2014; Vella et al., 2012). In 1987, the first antiretroviral drug azidothymidine (AZT, later called zidovudine) was approved for treatment. This drug component used to act as antagonist for the HIV enzyme reverse transcriptase, a key enzyme in the viral replication cascade. However, despite an initial decrease in morbidity after treatment initiation, efficacy diminished after some weeks of treatment. The cause was found to be the high mutation rate which rapidly led to emergence of resistant viral strains where the drug was ineffective. Drug formulations developed subsequently, and based on the same mechanism as AZT, suffered from similar resistance problems and frequently caused adverse effects due to drug toxicity. Early *Antiretroviral Therapy* (ART) consisted of these different drugs applied sequentially in

monotherapy, with the switch between these made after the virus had adapted to a specific drug. However, improvements in morbidity rates were modest.

A breakthrough in treatment efficacy occurred in the mid-90s where new drugs were approved which targeted different parts of the viral lifecycle. While still leading to rapid viral resurgence or drug resistance if used in monotherapy, it was found that certain different drug types act in synergy if administered in combination. These discoveries led to the development of *combination Antiretroviral Therapy* (cART) which still forms the core of today's treatment options.

### **2.3.2 Principal Mechanisms**

Among the most widely used drug classes are *Reverse Transcriptase Inhibitors* (RTIs) and *Protease Inhibitors* (PIs), (Arts and Hazuda, 2012). RTIs reduce viral infectiousness of healthy cells by preventing integration of the viral genome into the host DNA. PIs cause infected cells to produce non-functional virus by preventing a critical step in viral assembly. Figure 2.3 shows a schema of their effect at cellular level.

An overview of the classes of drugs currently recommended for state of the art *highly active antiretroviral therapy* (HAART) (AIDS.gov, 2009; FDA, 2013; WHO, 2013) along with their structure and abbreviations is given in Table 2.1. The tendency to become ineffective due to resistance differs among the drug classes, with PIs being most susceptible to resistance, (Rosenbloom et al., 2012).

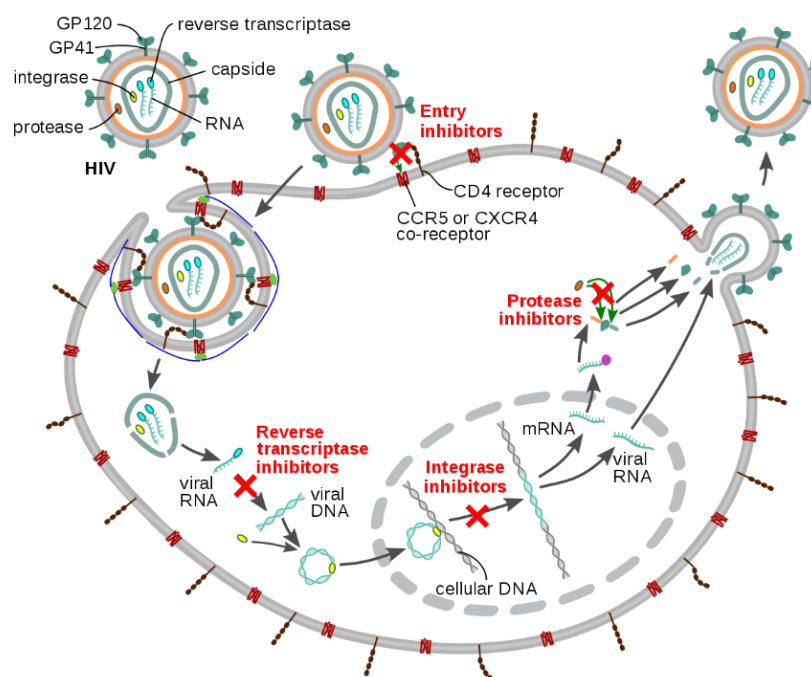


Figure 2.3: **Effects of antiretroviral drug classes.** Figure shows schematic of viral budding, fusion with host cell, reverse transcription and formation of new virus. Targets of antiretroviral drug classes are shown in red. Each target addresses a key protein in the viral replication cycle.

Image Source: Thomas Spletstoesser (www.scistyle.com) (2018) *File:HIV-drug-classes.svg*, *Wikimedia Commons, the free media repository.* Available at: <https://commons.wikimedia.org/wiki/File:HIV-drug-classes.svg> (Accessed: 6 March 2020). Use permitted under the Creative Commons Attribution License CC BY (<https://creativecommons.org/licenses/by/3.0>)

Table 2.1: Antiretroviral drug classes and mechanisms of action.

Drug class	Short name	Mechanisms of action
<b>Nucleoside Nucleotide Reverse Transcriptase Inhibitors</b>	/ NRTIs / NtRTIs	Short strands of RNA (NRTIs) or DNA (NtRTIs) bind competitively at virus RNA strand inhibiting Reverse Transcriptase enzyme function.
<b>Non-Nucleoside Reverse Transcriptase Inhibitors</b>	nNRTIs	Agents bind at allosteric centre of Reverse Transcriptase enzyme, non-competitive inhibition
<b>Protease Inhibitors</b>	PIs	Inhibits viral protease enzyme which is necessary for a cleavage step leading to immature virus
<b>Integrase Strand Transfer Inhibitors</b>	INSTIs	Inhibits viral integrase enzyme to block integration into genome
<b>Entry / Fusion Inhibitors</b>	-	Inhibit virus entry into host cells by interfering with receptors (or coreceptors) on the surface of HIV or CD4+ cells or by preventing fusion of the membranes.
<b>Pharmacokinetic enhancers</b>	-	Improve efficacy of other drugs by increasing their retention period in the organism.

Source: (FDA, 2013; WHO, 2013)

### 2.3.3 Treatment Regimen

The concentration of T-helper lymphocytes (CD4+) in blood serves as a biomarker for infection stage and treatment efficacy, (Fauci et al., 1996). In a healthy person, this concentration ranges from 500 to 1200 cells/ $\mu$ l blood, (AIDS.gov, 2010). In HIV infected persons these levels are decreased.

In their current recommendation, (WHO, 2013), World Health Organization sets the limit to start HAART to CD4+ levels below 500 cells/ $\text{mm}^3$  for adults. Compared to the previous recommendations, (WHO, 2010) where the limit was lower (350 cells/ $\mu$ l), this is an indication for treatment to start as early as possible in accordance with the results of current studies (Sáez-Ciri3n et al., 2013). About 20 different drugs have been approved for HAART, (United States Food and Drug Administration, 2014). A list of these drugs along with current combination recommendations is given in Appendix B.

The currently recommended combinations depend on the actual treatment ‘experience’ of the patient i.e. whether resistant strains have already built up. For ‘first line’ treatment, WHO recommends a ‘backbone’ of two NRTIs (refer to Table 2.1 for abbreviations) and one nNRTI, (WHO, 2013). If these medications lose effectiveness to suppress viral load, it is recommended to replace the nNRTI-based component with PIs. An NRTI component should remain as part of the regimen but a switch should be made to another drug, (i.e. AZT or TDF), depending on what was previously administered.

In contrast to the WHO-guideline, the guidelines coming from European, (European AIDS Clinical Society, 2014), and U.S. authorities, (U.S. Department of Health and Human Services, 2014), offer more options for first-line treatment. Combinations of NRTIs with nNRTIs or PIs or *Integrase Strand Transfer Inhibitors* (INSTIs) may all be used in certain circumstances.

## **2.4 Limitations of ART**

### **2.4.1 Viral Reservoirs**

Even though treatment with HAART leads to very low viral loads in peripheral blood, this does not imply complete healing. On cessation of therapy, viral rebound occurs within days, (Fischer et al., 2003). The only cases of apparent healing of an HIV infection after treatment removals are associated with special circumstances, such as a stem cell transplant following cancer chemotherapy, (Yukl et al., 2013), or treatment of a newborn child, (Persaud et al., 2013). However, in the latter case, the virus was found to have re-emerged several years later, (Cohen, 2014).

Under normal circumstances, it is not possible to eradicate every copy of the virus from the organism with available therapies. Latently-infected memory T-cells have been identified as viral reservoirs, (Chomont et al., 2009) where viral RNA has been integrated into cellular DNA. Other immune cell types, like macrophages and dendritic cells are also suspect in terms of infection retention, (Spiegel et al., 1992).

Another source of viral reservoirs are the so-called ‘sanctuaries’, which are physical compartments in the organism, which cannot be fully penetrated by antiretroviral drugs, (Cory et al., 2013; Solas et al., 2003). Concentrations of ART drugs in intracellular fluid of biopsies of lymphatic tissue were reported to be lower than in blood plasma, by orders of several magnitudes, remaining low even months after treatment initiation, (Fletcher et al., 2014). Also, measurements of viral RNA showed detectable concentrations in tissue despite total suppression in plasma.

The role of pharmacokinetics and drug penetration has been revealed only in recent years, (Cory et al., 2013; Moreno-Gamez et al., 2015). In particular, gut-associated lymphoid tissue (GALT), lymph nodes (LN) and the central

nervous system (CNS) have variously been identified as sanctuaries, (Svicher et al., 2014).

### **2.4.2 Drug Pharmacology**

Treatment efficacy of antiretroviral drug over time and concentration within a host are quantified by *Pharmacokinetics and Pharmacodynamics*, respectively.

*Pharmacokinetics* (PK) describes the course of the drug concentration in an organism over time following its administration. *Pharmacodynamics* (PD) describes the physiological effect of the drug over its concentration. To have a complete view on drug effect over time a combination PK/PD profile is required. HIV drugs are well characterised in terms of PK and PD parameters, with large differences between single drugs, (Sampah et al., 2011). HAART requires a strict regime with administration of at least one and up to three doses per day. Values for plasma half-life vary from several days to 4 hours, (Rothenberger et al., 2015). The primary WHO recommendation is for drugs with longer half-life, needing administration only once or twice a day, (WHO, 2013). However, all pharmacological parameters are based on drug concentrations obtained *in vitro* from serum, (Rosenbloom et al., 2012), which may not reflect true drug efficacy for the organism as a whole, (Cohen, 2011).

### **2.4.3 Drug Resistance**

Certain mutations in the HIV genome lead to resistant strains which respond less well to antiretroviral therapy leading to positive selection of these mutants. This may cause the current drug regimen failure to keep viral replication under control, making it necessary to switch to other drug classes, (WHO, 2013), (not always guaranteed to be available in resource-limited regions, (Cambiano et al., 2013)). Further, recent studies on the

Pharmacodynamics of individual antiretroviral drugs found a connection between dose-response ratios and drug resistance, (Rosenbloom et al., 2012; Sampah et al., 2011).

## **2.5 Discontinuation of ART**

### **2.5.1 Treatment Adherence**

Since HAART cannot eradicate the virus completely from the host, HIV infection is considered a *chronic* condition, requiring life-long treatment administration. The mandatory daily doses (to ensure effective viral suppression) necessitate a high degree of adherence and frequently cause side effects. Hence, (unstructured) interruptions of antiretroviral treatment are common in all regions of the world, (Kranzer and Ford, 2011). The reasons for such interruptions are many: relief from antiretroviral drug side effects (Ammassari et al., 2001), desire to conceal infection due to fear of stigma, (Katz et al., 2013; Murray et al., 2009); lack of knowledge and false beliefs regarding HIV infection, (Nozaki et al., 2013); inadequate access to therapy in resource limited regions, (Mann et al., 2013), are among the most common. Knowledge of the virologic and immunologic implications in suspension of treatment is consequently of importance for successful treatment management.

Consequences of HIV treatment interruptions identified to date are multi-faceted, occurring over very different time scales. Drug pharmacology effects are observable in the short-term, (i.e. of the order of hours), even where rise in viral activity is not yet measurable, a higher risk of drug resistance mutation may apply, (Rosenbloom et al., 2012). Virus levels becomes detectable in blood about ten days after interrupting therapy, (Rothenberger et al., 2015). Options for relief include ‘drug holidays’ or a personalised regimen, where ideally antiviral rebound may be managed.

Over longer time scales, moreover, several clinical studies, (e.g. (Lau et al., 2019)), have been conducted to investigate the effects of treatment interruption by applying them in a structured manner. These investigations are summarised briefly here.

## **2.5.2 Structured Treatment Interruptions**

Several hypotheses have been explored in the context of structured treatment interruptions, (Benson, 2006), with medication cost reduction being one target, and immunological aspects another. Regarding the latter, treatment removal was thought to provide a re-activation of the immune response, ideally stimulating the immune system's ability to control infection without requiring further medication, (Rosenberg et al., 2000). Other clinical studies assessed the potential of treatment interruptions to remove drug resistant mutations from the organism. It was hypothesised that (drug susceptible) wild-type<sup>9</sup> virus would outgrow drug resistant viral strains (which are usually less fit) during interruptions which would lead to improved response to treatment upon re-initiation, (Benson et al., 2006).

Accordingly, two basic designs of STIs have been proposed, (Ananworanich and Hirschel, 2007). In the simplest case, decisions on treatment removal and re-initiation depend on fixed time periods. These treatment interruption schedules are termed 'fixed cycle' with different durations explored, e.g. 'one week on, one week off' (treatment), (Dybul et al., 2001), or 'two weeks off, eight weeks on', (Fagard et al., 2003), among others. These fixed-cycle interruption patterns were somewhat crude, since they were independent of individual patient characteristics such as infection

---

<sup>9</sup> Virus, where the genome has not been subject to mutations leading to drug resistance.

progression speed or pre-existing immune system depletion and results were mixed.

To better consider the immune system state of an individual patient, more sophisticated approaches were suggested. Since the CD4<sup>+</sup> count is a key marker in infection progression and fitness of the immune system, it was employed by various clinical studies (see Appendix E) to make treatment interruption decisions. The diagram in Figure 2.4 shows an example where treatment is interrupted once the CD4<sup>+</sup> count of a subject exceeds 350 cells/ $\mu$ l blood and is re-introduced once it drops to 250 cells/ $\mu$ l. Other limits have been suggested and refined in further clinical studies, (Hirschel and Flanigan, 2009).

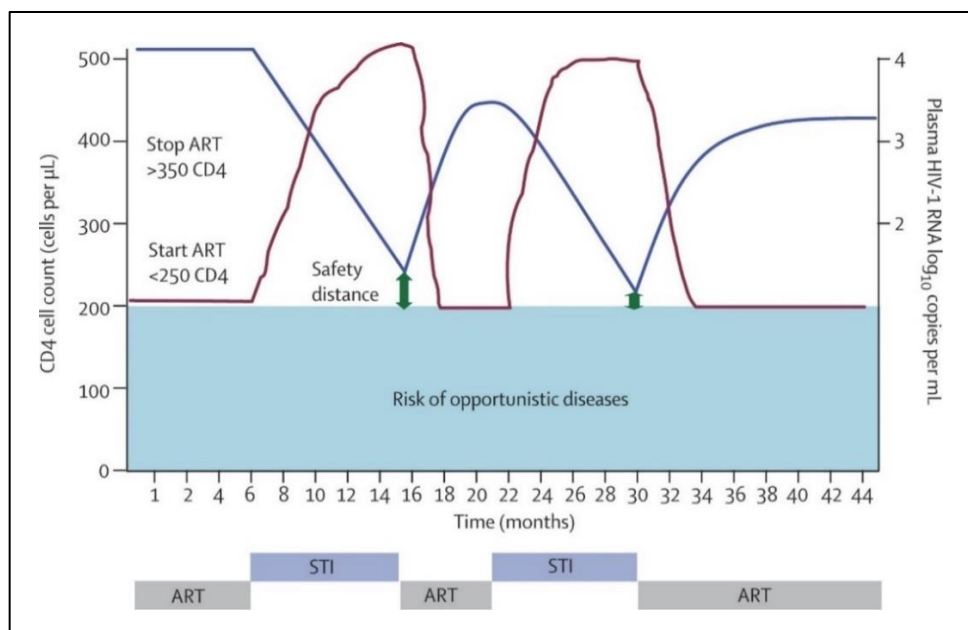


Figure 2.4: **Effect of CD4<sup>+</sup> guided structured treatment interruptions on viral load and T-cell levels.** For CD4<sup>+</sup> counts (blue) above 350 cells/ $\mu$ l, Antiretroviral Treatment (ART) is suspended followed by an increase of viral load (red) and decline of CD4<sup>+</sup> count. ART is re-initiated at CD4<sup>+</sup> counts below 250 cells/ $\mu$ l, thus allowing for a safety distance to critical CD4<sup>+</sup> levels.

Image source: Battegay, M. *et al.* (2006) 'Immunological recovery and antiretroviral therapy in HIV-1 infection', *Lancet Infectious Diseases*, 6(5), pp. 280–287. doi: 10.1016/S1473-3099(06)70463-7. Reproduced by permission from Elsevier

Nevertheless, results have been found to be contradictory and sometimes controversial, (Lau et al., 2019). While immune boosting capabilities have been observed only in rare cases, (Rosenberg et al., 2000), safe margins for treatment interruptions are still a matter of discussion, (Hirschel and Flanigan, 2009). As a consequence, medical authorities continue to recommend that treatment should be administered continuously, (WHO, 2013), in the interest of patient safety, while further clinical studies on treatment suspension are discouraged. However, the incidence of such interruptions is frequent so that wider knowledge of their impact remains desirable.

## **2.6 Summary**

HIV infection poses a complex and persistent threat. The need for lifelong, continuous treatment requiring perfect adherence and drug availability is a weakness of the otherwise potent state of the art combination ART. Treatment interruptions are inevitable, but knowledge of their implications is limited. Due to contradictory results of clinical trials on structured interruptions, further human-based studies are currently discouraged, with data on the issue scarce and sometimes outdated. The known mechanisms of HIV infection can be used, however, to construct models to complement clinical trial data and aid interpretation. Considerations of model type and construction are discussed in what follows next.

## 3 Mathematical and Computational Models for HIV Infection

### 3.1 Introduction

#### 3.1.1 Scale Considerations

Scale and the level of detail are key factors for the informative value of any model. Hence, a brief overview on commonly used formalisms in Biology for large to small scales is relevant here.

In the 18<sup>th</sup> century, Malthus investigated population growth in relation to available resources, (Malthus, 1798). Another major milestone was the description of constrained growth using the logistic equation, first reported by Verhulst, (see e.g. (Cramer, 2002)). This model used a ‘carrying capacity’ to describe an upper population limit, where growth slows down as this is approached. In the early 20<sup>th</sup> century, Lotka and Volterra formulated a model of two interacting species (predator and prey) represented by two coupled Ordinary Differential Equations, (ODEs, see e.g. (Berryman, 1992)), and based on the logistic equation. Hugely successful in helping to understand population fluctuations observed in nature, the predator-prey model was subsequently modified and extended to address related problems, such as transmission of infectious diseases, (Anderson and May, 1979). More recently still, models based on individuals and aggregated for population behaviour have grown in popularity.

The choice on formalisms chosen to cover interactions *between cells*, whether microorganisms or cells within larger organisms, is quite similar. The ODE approach can be applied to approximate a cellular population. However, treating a discrete number of cells as a continuous flow limits the power of ODE representation. The importance of spatial effects due to cell motility,

(Graw and Perelson, 2013), is now widely recognised. Extending the ODE system by an additional derivative for space leading to a system of Partial Differential equations (PDE), (Marinho et al., 2012; Su et al., 2009), adds realism but also complexity. Discrete Agent-Based Models are, however, especially suitable at this scale.

At the lowest level, Biology consists of complex *biochemical reactions* which take place all the time *inside a cell*. As more and more of these pathways have come to light, a vocabulary for expressing these interactions has become necessary. In consequence, both ODEs and formal methods from concurrent systems have been applied to biological systems, mainly to metabolic pathways, signal transduction pathways or genetic regulation. An example of the latter approach is pi-calculus, (Miller et al., 1992), one of an extended group of process calculi used to describe these biological reaction networks. Since these formal description languages were originally invented for computer science, the suitability of the vocabulary for biological systems is not comprehensive, hence kappa-calculus has also been employed, (Miller et al., 1992).

### **3.1.2 Modelling Strategies**

While scale is important, so is deciding how to view the system; a common modelling strategy is to look at the whole system in a *top-down* fashion and describe it by simple rules while considering what is known about its mechanisms. Ideally, such top-down approaches reduce the problem to a set of mathematical equations, enabling mathematical analysis and modest computational resources for numerical solution, (which might explain their popularity). However, many of the HIV top-down approaches are derived from chemical reaction models, which assume equilibrium and a well-mixed environment, which is typically an oversimplification for the problem, (Beauchemin, 2006).

An alternative strategy is *bottom-up* modelling of the system in terms of its component small entities. Systemic properties emerge as a consequence of the behaviour of multiple entities, reflecting a system, which is more than the sum of its parts, (Bianca and Pennisi, 2012).

Given the importance of scale (e.g. ranging from an isolated biochemical reaction cascade inside a single cell to world-wide population dynamics), a third modelling strategy is frequently mentioned for biology – namely *middle out*, (Castiglione et al., 2014). The idea is to start by focusing on an intermediate scale where the cellular level has been suggested as an ideal foundation, (Walker and Southgate, 2009). From this base, extensions are incorporated either to larger units (e.g. tissue) or smaller (e.g. genome) thus resulting in a multi-scale model.

In terms of modelling strategy, ODE formalisms are typically used for top-down modelling and the agent-based paradigm and variants for bottom-up or middle-out modelling. Some relevant examples and applications for model formalisms are given in Appendix B. In the following, their use for aspects of HIV infection is highlighted.

## **3.2 Top-Down Modelling**

### **3.2.1 Model Forms**

The advantage of ODE-based approaches is that they enable a wide range of mathematical means. Linear Algebra may be used to extract powerful metrics on the behaviour of the system, with the solution of more complex systems using numerical methods well researched, (e.g. (Miao et al., 2011)) and computationally inexpensive due to availability of potent mathematical tools, (MathWorks, 2015a). Typically deterministic, these require, in principle, just one simulation run to obtain desired characteristics. With Maximum Likelihood Estimation (MLE) for parameter estimation, computational effort,

in principle, is modest. However, the power is limited in the sense that a high level of abstraction applies to values obtained. Discrete events, which contribute to these, are not considered, which limits conclusions on the underlying causes of system behaviour. Nevertheless, top-down methods have been widely applied in Biology, (see (Gratie et al., 2013) for an overview).

### 3.2.2 Application to HIV Progression

Top-down models were used at an early stage to describe HIV progression, (Perelson and Nelson, 1999; Perelson and Ribeiro, 2013; Xiao et al., 2013). Initially, a system of ODEs was used to model the spread of the epidemic in communities, (Anderson et al., 1986), re-formulated to deal with within-host progression, considering aspects of population dynamics, (Perelson et al., 1993), to include immune response, (Nowak and Bangham, 1996), resistance, (Nowak et al., 1996), drug response, pharmacology, (Bonhoeffer et al., 1997), and so on. Typically, these models involve multiple linked equations, known as *compartments*<sup>10</sup>, with each DE in the system representing one cell type or virus.

In this context, the most commonly used to describe short-term effects of HIV infection, (Perelson and Ribeiro, 2013), is given, expression (3.1).

$$\begin{aligned}\frac{dT}{dt} &= \lambda - dT - \beta TV \\ \frac{dI}{dt} &= \beta TV - \delta I \\ \frac{dV}{dt} &= kI - cV\end{aligned}\tag{3.1}$$

---

<sup>10</sup> Hence, these forms are also referred to as ‘compartmental models’

This model has 3 compartments, where  $T$  denotes number (or concentration) of healthy T-helper (CD4+) cells,  $I$  of infected T-helper cells and  $V$  of free virus particles in the blood stream. This environment was chosen since the model form only works under the assumption of properties (or reactants) being sufficiently well-mixed, (as assumed the blood stream). The DEs then describe rates of change of infection over time with positive terms adding into the respective pool and negative terms reducing it.

Healthy cells  $T$  are produced at constant rate  $\lambda$  in the bone marrow. Death of these cells (due to causes not related to infection) is modelled by removing a fraction  $d$  at a given time interval. Finally, the number of cells removed from  $T$  due to infection and entering the infected state  $I$  is proportional to both virus  $V$  and healthy cell concentration  $T$ , where infectiveness is denoted by factor  $\beta$ . Infected cells  $I$  have no other source than from infection of healthy cells and their death occurs at a constant fraction  $\delta$ , which is typically higher than  $d$ . Each infected cell sheds a number  $k$  of virus  $V$  at each time interval with a constant fraction  $c$  of virus removed due to immune system activity.

This simple model can be used to observe some characteristics of acute HIV infection and to establish the *viral set point*. While the assumption of constant rates is overly-simplistic, insight was nevertheless provided e.g. on high turnover rates of both infected CD4+ cells and virions over the course of infection (Ho et al., 1995). Obtaining closed form solutions, however, is not trivial. Model reduction is required to obtain a simplified statement to describe a specific problem adequately.

This class of models may be extended with additional compartments or treatment effects, e.g. as for expression (3.2).

$$\begin{aligned}
\frac{dT}{dt} &= \lambda - dT - \beta(1 - \eta_{RTI})TV_I \\
\frac{dI}{dt} &= \beta(1 - \eta_{RTI})TV_I - \delta I \\
\frac{dV_I}{dt} &= k(1 - \eta_{PI})I - cV_I \\
\frac{dV_{NI}}{dt} &= k\eta_{PI}I - cV_{NI}
\end{aligned} \tag{3.2}$$

This approach, (Xiao et al., 2013), includes treatment with two drug classes (RTI and PI) and one additional compartment  $V_{NI}$  which denotes non-infectious virus particles. Effectiveness of treatment with the respective drug class is represented by  $\eta$  while the other parameters are as for (3.1). It can be seen that RTI has a direct effect on the rate of infection of T-cells, whereas PI influences the non-infectious virus fraction. Although the above model provides granularity between the effects of different treatments, it is still unsuitable for treatment interruption studies since it omits the latent reservoir of infected cells. Expression (3.3) describes an ODE model more suitable for this type of study, introduced, (Conway and Perelson, 2015):

$$\begin{aligned}
\frac{dT}{dt} &= \lambda - dT - (1 - \eta)\beta TV \\
\frac{dL}{dt} &= \alpha_L(1 - \eta)\beta TV + (\rho - a - d_L)L \\
\frac{dI}{dt} &= (1 - \alpha_L)(1 - \eta)\beta TV - \delta I + aL - mEI \\
\frac{dV}{dt} &= kI - cV \\
\frac{dE}{dt} &= \lambda_E + b_E \frac{I}{K_B + I} E - d_E \frac{I}{K_D + I} - \mu E
\end{aligned} \tag{3.3}$$

The compartment  $L$  denotes a pool of latently infected cells where the growth rate is given by a fraction  $\alpha_L$  of the overall number of cells becoming infected at each time interval. These latently infected cells multiply (proliferate) through cell division with a rate  $\rho$  or die with rate  $d_L$ . Activation of the latent reservoir is modelled by a fraction  $a$  exiting the compartment of latently infected cells and entering  $I$  at each time interval.

The model in expression (3.3) also includes an *active immune response* represented by property  $E$  ('Effector cells') causing reduction of infected cell number  $I$ . This reduction is proportional to the numbers of infected and effector cells and a factor  $m$ . Dynamics of  $E$  depend on a constant replenishment rate for Effector cells  $\lambda_E$  and a proportional death rate  $\mu$ . Multiplication due to immune activation and death due to cytotoxic activity are represented by two terms based on Michaelis-Menten (M-M) kinetics, (Michaelis and Menten, 1913). Rates of Effector cell multiplication and death are given by their maximum values  $b_E$  and  $d_E$ , and the M-M constants  $K_B$  and  $K_D$  respectively, (where these define the values of  $I$  where the rates reach half of their maximum values).

This more comprehensive and complex model was used to assess viral reservoir kinetics and viral control after treatment discontinuation, (Conway and Perelson, 2015), using numerical solution methods. However, the basic model building block (expression (3.1)) remains clear.

The effort to improve biological realism has led to further modifications of the ODE formalism. For example, during early HIV infection, viral numbers are low and random events may have greater impact, accounted for by inclusion of stochastic terms to form Stochastic Differential Equations (SDEs), (Perelson et al., 1993), where multiple model runs with the same initial conditions show different progression, (Tuckwell and Le Corfec,

1998). The intracellular delay associated with HIV infection<sup>11</sup>, has also prompted use of Delay Differential Equations (DDEs), with the ODE formalism incorporating delay terms associated with system rates, (McGuinness, 2012). Partial Differential Equations (PDEs) also permit inclusion of more dependencies into the DE system e.g. spatial relations, (Su et al., 2009), or the age structure of cells, (Wang et al., 2015).

In summary, the choice of model granularity depends on the question which is to be addressed. The addition of more compartments allows inclusion of more detailed biological mechanisms, but additional parameters inevitably increase complexity while baseline values cannot always be obtained from clinical data which may lead to ‘overfitting’ the model to existing data.

### **3.3 Bottom-Up Modelling**

#### **3.3.1 Attempts to Describe**

Bottom-up models typically observe emergent behaviour of individual, discrete entities. Description in terms of equations is less viable and no unified language exists to describe such models, although common grammars have been proposed. Prominent examples include state charts, (Harel, 1987), which aim at describing complex systems in a graphical way. The proposed hierarchical graphs (*higraphs*), (Harel, 1988) combine entities and relations with hierarchies. A similar concept is represented by P-Systems, (Păun, 2000), which relate the hierarchical graphs to biological cells with organelles and compartments separated by *membranes*. Similar ideas are exploited to describe business processes and software architecture (e.g. Unified Modelling

---

<sup>11</sup> Like the time lag between when a cell becomes infected and when it starts to shed virus.

Language, UML), but adoption for Biology has been slow, (Roux-Rouquié et al., 2004); in part this may be due to poor accessibility and discipline-specific experience needed for effective use of such concepts.

In consequence, a unified approach has not yet been adopted for HIV models, where descriptions often omit sufficient detail, thus impeding reproducibility, (Bauer et al., 2009).

In considering discrete entities in a virtual environment, Cellular Automata (CA) approaches handle mobility well and are discussed in detail in the next section. In short, CA assumes cells are fixed on a grid, controlled by global rules which are executed in constant discrete time steps. More generally, agent-based models (ABMs) deal with autonomous agents. The distinction is often difficult to draw, since more complex CA models also assign properties to lattice cells and even allow for movement, (Lin and Shuai, 2010; Mannion et al., 2002). Nevertheless, true agents possess autonomy to a certain degree, have individual properties and event cues and means of communication with the environment and other agents, (Wooldridge and Jennings, 1995). ABMs are widely used in Economics, (Fagiolo et al., 2019) and Social Sciences, (Keuschnigg et al., 2018), but also in Physics, (Sornette, 2014), Chemistry, (de Korte and Brouwers, 2013), and Biology, (Shinde and Kurhekar, 2018).

### **3.3.2 Examples for HIV Progression**

Earlier work, (Grilo et al., 2002), reported a multi layered model with a lattice populated by autonomous agents, while a multi-agent model proposed, (Zhang and Liu, 2005), demonstrated the 3 phase dynamics commonly associated with HIV infection. Further, focus on direct modelling of a lymph network, (Perrin et al., 2010), saw effective use of distributed computing to handle mobility.

In achieving detailed biological representation of system response to infection, an elaborate model (C-S) of antigen recognition and immune

activation was proposed, (Celada and Seiden, 1992). A central concept is the assignment of bit strings of variable length to immune cells which are generated at random, with antigen also represented by a bit-string. The Hamming distance measures probability of a successful interaction between string entities. To interact, two cells have to occupy the same site, so the model permits basic movement. Extensions include additional immune interactions, e.g. (Baldazzi et al., 2006; Castiglione et al., 2019) or adaptations to specific organisms, e.g. fish, (Madonia et al., 2017). One important aspect is the effect of treatment on immune system components, (Castiglione et al., 2007; Mancini et al., 2012).

### 3.4 Modelling Treatment Interruptions

#### 3.4.1 Commonly used Model Forms

A comprehensive review of the Literature on the model forms commonly used to assess treatment interruptions was undertaken, (Hillmann et al., 2017a), and indicated a decided preference to date for top-down forms. This result was confirmed by a repetition of the search in August 2020. In total, we identified 44 separate studies relying on mechanistic models. These are summarised in Table 3.1 according to formalism used and inclusion of biological features.

Table 3.1: Summary of model forms used in treatment interruption studies.

Formalism	Models including biological features					
	Total number of models	Immune response	Resistance	Pharmacology	Latent Reservoir	Spatial aspects
<b>ODE</b>	35	14	20	12	13	0
<b>ABM</b>	5	5	0	0	5	5
<b>Exponential</b>	1	0	0	0	0	0
<b>SDE</b>	1	0	1	0	0	0
<b>Stoch. Sim.</b>	2	0	2	1	2	0

Models of ODE type, which build on the basic form as in expression (3.1), have been amended to include certain biological features important for HIV, including details of immune response and a latent reservoir (included in (3.3)), as well as emergence of drug resistance and pharmacology details. Antiretroviral Therapy was incorporated into these models, typically in terms of a *reduction of infection rates* with effectiveness factor  $\eta$  ranging from zero to unity (as for expression (3.2)).

Subsets of the models identified have been used to investigate treatment interruptions and the conditions under which treatment failure may occur. The effect of missed doses on the Basic Reproductive Ratio<sup>12</sup> of both wild type and drug-resistant viral strains has been examined, (Wahl and Nowak, 2000). Another modelling approach suggests dynamics of infected cell numbers exhibiting damped oscillations being the cause of treatment failure associated with STIs, (Breban and Blower, 2006). However, the underlying assumptions could not be validated *in vivo*, (Oña et al., 2013).

Finding an ideal STI regimen by employing optimal control theory, (Adams et al., 2004; Ernst et al., 2006; Krakovska and Wahl, 2007; Kubiak et al., 2001; Kwon, 2007; Neri et al., 2007; Pannocchia et al., 2010; Xu et al., 2014), has been found to be another prominent application for ODE models. Unfortunately, formulation of an optimal control model requires rather detailed knowledge of the underlying processes of disease spread, together with a biologically realistic range of values for every parameter, which are seldom available. In consequence, these approaches often omit biological facts such as the clinical infeasibility of a continuous dataflow for CD4+ and

---

<sup>12</sup> Commonly denoted  $R_0$ , is a measure for the average number of new infections caused by one infected individual. First used in epidemiology, it has also found application for within-host modelling where susceptible and infected cells are observed. Values of  $R_0 > 1$  indicate that the infection will spread, on the other hand ( $R_0 < 1$ ) infection will die out in the long term.

virus concentration from patient blood, acknowledged, (Attarian and Tran, 2017); the immune system is far more complex than a thermostat, (Louzoun, 2007). The underlying reasons for failure are not elaborated in the reported work.

In summary, treatment interruption models based on ODEs typically have a single specific focus in order to restrict the number of differential equations and parameters to be estimated.

### **3.4.2 Bottom-Up Approaches**

Treatment interruptions have not been found to be extensively studied using bottom-up approaches. Exceptions include simulations with the ImmSimm platform, (Castiglione et al., 2007; Mancini et al., 2012). The latter is based on the C-S model, (Celada and Seiden, 1992), focusing on antigen recognition and immune activation.

However, simulations with ImmSim and variants are computationally expensive as the model scope includes an array of immune reactions, demanding high computing power or the omission of certain feature details, as a compromise to biological exactness. ImmSim studies on treatment interruptions examine the effectiveness of three fixed STI regimen by challenging the simulated immune systems with an opportunistic disease. All STI regimen were found to be inferior to continuous treatment in terms of mortality of the virtual patients. An optimal STI regimen was investigated subsequently, using the same modelling setup but an inverse problem approach; a Simulated Annealing algorithm with a fitness score depending on health and drug uptake of the ‘virtual patients’ was applied.

However, introduction of treatment and introduction of opportunistic disease were assumed to occur at *fixed time intervals* for each simulation which is not realistic, as timing of treatment initiation has important implications for disease management. Further, the STI regimen simulated was

of basic fixed-cycle form and no adaptive mechanisms (such as CD4+ guidance) were considered.

Furthermore, neither drug resistance, nor pharmacodynamics aspects of antiretroviral drugs were taken into account. In the context of treatment removal, (Paci et al., 2011), also used the ImmSim platform to examine viral rebound after interruption by analysing clinical data and comparing with model results. They found that initiation at a very early phase of the disease, (before seroconversion), facilitates viral suppression during a subsequent treatment removal with the model qualitatively replicating this behaviour.

### **3.4.3 Model Parameterisation**

Complex bottom-up models, such as ImmSim require accurate estimates for numerous parameters, relatively few of which are known to sufficiently high precision. The inevitable cumulation of errors may have major implications on simulation outcomes as described, (Castiglione and Celada, 2015).

Unfortunately, the same applies for higher order equation systems in top-down models employed to facilitate improved biological ‘realism’, e.g. (Ferreira et al., 2011). Parameter values must be assumed if not available from the Literature with solutions typically obtained by numerical simulation, (non-trivial, particularly for PDE systems, (Marinho et al., 2012)).

From our extensive review of the Literature, (Hillmann et al., 2017a), the strong indication, (despite intensive HIV research), is that very few clinical data suitable for model calibration or even validation appear to exist at all for the case of treatment interruptions. While ethical considerations clearly have priority, this lack does prohibit a clear-cut answer to regular practitioner queries on what data are used in modelling, with corresponding reservations on credibility of the results obtained. Understanding of the data limitations and more informed inter-disciplinary interaction remain critical to exploit gains offered by modelling alternatives to human clinical trials

### **3.5 Summary**

Modelling approaches for treatment interruptions have almost exclusively focused on short term effects and ODE modelling. Models describing long term effects of HIV infection are scarce and rely on assumptions which ignore newer clinical findings such as lymphoid tissue involvement.

In addition, clinical data, available for validation of these models, remains limited, with implications for perceived overall value. In these circumstances, bottom-up models offer potential for a better understanding of treatment interruption effects. This might be achieved with some reduction in complexity (e.g. compared to ImmSim), whilst specifically taking into account more recent clinical findings on HIV progression in lymphatic tissue.

## **4 Methods for Bottom-Up Models**

### **4.1 Introduction**

Elaborating on techniques and methodology introduced previously, I briefly illustrate the history of the CA formalism and expand on its applications in immunology, for HIV infection and for the present research. The background to both forward and inverse MC simulations is given and implementation options for optimal performance on modern cluster architectures are discussed.

### **4.2 Cellular Automata**

#### **4.2.1 Early Developments**

The Cellular Automata (CA) formalism idea is to compute neighbourhood effects by approximating the system in question by a regular grid, which, in theory, is not constrained in dimensionality or topology, (Ulam, 1962). The diagrams in Figure 4.1 illustrate topologies (and neighbourhoods) for the case of 2 dimensions. The concept was subsequently developed in combination with automata, (theoretical machines), which may assume states from a finite set, where state changes were based on a finite set of rules, (von Neumann, 1969). The resulting Cellular Automata formalism was successfully applied to address problems in computer theory. A noteworthy model in this context is the Universal Constructor, a theoretical machine able to replicate itself using CA rules. Ultimately, the whole universe might be taken to consist of lattice-like structures, which change states due to deterministic rules giving rise to phenomena based at quantum level, (Zuse, 1969).

Due to limitations in digital computing power, CAs remained mostly a theoretical concept until the 1980s. An exception and an implementation, which gained some popularity, was ‘Conway’s Game of Life’, (Cardner,

1971). The CA on a two-dimensional grid with relatively simple rules could produce effects, which appeared life-like or chaotic, despite being completely deterministic. The potential for modelling phenomena in all natural sciences was stimulated, (Wolfram, 2002, 1983), where these examples were mostly based on the progression of a simplistic model of a 1-dimensional CA, giving rise to a range of possible outcomes depending on the set of rules and initial conditions.

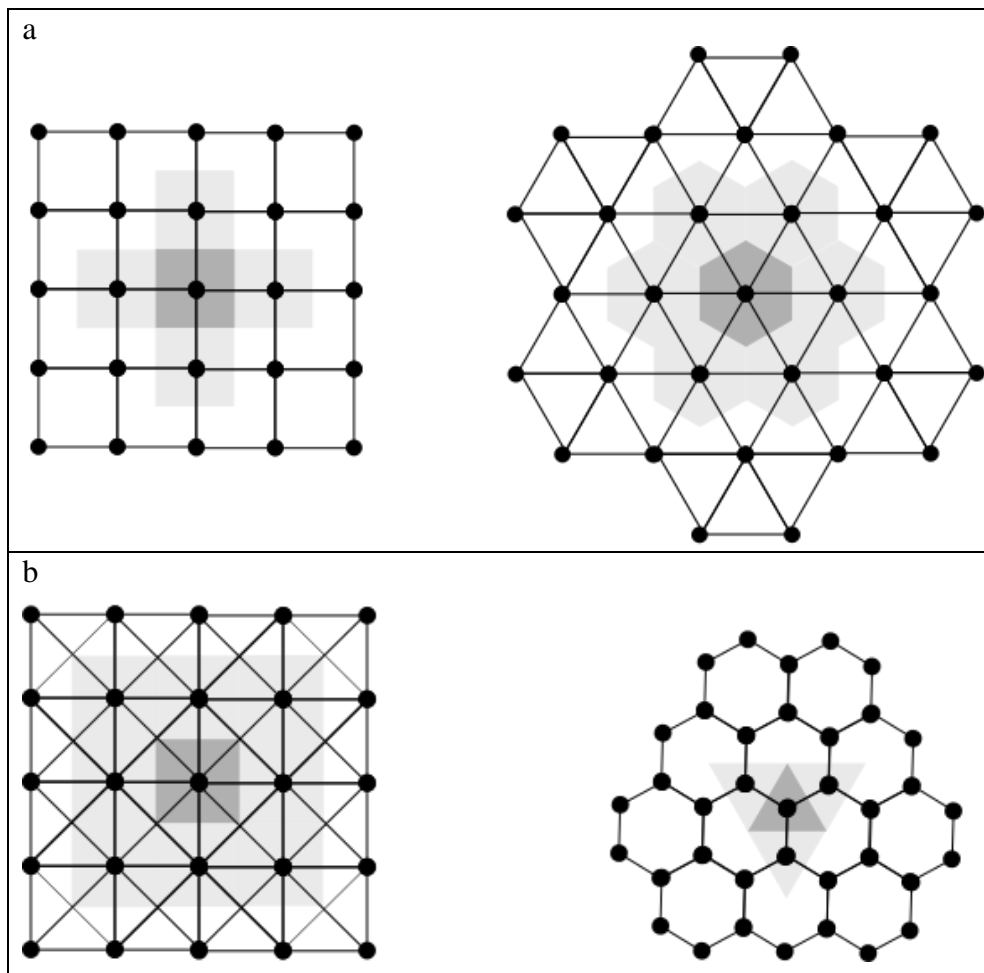


Figure 4.1: **Different lattice types and neighbourhoods** (solid wireframes and shaded overlays). (a) left: Square lattice - von Neumann neighbourhood; right: hexagonal lattice; (b) left: Square lattice - Moore neighbourhood; right: Honeycomb lattice.

### 4.2.2 Use in Immunology

The use of discrete models in Immunology evolved from the concepts of Immune Network Theory, (Jerne, 1974), (for more detail see Appendix C.3). Notably, a discrete deterministic model describing key properties of the immune system was proposed, (Kaufman et al., 1985), based on an earlier approach to model gene regulation, (Kauffman, 1969). A set of Boolean variables was used to represent whether a specific type of immune cell was present or not, hence the state space could be described conveniently using decimal numbers resulting from *bit combinations* of the different states. State changes occurred due to a set of Boolean rules representing known biological mechanisms on the immune system, such as T-cell activation. Thus, each initial state of the system (written as a bit string) yielded a pattern of transitions to other intermediate states prior to reaching an equilibrium state. The approach was extended to more complex immune mechanisms, (Weisbuch and Atlan, 1988), still assuming states to be present at the same location (mean field) and updated synchronously.

While these types of model could be used to explore the complex state space of the underlying Boolean network and to identify certain attractors, spatial effects were not accounted for. This was addressed, (Dayan et al., 1988), by transforming the Boolean network rules to a two dimensional lattice and employing nearest-neighbour interactions while preserving deterministic rules. A major extension of this approach was reported, (Pandey and Stauffer, 1989), retaining the representation of entities as Boolean variables but with execution of CA rules subject to *discrete probabilities*; the first attempt to describe immune system heterogeneity with Stochastic Cellular Automata (SCA). Subsequently, major effects of HIV infection on the immune system were observed with a modified SCA model for the first time, (Pandey, 1991) and extended for effects of mutation and cellular motility, (Pandey, 1998). These effects were also taken into account, (Mannion et al., 2000), using

*asynchronous* updating of lattice sites. In contrast to updating all sites at once, (as in all previous models), cells were updated one-by-one, taking into account specific neighbourhood configurations at the time of update, where this variant is arguably more suitable for biological environments.

### 4.2.3 Applications for HIV

The impact of HIV on Boolean immune system interactions, taking into account viral mutation, was described, (Mielke and Pandey, 1998), and extended for cellular mobility, (Mannion et al., 2000). These models (also based on Boolean network interactions) were limited to early infections and treatment effects were not included.

A hybrid formulation for HIV infection, using concepts from CA and the Celada-Seiden (C-S) model was reported, (Lin and Shuai, 2010). The CA rules are relatively simple but reflect biological functions of T-cells proliferation. Additionally, bit strings were used to model receptor shapes, while interaction probabilities are determined by the *Hamming distance* between two strings. While the 3 phases of HIV infection in a human host could be successfully reproduced, the validity of the underlying assumptions remains untested.

In an influential paper, a new type of CA model, (denoted *ZdSC* model from henceforward), was proposed, (Zorzenon dos Santos and Coutinho, 2001). In contrast to the former models, this focused on discrete states assigned to lattice sites (e.g. healthy, infected) along with a set of simple rules (details elaborated in Appendix D). Despite its less complex state space, the model faithfully reproduces the three-phase dynamics of HIV infection and a number of variants has been proposed, e.g. to introduce aspects of varying viral load, (Shi et al., 2008) and to consider coupling of lymphatic tissue to the blood stream, (Moonchai et al., 2010). An alternative approach, due to (Corne and Frisco, 2008), aimed at improved realism, with a highly complex

CA model making use of Conformon-P systems. However, some 44 rules (compared to 4 in the ZdSC model) were required and consequently validation of the results was both difficult and questionable, having little apparent relation to biological mechanisms observed in the context of HIV.

However, as pointed out, (Strain and Levine, 2002), interpretations in terms of clinical relevance of results obtained with the ZdSC model (and its variants) are also unsatisfactory due to the very loose relation of CA states and parameters to biological entities and mechanisms. Due to the deterministic nature of the ZdSC model, lattice configurations typically show wave-like structures of infected sites slowly progressing over the 2-dimensional lattice, (see Figure 4.2), used to approximate lymphatic tissue. Such regular structures appear to be artefactual rather than relating to the biological context of HIV. Despite the suggestion that such patterns follow Markovian behaviour and might be useful to assess treatment effects, (Hawkins and Molinek, 2015), their value remains questionable.

Few CA based models have considered effects of antiretroviral treatment. Initially, non-uniform CA were used to extend the ZdSC model based on a stochastic alteration of model rules, (Sloot et al., 2002). However, this leads to disruption of the wave-structures (as in Figure 4.2) due to underlying deterministic assumptions, radically altering model behaviour with the simulated infection progression being drastically accelerated and the lattice being completely covered by irregular structures after few 'simulated weeks', (González et al., 2013a). With respect to treatment interruptions, application of CA-based models is even more limited, with few examples available, (Haines and Corne, 2006; Rana et al., 2015), which did not re-evaluate the underlying assumptions of the ZdSC model.

However, subsequent research has aimed at partially addressing questions on biological plausibility of the ZdSC model and its variants, (Precharattana and Triampo, 2014). Here, the model focuses on spatial immune response kinetics during the early phase of HIV infection. To this end, cell types have

been linked to biologically meaningful analogues and parameters obtained, using clinical data, and indicating a potential path for further model expansion.

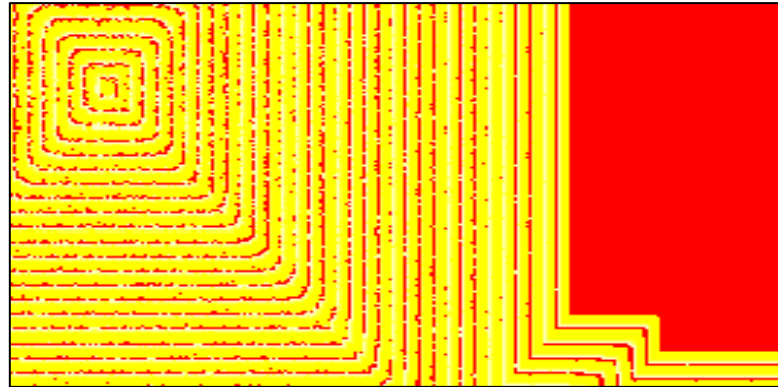


Figure 4.2: **Lattice segment of the ZdSC model** during simulated infection. Lattice sites may either assume a ‘healthy’ (red) or ‘infected’ (yellow/white) state. Simulated infection depends on ‘infected’ sites in the neighbouring of ‘healthy’ sites. Image shows wave-like structures of alternating ‘infected’ and ‘healthy’ sites. These structures are propagating slowly, eventually covering the whole lattice.

## 4.3 Monte Carlo Simulation

### 4.3.1 Direct Monte Carlo

Monte Carlo (MC), a term coined by Ulam to denote the inherent stochasticity of the simulation method, aims at the solution of a system, which is not tractable by other means, through repetition of numerous random sampling experiments to estimate relevant parameters. Outcomes of simulation runs are assessed to provide a numerical score (or ‘energy’ in the original sense of MC) to determine if the cycle of parameter modification, simulation and evaluation has converged on an estimate value or the system has attained equilibrium. While practical applicability was limited in the early days, MC methods found application in numerous areas of science and technology, with the advent of ubiquitous computing, (Kleijnen, 2004).

Subsequently, both *direct* and *inverse* Monte Carlo methods have found wide application. The direct (or forward) case requires a faithful parametrised representation of the system in computational terms. Results of random experiments conducted on this idealised system are thus comparable to results of the underlying ‘real’ system. An example of forward method might be the determination of the pi number by MC simulations (see Figure 4.3).

Unfortunately, while knowledge of a system may be sufficiently detailed to define a system function for some physical systems, for most (realistic) cases (not least in biology and medicine) it is not. However, where data are available, *inverse* MC methods may be used to obtain parameter estimates.

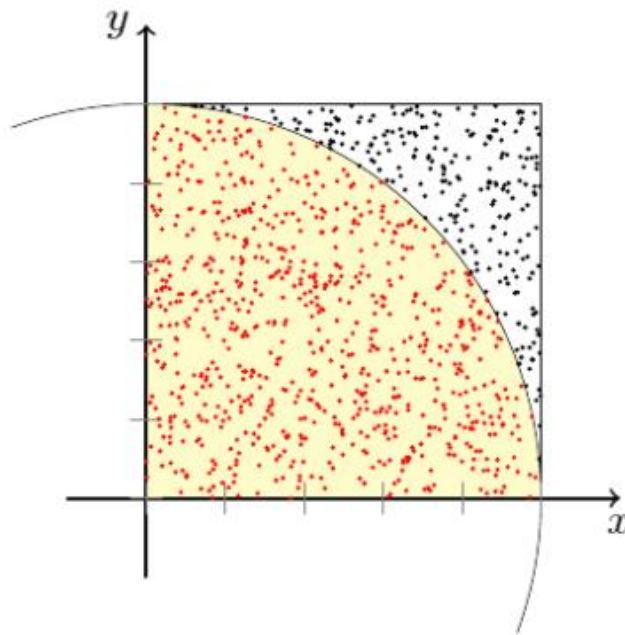


Figure 4.3: **Approximation of pi using direct MC simulation.** Samples are placed at random on a unity square. Objective function determines whether samples are inside (red) or outside (black) a quarter circle with unity radius. The proportion of red samples approaches  $\pi/4$  for large sample sizes.

Image source: Springob (2004) *Pi\_statistisch*, *Wikimedia Commons*, the free media repository. Available at: [https://commons.wikimedia.org/wiki/File:Pi\\_statistisch.png](https://commons.wikimedia.org/wiki/File:Pi_statistisch.png) (Accessed: 15 June 2020). Use permitted under the Creative Commons Attribution License CC BY-SA (<http://creativecommons.org/licenses/by-sa/3.0/>)

### 4.3.2 Inverse Monte Carlo

Biological systems are inherently complex and multi-faceted and detailed knowledge on all underlying mechanisms is typically limited. Despite intensive clinical research, this is also still the case for HIV pathology. Clinicians and Biologists thus have to rely on data from clinical trials and *in vitro* experiments to reconcile knowledge on the mechanisms involved.

This poses an *Inverse Problem*, (Tarantola, 2005), where the aim is to identify likely model parameterisations (commonly written as *parameter vector*  $\theta$ ) in the light of the experimental data. Hence, a cycle of *inverse* MC (iMC) typically draws samples from the available *parameter space* for a mechanistic model. The model with sampled set of parameters is then executed and the output is scored against available experimental data. The iMC cycle involves numerous iterations with the aim of exploring the parameter space, approximating the distribution of parameters.

Thus, the inverse process is essentially *Bayesian*. A simple Bayes formula for the Posterior  $P(\theta|y)$  (for some experimental data  $y$ ) is given by (4.1).

$$P(\theta|y) = \frac{P(y|\theta)P(\theta)}{P(y)} \quad (4.1)$$

Here,  $P(y|\theta)$  is the Likelihood that data  $y$  is observed with the given parametrisation  $\theta$  with  $P(\theta)$  the probability distribution assumed for  $\theta$  in absence of data. In the simplest case, a uniform probability distribution over the parameter space might be used (*uninformed* Prior). The probability distribution  $P(y)$  of obtaining the data is usually not known.

In the context of iMC, regions in the parameter space where the Likelihood is high are obviously the most interesting. Hence, drawing random samples from any location is not efficient, so an algorithm such as *Metropolis-Hastings* (M-H), (Hastings, 1970) is widely applied. The algorithm is based

on the Markov Chain principle, which in this case means that it is aware of the scores of the set of parameters sampled in the previous steps; if the score improves, the new sample is accepted. If accepted, it serves as a mean value for subsequent samplings and so on. Hence, the M-H algorithm, circumvents a common problem of ‘hill-climber’ algorithms of becoming ‘trapped’ in a narrow region with a local score maximum. It is therefore very powerful in terms of exhaustively exploring high-scoring regions in parameter space. The schematic in Figure 4.4 highlights principal algorithm steps. However, due to the underlying Markovian property, which requires computations to be executed in strictly sequential order, it is less efficient on modern, parallel computing architectures.

An alternative is to use the Sequential Monte Carlo technique, also termed *Particle Filtering* (PF), (Doucet et al., 2001). The basic algorithm, originally proposed to analyse time-varying noisy signals, consists of more steps than the M-H algorithm making it slightly more complex but can improve performance. In an inverse MC setting, multiple samples of candidate parameter sets are drawn from parameter space forming a cloud of ‘particles’. After this ‘bootstrap’ sample, scores are obtained from simulations with these proposed parameter sets. These score values are used to assign weights to the particles, with low-scoring particles below a certain threshold rejected immediately. The remaining particles are then *resampled* around the weighted particles, where the number of samples drawn depends on the weight of the respective particle. After this step, termed ‘importance sampling’ the PF cycle is repeated. A graphical representation of the algorithm is given in Figure 4.5.

In comparison to the M-H algorithm it is possible to analyse a large region of the parameter space simultaneously, which is particularly suitable for parallel computing architectures. Given sufficient parallel processing capability, the application of the PF method may be expected to yield marked gains in computing performance.

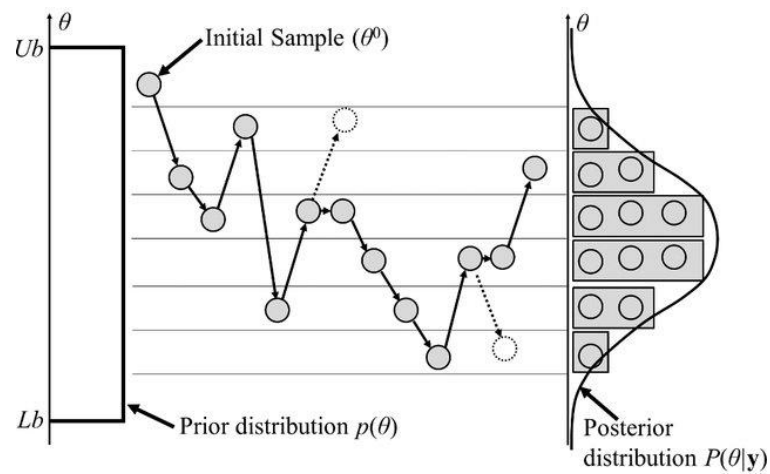


Figure 4.4: **Schematic of operation of the Metropolis-Hastings (M-H) algorithm.** The unknown Posterior distribution of parameter vector  $\theta$  can be approximated from some prior by a sequence of samples (grey dots w. arrows). Samples leading to lower scored than the previous sample may be rejected (dashed dots and arrows). ( $Lb$  -lower bound;  $Ub$  – upper bound)

Image source: Lee, J., Sung, W. and Choi, J. H. (2015) ‘Metamodel for efficient estimation of capacity-fade uncertainty in Li-Ion batteries for electric vehicles’, *Energies*, 8(6), pp. 5538–5554. doi: 10.3390/en8065538. Use permitted under the Creative Commons Attribution License CC BY (<https://creativecommons.org/licenses/by/4.0/>)

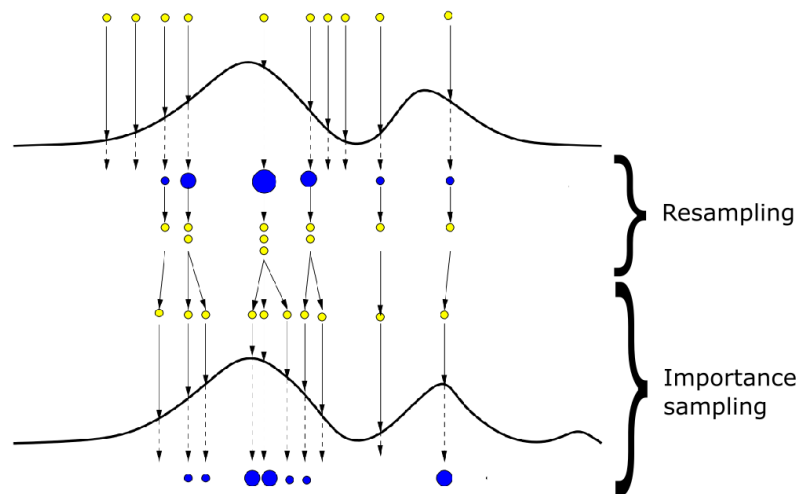


Figure 4.5: **Schematic of operation of the particle filtering (PF) algorithm.** Random samples (yellow dots) are drawn in parameter space and weighted against their Likelihood of fitting the data. Weighted samples (blue dots) are then resampled where the number of samples corresponds with the respective weights.

Image source: Doucet, A., de Freitas, N. and Gordon, N. (2001) *Sequential Monte Carlo Methods in Practice, Sequential Monte Carlo Methods in Practice*. Edited by A. Doucet, N. Freitas, and N. Gordon. New York, NY: Springer New York. doi: 10.1007/978-1-4757-3437-9. Adapted by permission from Springer Nature

## 4.4 Implementation of Bottom-Up Models

### 4.4.1 Tool Options

From the beginning of the 1990s, when large processing power became widely available, numerous toolkits for discrete models evolved, see (Nikolai and Madey, 2009) for a comprehensive review. Despite the range of methodologies proposed (e.g. (Macal and North, 2010)), however, there is no unified principle on technical implementation. The vast majority thus employ the syntax of popular programming languages like C or Java in addition to proprietary concepts.

General purpose mathematical tools also have been applied to agent-based modelling. MATLAB, (MathWorks, 2015b) has been a particularly popular choice for CA models, (Jafelice et al., 2009; Precharattana et al., 2011; Shi et al., 2008) due to its matrix-based architecture, which facilitates lattice representation.

The advantages of using modelling toolkits lie in their extensive documentation, the existence of a user community, the availability of examples and easy accessibility, (especially for scientists with no programming background). However, the tools have been designed with ‘typical’ scenarios in mind and often lack functionality or flexibility for specialised investigation. Performance is often a *disadvantage* as an agent-based model run is computationally expensive if a large number of agents is involved and has to be executed multiple times in stochastic terms. Modelling tools thus have a high calculation overhead compared to a high-level programming language. Of course, not all high-level languages are equally good either. Programs written in Java (due to its VM architecture) perform poorly compared to languages which access hardware more directly. Conversely, low-level programming languages like Assembler need extensive programming knowledge and pose problems of code maintenance.

Consequently, no general recommendation exists on an optimal tool for implementation of an ABM.

The C++ language represents a compromise between performance, complexity and maintainability (as it utilises the object-oriented approach). A high level of control on hardware resources is possible, together with some low-level programming knowledge, but significantly better performance can be achieved than for other high level languages, (Hundt, 2011).

#### **4.4.2 Model Design**

The model to be constructed needs to be meaningful in terms of the Biology and have measurable properties enabling comparison and verification against clinical data. While very large simulation size is advisable statistically, this numerical requirement must be balanced against computational resources available. Although a wide set of mechanisms on HIV interaction with the immune system has been the subject of research, a comprehensive model is both too complex and correspondingly limited in flexibility and predictive capability. One universal model example is that of ImmSim applied to HIV, (Paci et al., 2009). While the model is true to biology for wide-ranging immune mechanisms, computational requirements tend to be high limiting the number of simulations and time-line possible. A possible solution is to yet further increase scale and deploy even more computational resources to get closer to the actual system size (i.e. in terms of type and number of cells). While this has been attempted by Immunogrid (an EU-funded project), (Halling-Brown et al., 2010), results are still outstanding, indicative of the difficulty of the task. Moreover, despite its complexity, ImmSim still lacks basic features of HIV propagation, such as viral mutation and its effect on other cell types or tissues other than the cellular immune system. This implies at best partial view on some questions, such as HIV treatment interruptions, (Mancini et al., 2012).

Alternatively, a less complex model focusing on a subset of biological features, identified as important for the progression and this directly impacting on consequences of treatment interruptions, may be immediately useful. Biological features, having a minor role demand less detail, (for example, cellular infection with HIV and the immune response are typically events measured in time ranges of hours or days). To observe infection progression over an extended period, detail on these short-term effects can be simplified to reduce computation overheads in order to include mechanisms occurring at longer time scales. While this limits study of some interactions of the immune response, this modelling approach is in line with my objectives of obtaining an overall assessment of key factors influencing HIV progression following treatment suspension.

### **4.4.3 Computing Resources**

Performance is also inevitably affected by availability of the computing hardware. The co-founder of Intel, Gordon Moore, predicted a doubling of processor speed every 2 years, a relation which became commonly known as Moore's law, (Moore, 1965). The prediction mostly held for about 40 years but, due to physical limitations, the increase in processing speed for single processor units reached a limit a few years ago, (Kish, 2002). To cope with this issue, modern processor architectures combine multiple processing cores.

However, these still behave like separate processors which is a consideration for many-body programming. When using a high-level programming language, this can be achieved by splitting up the program into different threads executed in parallel. In some cases, threads can be run totally independently ('embarrassingly parallel'), but normally data exchange is required at some point. The necessary time needed for synchronisation and communication means resources run idle at times, inevitably impairing performance, despite attempts to minimise by good programme design. To

this end, libraries for high-level programming languages have been developed to reduce programming complexity and provide necessary functions in a convenient way. The Message Passing Interface (MPI) presents a de-facto standard for the implementation of programs running on distributed systems, (MPI Forum, 2019). The standard defines routines and describes their syntax and semantics for various programming languages, with various implementations available, the most common being OpenMPI, (Open MPI Project, 2020) and MPIch, (MPICH Collaborators, 2019). Where MPI puts focus on running threads on separate physical machines, the OpenMP library, (OpenMP Architecture Review Board, 2019), offers similar functionalities for shared memory systems with parallel processing capabilities (such as multiprocessor desktop computers).

#### **4.4.4 Parallelisation Techniques**

One utilisation of parallel processing for this research is to perform a large number of model runs with different parameter settings in order to analyse model behaviour and gain meaningful statistics. Since each run is independent, no communication overhead occurs, hence optimising computational resources.

However, this is not really possible as more complex models may be too demanding to run on a single thread. Hence, the components of the model have to be split in a sensible way to ensure best parallelisation. One needs to consider whether to split up computations into many small tasks, (small-grained) or to use less but larger tasks (coarse-grained) and run in parallel. The optimal choice may be a compromise between these two, depending on the model and computational resources available. In terms of a CA model, one can intuitively split up the simulation space in equally sized parts to run in parallel. Communications among parallel processes then need to ensure information on neighbourhoods is correctly passed. If neighbourhoods are

comprised solely of directly-adjacent sites, communication can be conveniently solved by introducing an additional layer of sites around each part of the simulation space. Communication is restricted to the sites of these ‘boundary layers’. If a site updates its state due to local CA rules, the updated state is copied to the corresponding site in the neighbouring part of the simulation space, (Perrin et al., 2006). If the number of sites in boundary layers is small compared to the size of each lattice part, parallel performance is markedly improved, (Hecquet et al., 2007).

## **4.5 Summary**

This chapter highlights the principles and evolution of SCA methods for immune modelling and HIV. Foundations of MC simulations, tool choices and options to achieving a detailed model, with strong performance are also considered. Application of these methods to the problem of HIV treatment interruptions is discussed in what follows.

## **5 Two Models for Lymphatic Tissue Changes**

### **5.1 Introduction**

In this chapter, I propose a novel computational model using a bottom-up approach with the CA formalism. Each aspect of the model is rooted in biological facts, using recently available data. To this end, additional required biological background is given. In subsequent sections I describe construction of a stochastic Cellular Automata model for tissue collagenation, translating known biological mechanisms into model rules. The model is further extended to investigate effects of CD4+ cell motility, adding further to our published work, (Hillmann et al., 2019). I focus briefly on implementation to demonstrate impact of the different parallelisation strategies highlighted in the previous section. Preliminary results are presented, and forms of simulated treatment introduced.

### **5.2 Biological Effects**

#### **5.2.1 Functions of Lymphatic Tissue**

The way in which this complex system maintains its balance (*homeostasis*) and the cause of its stability has long been a target for research: e.g. on the importance of lymphatic tissue for both functionality and stability of the immune system, (Mueller and Germain, 2010). The pathogenesis of HIV infection has long been known, (Brenchley et al., 2004; Pantaleo et al., 1993a), but only recently novel analysis techniques have enabled further insight into live tissue processes, (Schacker et al., 2002). These recent efforts suggest that the cells of tissue in lymph nodes play a key role in maintaining the delicate balance. The current knowledge and major mechanisms of the immune system in this context are briefly summarised in Appendix A, while the biological terminology is detailed in the Glossary.

Besides hosting most motile lymphocytes, connective tissue (or stromal) cells of lymph nodes also play a key role. Lymphatic tissue is roughly differentiated into T-cell zone and B-cell zones, similar to predominant immune cell types, (von Andrian and Mempel, 2003). Reacting to stimulus, immune cells migrate into the respective tissues, encountering antigen and binding to different types of antigen-presenting cells. A successful match triggers maturation and proliferation of the given cell type.

The B-cell zone tissue consists largely of *Follicular Dendritic Cells* (FDCs), providing an immobile matrix of antigen presenting cells. These cells are known to be a viral reservoir for HIV since they are able to bind viral particles, and release them slowly, (Spiegel et al., 1992).

The T-cell zone tissue makes up about 25% of total lymph node volume, (Mueller and Germain, 2010) and mainly consists of *Fibroblastic Reticular Cells* (FRCs), (Fletcher et al., 2015). These cells form a network structure, the *Fibroblastic Reticular Cell network* (FRCn), due to their association with fibres of connective tissue. In consequence, the function of these cells was thought to be limited in providing tissue structure for a long time. However, recent studies suggest that the FRCn plays a crucial role in guiding naïve T-cells which encounter antigen-loaded Dendritic Cells (DCs) by moving along network fibres, (Brown and Turley, 2015).

Structural aspects of the FRCn have not been widely researched. However, a recent study of *murine* experiments, aiming at quantifying regeneration capabilities of FRCs following ablation, suggested that the FRCn topology has aspects of both regular lattice and small-world<sup>13</sup> networks, (Novkovic et al., 2016), as illustrated in Figure 5.1.

---

<sup>13</sup> A network topology where most nodes can be reached from any other node with a small number of steps facilitated by a small number of highly connected nodes.

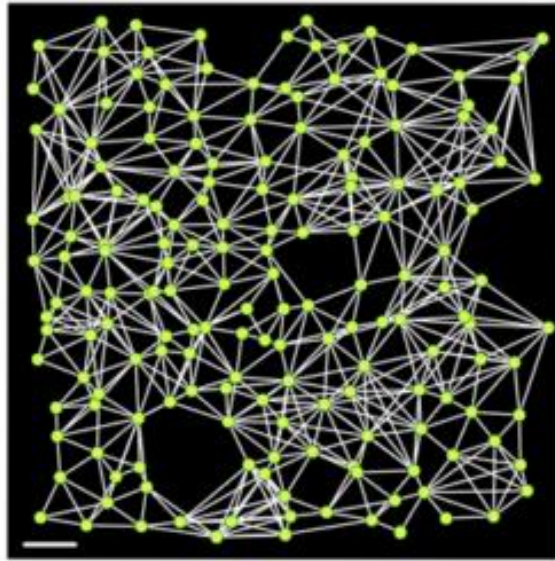


Figure 5.1: **Topology of a subset of the murine FRCn reconstructed from microscopic imaging.** Scale bar in bottom left corner represents 30 $\mu$ m

Image source: M. Novkovic et al., Topological Small-World Organization of the Fibroblastic Reticular Cell Network Determines Lymph Node Functionality, PLOS Biol. 14 (2016) e1002515. doi:10.1371/journal.pbio.1002515). Use permitted under the Creative Commons Attribution License CC BY (<https://creativecommons.org/licenses/by/4.0/>)

There is also a strong indication of a link between FRCs and naïve<sup>14</sup> CD4 T-cells, the main target of HIV, (Zeng et al., 2011). The presence of FRCs appears to improve the survival of naïve T-cells in their *neighbourhood* by secreting signalling molecules (cytokines) of type Interleukin-7 (IL-7). In response, naïve T-cells provide another cytokine, Lymphotoxin beta (LT- $\beta$ ) which, in turn, preserves fitness of FRCs (see Figure 5.2). This give-and-take relationship is assumed to play an important role in maintaining constant levels of naïve T-Cells (and the above-mentioned homeostasis), (Link et al., 2007).

---

<sup>14</sup> T-cells not yet in contact with antigen, i.e. not specific to any antigen.

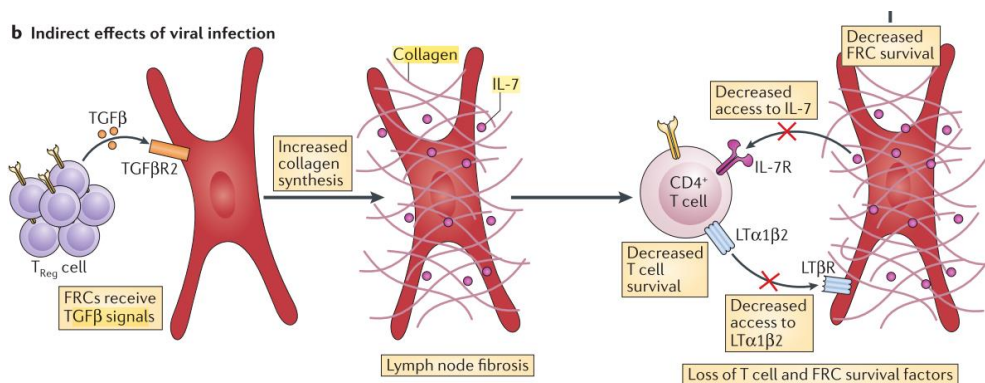


Figure 5.2: **Effects of chronic infection on FRCs.** Prolonged exposure to inflammation signals lead to an increase in collagen around FRCs. Collagenation limits the exchange of cytokines, e.g. for CD4<sup>+</sup> T-cells, leading to increased apoptosis.

Image source: A.L. Fletcher, S.E. Acton, K. Knoblich, Lymph node fibroblastic reticular cells in health and disease, *Nat. Rev. Immunol.* 15 (2015) 350–361. doi:10.1038/nri3846, copyright 2015. Reproduced by permission from Macmillan Publishers Ltd: Nature Reviews

## 5.2.2 HIV Infection on Cellular Level

HIV infection has a dramatic impact on both tissue structure and function in lymph nodes. Starting in the early infection phase, tissue images reveal the disruption of designated structures like B- and T-cell zones along with loss of functional tissue (see Figure 5.3). While these tissue alterations have been known for some time, (Haase et al., 1996), the causes have been subject to debate.

However, current research suggests that due to HIV-induced reduction of CD4<sup>+</sup> cell populations, levels of LT-β also decline in the lymph nodes which in turn decreases the number of FRCs. In this context, the function of *Regulatory T-cells* (Tregs) has been the subject of recent clinical research on HIV, (Kinter et al., 2007; Kleinman et al., 2018). This specific subset of T-cells also carries the CD4 receptor, together with additional receptors (FoxP3 and CD25), which promote its function, (Milanez-Almeida et al., 2015).

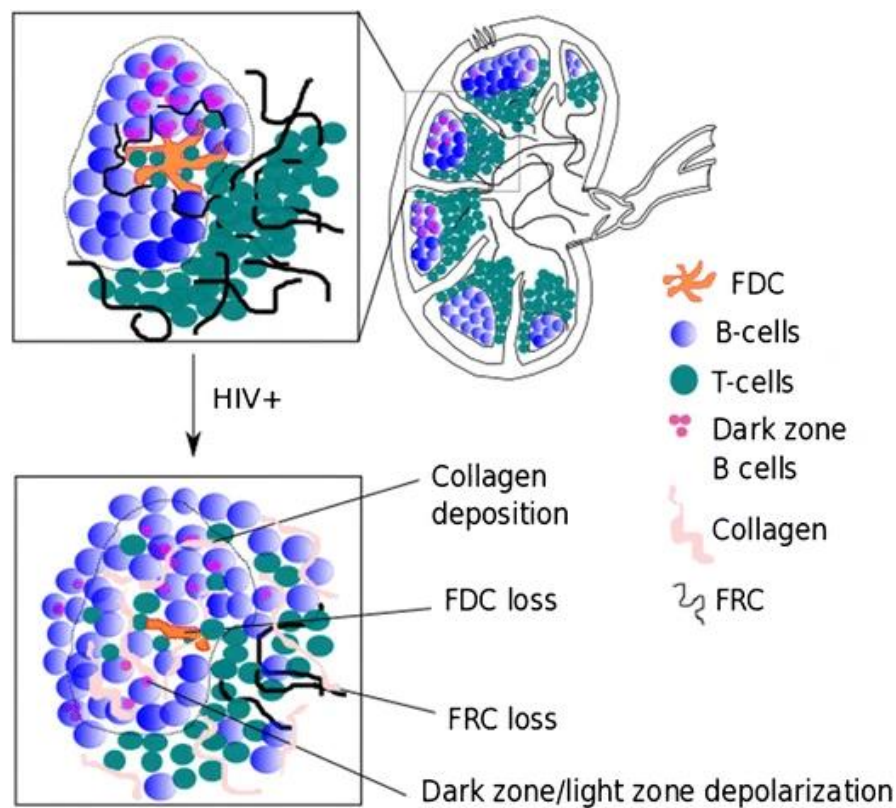


Figure 5.3: **HIV induced alterations on lymphatic tissue structure.** Diagram shows typical composition of a lymph node with stromal cell types and zones for T- and B-cells. Enlarged portion (top left) illustrates the structure of healthy lymphatic tissue. Image portion on bottom left indicates pathogenic alterations due to HIV infection.

Image Source: Dimopoulos, Y. et al., 2017. The Lymph Node in HIV Pathogenesis. *Current HIV/AIDS Reports*, 14(4), pp.133–140. Available at: <http://link.springer.com/10.1007/s11904-017-0359-7>. Reproduced by permission from Springer Nature

Unlike T-helper cells, Tregs *oppose and dampen* general immune response once activated. By reducing T-cell activation, Tregs limit the cellular immune response as well as downregulate cellular signals causing inflammation, (Yamaguchi et al., 2011). Their function has been found to be crucial in providing tolerance to certain types of antigen and in reducing systemic damage through ongoing immune activity. The role of Tregs in HIV-infection has been partly elucidated only recently, (Hasenkrug et al., 2018). Given the presence of the CD4 receptor, Tregs also constitute an HIV target, but as the total number of the CD4<sup>+</sup> T-cell population declines, the proportion of Tregs

has actually been found to increase (Nobrega et al., 2016; Presicce et al., 2011). The reason for this apparent immunity from infection, relative to other CD4+ cells, is as yet unknown (Kleinman et al., 2018).

However, Tregs become activated under HIV infection, expressing several cytokines, with both benign and malignant effects for the organism, (Chevalier and Weiss, 2013). In the former case, immune activation is in general damped down preventing damage originating from systemic inflammation due to infection while T-cell activation is reduced, limiting the number of HIV targets. Conversely, Treg activity also dampens the response of Effector cells (CD8+), reducing both their cytotoxic capacity and ability to target infected cells.

### **5.2.3 Implications for Lymphatic Tissue**

Fibrosis is the process of a pathogenic proliferation of (non-functional) connectivity tissue, mainly consisting of collagen fibres, often combined with functional impairment of the affected organ, (Wynn, 2008). In the case of lymphatic tissue, massive collagen deposition (or *collagenation*) has been observed following infection by HIV as illustrated in Figure 5.3. It is assumed that, when activated Tregs excrete tissue growth factor beta 1 (TGF- $\beta$ 1) in the vicinity of stromal cells, these start to produce collagen by elongation of existing fibres, (Fletcher et al., 2015; Theron et al., 2017). In the context of lymphatic tissue, this reaction affects the FRCn, whereby collagenation of the stromal tissues occurs gradually over time, (Maina et al., 2016; Nilsson et al., 2006; Zeng et al., 2012c, 2011).

A potentially harmful effect of this collagenation has been found to be the blocking of functional FRCs from the LT- $\beta$  of naïve CD4+ cells, (Fletcher et al., 2015), rendering them prone to apoptosis (see Figure 5.2). Tissue imaging, as illustrated in Figure 5.4 indicates a replacement of FRC-rich regions with non-functional collagen. Regeneration of this cell type is

impeded due to the collagen, which permanently reduces their number in lymphatic tissue, (Schacker et al., 2005; Zeng et al., 2012a). Experimental data suggest an ongoing ‘vicious cycle’ of CD4+ cell reduction, Treg activation, collagenation and FRC reduction during untreated HIV infection (see Figure 5.5). This ongoing process is assumed to contribute to the breakdown of the immune system, (Zeng et al., 2011), as observed in the chronic phase of infection.

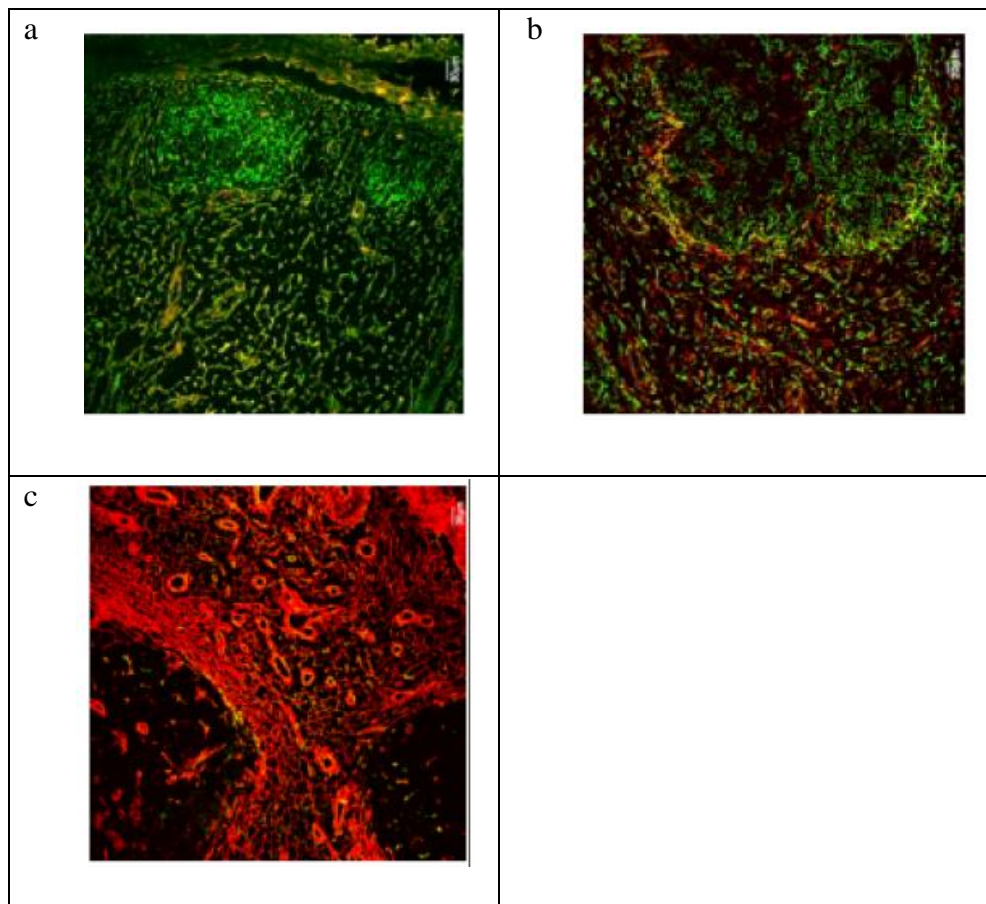


Figure 5.4: **Distinct stages of lymphatic tissue collagenation.** Imaging of lymphatic tissue for (a) uninfected, (b) early, and (c) late stages HIV infection. Green-staining denotes functional tissue, red-staining represents non-functional collagen.

Image source: Zeng, M. *et al.* (2012) ‘Lymphoid Tissue Damage in HIV-1 Infection Depletes Naïve T Cells and Limits T Cell Reconstitution after Antiretroviral Therapy’, *PLoS Pathogens*. Edited by G. Silvestri, 8(1), p. e1002437. doi: 10.1371/journal.ppat.1002437. Use permitted under the Creative Commons Attribution License CC BY (<https://creativecommons.org/licenses/by/4.0/>)

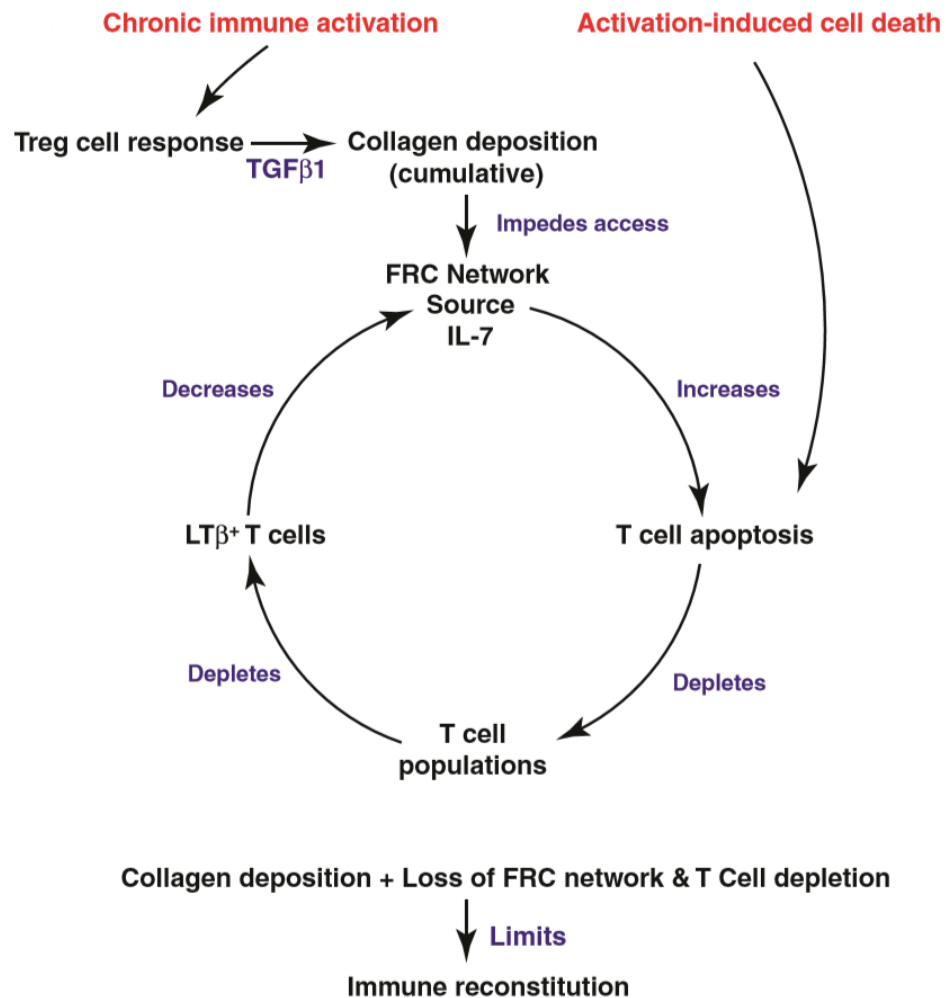


Figure 5.5: **Cycle of HIV induced collagenation and decay of T-cell.** Mechanisms associated with HIV infection (highlighted red) drive a reaction cascade leading to T-cell death and collagen deposition in lymphatic tissue.

Image source: Zeng, M., Haase, A. T. and Schacker, T. W. (2012) 'Lymphoid tissue structure and HIV-1 infection: Life or death for T cells', *Trends in Immunology*. Elsevier Ltd, 33(6), pp. 306–314. doi: 10.1016/j.it.2012.04.002. Reproduced with permission from Elsevier

## 5.2.4 Clinical Observations and Treatment

Considering varied rates of HIV infection progression, the disease experience of infected, but untreated persons can be markedly inhomogeneous, (Nilsson et al., 2006). On average, decline of the CD4<sup>+</sup> cell population takes

approximately 10 years if untreated, by which stage symptoms of immune deficiency become evident, (Fauci et al., 1996). However, cases of fast progression taking as little as 3 years have also been observed for CD4+ counts, (Maina et al., 2016), reaching levels below 200 cells / mm<sup>3</sup> blood. Conversely, cases of so called *non-progressors* or *elite-controllers* also occur, where high levels of CD4 counts are maintained over a long period, despite detectable viral loads in blood and absence of treatment, (Hunt et al., 2008). These subjects have been found to have higher numbers of effector cells in their blood, (enabling more efficient immune response), together with generally lower Treg activity, (Shaw et al., 2012). However, while some consideration has been given to Tregs suppression as a target for therapy to control infection, (Kleinman et al., 2018), this is inhibited by apparent higher incidence of inflammation-related conditions, such as cardiovascular and renal disease in elite controllers, (Hsue et al., 2009; Sanchez et al., 2015).

Further experiments, involving initiation of antiretroviral therapy, have produced evidence that the ability of FRCs to regenerate is largely dependent on the state of infection, (Zeng et al., 2012a). Conversely, collagenation does not appear to be *reversible* even after several months of treatment, (Zeng et al., 2012c). Further, while introduction of treatment leads to increase in numbers for all CD4+ cells, the Tregs proportion increases briefly prior to relatively *slow* decline, (Presicce et al., 2011). The proportion of Tregs may remain elevated for as long as 2 years after initiation, (Nobrega et al., 2016), increasing TGF- $\beta$ 1 concentrations and thus facilitating collagen formation.

Despite intensive research, quantification of Treg cell activity and the collagenation-mediated loss of FRCs under HIV infection, both with antiretroviral treatment and in its absence, remain difficult. Such quantification would be of clear benefit in investigation of Tregs as a potential target for HIV therapy, (Kleinman et al., 2018).

## 5.3 Stochastic Cellular Automata (SCA) Model

### 5.3.1 Surrounding Conditions

In the SCA model, the focus is specifically on FRC depletion and its relation to maintaining homeostasis. Comprehensive inclusion of the numerous factors connected with the depletion of immune functions under HIV, (Appay and Sauce, 2017), is not the objective here. Specifically, two effects, responsible for the depletion of CD4+ cells, (as reported by clinical studies), (Schacker et al., 2005), are considered, (i) HIV-induced direct killing of susceptible CD4+ cells and (ii) impairment of survival through depletion of FRCs and collagenation in the T-cell zone. Both factors influence the concentration of CD4+ cells in lymphatic tissue, with the time-scale of the former relatively short (days to weeks), (Cavert et al., 1997), while the latter is effective at longer timescales (months to years), (Zeng et al., 2012c). However, due to the regenerative capabilities of CD4+ cells, the first effect is reversible under antiretroviral treatment while only minimal regeneration has been observed for the second, (Zeng et al., 2012c). To be able to effectively simulate treatment interruptions, a model time step of one week is defined. This choice enables us to reproduce the clinical regimen on treatment interruption patterns and real-time adherence with appropriate time resolution while avoiding excessive computational costs, such as those for detailed cell-set-scale models (e.g. ImmSim), due to the prolonged simulation runs required.

We further assume that each cell has a connection to its four immediate neighbours, broadly in line with *in-vivo* imaging data, (Novkovic et al., 2016), and with regular topology. In terms of Cellular Automata computation, this corresponds to a *von Neumann* neighbourhood. To rule out artefacts due to edge effects, periodic boundary conditions are imposed, (Radjai and Voivret, 2013).

An average lymph node measures about 1 cm in diameter and is of approximately spherical shape. From murine experiments, it is known that the mean separation of the centres of mass of single FRCs is  $\sim 23 \mu\text{m}$ , (Novkovic et al., 2016). A human lymph node therefore consists of around 40 Million FRCs. A simplified view is acceptable in this case since it is not intended to aim at reproducing an anatomically correct representation of the organ (see e.g. (Kislitsyn et al., 2015)). My simulations are based on a smaller fraction, namely a 2-dimensional slice through a lymph node, consisting of approximately 250,000 single cells and representing less than 1% of the total volume. While clinical data provide little information on progression of collagenation over time, microscopic images, (see Figure 5.4) suggest that formation of collagen clusters occurs. I therefore assume that collagenation starts at random locations across the tissue matrix and that its increase occurs predominantly through elongation of existing collagen fibres. These assumptions give rise to the model rules described in the following.

### **5.3.2 Model Rules**

Before simulated infection occurs, the lattice is populated with both healthy FRCs and co-located CD4+ cells. In accordance to earlier research, (Graw and Regoes, 2012), it is assumed that each FRC is associated with the same number of CD4+ cells. In the initial, uninfected state, CD4+ cells are assumed to maintain equilibrium (homeostasis) as well as a stable concentration in lymphatic tissue, (Fletcher et al., 2015). However, on introducing simulated HIV infection, two effects are observed: Not only are CD4+ cells diminished directly by viral infection and mechanisms of cellular apoptosis but Treg activity is increased also, (Fletcher et al., 2015), due to preferential selection of this subset of T-cells. Though Tregs are not included in the model as separate entities, their activity is modelled by increase of tissue growth factors leading to collagenation.

As suggested by clinical observations, (Zeng et al., 2012c), the fraction of CD4+ cells, which are co-located with the collagenated tissue, tends to exhibit poorer survival than usually observed for co-location with healthy tissue. In addition, CD4+ survival is impaired by effects directly relating to viral infection of those cells. Treatment ameliorates the latter, however, which also reduces Treg activity due to reduction of viral load, (Nobrega et al., 2016). CD4+ cells and FRCs are therefore regenerated and the collagenation processes in lymphatic tissue are slowed down. Nevertheless, upon reinstatement of Treg activity (e.g. due to a treatment interruption), homeostasis is disrupted again. This gives rise to the state transition model shown in Figure 5.6, which contains the four possible combinations of CD4+ cells and collagen status as well as permitted changes. Transitions depend on stochastic parameters, which are described in Table 5.1. Transition rules are defined in the following:

**Initialisation:** The rectangular grid is seeded with collagenated cells  $C$  with probability  $hev$ , otherwise cells are assigned the healthy state  $H$ . Hence, each lattice site is occupied by either  $C$  or  $H$ .

**Rule 1:** A healthy cell  $H$  may assume a healthy collagenated state  $HC$  with probability  $treg$  for each cell with state  $C$  or  $HC$  ( $n_c$  and  $n_{hc}$  respectively) in its Moore neighbourhood. The latter considers only the 8 directly adjacent sites of the healthy cell on the rectangular grid, hence  $(n_c+n_{hc})$  may assume values from 0 to 8. Thus, the transition probability to the collagenated state represents a binomial distribution for having ‘success’ with probability  $treg$  and at least one sample of size of  $(n_c+n_{hc})$  as given by expression (5.1):

$$P_C = 1 - (1 - treg)^{(n_c + n_{hc})} \quad (5.1)$$

This collagenation resembles the activity of tissue growth hormone, normally excreted by Tregs, which have been found to be upregulated during untreated HIV infection.

**Rule 1a:** A healthy cell  $H$  may die and assume state  $D$  (representing an unoccupied site on the lymph network) with probability  $ap$  which resembles programmed cell death, (also upregulated in untreated HIV infection).

**Rule 2:** A vacant site  $D$  may become a collagenated site  $C$  with probability  $treg$  for each collagenated site ( $C$  and  $HC$ ) in its Moore neighbourhood as given by equation (5.1).

**Rule 2a:** A vacant site  $D$  may be regenerated to  $H$  with probability  $reg$  of self-regeneration of lymphatic tissue.

**Rule 3:** A  $HC$  cell may become collagenated  $C$  with probability  $cyt$ , which represents the cytotoxic effect of the collagenation (see. Figure 5.6, left).

**Rule 4:** A collagenated site  $C$  may regenerate into healthy collagenated state  $HC$  with probability  $reg$ .

Rules are applied in a synchronous manner, i.e. each site is updated at the same time. Each simulation step represents a week in real time. Model parameters are listed in Table 5.1 together with value estimates, where these could be identified from the literature. Model simulations give both an approximation of tissue destruction at the microscopic level (see Figure 5.7) as well as of immune system stability at the macroscopic level. The model can thus be used to assess effects including the way in which different levels of adherence to antiretroviral treatment impact on immune system damage.

Data from quantitative imaging analysis of lymphatic tissue, (Haase, 1999), suggest that in untreated HIV the (naïve) CD4+ cell counts are reduced to about 26% of those for the uninfected case. As mentioned above, initiation of antiretroviral treatment may also stimulate partial CD4+ cell count recovery. However, as it is reported to be less effective in tissue than in blood, (Fletcher et al., 2014), I assume only partial suppression of the viral lifecycle (and thus CD4+ depletion) under treatment in these experiments. An increase of the proportion of CD4+ cells (compared to uninfected) to about 62% at six

months after treatment initiation is suggested as realistic according to the clinical data, (Haase, 1999).

Considering these data, valid parameter estimation for the SCA model is still not trivial due to effects resulting from nonlinearities in the model. Monte Carlo methods were used therefore to ensure that parameter outcomes correspond well with available (published) data and to determine parameter sensitivity, - described in the next section.

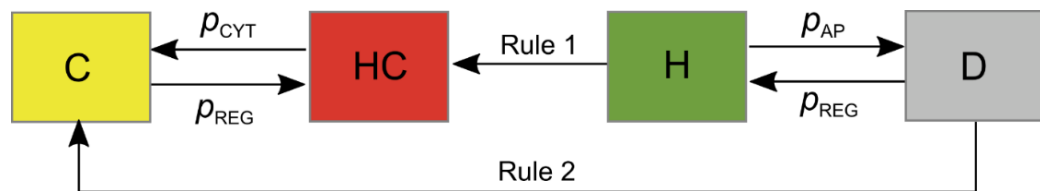


Figure 5.6: **State change diagrams of model rules.** H: healthy CD4+ cell; HC: healthy CD4+ cell co-located with collagen; D: dead CD4+ cell (empty); C: empty site co-located with collagen. Transition probabilities and rules are described in the main text.

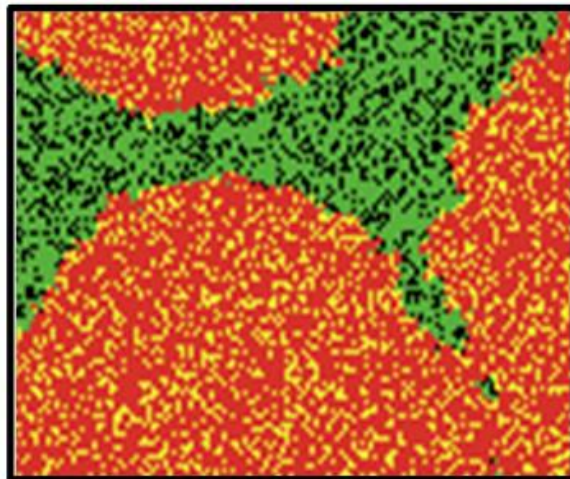


Figure 5.7: **Image of the lattice (SCA model).** Lattice configuration shows simulated lymphatic tissue in latent phase of HIV infection (300 time steps / weeks) with initially 1% of cells were collagenated. Colour coding: Green – healthy regions; Red, Orange – infected, collagenated; Black – dead cells.

Table 5.1. Model parameter value selection for CD4+ cell and collagen build-up dynamics.

Param.	Description	Value	Ref
$P_T$	Treatment effectiveness	0.0 - 0.9	(Cohen, 2011)
$P_{INF}$	Infection induced inflammation	0.06	(Zeng et al., 2012c)
$P_{REG}$	CD4+ cell / FRC regeneration	0.08	(Haase, 1999; Novkovic et al., 2016)
$P_{AP}$	CD4+ cell / FRC death through infection (apoptosis)	0.08	(Haase, 1999)
$P_{CYT}$	CD4+ cell / FRC death due to signalling (cytokines)	0.9	(Zeng et al., 2012c)

### 5.3.3 Parameter Sensitivity

To assess the model with regard both to sensitivity to parameter changes and comparison with available clinical data, distinction is made between the clinical phases of HIV infections, (Fauci et al., 1996). The SCA model is able to simulate each of these phases, as illustrated in Figure 5.8.

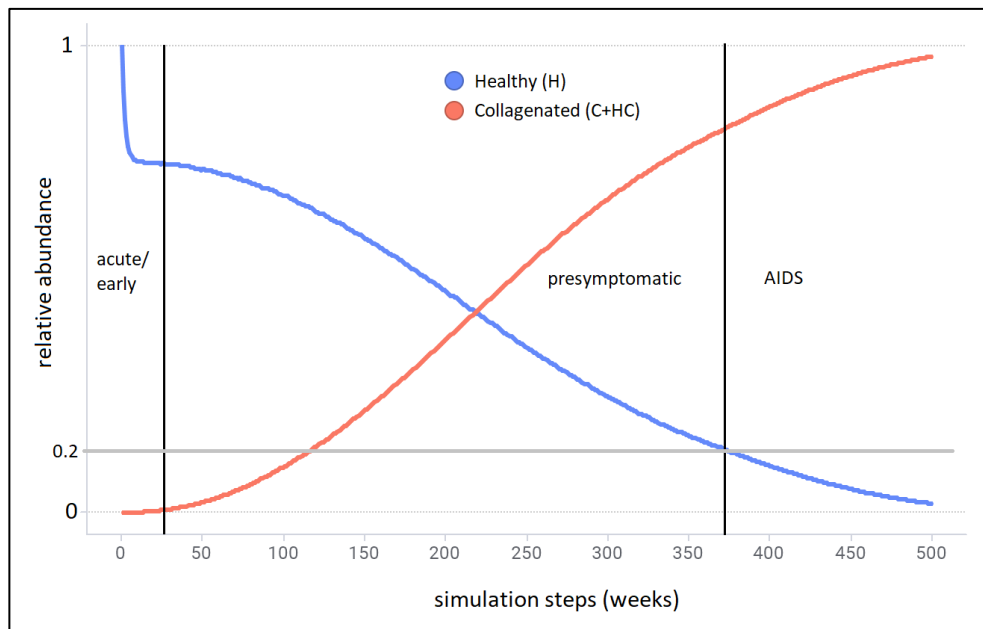


Figure 5.8: **Simulation data from SCA model showing phases of HIV infection.** Simulated data for amounts of healthy (blue) and collagenated (red) cells in a simulated fraction of lymph tissue. Acute/early phase occurs (3 to 25 weeks); pre-symptomatic phase - until proportion of healthy cells falls below 0.2 (grey line); after which the AIDS phase is entered and continues.

The Mean Squared Error, as defined in expression (5.2), is used as a simple cost function to evaluate model performance for given parameter selection.

$$J(treg, reg, cyt, ap) = \frac{1}{3} \sum_{i=1}^3 (\hat{Y}_i(treg, reg, cyt, ap) - Y_i)^2 \quad (5.2)$$

The subscript  $i$  represents the infection phases, as highlighted in Figure 5.8, where any phase is weighted equally for cost function purposes. For any of the three phases  $\hat{Y}_i$  denotes the model output for a given parameter vector  $(treg, reg, cyt, ap)$  in phase  $i$ , while  $Y_i$  signifies the corresponding clinical measure. Full factorial model design experiments were used for an initial sensitivity check to assess the impact of parameter selections on overall outcomes ( $2^5$  model runs).

**SCA(a)** A sensitivity analysis for parameter  $treg$ , (Figure 5.9) suggests a marked impact of changes of parameters  $treg$  and  $ap$  to outcomes of the cost function with the response pattern ideally requiring a more fine-grained exploration as described below.

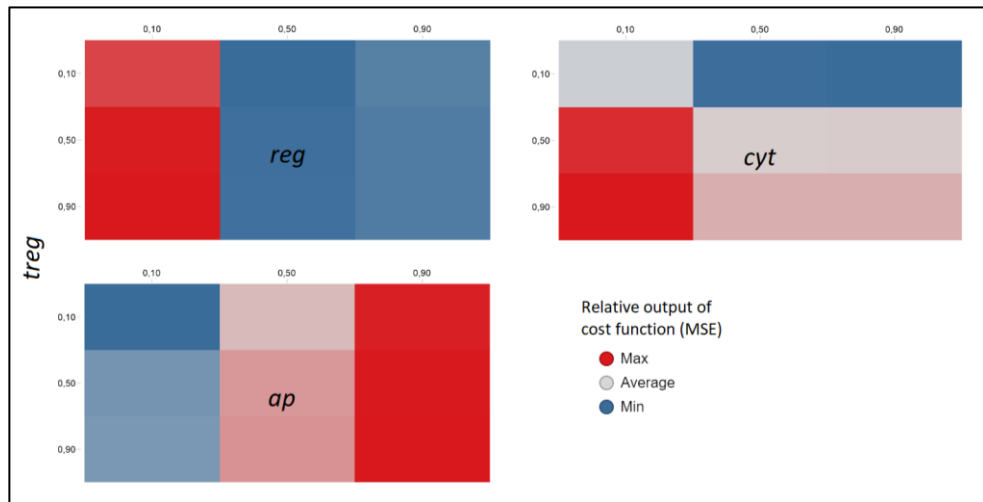


Figure 5.9: **Illustrative overview of sensitivity analysis of a selection of model parameters** *reg*, *cyt*, *ap* with *treg* (vertical axis). Color-coding represents Mean Square Error serving as a cost function. Diagram highlight complex interactions between the parameters.

Monte Carlo simulation and the Metropolis-Hastings algorithm was used to perform a local random walk on the parameter space and obtain approximate distributions of the model parameters. In the case of *treg*, *reg*, *ap* and *cyt*, a Normal distribution was assumed, which presents a reasonable choice for biological population data. However, there is some evidence that distributions of *reg* and *ap* may be skewed towards higher values, (Novkovic et al., 2016). The distribution for *hev* was chosen to be Log-Normal due to high variability of the HEV network, (Kumar et al., 2010). Simulation outputs for the sample model parameters were compared against available clinical data, (Zeng et al., 2012c). The resulting model error was used to either reject or accept the sampled parameter set, with the latter used to refine distributions for the next round of sampling. I obtained 6000 subsequent samples, each with 24 repetitions during the Metropolis Monte Carlo process, allowing for 1000 steps of burn-in to reduce dependencies on initial values. Execution took about 15 hours (wall clock time) with available computational resources. A subset of the results is displayed (Figure 5.10) where each point represents a

sample from a parameter distribution together with closeness of the corresponding simulations to clinical data.

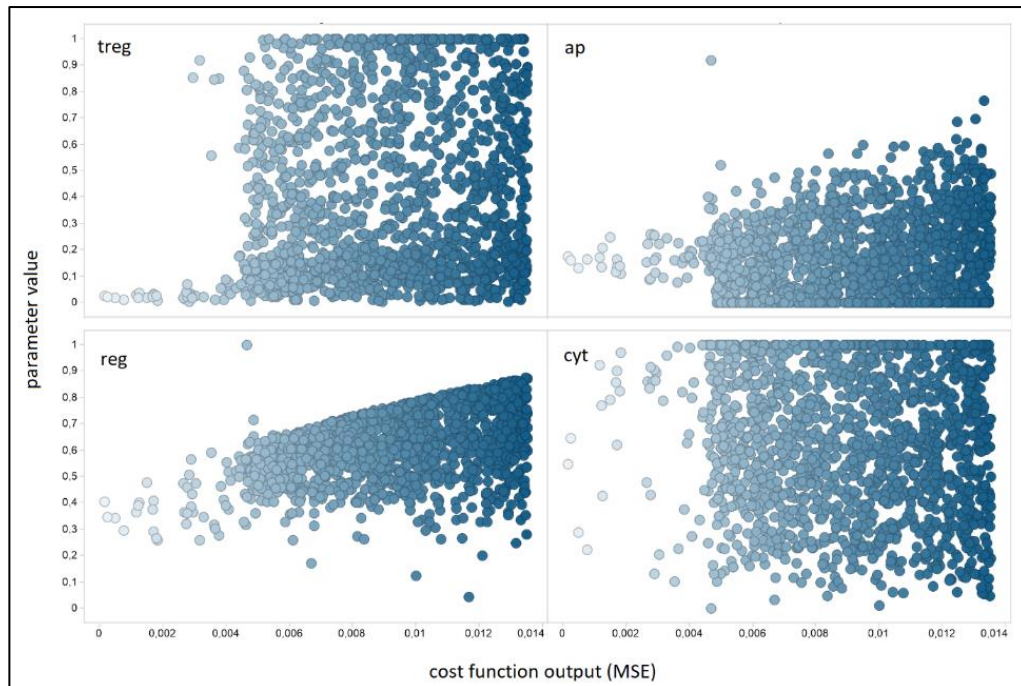


Figure 5.10: **Cost functions against proposed parameter value** (x-axis vs. y-axis). Results for *treg*, *ap*, *reg* and *cyt* (from top left to bottom right). Only the 1000 samples with lowest overall cost are shown to facilitate visualisation.

**SCA(b)** In addition, the detailed response surface for any promising parameter combination was obtained. The structure generated by the combined effects of *reg* and *ap*, as depicted in Figure 5.11 suggests a nonlinear relation with a (critical) region where the cost function changes very rapidly. With respect to estimation of optimal parameter ranges, data in Figure 5.10 suggest that best fits for *treg*, *ap* and *reg* converge within a narrow region of the parameter-space, (with values in good general agreement with indicative values as in Figure 5.8). Alternative values for the parameter *cyt*, do not appear to cause significant changes in outcome.

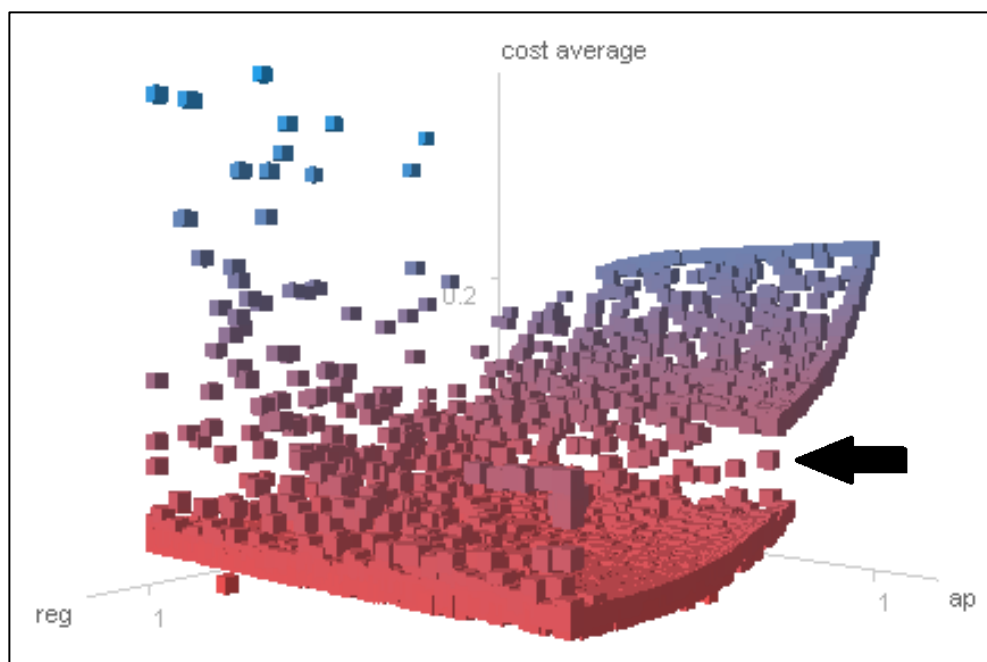


Figure 5.11: **Response surface visualisation** of reg and ap against cost function. Illustrative example shows significant distortion of surface (-see arrow) indicating possible transition (or critical) points.

## 5.4 CD4+ Motility (CM) Model

### 5.4.1 Model Overview

As with the previous model, the lattice represents a fraction of the FRCn of a lymph node, with sites in either a healthy or impaired state. Again, each site of the lattice is assumed to represent one FRC, directly connected to its  $n$  nearest neighbours. However, for this model, I take into account the *small-world topology* of the FRCn which has been suggested by analysing microscopic imaging data, (Novkovic et al., 2016). These small-world features provide (additional) connections to more distant sites, allowing for *non-local* (as opposed to neighbourhood) effects. In CA terms, these small-world properties are achieved by assigning states to a given fraction of

randomly selected sites with state changes obtained through neighbourhood-effects, (Yang and Yang, 2010).

For CD4+ motility, I adopt the assumption of a random walk suggested by microscopic data, (von Andrian and Mempel, 2003). Thus, I have a reasonable basis to assume that CD4+ cells enter the simulated lymphatic network only at *High Endothelial Venules* (HEVs), (Ager and May, 2015) and perform a random walk over simulated FRCn from these conduit sites. It is worth noting that T-cells may also enter lymph nodes via other routes (e.g. afferent lymphatics). However, the quantities of T-cells migrating through such routes in relation to HEVs are not sufficiently known. One possibility is that the process may be regarded as a baseline reduction of CD4+ cells, *independent of spatial considerations* such as those explored here for collagenation.

The assumed ‘1 week’ granularity of the model time step was chosen to better enable the assessment of both mid- and long-term-effects. These are typically occurring over weeks and years, like depletion of CD4+ cells, (Fauci et al., 1996), and collagenation (Zeng et al., 2012c), in contrast to effects directly related to viral dynamics, occurring over days, (Ho et al., 1995). Further, the present model considers the spatial effects of collagen formation and depletion of CD4+ cells. This reduction in cell numbers is due either to direct viral effects or to collagenation of the lymphatic tissue matrix where, under ART administration, the former is *reversible* but not the latter, (Zeng et al., 2012a).

To account for the marked computational cost required to track a large number of separate CD4+ cells passing through lymphatic tissue, I generate a probability distribution for a given cell being present at any lattice site. The cellular automata model was implemented in the C++ programming language with key features illustrated in Figure 5.12, with separate elements and their rationale described in more detail as follows.

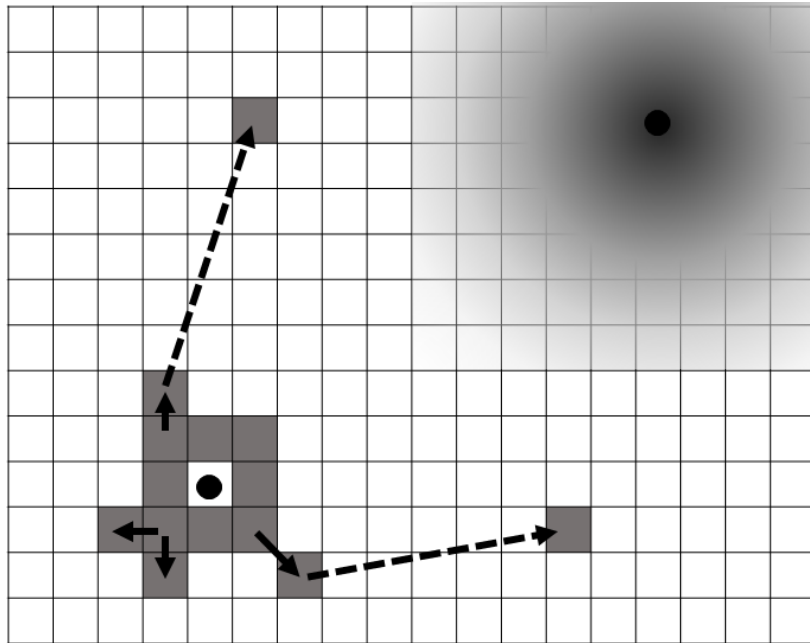


Figure 5.12: **Fundamental concepts of on-lattice collagenation model.** Left side: Solid arrows indicate neighbourhood effects. Originating from HEVs (black dots), collagen (solid grey boxes) spreads to adjacent non-collagenated / healthy sites (white boxes). Right side: Probability of CD4+ cells found present (grey shading/overlay) decreases quadratically with distance to HEVs, based on current assumptions of slow movement due to a random walk. In the event of more rapid T-cell dispersion (or influx from other sources) probabilities close to HEV regions would be relatively low, which corresponds to a more uniform distribution.

## 5.4.2 Model Setup and Rules

### Simulation Environment

A 2-dimensional square lattice with each site representing a single FRC forms the basis of all simulations. The actual FRCn occupies a 3-dimensional space in the approximately spherical lymph node. Human lymph node sizes range between 0.5 and 2 cm, (Ward et al., 2018). Diameters larger than 1.5 cm (short axis) are usually considered pathological, (Ganeshalingam and Koh, 2009; van den Brekel et al., 1998). For this study, an average diameter of ~1 cm is assumed, as for the SCA model, acknowledging that other sizes in the above-mentioned range are possible. Microscopic imaging data on the FRCn has been obtained using histological cuts of the actual organ, (Novkovic et al., 2016), offering some insight into the 3-dimensional topology of the reticular

network. Translating this data into an exact computational representation of the network structure along with different functional areas in a lymph node has been a focus of recent work, (Bocharov et al., 2015). However, to address broad questions of collagenation in the context of HIV, simplifications can reasonably reduce complexity while retaining enough information about the system. In this context, reduction of dimensions is used to address the problem in a ‘layered’ fashion and has been commonly employed in the context of investigating the spread of HIV in tissues, (González et al., 2013b; Precharattana, 2016; Strain et al., 2002). Considering clinical literature to date, a 2D representation and parameter ranges can capture qualified tissue features on which to base further hypotheses.

The mean distance between the centres of reticular cells (FRCs) has been determined to be in the range of 21 – 30 $\mu$ m, (Graw and Regoes, 2012), or of the order of 23 $\mu$ m according to recent murine experiments, (Novkovic et al., 2018). In any case, a histologic section through the whole organ would correspond to a square lattice with side length of approximately 500, again in line with the SCA model. Experimental data also suggest FRCs to be connected to 6 to 11 (median 8) other cells, (Novkovic et al., 2016). These connections either go to cells in the direct neighbourhood or to cells further away. To simulate these small-world properties in the CM model I consider the 8 nearest-neighbours (*Moore neighbourhood*) while a site might additionally be connected to a randomly-selected site with a probability  $P_S$ , (Yang and Yang, 2010). For each lattice site, I further assume one of two states:  $H$  (healthy FRC, no collagen), and  $C$  (covered by collagen, no FRC). During model initialization, all sites of the 500x500 lattice were assigned a state  $H$ , except for a random fraction  $P_{HEV}$  representing HEVs as entry points for CD4+ cells, with special state  $CH$ . The density of HEVs in the T-cell zone of a lymph node remains inconclusive and is apparently variable depending on immune system status, (Ager, 2017). Available data, however, indicate a

density of about 18 per square millimetre, (Shen et al., 2014), which translates to an estimate of  $\sim 0.01$  for  $P_{HEV}$ .

### **Tissue Collagenation Rules**

State changes (or transitions) at lattice sites follow a probabilistic set of rules, where at unit time step  $t$ , change from state  $x$  to a state  $y$  is represented by a probability  $P_{x \rightarrow y}$ ; (indices are assigned for clarity). While some transition probabilities have fixed values, others depend on the neighbourhood of a given site.

Updates are performed in discrete time steps, where each step represents  $\sim 1$  week in real-time. This choice of interval reflects the fact that collagenation occurs over years, i.e. slowly compared to other aspects of HIV infection (such as infected cell turnaround and corresponding immune response).

The model rules for collagenation spread are as follows, (designated by cell state type and mechanism).

**1. Rule  $H \rightarrow C$  (neighbourhood-driven):**

$$P_{H \rightarrow C(N)} = (1 - (1 - P_{INF})^N)$$

**2. Rule  $H \rightarrow C$  (random – small world):**

$$P_{H \rightarrow C(S)} = P_S$$

**3. Rule  $C \rightarrow H$  (regeneration)**

$$P_{C \rightarrow H} = P_R = 0$$

**Description:** Initially, collagenation is seeded by assigning state  $CH$  with probability  $P_{HEV}$  to random sites, which serve as origins of collagenation while all other sites are assigned to state  $H$ .

1. The first rule expresses the chance that a given site may become collagenated, depending on the amount of collagen already present in the neighbourhood, (as suggested by microscopic data), (Zeng et al., 2012c). The collagenation process is ascribed to factors, such as presence of Transforming

Growth Factor  $\beta 1$  (TGF- $\beta 1$ ), (Theron et al., 2017) which is commonly excreted by regulatory T-cells (Tregs). The number of these cells is high during HIV infection, possibly related to inflammation processes, (Hasenkrug et al., 2018): TGF- $\beta 1$  in the model here is taken to be a scalar represented by probability  $P_{H \rightarrow C(N)}$  which depends on the number of collagenated neighbours and is thus non-uniform. *Each* of  $N$  collagenated neighbours of a site with state  $H$  may cause collagenation of a given site with a probability  $P_{INF}$  (of inflammation) at each time step: the contribution to  $P_{H \rightarrow C(N)}$  is thus Binomial. It is assumed that  $N$  may take values from 0 to 8, (*Moore* neighbourhood).

**2.** Given the evidence of the FRCn having small-world topology, (Novkovic et al., 2016), state changes can also be ascribed to neighbourhood effects at random sites. Changes are triggered with probability dependent on the interconnection between different clusters, (Yang and Yang, 2010), where high values of interconnection lead to approximation by a random network. A cut-off distance for this random inclusion of sites, which might offer greater realism, does not apply here to keep the model simple. For random collagenation, therefore, the CA model mimics this process by introducing an alternative rule for  $H \rightarrow C$ , where a site selected at random assumes state,  $C$ , with a probability  $P_S$ . This rule is applied at each iteration in addition to rule 1 and leads to an accumulation of collagen at random sites (in addition to local accumulation). However, use of this rule is confined to preliminary experiments (see results) to determine an estimate for  $P_S$  while considering only the special case of  $P_S = 0$  for subsequent experiments to emphasize *local collagenation*.

**3.** Finally, I note that, while some clinical data do provide evidence of a small, albeit significant, FRC regeneration once antiretroviral treatment is initiated, (Zeng et al., 2012c), the strong general evidence is that collagenation is irreversible. Regeneration is thus assigned a probability of zero in these preliminary numerical experiments.

### **T-Cell Degradation Rules**

Collagenation progression is slow compared to traversal of CD4+ cells through the FRCn; a discrete probability is thus associated with random occupation of a given lattice site by a cell at each time step. Cell movement can be taken as random from entry points, as suggested by earlier modelling studies (Donovan and Lythe, 2012). Thus, the average distance of a cell from its entry point increases in a linear manner with the square root of time elapsed. Conversely, the distances of a large number of cells from their point of entry are assumed to follow a 2-dimensional Normal Distribution with discrete steps around the location of the HEVs as the mean. The Standard Deviation can then be validated from clinical data: Assuming an average cell movement time of 10 hours within a lymph node and a diffusivity of  $60 \mu\text{m}^2 / \text{minute}$ , (Ganusov and Auerbach, 2014), with average path length of  $23 \mu\text{m}$ , (Novkovic et al., 2016), a Standard Deviation of  $\sim 8.5$  lattice sites from HEV locations is indicated. The resulting distributions ( $P_1 \dots P_n$ ) describe the probability of a lymphocyte being present around each of the  $n$  HEVs in the model. Conflating these  $n$  distributions yields the overall probability distribution  $P(L)$  of presence of a lymphocyte for any lattice location. The heat map in Figure 5.13 illustrates this spatially heterogeneous probability.

We further state that an individual CD4 cell has a probability  $P(AP/L)$  of undergoing apoptosis when close to a collagenated site. A link between terminal tissue fibrosis and AIDS disease has been suggested, where AIDS is associated with an approximate reduction of 80% or more of CD4+ cells from baseline, (Fauci et al., 1996). This means that when collagenation spans the whole T-cell zone, like it is the case in the terminal phase of infection, CD4+ cells are reduced to about 20% of the amount found in a healthy state. In consequence, an approximate value of 0.8 is initially chosen for  $P(AP/L)$ . Due

to patient-specific variations of the amount of CD4+ cell decline until AIDS emerges, other values within the range (0.7, 1.0) are also possible.

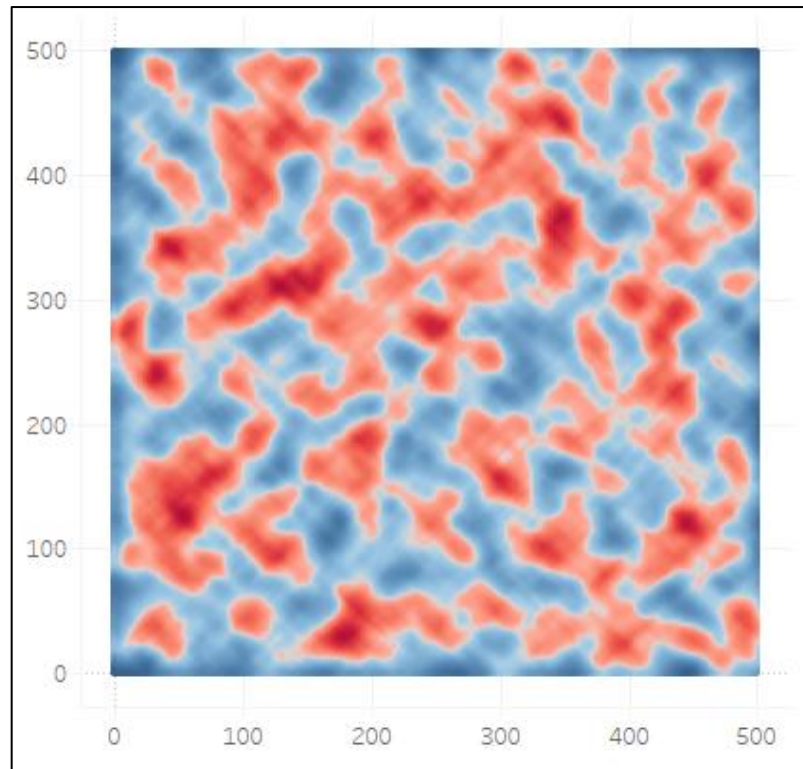


Figure 5.13: A (500 x 500) lattice section for lymphatic tissue showing spatially heterogeneous probabilities of CD4+ cell presence. Regions around HEVs (conduit entries for CD4+ cell movements; red) are associated with high probabilities, compared to non-HEV areas (blue).

Bayes Theorem is employed, (given in general form, expression (4.1),) and rearranged for  $P(y)$ , where the latter relates to the overall probability distribution  $P(AP)$  (apoptosis of a CD4+ cell at any lattice site). Since apoptosis may only occur for a site with Lymphocytes present,  $P(\theta/y)$  (relating to  $P(L/AP)$ ) in the denominator becomes unity, hence,  $P(AP)$  is calculated by the simple product of  $P(AP/L)$  and  $P(L)$  ( $P(y/\theta)$  and  $P(\theta)$ ) The resulting spatially dependent probability distribution for apoptosis is computed for every time step.

### 5.4.3 Parameter Estimates

Parameter estimates, as described above, are summarized in Table 5.2, with clinical data sources cited. Obtaining estimates for  $P_{INF}$  and  $P_S$  which control collagenation progression in the model is challenging due to the difficulty of obtaining lymph tissue samples over the time course of HIV infection. A pool of patients was studied, (Zeng et al., 2012c), with individuals assigned to one of three disease stages of HIV infection, (healthy, pre-symptomatic, AIDS), based on their CD4+ counts. The patients who did not receive antiretroviral treatment prior to the study were subject to lymph node biopsies, where analysis gave rise to quantification of FRCn and collagen. The procedure was repeated some months after patients started Antiretroviral Therapy. A remarkable result was that collagen accumulation remained constant after months of treatment, while FRCn levels recovered to a certain degree. These classifications provide coarse guidance on progression of collagenation with time, but since the asymptomatic phase of HIV infection can last for 10 years, granularity is low.

Table 5.2: Parameter estimates for the spatial CA Tissue Model (from the literature).

Parameter	Parameter value (range)	Source
$P_{HEV}$	0.01 (0.006; 0.016)	(Shen et al., 2014)
$P_R$	0 (-6.3E-3; 7.7E-03)	(Zeng et al., 2012c)
$P(L)$	$N \sim 0, 8.5$	(Ganusov and Auerbach, 2014)
$P(AP/L)$	0.8 (1.0; 0.65)	(Fauci et al., 1996)
Lattice side length	$500 \pm (250; 1000)$	(Novkovic et al., 2018)
Neighbourhood	8 (7.91; 8.558)	(Novkovic et al., 2016)

However, the amount of collagenation over a period of time has been found to be inversely correlated with CD4+ cell count in lymphatic tissue, (Estes, 2013), similar to findings for blood. In consequence, I utilize clinical data on progression of CD4+ counts in blood (Fauci et al., 1996), where these show linear decline. Assuming a similar relation for lymphatic tissue in this model, a decrease of 0.19% of baseline CD4+ cells per week is assumed when

no treatment is applied. As stated in section 5.2.4, this value is based on a population average of ~10 years from infection until AIDS symptoms emerge (in absence of treatment). Extreme cases e.g. with a period as short as 3 years to AIDS symptoms ('fast progressors') has been observed, (Ruffault et al., 1995), ranging to decades without visual depletion ('elite controllers'). It should be noted, however, that such cases (specifically the latter) are extremely rare. A more detailed exploration of these extreme values must motivate future sensitivity analysis.

#### 5.4.4 Simulation Setup

Our primary aim is to assess the contribution of spatial effects on the overall decrease of CD4+ cells through lymph tissue collagenation and the related FRC loss. In this context, it is interesting to observe differences in the overall result if spatial effects are cancelled out, i.e. if collagenation is allowed to take place exclusively due to random effects. In the latter case, only random collagen growth is permitted i.e. lattice cells may change their state from  $H$  to  $C$  with a fixed probability  $P_{rand}$  at each time step (termed 'random model' in the following). To determine spatial contribution, an amount of collagen in the context of apoptosis risk (used as a measure for CD4+ survival), is assigned by implementing computer simulations for the two models (spatial / random model), highlighted above.

In this context, specific parameter estimates ( $P_{INF}$ ,  $P_S$ ,  $P_{rand}$ ) cannot be obtained directly from the literature, so required implementation of an inverse Monte Carlo approach, (McGreevy, 2001). This enabled exploration of the parameter spaces of the respective models (the 'spatial' or localized/small world and random versions). Repeated sampling is used to find *candidate parameter combinations* which are scored on the basis of closeness of the simulated CD4+ apoptosis rates to CD4+ decline rates from clinical data, using a Root Mean Square Error (RMSE) measure. CD4+ cell loss shows

great patient-specific variability with AIDS symptoms emerging from three years to decades post infection, (e.g. (Okoye and Picker, 2013)). For this study, I use a population average obtained, (Fauci et al., 1996; Greenough et al., 1999), indicating a constant CD4+ cell loss of 0.19% per week from baseline (zero order). Depending on the score change at each iteration the candidate parameter refinement is either accepted (and used as the new basis for sampling) or rejected, while employing a typical M-H algorithm to avoid local minima.

Finally, in order to show the contribution of spatial heterogeneity to CD4+ count decrease during antiretroviral treatment interruptions, treatment initiation was mimicked by effectively stopping simulated collagenation (setting respective probabilities to zero) at different simulated infection stages, then subsequently interrupted for fixed time periods of treatment.

### 5.4.5 Simulation Results

From the simulations with the CM model, the following results were obtained:

**CM(a)** For calibration of the spatial model 5000 inverse Monte Carlo steps were performed in total, with different starting values for  $P_{INF}$  and  $P_S$  chosen at random every 1000 steps. Figure 5.14 shows results for a subset of the generated data, namely the 1000 points with near-optimal scores, where candidate values of the parameter describing neighbourhood effects  $P_{INF}$  are plotted against their score function (RMS). The curve indicates a minimum RMS around values of  $P_{INF}$  between 0.0015 and 0.0045 depending on the setting of the ‘small world’ parameter  $P_S$  chosen. I found  $P_{INF}$  and  $P_S$  to be correlated in a power law fashion as suggested, (Yang and Yang, 2010), with  $P_{INF} = 0.0021 * P_S^{-0.195}$  in this case. While linking these directly to clinical outcome is tentative, however, due to insufficient data about the degree of small world in lymph tissue, the potential for refinement is clear. Given the availability of more detailed data, it should be possible to narrow down the range of possible values for  $P_{INF}$  and  $P_S$ , which would in turn provide a more exact representation of FRCn structure in the CA model with corresponding improved viability of simulation outcomes. As noted above, I assume the special case of  $P_S$  to be zero for subsequent spatial model simulations since my emphasis is on local collagenation patterns. The random model with one parameter was calibrated using 1000 Monte Carlo steps, where a clearly defined minimum in terms of RMSE could be identified at  $P_{rand} \sim \updownarrow 0.0035$  (see Figure 5.15).

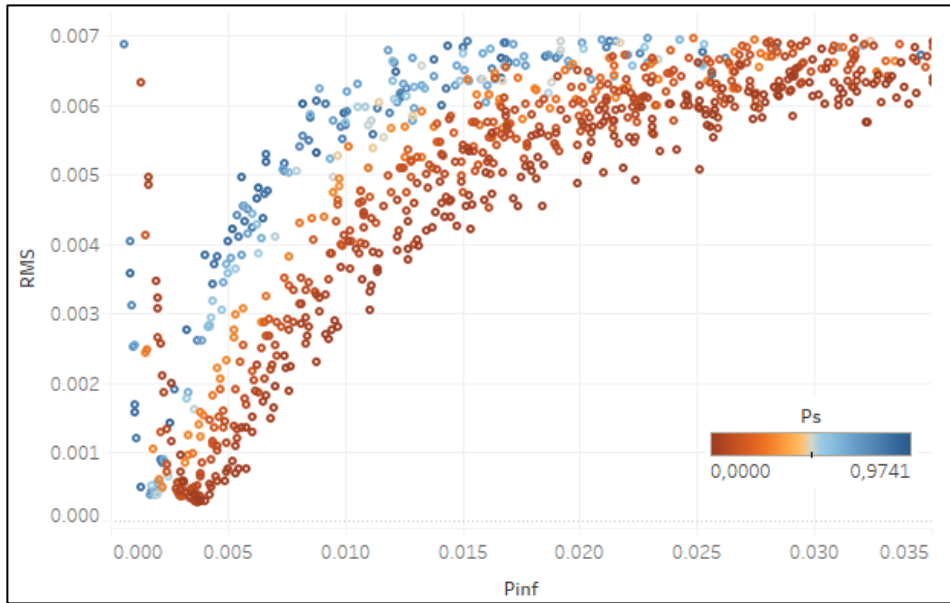


Figure 5.14: **Result of 1000 inverse MC steps for the spatial model.** The X-axis denotes possible values for spatial collageneration parameter  $P_{INF}$  while the Y-axis corresponds to RMSE w.r.t. clinical data match. Marker colouring indicates value of corresponding 'small world' parameter  $P_s$ .

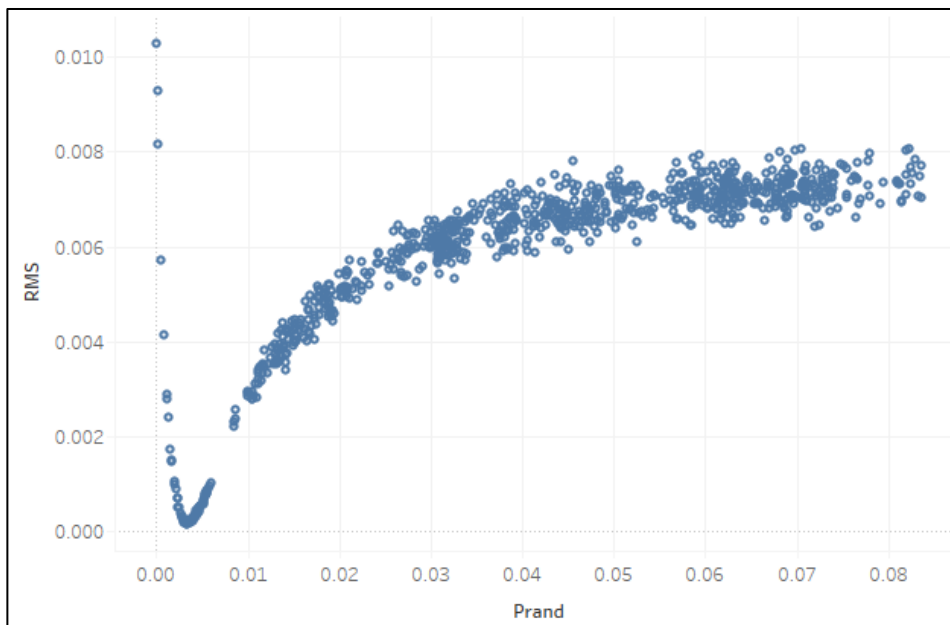


Figure 5.15: **Result of 1000 inverse MC steps for the random model.** The X-axis denotes possible values for random collageneration parameter  $P_{rand}$  while the Y-axis corresponds to RMSE w.r.t. clinical data match. Minimum RMSE value is obtained for  $P_{rand} \sim 0.0035$ .

**CM(b)** To account for the heterogeneous progression rates of untreated HIV infection observed in clinical practice, I varied the CD4+ decline rates used for model calibration, using known extreme values in both directions. Hence, to account for *fast progressors* I used a decline rate twice as high as the average case. Conversely, I used a decline rate half the normal rate to account for *long term (non-) progressors*. Estimated data for  $P_{INF}$  and  $P_{rand}$  obtained by inverse MC simulations for a range of progression speeds are presented in Table 5.3. Such a sensitivity analysis is useful to test model robustness and to determine valid parameter ranges. Results indicate clearly defined parameter ranges for  $P_{INF}$  and  $P_{rand}$ ; however, for steeper slopes of CD4+ decline (as for fast progressors) the range of possible parameter values is wider, (i.e. is less precise). Also, both parameters appear to change proportionally with progression speed. Doubling or halving progression speed is reflected in similar proportional changes in  $P_{INF}$ , while the factor for  $P_{rand}$  is around three.

Table 5.3: Estimates for  $P_{inf}$  and  $P_{rand}$  obtained by inverse MC simulations in relation to different infection progression speeds. Values denote averages and standard deviations of the 50 lowest scoring MC samples.

Parameter	Infection progression (years until CD4+ depletion)		
	<i>Fast (5 years)</i>	<i>Average (10 years)</i>	<i>Slow (20 years)</i>
$P_{INF}$	0.0093 (0.0011)	0.0042 (0.0028)	0.0024 (0.00024)
$P_{rand}$	0.011 (0.0027)	0.0035 (0.00070)	0.0012 (0.00028)

The different dynamics for the random and spatial model are illustrated in Figure 5.16. Both panels show collagenation patterns for 100 time steps (~2 years) after simulated infection for a similar degree of CD4+ apoptosis. For the spatial model (Figure 5.16 a) it is clear that collagen is concentrated in *specific regions* (coloured red), predominantly around HEVs where CD4+ cells have a high probability of being present, whereas for the random model (Figure 5.16 b), collagen is more diffused (coloured blue) over the simulated tissue. The consequences of those differences in collagen clustering on CD4+

apoptosis are illustrated in Figure 5.17. The ratio of the total reduction of CD4+ cells due to collagenation to total collagen accumulation is defined here as ‘relative apoptosis’.

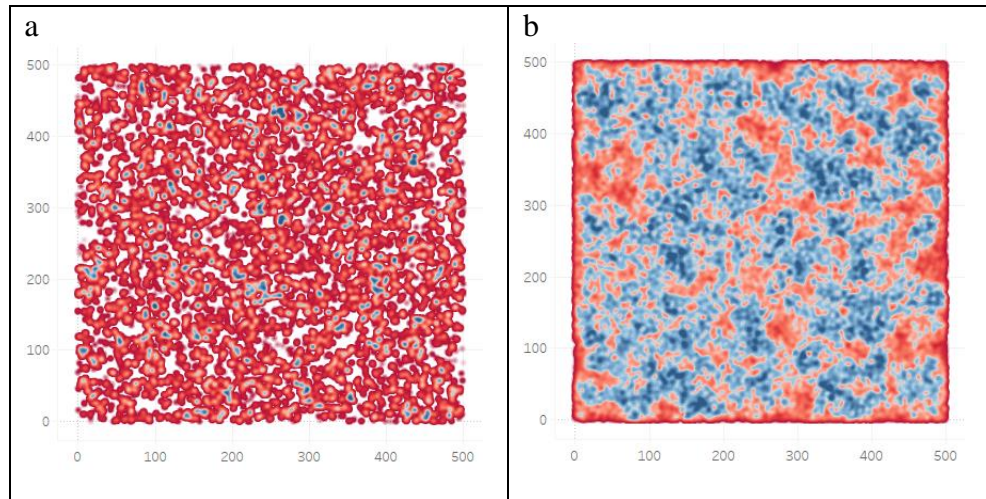


Figure 5.16: **Lattice snapshots of simulated collagen localisation** for spatial model (a) and random model (b), at simulation time step 100 (equivalent to ~2 years). Collagenation forms more distinct clusters (a) compared to (b). Colors indicate simulated collagen density (red – high; blue – low; white - none).

**CM(c)** Since collagen formation starts at sites with high CD4+ throughput (HEVs) for the spatial model (Figure 5.17 a), relative apoptosis starts high but reaches a plateau over time as collagenation spreads to regions with fewer CD4+ cells. In contrast, relative apoptosis remains constant for the random model since collagen appears at random locations, irrespective of CD4+ cell occupation. Thus, for total collagen percentage over time, as shown in Figure 5.17 b, curve shapes are markedly different. Despite constant decay of CD4+ cells (zero order), neither curve is linear, suggesting that exact mechanisms of collagen formation patterns are yet to be completely identified. Nevertheless, these results clearly show that both spatial and random models agree with clinical data in terms of showing CD4+ count decline. However, different predictions for the ratio of total CD4+ reduction and collagenated

areas (relative apoptosis) are obtained, since collagenation is more marked in the spatial model. The fact that both models do not give the same results concerning collagen accumulation and CD4+ decline, may provide a link for clinical research in assessing the impact of spatial collagenation patterns in greater detail.

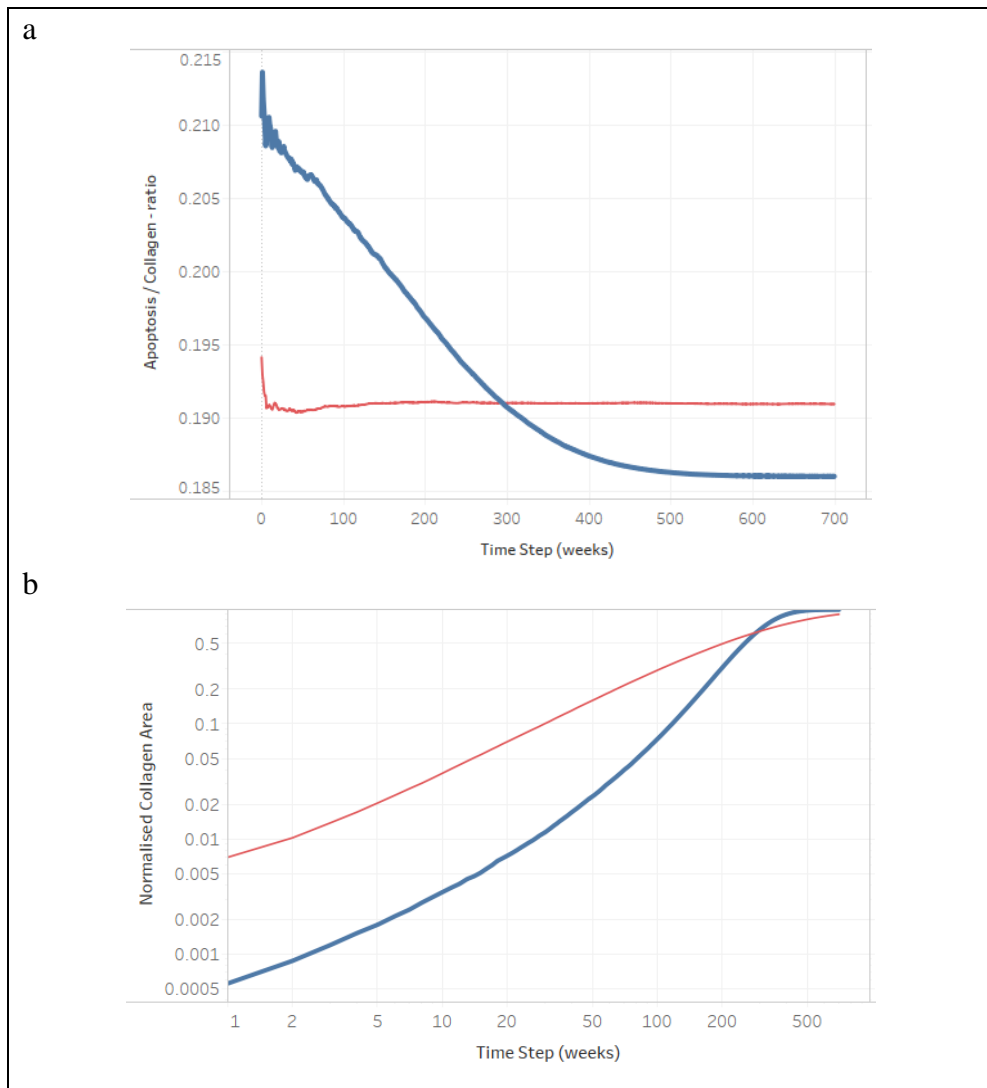


Figure 5.17: **Apoptosis rates per collagenated area (a) and log-log plot of profiles of collagen growth over time (b)** for the spatial model (thick blue line) and random model (thin red line). Y axis denotes ratio between the total reduction of CD4+ cells due to collagenation and total collagen accumulation. (Parameters. spatial model:  $P_{INF} = 0.035$ ,  $P_S = 0$ ; random model:  $P_{rand} = 0.0035$ , Y-scale in (a) truncated for visibility).

## 5.5 Implementation Performance

### 5.5.1 Parallelisation Performance

Details of the computing platform used are given in Table 5.4, with processing power divided between 96 single processors (cores). To capitalise on its power, multi-threading is attained in various ways, depending on the programming language used and the underlying programming model, (Diaz et al., 2012).

Table 5.4: Specifications of the set up used for experiments with the SCA model.

<b>Server hardware</b>	2 x 12 core 2.4 GHz Intel Ivy Bridge processors, 64 GB RAM, FDR InfiniBand network adaptor
<b>Nodes</b>	4
<b>Total TFlops</b>	1.75

Here, for code developed in C++, the implementation employed the Message Passing Interface, (OpenMP / MPI) (MPI Forum, 2019; Open MPI Project, 2020). A hybrid MPI-OpenMP approach was used to combine distributed memory parallelisation and shared memory parallelisation between and within computational nodes respectively, (Rabenseifner et al., 2009). The OpenMP library, (OpenMP Architecture Review Board, 2019), was chosen for parallelisation *within* a simulation run by dividing up the lattice into evenly-sized fragments (*spatial* parallelisation), with MPI, (MPICH Collaborators, 2019), chosen for parallelisation *between* simulation runs (*time* parallelisation), (Hecquet et al., 2007). A first step in balancing these approaches consisted of finding the optimal setup for spatial parallelisation. Intuitively, while a high number of spatial fragments is advisable in this context, the more frequent communication and synchronisation of threads outweighs the advantages.

Thus, an analysis of relative run times for different OpenMP setups (see Figure 5.18) indicates a minimum run time for the lattice divided into 6 parts, but gains in performance diminish for higher number of spatial segments due to communication demand between threads. Since a setting of 4 parts performed almost as well, it was adopted for subsequent experiments with remaining threads used for time parallelisation.

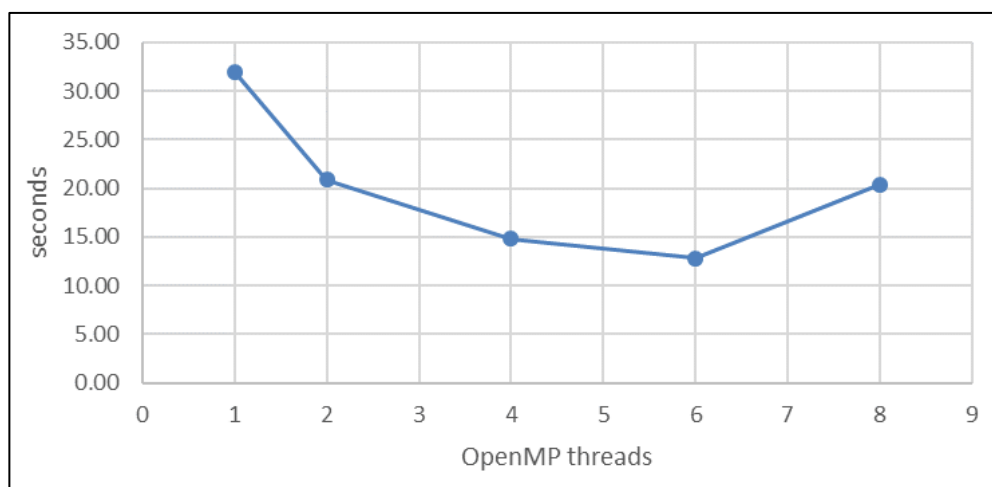


Figure 5.18: **Comparison of run times.** Diagram shows averages of 24 parallel runs with different degrees of spatial parallelisation for 700 simulation steps with a 500 x 500 lattice.

## 5.5.2 Lattice Size

In initial experiments, (Hillmann et al., 2017b), a lattice size of 500×500 was chosen to represent a small section of a lymphatic organ, specifically a ‘cellular layer’ of a cross-section of the lymph node, (Kislitsyn et al., 2015). To estimate the number of experimental repeats needed for reliable statistical inference, I investigated the effect of lattice size on *between-run* variation. Results for different sizes (Figure 5.19) indicate that variations are small irrespective of lattice size until simulation times of around 450 steps. Subsequently, larger lattice size runs showed markedly lower variance. Since the main interest was in the disease phase up to 540 steps (representing a real-

time span of around 10 years), the lattice dimension (tissue cellular-layer cross-section) of 500 was retained and achieved good precision.

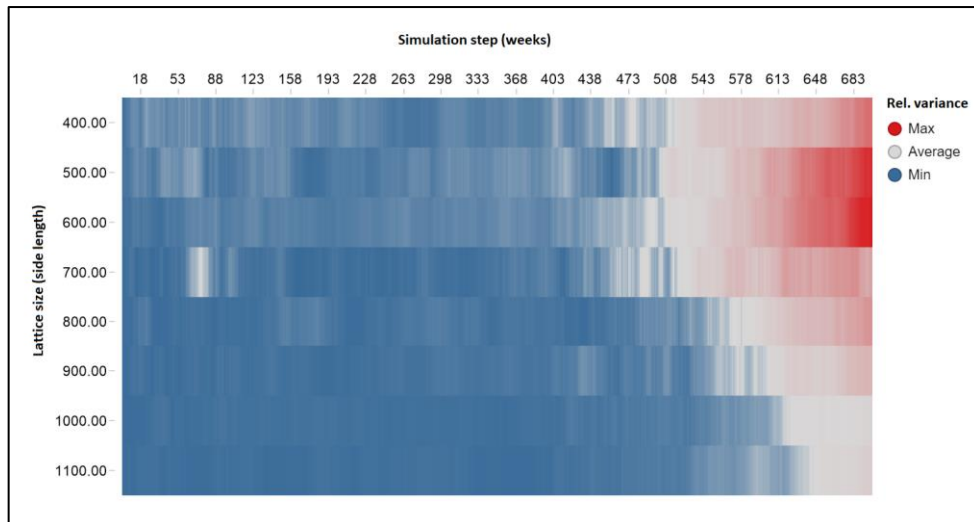


Figure 5.19: **Influence of square lattice size on inter-run variance** (250 runs respectively with 700 simulation steps each) by simulation step. Variance increase (red colour) occurs towards end of simulations due to incremental stochastic error (less pronounced for larger sizes). Overall variance is low for sample size chosen.

## 5.6 Summary

We have developed models to investigate effects of treatment interruptions on lymphatic tissue. To account for lymphatic tissue collagenation I constructed a novel Stochastic Cellular Automata model, in which principal mechanisms were obtained from recent clinical findings. Parameters were assessed for sensitivity, where I discovered a complex response surface with defined transition areas as in SCA(a,b). Furthermore, the model was adapted with the aim of exploring the impact of CD4+ motility (CM model). Using this model, I explored the influences of random collagen spread (as opposed to spatial spread). In the next chapter these findings are used to explore how collagenation and progression are impacted by treatment interruptions.

# 6 Effects of Treatment Interruptions on Lymphatic Tissue Structure

## 6.1 Introduction

In seeking to evaluate the impact of treatment interruptions I refer to past clinical findings and simulate designs of unstructured and structured treatment interruptions with the SCA model. The CM model of the previous chapter is also used to address different aspects of spatial infection progression, such as the impact of clusters of collagen, augmenting our recent article, (Hillmann et al., 2020).

## 6.2 Clinical Studies

Most clinical trials for *structured* treatment interruptions were conducted in the late 1990s and early 2000s. Major trials together with their designs are listed in Appendix E. The largest clinical trial on STIs, the SMART study, (Siegel and El-Sadr, 2006), represents the main source of knowledge on the effects of treatment interruption to date. The study was of type ‘CD4+ guided’, i.e. when the CD4+ count in blood for a patient falls below a certain limit, treatment is reintroduced and subsequently interrupted if the count exceeds an upper boundary, (Benson, 2006). However, data from this trial showed an increase of serious events such as opportunistic disease and effects not generally associated with HIV, such as cardiovascular risk or cancer. These events tended to emerge months or years after initialisation of treatment interruption, indicating the possible long-term downstream consequences of such actions, (Silverberg et al., 2007). As a result of these findings, a general ban on interrupted treatment has been advocated by some researchers, but the design of the SMART study has been subject to criticism also, (Hirschel and Flanigan, 2009). In particular, threshold values of CD4

cell concentrations, chosen for interruption and re-initiation of therapy (250 and 350 cells/ $\mu$ l), are considered to be too low by current guidelines, (WHO, 2013), which recommend at least 500 cells/ $\mu$ l (see Section 2.3). In addition, the study did not consider participants' prior immune system status. Serious HIV/AIDS opportunistic disease events are associated with low CD4 counts and high viral load, indicating that a weakened immune system may contribute to harmful outcomes of treatment interruption, (El-Sadr et al., 2006). A similar study, LOTTI, (Maggiolo et al., 2009), conducted around the same time as SMART used slightly higher ranges of CD4+ counts for treatment removal and re-initiation. It did not, however, report a rise of adverse events for patients with treatment interruptions. In contrast, harmful effects associated with drug toxicities, were significantly lower under STI. A comparison of the two study setups is given in Appendix F. Also, several newer studies involving patients at early stage HIV, with immune function predominantly unimpaired, showed *no adverse effects* to (short-term) interruptions, (Goujard et al., 2012; Grijsen et al., 2014).

*Unstructured* treatment interruptions, on the other hand, where the main cause is lack of adherence, have been associated with formation of drug resistance mutations, necessitating regimen switching, (Glass and Cavassini, 2014). However, increasing viral levels despite treatment (i.e. virologic failure), often observed for the drug class of protease inhibitors (PI) is not completely understood, (Rabi et al., 2013).

In summary, treatment interruptions have been commonly associated with treatment failure and possibility of drug resistant mutations. The mechanisms underlying these relations, such as involvement of immune system damage, however, have been partially investigated only to date, (Hammer et al., 1997). Increased knowledge of these mechanisms may help in exploiting potential benefits of treatment interruptions, preventing adverse side effects and promoting drug sparing.

## 6.3 Treatment Simulation

### 6.3.1 SCA Model Setup

With the parameterisation specified for the SCA model, the aim was to test the long-term effect of different patterns of *unstructured* interrupted treatment on collagenation (and thus immune system degradation). To simulate interrupted treatment, ‘average’ adherence was assumed: (the probability that the simulated patient takes the medication regularly each week), (Glass and Cavassini, 2014). Further, the effect of *treatment initiation timing* was assessed, where clinical studies have indicated possible impact on long-term progression, (Lundgren et al., 2015). Table 6.1 summarizes parameter values chosen for the simulation runs. After the treatment period (corresponding to ~ 5 years), increase in collagenation, compared to that at treatment initialization, is determined.

Table 6.1: Simulation parameters for treatment interruptions using the SCA model.

	<b>Value range</b>
<b>Time step</b>	1 week
<b>Treatment initiation</b>	0, 50, 100, 150, 200 timesteps
<b>Treatment adherence</b>	0%, 20%, 40%, 60%, 80% 100%
<b>Treatment period duration</b>	250 timesteps
<b>Total simulation length</b>	500 timesteps (~ 10 years)

Additionally, the effects of *structured* treatment interruptions are investigated, with an illustrative example of a *fixed-cycle* approach shown in Figure 6.1. However, in the following I am adopting the *CD4+ guidance* approach, pursued in multiple clinical trials, (Benson, 2006). This uses a threshold value of CD4+ cell count in a patient as a *surrogate marker* to decide on interruption or initiation of antiretroviral treatment. Limits obtained in two previously mentioned CD4+ guided clinical studies, SMART, (El-Sadr et al., 2006) and LOTTI, (Maggiolo et al., 2009), were used for the SCA

model, where these reported highly diverse outcomes despite their similar structure. Due to practical reasons, follow-up for each patient was restricted on average to 48 months (SMART) and 50 months (LOTTI). In order to attempt an explanation for the clear lack of agreement, the SCA model was used to investigate the effects of the respective interruption thresholds for prolonged periods of simulation, with outcomes observed after 500 model timesteps (equivalent to weeks).

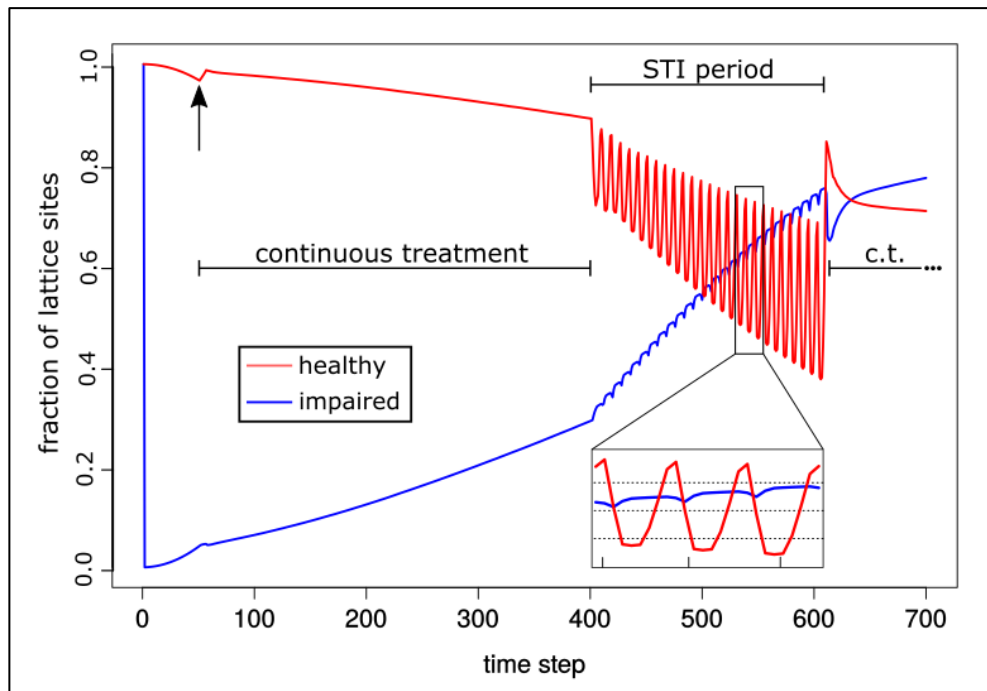


Figure 6.1: **Effect of a structured treatment interruption period on model behaviour.** Continuous treatment initiated at time step 50 (arrow). Start of STI period (fixed cycle – 4 weeks on 4 weeks off) from step 400 to 600, followed by resumption of continuous treatment (c.t.). Enlarged portion of the graph shows the patterns of healthy cell decline, and damage spread in more detail.

Transition probabilities for Rules 1 and 2 ( $H$  to  $HC$  and  $D$  to  $C$ ) also depend on the number of collagenated 4 directly adjacent neighbouring sites  $N$  (according to *von Neumann* definition) and the cumulative binomial probabilities calculated using the expression:

$$(1 - P_T) \left( 1 - (1 - P_{INF})^N \right) \quad (6.1)$$

In a similar manner, ART is assumed to limit the effects of CD4+ apoptosis, calculated according to the expression:

$$(1 - P_T) P_{AP} \quad (6.2)$$

In both expressions, parameter  $P_T$  denotes effectiveness of ART, limiting both the spread of collagenated regions and elimination of CD4+ cells. ART has found to be less effective in lymphatic tissues than in blood, (Fletcher et al., 2014), which is reflected by parameter choices (see Table 5.1).

To investigate treatment, interrupted in an *unstructured* way, ART is assumed administered with fixed probability during the week, (i.e. an *adherence* measure). Non-administration of ART (*non-adherence*) is simulated by setting the probability of the drug being effective ( $P_T$ ) to zero for the duration of the time step. This simplified notion follows the definition of ‘taking adherence’, in clinical settings (Glass et al., 2010).

To explore the importance of a patient’s underlying immune status, (Hirschel and Flanigan, 2009), and its influence on outcomes, I use the SCA model to simulate different levels of prior *immune damage* and assess their influence on CD4+ counts when applying different patterns of treatment interruptions.

### 6.3.2 Unstructured Interruptions

An example model run is depicted in Figure 6.2, illustrating the effects of *unstructured* treatment interruptions (e.g. due to incomplete adherence) on levels of collagen and CD4+ counts. I simulate these by randomly missing out a week of treatment using Bernoulli probability. Clearly, this is a preliminary check, as adherence has been found to be a dynamic process, with patterns changing over time, (Glass et al., 2010).

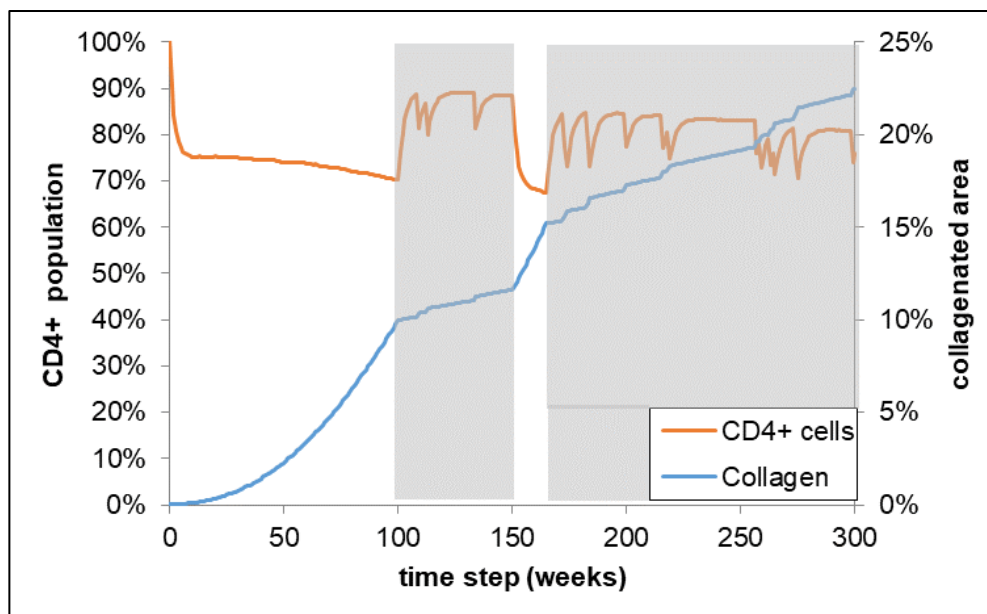


Figure 6.2: **Dependency of collagenation and CD4+ concentration.** Collagenation (blue line) and population of CD4+ cells (red line), grey rectangles superimposed on periods of treatment. Treatment starting at time step 100 with 90% effectiveness. During treatment period, there is a 10% probability that treatment is left out for a week to simulate incomplete adherence which is visible as temporary decrease of CD4+ counts during treatment. Extended period (12 timesteps) of ‘drug holiday’ from time step 150.

Our data show a rapid drop in the count of CD4+ cells after simulated infection at timestep zero (characteristic of the acute phase). The decline then continues, albeit at a slower rate, during the chronic phase of infection. Upon initiation of simulated treatment at time step 100, a significant recovery in the

number of CD4+ cells occurs. Incomplete adherence to the treatment regime, simulated by a random chance of omitting treatment for time step (10% in Figure 6.2) causes a temporary drop in cell numbers (signified by the irregular saw tooth pattern), as well as an overall decline in the long term. This decline accelerates as the treatment period persists. Collagenation, however, exhibits constant increase, albeit with less-pronounced slope during treatment.

The influence, of treatment initiation timing and subsequent adherence, on collagenation build-up was also investigated, (Figure 6.3). The concave shape of the respective classes of relative collagen increase is caused by potential sites already being saturated with collagen for *late* treatment initiation. Hence, the *apparent* decrease is caused by the metric of *relative* collagenation chosen.

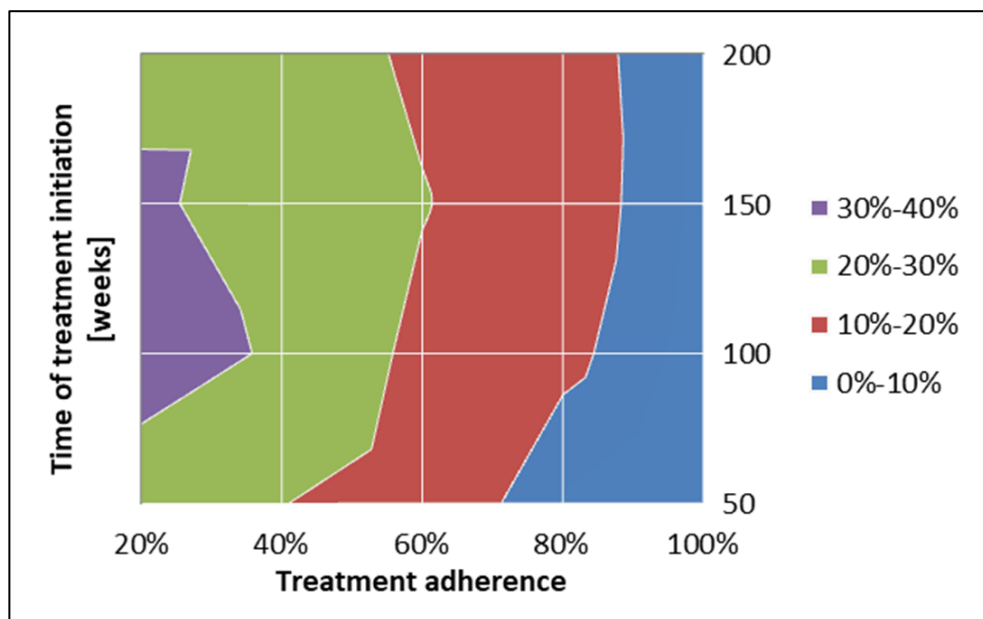


Figure 6.3: **Effect of treatment adherence and initiation timing on increase of collagenation.** Different colours denote levels of collagen increase. Graph shows relative increase from time of treatment initiation.

*Treatment initiation timing* appears to have a less-pronounced effect than adherence to treatment. Nevertheless, if treatment is introduced during the early phases of infection (within the first 2 years), it has greater impact than if initiated at a later stage in disease progression. However, with good adherence to treatment (80% and above), collagenation can still be kept within *acceptable bounds* even for late treatment initiation. An acceptable outcome is taken to be *a total collagenated area of less than 75% at the end of the simulated 10 years*, where this is guided by clinical data, (Zeng et al., 2012c), and indicates a threshold above which onset of AIDS or AIDS-related disease is imminent.

### 6.3.3 Structured Interruptions

Prior to simulation, absolute values of CD4+ count limits from clinical literature were normalized for use with the SCA model by assuming an initial cell count of 1000 cells/ $\mu$ l. Results were again obtained after 500 timesteps (~ 10 years). The projected results (see Table 6.2) show a marked difference for both collagenation and CD4+ count for the earlier studies.

Table 6.2: Experimental results for CD4+ guided structured treatment interruptions.

Clinical study	CD4+ count limits [cells/ $\mu$ l]		Simulation (timestep 500)	results
	Interruption	Resumption	Collagenation	CD4+ count
SMART (El-Sadr et al., 2006)	350	250	97%	260
LOTTI (Maggiolo et al., 2009)	700	350	81%	380

Using the thresholds of the LOTTI study for a prolonged period would still yield average CD4+ counts which are well above the critical value of 200 cells per microliter.

A further SCA model experiment on *CD4+ guided* structured treatment interruptions, aimed at assessing the amount of collagenation (and immune

system impairment) in conjunction with different thresholds of treatment re-initiation where the latter had been suggested to be crucial in clinical STI studies, (Hirschel and Flanigan, 2009). The simulation setup included (i) allowing CD4+ counts to decrease to the respective threshold and (ii) no collagenation to be present at the start. Treatment resumption thresholds were then varied and simulated tissue collagenation observed. Figure 6.4 shows that the collagenated area appears inversely proportional to the treatment re-initiation threshold *only* for the case of no previous impairment. Where pre-existing collagenation exists and is already high, the re-initiation threshold does not appear to have any influence. These results indicate that immune system failure is likely to occur if pre-existing immune damage exists at the start of CD4+ guided treatment interruptions, irrespective of the re-initiation threshold chosen. The results may also allow quantification of the pre-existing immune system impairment and may in part explain the negative outcome of the SMART study, given its patient characteristics.

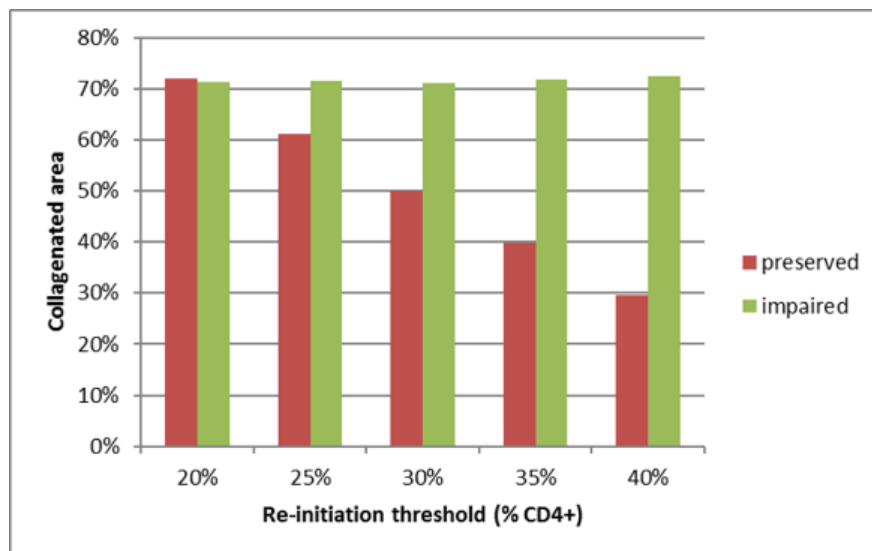


Figure 6.4: **Effect of different treatment re-initiation thresholds on long term progression of collagenation.** Model simulation with CD4+ thresholds normalized to values before infection. Percent area covered by collagen evaluated after 520 timesteps (~ 10 years in real time). ‘preserved’: Treatment interruption regimen was applied immediately; ‘impaired’: TI regimen was applied after CD4 level reached 20%.

## 6.4 Impact Assessment of STIs

### 6.4.1 SCA Model

#### Experimental Setup

While the model is useful to gain general insights into long-term tissue dynamics associated with HIV-infection, I now focus on the aspects of treatment and interruptions. Specifically, I want to assess the effect of *treatment initiation timing* on the outcomes of subsequent treatment interruptions to probe the contradictory results of treatment interruption studies. Further, I aim to investigate the impact of unstructured interruptions or adherence on long-term prognosis.

The *objectives* of my experiments here are as follows:

**SCA(a)** The *amount of collagenation* is measured both before and after a brief treatment interruption, together with the *progression of collagenation* over the experimental period. Additionally, the effect of the timing of the interruption itself on *overall collagenation* is evaluated.

**SCA(b)** Further, the effect of various levels of adherence on FRC decline and collagen accumulation is investigated. In this regard simulated treatment is started at time step (week) 50 to allow the FRC level to stabilize, after which different *adherence protocols* are applied by defining a discrete probability of ‘missing a dose’ at each time step. In terms of the model, this is achieved by setting treatment effectiveness  $P_T$  to zero for random time steps according to a probability defined by the level of adherence, (providing a slight simplification of the adherence patterns observed in clinical practice), (Glass and Cavassini, 2014). Every 50 timesteps (approx. one year), no doses are missed to allow for observation of FRC regeneration and to determine its peak. In total, four periods are introduced for each level of adherence.

**SCA(c)** Here, the aim is to quantify treatment initiation timing in combination with a structured treatment interruption. While a potentially

beneficial effect of early treatment initiation has been the subject of recent clinical research, (Lundgren et al., 2015), its impact on FRCn integrity is not well understood.

**SCA(d)** The intent here is to assess the impact of a heterogeneous distribution of cytokines in the microenvironment of the FRCn, an important aspect and a matter of recent discussion, (Dimopoulos et al., 2017). A homogenous distribution would lead to collagen depositions which spread randomly over the network, yet imaging data suggest that collagen build-up has a localised structure. To simulate variations of neighbourhood effect contribution, I introduce an additional probability for *random* collagenation with no neighbourhood dependency contributing to  $P_{H \rightarrow Hc; D \rightarrow C}$  in this model. With this modified model I perform multiple simulation runs while reducing the effect of the neighbourhood-induced collagenation (by lowering parameter  $P_{INF}$ ) in such a way that the overall collagen build-up after 10 simulated years remains constant.

Parameters along with estimated values from clinical sources are listed in Table 5.1, (see chapter 5.3.2). Parameter estimates represent population averages. Different treatment interruptions patterns (see above) are applied to this population. To account for stochasticity, results are obtained by taking the average of the outcomes of 100 simulation runs with identical setup. Sample values for simulated collagenation and FRCs were obtained for each simulated week from the averaged runs.

## **Results**

From the simulation experiments, the following results are obtained:

**SCA(a)** Analysis of regeneration capabilities of FRCs after treatment re-initiation following a treatment interruption of 50 steps indicates a decrease for both baseline and maximum proportions (see Figure 6.5), which appears to accelerate for each subsequent interruption period. The chart shows the

treatment periods where doses were missed (starting at 50, 150, 250, 350 steps respectively), as well as recovery periods where no dose was missed in-between.

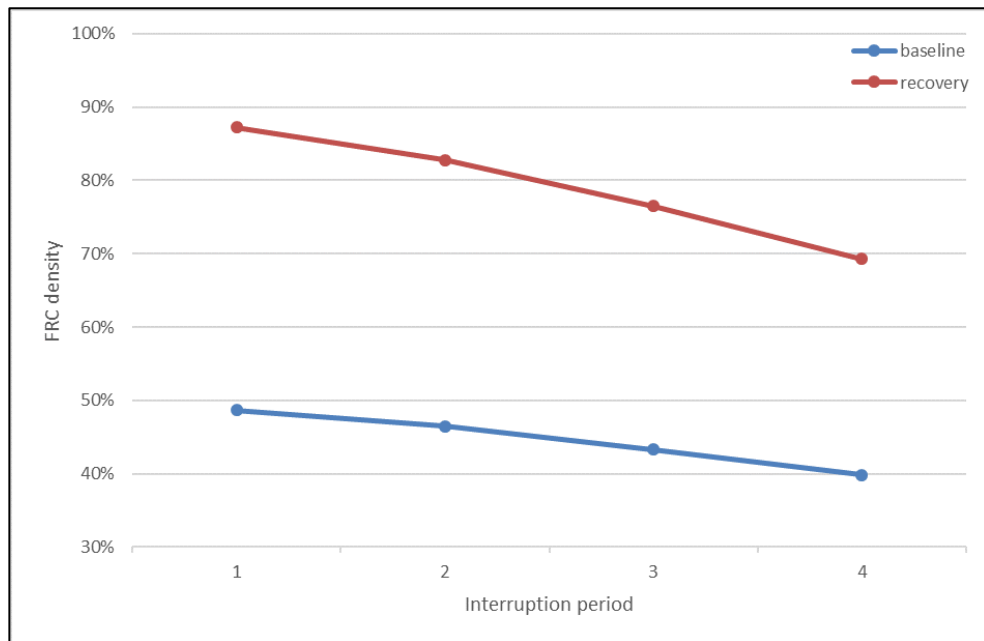


Figure 6.5: **Interruptions affect FRC baseline.** Graphs shows FRC densities (Y-axis) before (blue) and after (red) treatment re-initiation for four subsequent interruption periods (X-axis). The respective interruption patterns were 50 weeks of no treatment followed by 50 weeks of treatment with perfect adherence.

**SCA(b)** A dependency between FRC regeneration capabilities and *different adherence protocols* is marked (see Figure 6.6). Lower probabilities of missing a dose show more of a gradual decrease in contrast to higher probabilities where decrease is parabolic suggesting the impact of pre-existing damage fuelling decay. This result corresponds to the build-up of collagen between subsequent periods where different adherence protocols apply (see Figure 6.7).

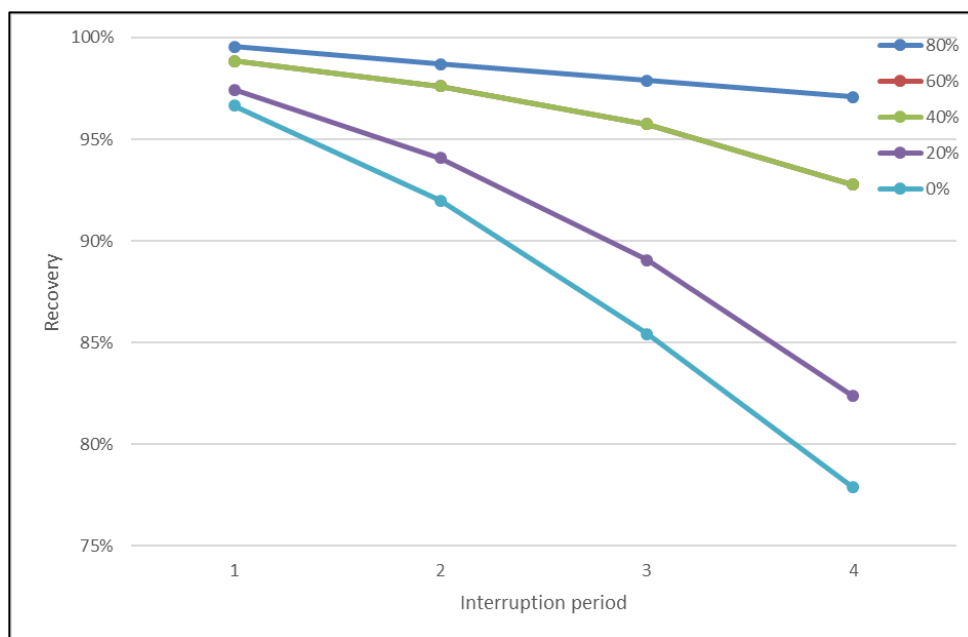


Figure 6.6: **Treatment adherence effect on FRC regeneration.** FRC levels (Y-axis) after multiple periods (X-axis) of occasional treatment, which was only applied in a proportion of weeks (see legend) The respective patterns were 50 weeks of occasional followed by 50 weeks of full treatment for each period.

In summary, these results indicate marked impact of treatment interruptions or infrequent drug taking in terms of progression of lymph tissue fibrosis and loss of FRCs. Different probabilities of missing a dose together with interruption duration, affect these properties non-linearly where degradation is faster for pre-existing damage. Upon treatment re-initiation a high degree of FRC regeneration can be observed, possibly contributing to CD4+ increase and restoration of immune functions. However, results also show that FRC loss for treatment interruptions is highly dependent on the accumulation of collagen, as suggested, (Zeng et al., 2012c). In consequence, the level of lymphatic tissue collagenation may be a ‘missing piece in the jigsaw’ when considering treatment interruptions on a clinical basis.

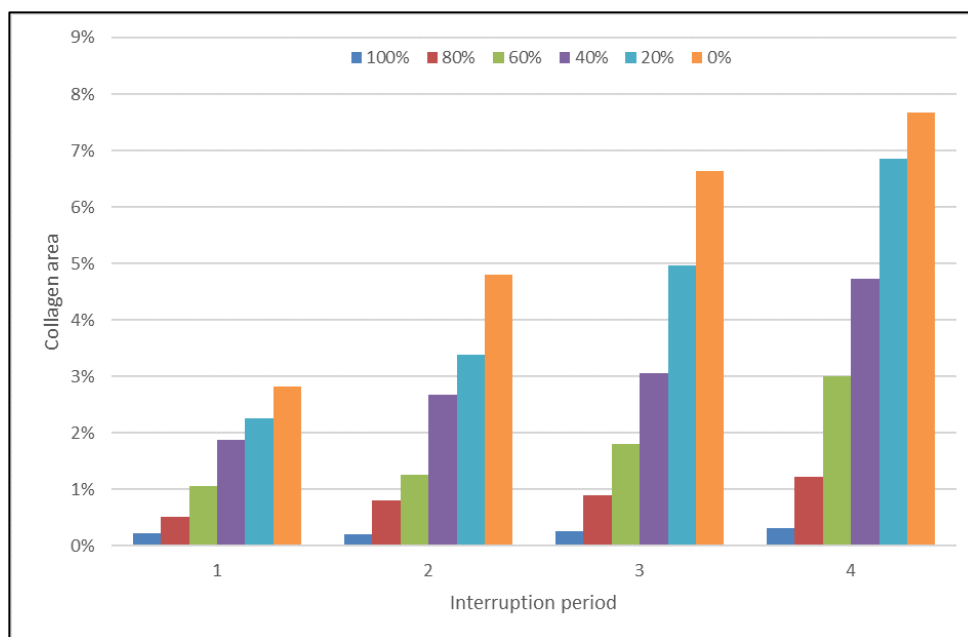


Figure 6.7: **Collagen build-up depends on adherence level.** Coloured bars indicate collagen coverage after multiple periods (X-axis) of occasional treatment, which was only applied in a proportion of weeks (see legend) and after treatment interruption periods (X-axis) using the interruption pattern of 50 weeks of occasional followed by 50 weeks of full treatment.

**SCA(c.1) Early treatment initiation**, during primary phase of the infection, has been found to be associated with lower declines of CD4+ count following an interruption (Fidler et al., 2013; Sáez-Cirión et al., 2013), with immune system functions largely preserved. Considering this apparently key factor of treatment initiation timing, I varied simulated treatment onset while keeping the time of interruption constant. Further, my experimental setup considered clinical findings of incomplete antiretroviral drug penetration into lymphatic tissue, (Cohen, 2011), by assuming a treatment effectiveness less than 100%. According to my results, the progression of collagenation over time following infection diagnosis, (see Figure 6.8), indicates strong dependency for overall collagenation on start of treatment (i.e. the state of disease progression which it commences). This important result reinforces outcomes of recent large-scale clinical studies on treatment initiation timing, endorsing the earliest possible treatment commencement, (Lundgren et al., 2015).

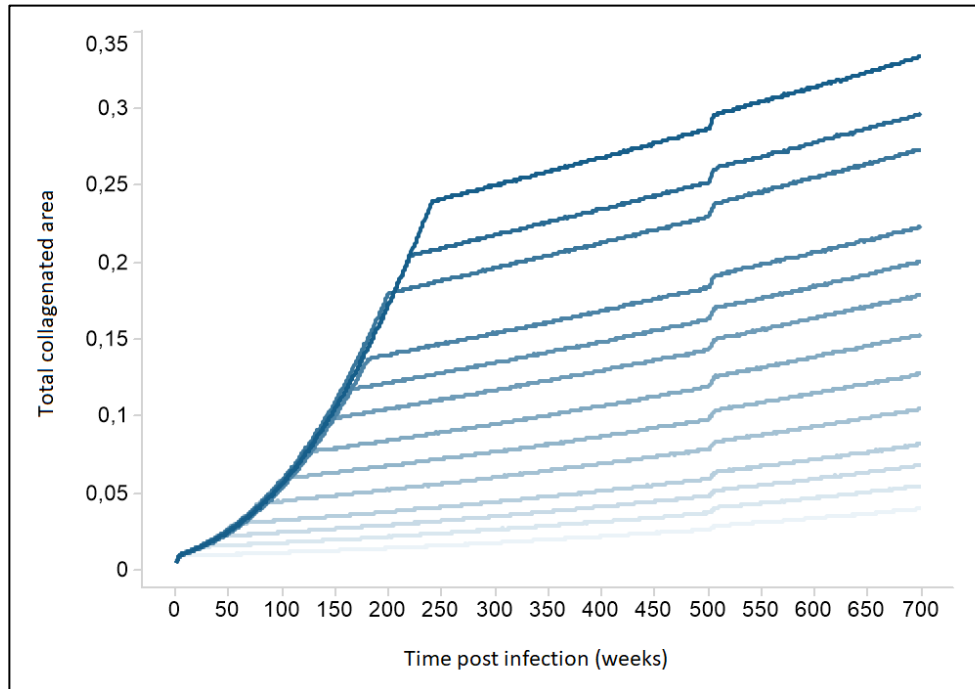


Figure 6.8: **Treatment initiation timing affects collagen build-up.** Shaded lines indicate different times of treatment initiation (0 – 240 weeks, see legend). Treatment interruption displayed takes place between weeks 500 to 505, visible as brief, rapid increase in collagen build-up. Treatment effectiveness was assumed to be 90% on average.

**SCA(c.2)** Results further show that, for each week that treatment initiation is delayed, irreversible collagenation grows *quadratically*. This is a vital finding as it provides a metric. Findings show conclusively that the collagenation increase after *later* treatment initiation occurs at a faster rate than when treatment is introduced *earlier*, (something not reported previously in the literature). From Figure 6.8, this effect appears to be less pronounced than pre-treatment collagenation. However, looking at the rates of collagenation in more detail (see Figure 6.9), they appear to increase in a *linear* fashion with treatment initiation times. This finding also reinforces the hypothesis that early initiation is essential to limit the infection progressing, (Buzon et al., 2014).

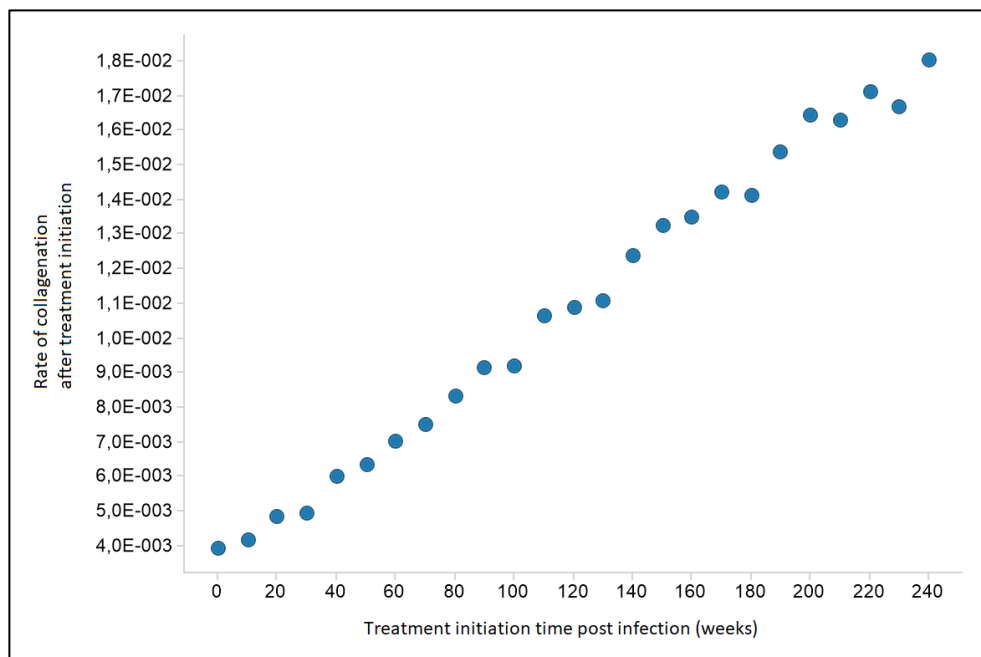


Figure 6.9: **Collagenation rates under treatment depend on treatment initiation timing.** Markers show rates of collagenation (Y-axis) after treatment initiation against time of treatment initiation (X-axis) after infection. Treatment effectiveness was assumed to be 90% on average.

**SCA(c.3)** The *persistent* effects of treatment *interruptions* also appear to be related to treatment initiation timing or pre-existing immune damage. Treatment interruption shows an increase in collagenation (see Figure 6.8, time step 500), which is halted but *not reversed* after re-initiation. Details of this sharp increase, displayed in Figure 6.10, indicate that the amount of interruption-induced *extra* collagenation *increases steadily* over time of treatment initiation. This result is interesting since one would expect a constant increase for each interruption, because interruptions have the same time span. However, simulations indicate that larger areas of collagen (as present in late stages) tend to spread in a more rapid manner if treatment is removed. A reason for this behaviour might be that collagenated areas have a larger contact surface as compared to yet un-collagenated regions. This

finding may be useful for further clinical investigations on the collagenation process.

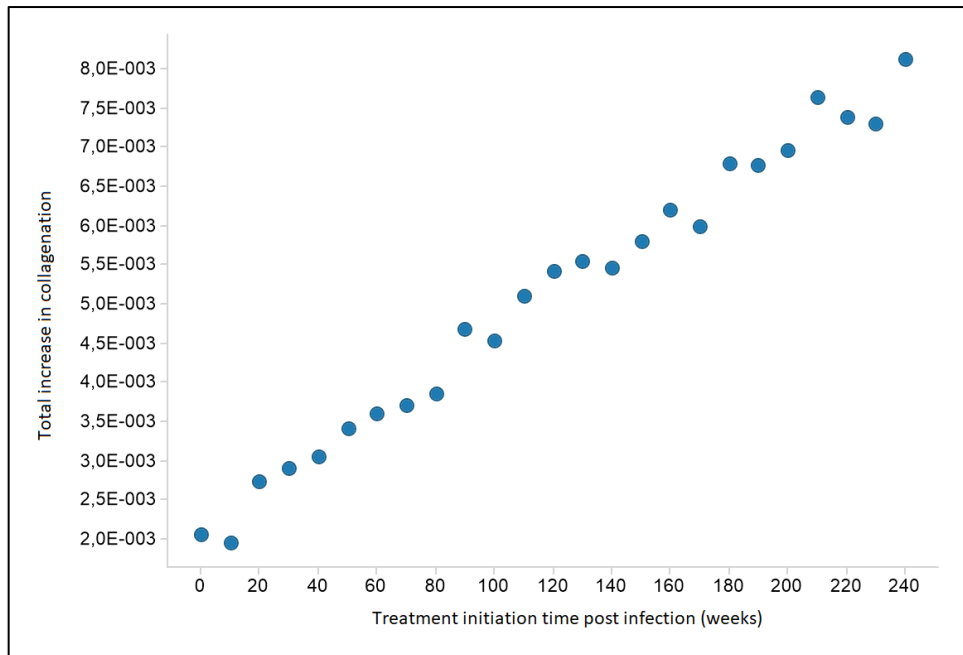


Figure 6.10: **Collagenation following interruptions depend on treatment initiation timing.** Markers denote total increase in collagenation (Y-axis) during the interruption period against time of treatment initiation (X-axis). Treatment interruption displayed takes place between weeks 500 to 505. Treatment effectiveness was assumed to be 90% on average.

**SCA(d)** The introduction of random effects (in addition to neighbourhood effects) leads to variations in the collagenation patterns (Figure 6.11). Stronger neighbourhood dependencies lead to clustering of collagen, as observed in microscopic imaging, (Zeng et al., 2011). A steady *build-up* in collagenation, as suggested by clinical data, (Zeng et al., 2012c), is only achieved by a combination of random and neighbourhood effects.

If only random effects are considered (0% contribution from the neighbourhood), collagen accumulation does not increase in a linear manner. It is noted that, after a comparatively quick build-up at the start, the curve flattens indicating slower rate of collagenation towards the end. As the model

setup included imposing periodic boundary effects, edge effects are less likely here. Hence, my assumption is that this is actually ‘saturation’, i.e. lack of available non-collagenated cells. A stronger focus on neighbourhood effects, however, leads to attenuated collagenation, which starts slowly then exhibits accelerated collagen build-up until the end of simulation, probably due to increase in the overall contact area of collagenated with healthy tissue, fuelling the process.

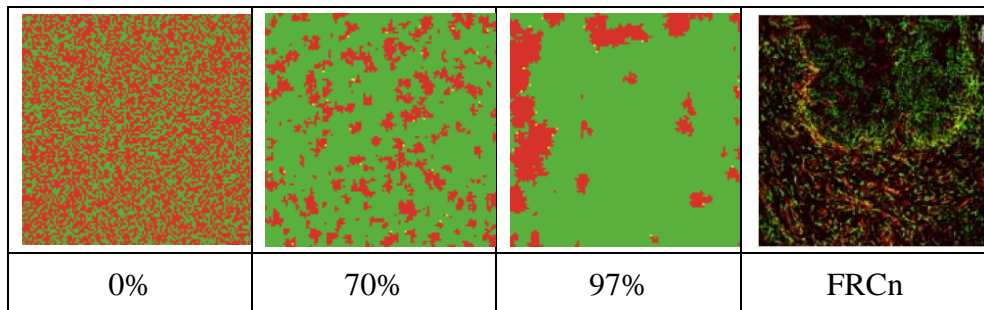


Figure 6.11: **Collagenation patterns obtained by alteration of neighbourhood effects in comparison to tissue imaging.** Panels on left, centre-left and centre-right show simulation results obtained at time step of 250 weeks. Regions with red colours indicate collagen and healthy cells coloured green. Colour coding applies for simulated and stained tissue. Leveraging settings for effects of neighbourhood collagenation account for different collagenation patterns. Percentages indicate whether sites are collagenated at random (0% neighbourhood effects) or mainly due to neighbourhood effects (97%). Panel on right shows an image of FRC tissue during chronic phase of HIV infection showing curved line separating areas with different collagenation densities.

Image source (right): Zeng, M., et al., PLoS Pathog. 8, e1002437 (2012). Use permitted under the Creative Commons Attribution License CC BY (<https://creativecommons.org/licenses/by/4.0/>)

The change in shape observed in the resulting curves (Figure 6.12) is marked, suggesting significant influence of the neighbourhood effect. An approximately (at best) linear relation is observed when neighbourhood effects contribute around two thirds of total collagenation. However, for neighbourhood effects predominating, non-linearity is less marked, given the long-time scale of FRC decline during untreated HIV.

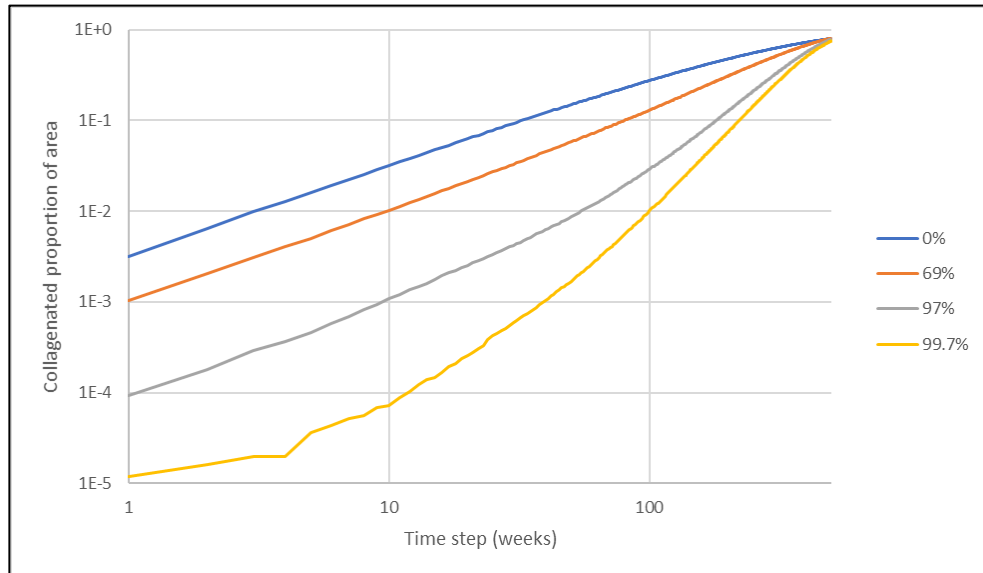


Figure 6.12: **Contribution of modelled neighbourhood effects to total collagenation progression.** Model parameters were chosen that after 500 timesteps (weeks), 80% of the tissue matrix would be covered with collagen, resembling the terminal phase of infection. Legend shows proportion of neighbourhood effects vs random effects. In this context, 0% represents no collagenation due to neighbourhood effects (i.e. all collagenation caused by random effects). Values were chosen arbitrarily for illustration purposes and double logarithmic scale was chosen for better comparability.

## 6.4.2 CM Model

For the CD4+ Motility model, *persistent* effects of treatment *interruptions* also appear to be related to treatment initiation timing or pre-existing immune damage, (Hillmann et al., 2017b). Using either the spatial or the random CM model, treatment interruption shows as an increase in collagenation, which is halted but *not reversed* after re-initiation. This sharp increase, (Figure 6.13), illustrates the opposite effect of both models in terms of collagen build up.

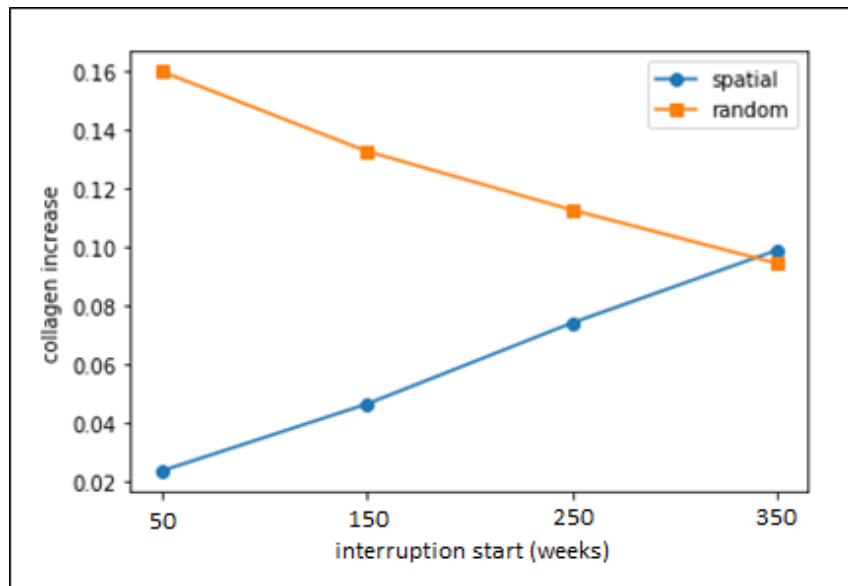


Figure 6.13: **Differences in collagenation increase following interruptions for spatial and random model.** Increase depends on amount of pre-existing collagenation for spatial (blue circles) and random model (orange squares). Markers denote total increase from baseline in collagenation (Y-axis) during subsequent interruption periods starting at specific time steps (X-axis) with respective duration of 50 time steps / weeks.

**CM(a)** For both, spatial and random models, results indicate that the amount of collagenation, caused by repeated treatment interruptions of the same length, is *not constant*. Instead, a *steady change* (increment or decrement) in the amount of collagen can be observed for any subsequent interruption and re-initiation.

However, the *slope directions* differ markedly in the spatial and the random model, as indicated in Figure 6.13. Considering only random collagen spread, the rate of collagen formation is more pronounced for the first few treatment interruptions, presumably due to the high availability of healthy cells. When more and more cells become collagenated, the collagen increase appears to slow down slightly (for the four points of data obtained). Conversely, the spatial model exhibits an *inverse slope*, with the slow rate of collagenation for early treatment interruptions increasing for each subsequent interruption. This profile of rate change also indicates that large collagenated

areas, (present at later stages of infection), will inevitably spread more rapidly in the spatial model if treatment is removed, since the contact boundary with healthy areas is also larger. Periodic boundary conditions, as imposed for the SCA model, prevented visible artefacts resulting from edge effects. The implications of the nature of collagen deposition for treatment interruptions are particularly clear. While few interruptions are less deleterious only *if* collagen spread occurs due to neighbourhood effects, a deposition of collagen at random locations implies that a first interruption is associated with the *most severe* collagen increase. The question, of which type of collagen deposition (spatial/random) predominates in real terms, remains open.

## 6.5 Summary

The potential of the present modelling approach for simulating treatment interruptions is demonstrated by results, which show a distinct relation between duration of the interruptions, pre-existing damage and damage caused by the suspension of treatment, as indicated respectively by SCA(a,b,c,d). In particular, pre-existing damage was not comprehensively considered by earlier clinical studies. Further, results in CM(a) indicate the marked influence on overall progression for multiple interruptions in terms of the way in which collagen spread occurs, (spatial/random).

However, to fully understand and offer explanation of results of past clinical trials on STIs, I need to upscale my approach to simulate a whole study population. In the next chapter, I propose such a ‘clinical trial model’ and demonstrate its capabilities for parameter estimation and distribution identification, using an inverse approach.

## **7 Upscaling: iCTS Model Components and Inverse MC**

### **7.1 Introduction**

Having considered treatment interruptions at the cellular and tissue level in previous chapters, I now turn to the ‘population scale’ of clinical study cohorts. While a review and extension of clinical trial designs would be a thesis topic of its own, I will focus on trial formats of studies previously used to investigate structured treatment interruptions. Lacunae in clinical trial design can be addressed only by new trials, but recent research may throw light on previous findings, which are not clear-cut.

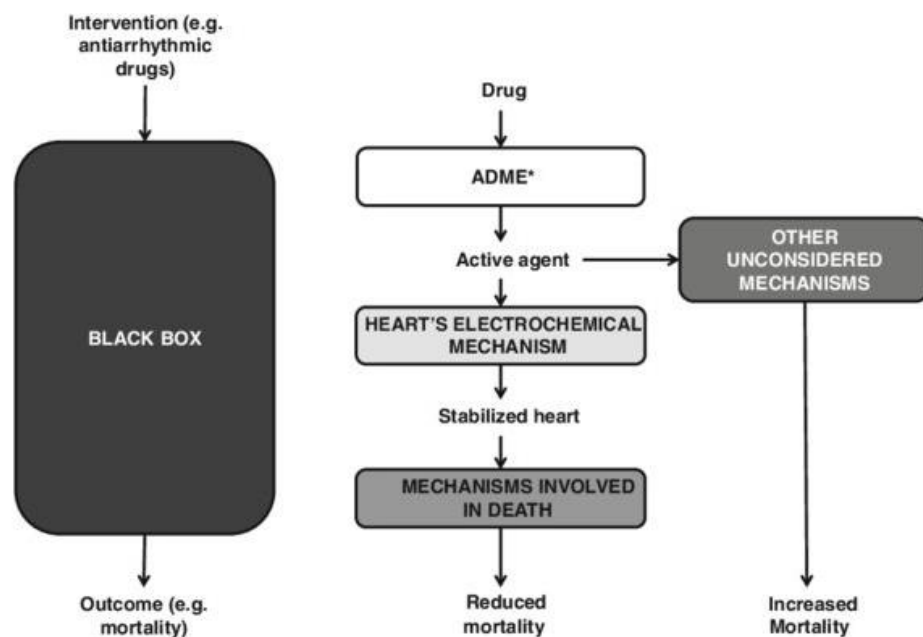
Further, *clinical trial simulation*, with different designs simulated using *virtual patient groups* have now achieved some measure of popularity, in order to consider alternative design options in a cost-effective way. In this chapter, I rely on the findings obtained previously to simplify and upscale my approach to simulate treatment interruption trials with a large group of patients. Inverse Mont Carlo methods are used to draw conclusions on specific properties of the patient populations, not considered in the original study, but of potential importance in explaining outcomes.

### **7.2 Data from Clinical Sources**

#### **7.2.1 Clinical Evidence**

The common approach to obtaining evidence on efficacy of some treatment is to assess the emergence over time of so-called *clinical endpoints*, (defined at the design stage). These endpoints may be specific events, such as emergence of disease or death or less drastic biomarkers, such as event-free progression. In the case of the SMART study, (Siegel and El-Sadr, 2006),

these endpoints were defined as various types of adverse effects, which a patient with HIV infection might encounter, e.g. AIDS-related disease, non-related diseases or death (due to AIDS or any cause). A common way to display information collected on events over time is by a ‘survival’ model (displayed e.g. as a *Kaplan-Meier* chart), which indicates the fraction of patients remaining free of a specific event. Statistical correlation is used typically in clinical studies to compare randomised treatment and control groups and assess efficacy (or non-efficacy) of a treatment, (Sackett, 1997). Rather less emphasis is placed on *how* results occur, with the study effectively a ‘black box’, with defined inputs and statistical outputs (see Figure 7.1, left).



\*absorption, distribution, metabolism, and excretion mechanisms

Figure 7.1: **Example (cardiac drug) demonstrating drug efficacy through evidence-based and mechanistic reasoning.** Left diagram shows purely evidence-based approach by observing inputs and outputs and treating the system as a ‘black box’. Consideration of mechanisms (middle) enables improved system insight but bears risk of false results if not all relevant mechanisms are known.

Image source: J. Howick, P. Glasziou, and J. K. Aronson, ‘Evidence-based mechanistic reasoning,’ *J. R. Soc. Med.*, vol. 103, no. 11, pp. 433–441, Nov. 2010. Use permitted under the Creative Commons Attribution License CC BY (<https://creativecommons.org/licenses/by/4.0/>)

Whereas this approach is sufficient to infer statistical properties, it is less suitable to obtain insight into the underlying *biophysical mechanisms* (see Figure 7.1, middle). Such knowledge is usually not incorporated in these studies, since the corresponding mechanisms introduce additional uncertainty and risk omission of important side effects (see Figure 7.1, right). Nevertheless, useful additional insights may be provided, especially in cases where data are sparse, (Howick et al., 2010).

## 7.2.2 Clinical Trial Simulation

In addition to factors above, multi-phase clinical trials are expensive and time-consuming with a large patient sample required to provide reliable statistical evidence, (Holford et al., 2010). To minimise patient (and other) risks, *Clinical Trial Simulation* (CTS), (Ogenstad, 2018), has been proposed to test certain trial designs *in silico* by utilising prior knowledge of the biophysical mechanisms associated with intervention, and with the aim of selecting the most promising for assessment.

Most applications of CTS follow a ‘forward’ approach i.e. their aim is to provide optimal design for clinical studies based on prior knowledge (see Figure 7.2). Models used in this context mostly originate in Pharmacokinetics / Pharmacodynamics (PK/PD) and put emphasis on the drug or active component, (Mould and Upton, 2013; Sheiner and Steimer, 2000). Pharmacokinetic models obtained from *in vitro* data have been considered a valid approximation for data obtained *in vivo* under certain circumstances (termed *in vitro in vivo correlation*), (Emami, 2006). Apart from this promising approach, regulatory authorities have been slow to adopt the whole concept of CTS as a complement of *in vivo* trials, (Pappalardo et al., 2018). However, recent approaches have seen some amelioration of the wholly pharmacologically centric view to allow for more general simulation of patient populations. In the HIV-context, data from historical clinical trials and

simulation were used, (Abbas et al., 2008), to optimise trial design for antiretroviral therapy interventions, while an agent-based epidemiological model was employed to assess different interventions to prevent infection, (Cuadros et al., 2014). Further, a stochastic CTS model was employed, (Braithwaite et al., 2005), to investigate co-morbidities under HIV infection with adherence to antiretroviral therapy considered. This model was extended also to take into account additional intervention types and covariates (such as age, gender, alcohol consumption), (Ruggles et al., 2017). While these recent examples highlight the potential of CTS, they still rely on forward simulation for prospective study planning and have not been widely adopted for STIs.

In Chapters 5 and 6 I built computational models to study immune system fitness decline due to lymph tissue damage in conjunction with treatment interruptions. My previous results can be used, therefore, to construct a model permitting *inversion* of the CTS process (Figure 7.2).

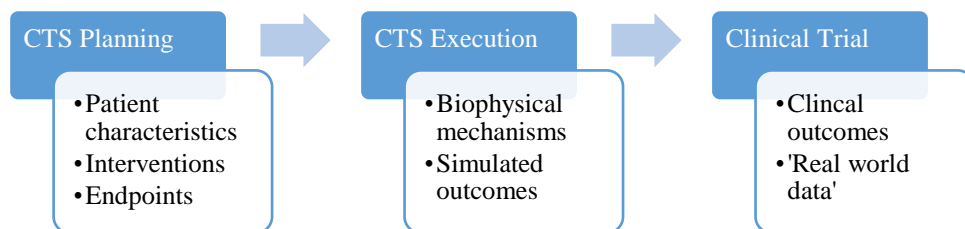


Figure 7.2: **Concept model for CTS studies** showing the three main steps and subtasks.

The resulting concept of *inverse clinical trial simulation* allows predictions for patient population characteristics, using outcome information, together with knowledge of the biological mechanisms involved. Consequently, the re-use of existing data on historical clinical trial outcomes is possible, even where these are relatively sparse or incomplete in current terms. The aim is to derive plausible information on patient population features, which may not have been considered at the time of the original

clinical trial, (including lymphatic tissue status and immune system impairment in this case).

In the following, mechanistic modelling of HIV is briefly reviewed, and construction of a simplified version of the LT-model, (Hillmann et al., 2020, 2017b), is discussed. Model capabilities are demonstrated in ‘forward simulation’ and subsequently apply an inverse approach to simulated and original STI clinical trial data and outcomes.

## **7.3 Mechanisms and Data**

### **7.3.1 Observed and Hidden Data**

In chapter 3, I noted that models, which incorporate known biological mechanisms of HIV infection are still predominantly of predator-prey compartmental type. In these, the virus acts on cells from the immune system, where the basic setup consists of three compartments, each represented by an *Ordinary Differential Equation* (ODE) and describing concentration changes of a specific property over time. In the case of HIV these are commonly concentrations of the virus and a type of white blood cells (CD4+ T-cells), the main target of the virus. A core condition of this class of models is that all ‘reactants’ are sufficiently well mixed, (arguably true for the bloodstream, (Beauchemin, 2006)). The dynamics of such ODE-systems have been widely researched and the basic model has been refined over time (e.g. (Conway et al., 2019)). However, recent clinical results strongly suggest that HIV infection is much more multi-faceted in terms of its impact on various components of the immune system than model assumptions allow, (Appay and Sauce, 2017).

One major aspect, which has largely been neglected to date, is lymphatic tissue degradation through collagen deposition, as described in Section 5.2. These alterations may be induced by infection-related alterations of cellular

signalling, (Fletcher et al., 2015; Schacker et al., 2005; Zeng et al., 2012a). Antiretroviral therapy has been found to slow down this process but not to reverse it, (Zeng et al., 2012c), leaving permanent impairment of immune function, despite apparent CD4+ restoration. The intervals between structured treatment interruptions may also influence these alterations, but this has not yet been observed directly. Figure 7.3 illustrates the impact of direct and indirect adverse effects of HIV infection and treatment interruptions, as observed in clinical studies.

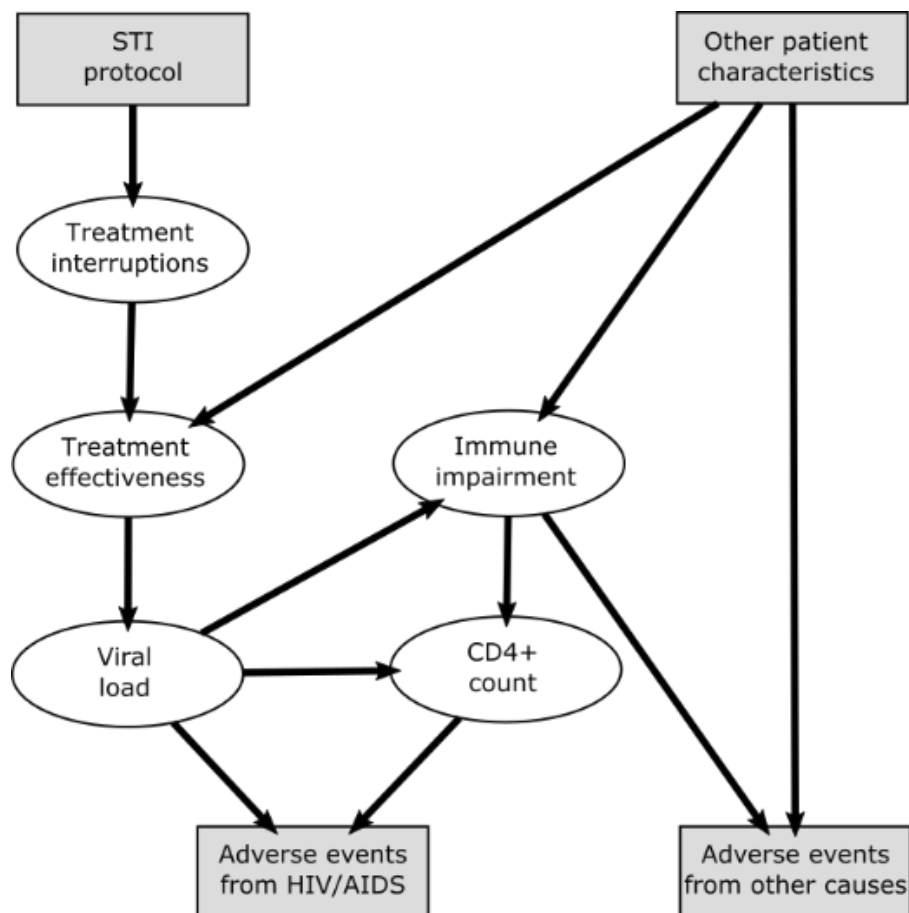


Figure 7.3: **Relationship diagram for a treatment interruption study.** Grey boxes denote data captured during the clinical study while ovals denote factors at least partially hidden e.g. replacement of lymphatic damage with something like immune damage where the former is not directly observable.

Adverse events may be caused directly, (e.g. through destruction of CD4+ T-cells, due to the virus) or indirectly, (from immune system depletion). In the SMART study, events directly attributable to HIV infection (i.e. through opportunistic disease) were rare and numbers did not differ significantly from the control group. However, a statistically significant increase in non-HIV infection related cases (of cancer and even death) was detected, (Silverberg et al., 2007). More recent research has associated such events with ageing of the immune system, (Appay and Sauce, 2017).

Antiretroviral treatment limiting the viral concentration in body fluids may thus have the *twofold* effect of preventing direct infection of CD4+ cells (allowing regeneration) and restoring cellular signalling to ‘normal’ levels preventing further permanent damage. The detailed mechanisms of infection progression responsible for those outcomes are described and quantified in the next section.

### **7.3.2 Infection Progression**

During untreated HIV infection, different kinetics for various biomarkers can be observed. In addition to the concentration of viral copies in peripheral blood, and proteins used for cellular signalling (cytokines), (Duprez et al., 2012), CD4+ T-cell concentration is the most commonly used marker for determination of the status of infection progression, (Fauci et al., 1996). This concentration (denoted CD4+ count) exhibits a marked decline during untreated infection (see Figure 7.4).

As remarked in section 2.2.3, the decline is roughly categorised by three distinct phases: In a healthy person, the CD4+ count is in the range of 800 - 1500 cells/mm<sup>3</sup> blood. In the *acute phase* (first 12 weeks after HIV infection), a rapid decline and subsequent (incomplete) recovery of CD4+ T-cell levels occurs, accompanied by flu-like symptoms; (CD4+ counts in blood then stabilise on a level lower than that prior to infection); in the subsequent

*chronic phase*, which is largely asymptomatic, levels of CD4+ concentrations tend to decrease in a steady manner, (Fauci et al., 1996); the final phase, associated with immune system breakdown and AIDS-related disease, is defined by CD4+ concentrations dropping below 200 cells/mm<sup>3</sup>. Clinical data suggests an acceleration of CD4+ level decline accompanied by emergence of AIDS-related symptoms and opportunistic disease leading to death within a few months, (Fauci et al., 1996). In the following, I focus on the chronic phase, (the greater part in HIV infection progression). Nevertheless, the time period involved is subject to patient-specific variations. These have been identified and described earlier in terms of fast-progressors, slow progressors and the rare cases of elite controllers or non-progressors (Section 5.2.4). In any case, all available data sets record a steady decline of CD4+ concentrations in blood, typically of the order of 5.25 cells/mm<sup>3</sup>/month, (Fauci et al., 1996; Greenough et al., 1999).

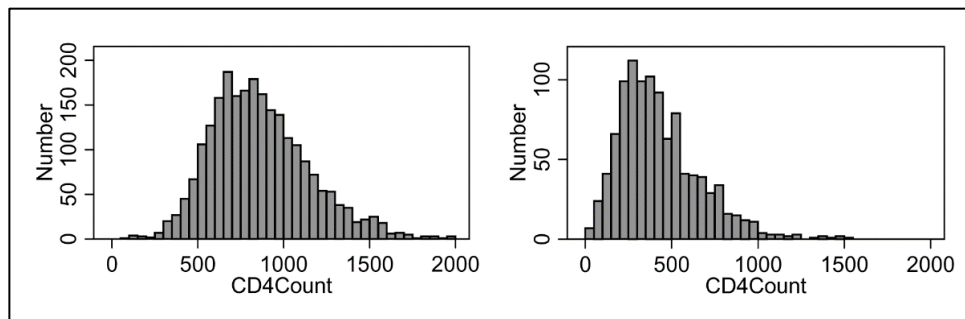


Figure 7.4: **Histograms of CD4+ counts** for groups of HIV-uninfected (left) and infected (right) individuals. Increase in fatalities due to low CD4+ counts lead to asymmetric distribution shape for the HIV infected group.

Image source: A. Malaza, J. Mossong, T. Bärnighausen, J. Viljoen, and M.-L. Newell, ‘Population-Based CD4 Counts in a Rural Area in South Africa with High HIV Prevalence and High Antiretroviral Treatment Coverage’ PLoS One, vol. 8, no. 7, p. e70126, Jul. 2013. Use permitted under the Creative Commons Attribution License CC BY (<https://creativecommons.org/licenses/by/4.0/>)

To obtain a more detailed picture of the underlying distribution of progression times in a patient population, I analysed publicly available data from a patient cohort of HIV infected individuals in the *Amsterdam Cohort*

*Study*, (Coutinho, 1998). The patients were observed over the whole course of infection until AIDS symptoms emerged. The risk data presented in Figure 7.5 (a) indicates a variable event rate, increasing from year 3 after infection, levelling off for times above 10 years. This observation is in line with other sources, (Fauci et al., 1996; Greenough et al., 1999), of fast- and slow- or long-term non-progressors.

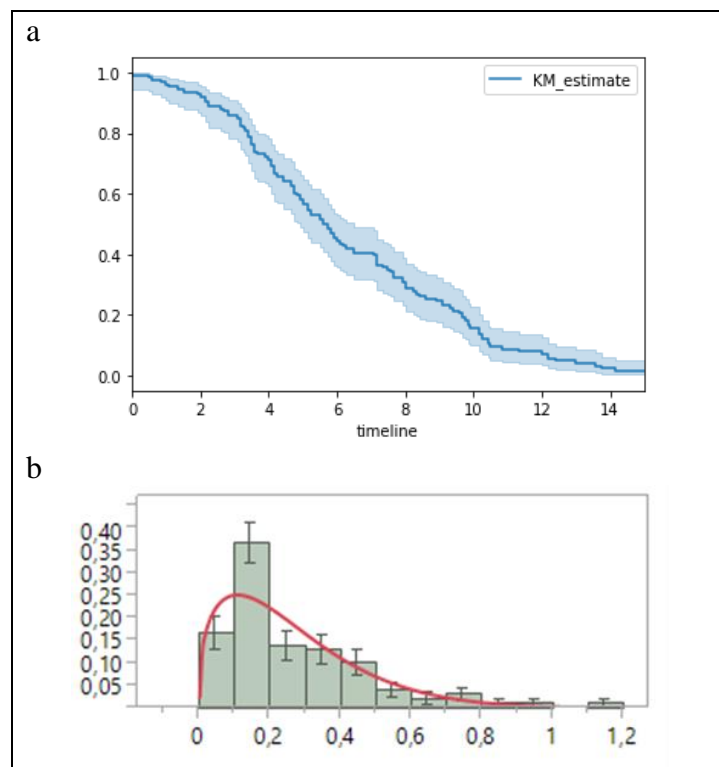


Figure 7.5: **Distribution of time-to-AIDS in a patient cohort.** (a): Risk chart indicating proportion of patients with no HIV (at risk, y-axis) against time since seroconversion (years, x-axis); sample size  $n=125$ . (b): Histogram of relative incidence (y-axis) of CD4+ decline rates (cells/mm<sup>3</sup>/day, x-axis), pooled in 0.1 intervals until AIDS onset; and best fit with Weibull distribution.

The average loss of CD4+ count per patient was calculated using the same set of data. The resulting histogram, Figure 7.5 (b), illustrates slow progression with the distribution positively skewed towards higher times. I

found the best mathematical representation of this behaviour to be a 2-parameter Weibull distribution (with parameters scale 7.2; shape 1.9) though the Lognormal is also feasible. Consequently, by sampling from the Weibull [7.2, 1.9], a patient population with a realistic distribution of progression rates can be generated, (and is used for the following progression modelling).

## 7.4 iCTS Model Components

### 7.4.1 Infection Progression Model

To relate the *hidden* property of permanent immune system impairment for a specific individual to the *observable* property of CD4+ cell concentration I construct a mathematical model (termed *trial model*) based on Ordinary Differential Equations with two compartments: the former,  $T$ , denotes CD4+ count in blood, while  $T_C$  denotes the ability of the immune system to regenerate. This latter property is diminished during infection through permanent damage effects caused by HIV (e.g. lymph tissue collagenation). I use established ODE formalism in preference to the biologically more realistic models (described in Sections 5.3 and 5.4), as this is simpler to implement as a first attempt and with limited computational resources. In this case, therefore, a detailed calculation of lymphatic tissue damage is not included. Rather, I present a proof of concept, which may be adapted to include more complex model forms (see extensions following). For now, I take  $T_C$  to be the lowest value that  $T$  can assume at a given time, so that in the case of no treatment ever having been applied,  $T$  and  $T_C$  are equal. Further, I assume identical units (cells/mm<sup>3</sup>) for  $T$  and  $T_C$ , although the latter strictly speaking is a virtual or idealised concentration only of CD4+ cell count as a measure of the ability of the immune system to fight infections or in the absence of any previous treatment. It is useful as a quantitative comparison of patients or patient populations in terms of immune system impairment.

Most ODE models addressing HIV focus on underlying viral infection processes. However, these have a very short turnaround of approximately two days, (Ho et al., 1995), important in modelling short-term responses to treatment, (e.g. (Perelson and Nelson, 1999)). Since the timeframe in this case ranges from weeks to years, however, viral replication is indirectly represented as *pressure* on the immune system (affecting degradation and recovery rates in the compartments).

Thus, for the case of an individual who never received treatment (*treatment-naïve*) the system is represented by the following system of two equations:

$$\begin{aligned} \frac{dT}{dt} &= -d_{\max} \\ \frac{dT_C}{dt} &= -d_{\max} \end{aligned} \quad (7.1)$$

Using expression (7.1), I assume that CD4+ concentration decline, and immune system depletion occur at the same constant rate,  $d_{\max}$ . This is suggested by the CD4+ count being a strong predictor of infection progression if no treatment is introduced, (as observed in the pre-ART era, (Fauci et al., 1996)). Further justification for assuming this relation are that rates observed for T-cell decline and lymphatic tissue collagenation are strongly proportionally-related, (Zeng et al., 2012c).

## 7.4.2 Medical Intervention Model

Initiation of Antiretroviral Therapy has been found to lead to a drastic reduction of viral load in blood, (Dixit and Perelson, 2004). This slowdown of viral activity is accompanied by downregulation of immune activity and subsequent recovery of CD4+ cell levels. This increase in concentration is most pronounced in the first few months after treatment initiation with

recovery rates in the range of 20 to 30 cells/mm<sup>3</sup>/month, (Corbeau and Reynes, 2011). Increased migration of lymphocytes from lymphoid organs into the bloodstream is assumed to be a key contributor to this rapid rise. This slope levels off subsequently but CD4<sup>+</sup> counts in blood continue to rise more slowly for 5 to 6 years of continuous therapy, (Moore and Keruly, 2007) with the increase assumed to be caused by homeostatic proliferation until CD4<sup>+</sup> levels reach a steady state. The plateau achieved has been found to be associated with baseline CD4<sup>+</sup> counts (*nadir*; pre-treatment level or lowest CD4<sup>+</sup> count detected) for the patient, (Falster et al., 2009). Overall, the final CD4<sup>+</sup> concentration stabilises at approximately 300-350 cells/mm<sup>3</sup> above this baseline. Interestingly, individual baseline levels do not appear to impact on the pattern of recovery rates as described above, (Nobrega et al., 2016). The limitation of CD4<sup>+</sup> cell recovery appears due to multi-faceted causes, (Corbeau and Reynes, 2011), and is not yet fully resolved, but research to date suggests that production of defective naïve T-cells and increased apoptosis are key contributing factors, (Aiuti and Mezzaroma, 2010). In addition, there is strong evidence that these factors are linked to lymphatic tissue damage, (Zeng et al., 2012b). A mathematical approximation for constrained growth (as observed in this case) is the common 1-parameter logistic formula. Recent data indicate that biomarkers associated with inflammation and immune system upregulation remain elevated for *more than a year* after therapy initiation, (Osuji et al., 2018). To better allow for these combined effects of medical intervention, I extend system (7.1) to allow for a non-constant immune system decay rate  $D$  and constrained recovery / immune system impairment:

$$\begin{aligned}
\frac{dT}{dt} &= r \left( 1 - \frac{T - T_C}{b} \right) \\
\frac{dT_C}{dt} &= -D \\
\frac{dD}{dt} &= -\alpha D
\end{aligned}
\tag{7.2}$$

In the modified system represented by expression (7.2), rate  $r$  represents the maximum observable recovery rate for CD4+ T-cells, while  $b$  denotes the regeneration limit. I further assume that, while rate  $d_{max}$  from expression (7.1) is not immediately reduced to zero for the  $T_C$  compartment when treatment is initiated, it follows an exponential decline with rate  $\alpha$ . This property is possibly correlated with the frequency of *regulatory T-cells* (Tregs) relative to the CD4+ T-cell population as indicated in Section 5.2. This percentage of Tregs has been found to be significantly elevated during HIV infection, (Shaw et al., 2012). However, during the first months after treatment initiation and during CD4+ regeneration, the relative frequency of Tregs drops rapidly and approaches pre-infection levels, (Nobrega et al., 2016). Assuming a similar kinetic and based on this information, a value for  $\alpha$  was chosen such that the decline of  $D$  has a half-life of around one month. Since immune system depletion is assumed to be irreversible,  $T_C$  may not increase irrespective duration or effectiveness of treatment.

### 7.4.3 Therapy Removal Model

The first remarkable phenomenon associated with antiretroviral treatment discontinuation is the rapid increase of viral concentration in blood, (detectable after about 10 days), known as *viral rebound*, (Rothenberger et al., 2015). It is assumed that this rise is caused by activation of ‘dormant’ virus in so-called *latently infected cells*, (as noted in section 2.4 previously) (Conway et al., 2019), or by ongoing viral replication in lymphatic tissues,

not accessible with *in-vivo* assay techniques, (Fischer et al., 2003). These short-term viral dynamics are well-characterised, (Hill et al., 2016), but CD4+ dynamics over longer time scales following treatment cessation are less well-known. A rapid drop in the CD4+ cell concentration in blood within the first month after a treatment interruption has been detected, but this loss of immune cells has been found to be strongly correlated with baseline levels for a specific subject, (Thiébaud et al., 2005). In cases of low CD4+ baselines ( $< 200$  cells/mm<sup>3</sup>) average losses of 365 cells / mm<sup>3</sup> have been reported for the first month of treatment interruption.

For higher baselines, this loss was less pronounced ( $\sim 154$  cells / mm<sup>3</sup>) in the first month. From month 2 after treatment discontinuation, the loss rate is lower and constant,  $\sim 17$  cells/mm<sup>3</sup>/month, (Thiébaud et al., 2005), or 24 cells/mm<sup>3</sup>/month, (Maggiolo et al., 2004), have both been reported. It is questionable whether treatment interruption loss rates for CD4+ cells would decline sufficiently to approach (markedly lower) *treatment-naïve* loss rates, (given in 7.3.2).

Hence, the system (7.2) is modified to allow *constrained decay* of  $T$ :

$$\begin{aligned} \frac{dT}{dt} &= -c \left( 1 - \frac{T_{int} - T}{T_{int} - T_c} \right) \\ \frac{dT_c}{dt} &= -D \\ \frac{dD}{dt} &= \beta D \left( 1 - \frac{D}{d_{max}} \right) \end{aligned} \tag{7.3}$$

In this ODE system, parameters  $T_{int}$  and  $c$  represent CD4+ T-cell concentration and maximum loss rate of T-cells at the start of interruption respectively. I assume  $c > d_{max}$ , to allow for the rapid decline of CD4+ concentration following treatment interruption, as indicated, (Maggiolo et al., 2004). For the rate of change for  $T_c$  I assume an exponential  $d_{max}$  with

doubling time  $\beta$  where  $\alpha < \beta$  and take  $\beta$  values to be ranged in time around viral rebound, (Rothenberger et al., 2015). This system thus defaults to expression (7.1) for longer periods of treatment interruption.

All parameters used for the models formulated, along with parameter ranges suggested by the literature are summarised in Table 7.1 .

Table 7.1: Parameter estimates for the CTS model.

Model	Param.	Description	Value	Literature
Infection progression	$d_{max}$	Maximum depletion rate of CD4 T-cells (Weibull distributed)	62.8 cells/mm <sup>3</sup> /year	(Fauci et al., 1996; Greenough et al., 1999)
	$r$	Initial regeneration rate of CD4+ T-cells on treatment	305 cells/mm <sup>3</sup> /year	(Corbeau and Reynes, 2011)
	$b$	Regeneration limit	350 cells/mm	(Corbeau and Reynes, 2011; Moore and Keruly, 2007)
Medical Intervention	$a$	Slowdown rate of depletion rate.	9 per year	(Nobrega et al., 2016)
	$c$	Maximum depletion rate of CD4+ cells at start of treatment interruption.	204-288 cells/mm <sup>3</sup> /year	(Maggiolo et al., 2004; Thiébaud et al., 2005)
	$\beta$	(Maximum) acceleration rate of Depletion rate.	25 per year	(Rothenberger et al., 2015)

#### 7.4.4 Risk Model

As noted above, clinical studies typically observe the emergence of specific outcomes (or *endpoints*) which are defined during study setup. These endpoints then provide evidence to prove (or disprove) study hypotheses. For the STI studies referenced, endpoints were chosen to test neutrality of the STI regimen (so were related to fatalities or emergence of disease). For example, the most extreme case, (increase in death rate due to AIDS-related or other causes), has been found to show elevated incidence for the STI group in the SMART study, (El-Sadr et al., 2006).

To quantify the relationship between immune system impairment and chance of an extreme event, I use clinical data of the last measured CD4+

counts for a cohort of untreated (or treatment naïve) patients, (Coutinho, 1998), (measured 3 months or less prior to death), (May et al., 2016; Palella et al., 2006). As stated in section 7.4.1, I assume the CD4+ count *for treatment naïve subjects* to be a valid representation of actual immune system impairment. The relationship was found to be well-represented by a power law, (Figure 7.6). Using non-linear regression, we obtain the following function to determine the risk of experiencing a fatal event for a given immune state:

$$P(T_C^{naive}) = 1.38x^{-0.814} \quad (7.4)$$

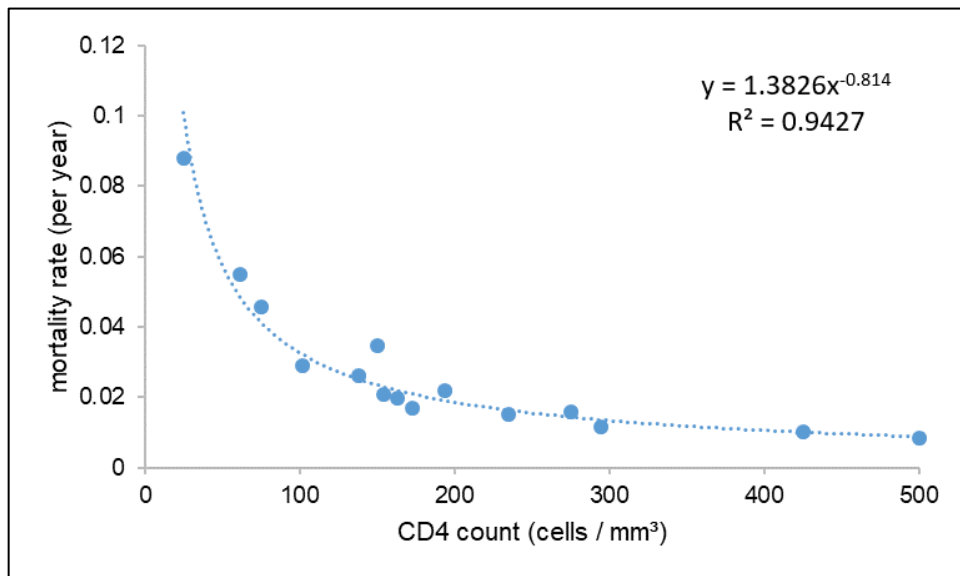


Figure 7.6: **Mortality rates of HIV-infected patients in relation to latest measurements of CD4+ counts.** Measurements from pooled clinical datasets, (May et al., 2016; Palella et al., 2006). Dashed line shows fit using a power-law function indicating asymptotic behaviour.

With the mechanistic ‘trial model’ described above, we are now able to simulate trajectories over time, for CD4+ counts and immune system impairment, together with associated risks for fatal events under various treatment regimens for *simulated patient cohorts*. These *virtual patients* also may differ in their initial predisposition and response to infection and

treatment. In the following, I define a theoretical framework of use for further experimentation.

## 7.5 Inverse Monte Carlo Framework

### 7.5.1 Inputs and Outputs

To highlight the concepts underlying my approach, I combine and simplify model relations from section 7.4 by defining a function describing the ‘risk of a fatal event’ over time  $E$ :

$$\begin{aligned}
 E(t) &\equiv f(\Theta, t) \\
 &\text{with} \\
 \Theta &= [T_0, T_{C0}, d_{\max}, r, b, c, \alpha, \beta]
 \end{aligned}
 \tag{7.5}$$

In expression (7.5), the non-linear function  $f$  describing the event rate over time depends on parameter vector  $\Theta$ , which consists of initial values of  $T$  and  $T_C$  and parameter values chosen for the progression model. Each *virtual patient*  $i$  can then be represented by a parameter vector  $\theta_i$  with a unique set of values from biological meaningful ranges for each parameter. It is then assumed that each parameter in  $\Theta$  can be represented by some distribution over the patient population.

In the context of clinical trial simulation, such variations are commonly described using *Non-Linear Mixed Effect Models (NLME)*, (Wu, 2005). Using this NLME methodology, each parameter (or covariate in the NLMEs), is assumed to be either fixed or variable. Variation to account for different individuals (*inter-patient*) typically follow a Normal (Gaussian) distribution with parameters mean  $\mu$  and standard deviation  $\sigma$  in NLME. In this case  $T_0$  and  $T_{C0}$  are assumed to be variable due to natural variation. Further, distributions differ between clinical studies, possibly due to different

enrolment criteria for participating patients. Other parameters are also assumed to show inter-patient variations but are not linked to the study setup. In this context,  $d_{max}$  is assumed to be variable due to different progression rates observed for HIV infection. For rates  $r$  and  $c$  representing regeneration or depletion of CD4+ cells, variability is also assumed, based on evidence from clinical data. The remaining parameters  $b$ ,  $\alpha$ ,  $\beta$  are assumed to be fixed, since the clinical data indicate little variation for the regeneration limit  $b$ , (irrespective of the phase of infection), while the acceleration of depletion rate  $\beta$  is mostly influenced by viral properties like the (non-patient-specific) turnaround rate, (Rothenberger et al., 2015). Finally, slowdown of the depletion rate under treatment  $\alpha$  is assumed fixed due to the kinetics of Regulatory T-cells, for which available clinical data, (Nobrega et al., 2016), suggest little inter-patient variation.

Though some parameters may be related, publicly available data are limited, hence independence is also assumed here. From initial remarks on parametrisation (see section 3.4.3), estimates for most parameter distributions can be obtained from the literature (e.g. (Coutinho, 1998)). However, for historical STI studies, pre-existing immune system impairment  $T_{C0}$  has typically not been reported. Analytical solutions are unavailable, so one might rely on sampling-based techniques. Data for serious events, however, (e.g. death, opportunistic disease) are available from study records. Hence, I apply an *inverse Monte Carlo method*, as described in section 4.3.2, to obtain an approximation of  $T_{C0}$ . From inverse MC, a candidate value for  $T_{C0}$  can be obtained by sampling the distribution parameters  $(\mu, \sigma)$ . A rich sample from the resulting distribution is generated, which represents a virtual study population. To address further inter-patient variation, estimates for the remaining model parameters may be also obtained by sampling from the respective distributions. With the population generated, the model is applied to simulate the time course for  $T$  and  $Tc$  for each population member in order

to obtain an approximation for  $E(t)$ . The closeness of this solution to clinical outcomes is then quantified using the Mean Squared Error (MSE):

$$MSE = \frac{1}{N} \sum_{i=1}^N (E_i^{obs} - E_i^{sim})^2 \quad (7.6)$$

Since we are interested in solutions for  $E(t)$  which are close to observed clinical findings, an iterative approach, such as the Metropolis-Hastings algorithm must be applied (see Section 4.3.2). In case of this model, each Metropolis step  $n$  introduces small, random changes to the parameter vector  $\theta$  and obtains the MSE for  $n$ . The new parameter vector  $\theta_n$  is then accepted with a probability using the following relation and rejected otherwise:

$$P(\text{accept } \theta_n) = \begin{cases} MSE_n \leq MSE_{n-1} & 1 \\ MSE_n > MSE_{n-1} & \frac{MSE_{n-1}}{MSE_n} \end{cases} \quad (7.7)$$

## 7.5.2 Computational Model

An analytical solution of the equation system (7.1) – (7.3) is non-trivial, as treatment settings depend on STI protocol, hence I rely on numerical simulation methods. To simulate a ‘CD4+’-guided STI strategy, as used in the SMART and LOTTI studies, evaluating levels of  $T$  and  $T_C$  at fixed incrementally simulated time steps is necessary to assess risk of events or need for changes in treatment settings. In this case, common efficient algorithms for solution of ODE systems with variable step length (e.g. *Runge-Kutta* methods, see (Butcher, 1996) for a review) are not applicable. Solutions involving fixed steps, (such as the *Euler* method), however, tend to accumulate error rapidly for large step widths. Hence, I choose a discrete simulation step representing one day in the model space which is small

compared to the typical duration of HIV infection ( $> \sim 1500$  days) and offers a valid approximation interval. In observing the trajectories of both  $T$  and  $T_C$  (see Figure 7.7) an irreversible decline in  $T_C$  during a phase of treatment interruption is noticeable which is in line with clinical observations, (Zeng et al., 2012c).

Fixed time intervals enable the use of *Markov Chain Monte Carlo* (*MCMC*) methods where trajectories of simulated T-cell concentrations and immune system impairment are represented by a series of successive states. For systems of equations (7.1) – (7.3) the inter-dependency of  $T$  and  $T_C$  is clearly noted. The property  $T_C$  typically can not be observed in a clinical setting due to its complexity, but property  $T$  is routinely obtained (CD4+ count) and regarded as a proxy for  $T_C$ .

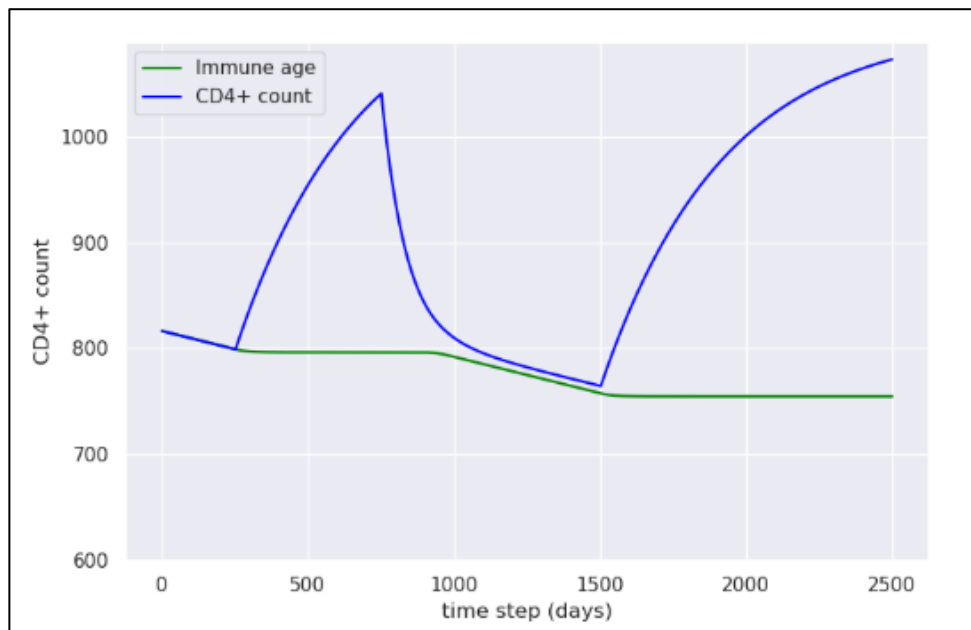


Figure 7.7: **Sample run of modelling framework using typical choices for parameter estimates.** Simulated treatment initiation occurs at timestep 250 with interruption at timestep 750 and subsequent re-initiation at timestep 1500 time steps (CD4+ count –  $T$ ; Immune age –  $T_C$ ; each step is equivalent to one day in real time).

Consequently, conditions for a *Hidden Markov Model (HMM)* apply (see. Figure 7.8). This type of models has wide applicability to problems in computational biology, (Schuster-Böckler and Bateman, 2007). Though mathematically intractable for most complex systems, sampling-based methods can again be used to overcome this limitation.

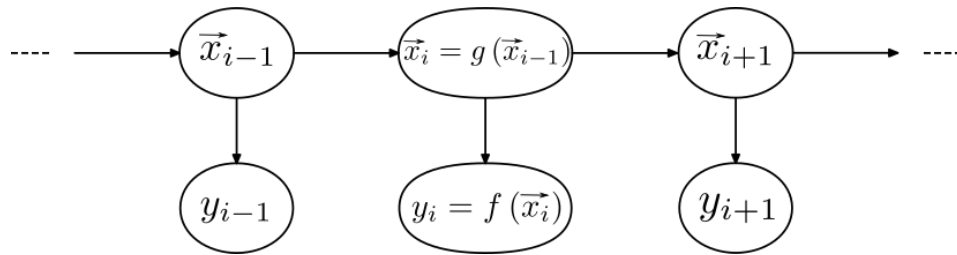


Figure 7.8: **Graphical representation of a Hidden Markov Model.** Circles denominate states (y – observed; x – hidden), arrows dependencies between states.

In the following I aim first to demonstrate the capabilities of the computational model based on equations (7.1) – (7.3), performing forward simulations and comparing results with data from clinical settings. Expanding on this, I use MCMC techniques to analyse clinical data from STI trials to gain additional insight on outcomes.

## 7.6 Simulation and Results

### 7.6.1 Forward Simulation

Each model run follows the steps, described in this section.

1. To initialise the model (or simulated clinical trial), I generate a number  $n$  of *virtual patients* by generating  $n$  corresponding vectors  $\theta_i$  ( $i = 1, \dots, n$ ). These parameter estimates are obtained by sampling the distributions given in Table 7.1, above. Distributions are assumed to be Normal except for  $d_{max}$  which follows the Weibull distribution. The assumption of Normally distributed

parameters is common in clinical settings for large patient groups, (Whitley and Ball, 2002). Parameters assumed to be fixed do not relate to inter-patient variation and are based on values from the literature (see Table 7.1). For starting values for  $T$  and  $T_C$ , the bell-shaped Normal distribution ( $\mu = 742$ ,  $\sigma = 305$ ) of CD4+ counts used to fit data of a treatment-naïve patient population, (Coutinho, 1998), (see Figure 7.9) is assumed. However, for STI trials, patients were mostly not treatment naïve (possibly distorting the Normal form), suggesting that an alternative distribution may be more appropriate. The assumption of Normality is acknowledged, therefore, to be a simple and convenient initial choice in this instance. After initialising the virtual patient population, model execution is started.

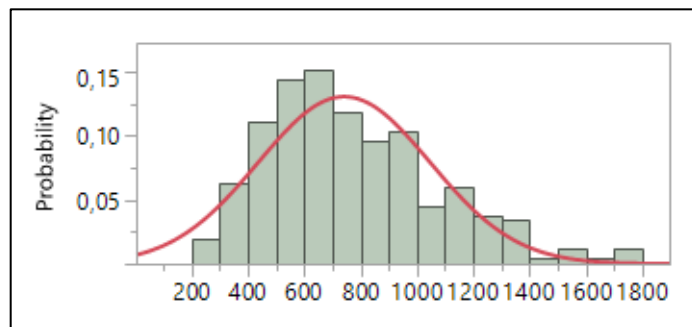


Figure 7.9: **Distribution of CD4+ T-cell counts at start of chronic phase of HIV infection.** Histogram height illustrates binned proportions of T-cell concentrations ( $n = 273$ ) obtained from the Amsterdam Cohort Studies on HIV / AIDS, (Coutinho, 1998). Red line shows fitted Normal distribution ( $\mu = 742$ ,  $\sigma = 305$ ).

2. At the start of each model time step, treatment status (either naïve, on or off treatment) is evaluated for each simulated patient. Depending on this status, equation systems (7.1) - (7.3) are employed to obtain values for the next time step.

**3.** Every 30<sup>th</sup> time step, results for CD4+ counts are evaluated for each patient (simulating a clinical visit). Depending on the outcome and CD4+ limits imposed for the simulated trial, treatment is adjusted accordingly.

**4.** The risk of experiencing an adverse event (like opportunistic disease, AIDS or death) is calculated for every time step using expression (7.4). A discrete event is simulated by comparing the individual patient risk with a random number. Upon occurrence of an event for one patient, the result counter for this time step is incremented by one and the patient is removed from the study.

**5.** The framework also assigns a discrete probability to study dropouts due to other reasons, i.e. ‘loss to follow-up’. The latter, however, does *not* cause an increase of the result counter.

**6.** After updating the virtual study population, the time step is incremented by one and the next iteration is started with model step **2**.

**Note:** The withdrawal of subjects (as in steps 4 and 5) is very common for clinical trials due to various reasons. Termed *censoring* in statistics, multiple methods have been proposed to deal with such truncated data, (e.g. classically, (Lindsey and Ryan, 1998)).

An example of data generated by simulation is shown in Figure 7.10. The property of immune system impairment (Figure 7.10 (b)) can not be observed as such under clinical conditions. Despite CD4+ counts well above critical levels at the end of study (Figure 7.10 (b), red bars), immune system function has markedly declined in contrast to study initiation (green bars).

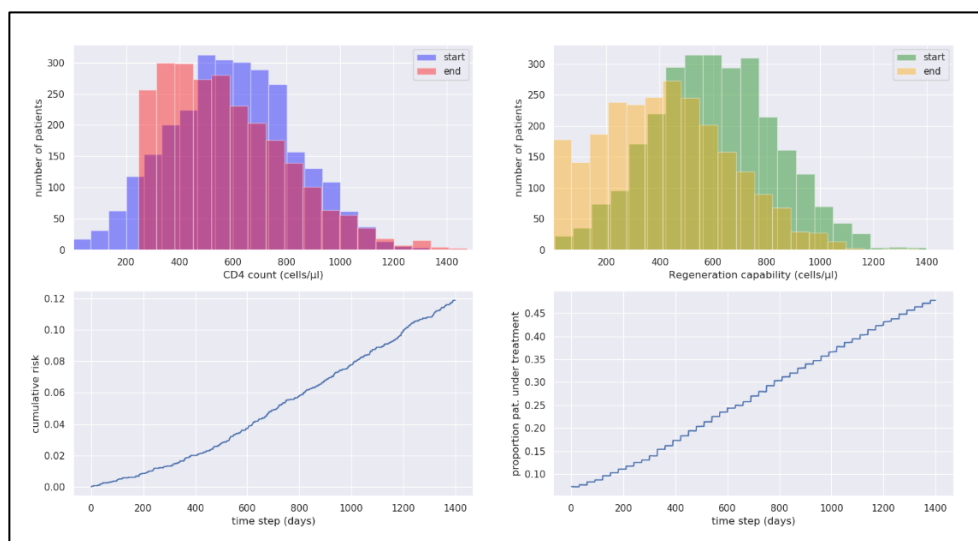


Figure 7.10: **Example of a simulated treatment interruption study.** The simulation starts with 2800 patients, treatment interruption occurs for CD4+ counts above 350 cells/mm<sup>3</sup> and (re-)initiation at CD4+ counts below 250 cells/mm<sup>3</sup>. (a) Distributions of CD4+ count at start (blue) and end (red) of study. (b) Distributions of Immune regeneration capabilities at start (green) and end (brown) of study. (c): Cumulative risk of adverse events study period. (d): Proportion of patients under treatment over study period.

In a real-world study, this decline can only be diagnosed indirectly by observing risk (Figure 7.10 (c)) or parameters such as treatment status or patients, (Figure 7.10 (d)). Besides population specific properties, the model also relies on parameters which are patient independent. The ‘trial model’ can be used to generate data sets on risk (similar to Kaplan-Meier charts) for a virtual study population where specific STI patterns are applied, where data are lacking for real study populations.

## 7.6.2 Parameter Sensitivity

To determine influence of non-patient specific model parameters  $\alpha$ ,  $\beta$  and  $b$  on risk progression, estimates (see Table 7.1 above) are varied by a factor of 2 and compare simulation outcomes. Simulations are set up to follow the protocol of the SMART STI study, (El-Sadr et al., 2006), but with an increased number of simulated patients (100,000) for improved statistical

power. I further use the total accumulated risk after simulation time = 2500 (days) as a measure for sensitivity. Results, (Figure 7.11) indicate marked impact of  $\alpha$  whereas other parameter changes appear to have a less profound influence.

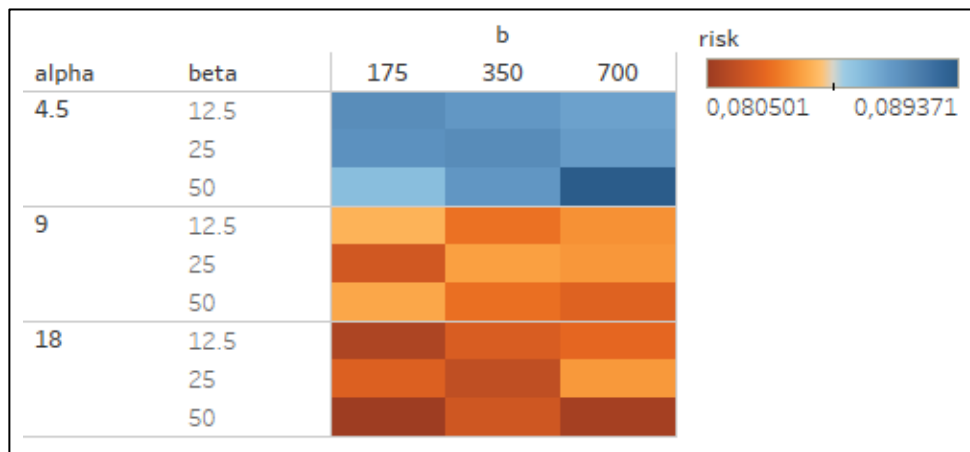


Figure 7.11: **Impact of non-patient specific parameters on total risk.** Heat map shows accumulated risk after 2500 simulation time steps (weeks) by colour in relation to different parameters selections.

As parameter  $\alpha$  controls the reduction of the immune system decay rate  $D$  under treatment, as defined in expression (7.2), low values result in ongoing decay even under treatment, permanently impacting CD4+ recovery and terminally increasing risk. Parameter  $b$  has less influence on risk, as it only impacts CD4+ recovery directly during treatment (expression (7.2)) and has no influence on immune system decay. Lastly, as parameter  $\beta$  controls immune system decay rate  $D$  when treatment is interrupted (expression (7.3)), the limitation of  $D$  to  $d_{\max}$  as maximum value might explain the lack of influence of  $\beta$  on overall outcome.

We next use the ‘trial model’ to generate data sets on risk progression for a virtual study population where specific STI patterns are applied, for which data are lacking for real study populations.

### 7.6.3 Comparison with Clinical Data

#### Simulation Setup

We assumed a virtual study setup and treatment interruption schedule, which followed the protocol of SMART, (El-Sadr et al., 2006), where key aspects are listed in Table 7.2. I chose the SMART STI study due to its controversial outcome and wide-ranging impact. Regarding prior immune system impairment, it has been reported that the SMART patient population consisted largely of immune-compromised subjects, (Hirschel and Flanigan, 2009), but no quantitative data on group condition exists. Hence, I simulate groups with *different degrees of immune system impairment* to explore the impact on outcomes for this specific study setup and compare simulated with clinical data.

Once again, the states of immune system impairment are taken to be Normally distributed, as for CD4+ count for untreated infection. Two different Normal distributions are sampled, representing different choices for these parameters, simulating both a group with immune functions largely intact and one with pre-existing impairment (see Table 7.2).

Table 7.2: Virtual study setup, (following basic parameters of SMART STI study) and characteristics of patient groups.

		Mean (SD)
<b>Study population (STI)</b>		2720
<b>CD4+ count (cells/mm<sup>3</sup>)</b>		597 (240)
<b>CD4+ threshold (cells/mm<sup>3</sup>)</b>	Lower	250
	Upper	350
<b>Patient immune functions</b>	degraded	750 (300)
	intact	1200 (300)

#### Results

Simulation results in terms of cumulative risks of death are compared with corresponding data from the SMART clinical study (Figure 7.12). The main findings for the forward simulations (denoted **F**) are as following:

**F(a)** The results indicate good agreement for risks of fatal events for clinical data (solid orange line) with the simulated data of the group with impaired immune functions (dashed blue line), at least during early phases.

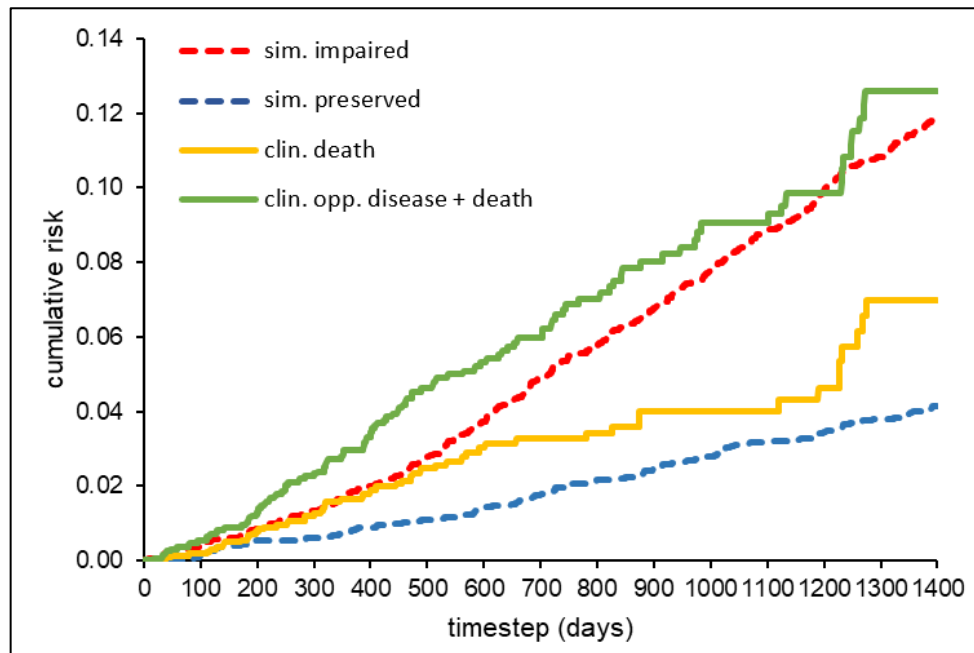


Figure 7.12: **Comparison of risk progression data** from SMART STI study (solid lines) - rates of death (orange) and opportunistic disease and death (green), with simulation data (dashed lines) for different initial choices of either intact (blue) or impaired (red) immune system function. Clinical data shows as more coarse-grained towards the end, (from censoring).

However, clinical and simulated data diverge from ~500 days, where simulation predicts higher values than were observed in the clinical study. In assessing this divergence, it is useful to note that the study ethics protocol obviously required patients to be removed / censored upon emergence of opportunistic disease, indicating immune system breakdown. This withdrawal and subsequent re-initiation of fully suppressive treatment aimed to prevent fatal events, which might otherwise have occurred had a vulnerable patient remained in the study.

**F(b)** I therefore included clinical data on risk of opportunistic disease in addition to fatal events (solid green line). It is noticeable that for this

combined measure, clinical and simulation data of the ‘trial model’ are in better agreement at a late phase of the clinical study.

To attempt derivation of the initial distribution of immune system states, I applied an inverse Monte Carlo (iMC) method to approximate the Normal distribution parameters, highlighted in the previous section.

## 7.6.4 Inverse Monte Carlo Simulations

### Simulation Setup

Using the framework described earlier, I initially aimed to validate the approach by deriving the known initial distributions for the two sets of data generated in the previous section, (parameters listed in Table 7.2). The sample size was again of ~2800 as in the forward simulations. An initial choice of  $\theta$  with ( $\mu = 742, \sigma = 305$ ) represented the typical distribution for a population at the start of the chronic HIV phase. Samples values for distribution parameters were restricted to within biologically plausible ranges ( $\mu$ : [0, 1500],  $\sigma$ : [0, 500]). For the first experiment, a run time of 100k Monte Carlo steps was implemented for each of the two simulated data sets. To enable better characterisation of regions of interest, (MSE low values) a negative log-transformation, (Feng et al., 2013) was applied in order to give a positive score  $S$ :

$$S = -\log_{10}(MSE) \quad (7.8)$$

In the following the results for the inverse Monte Carlo experiments (denoted I) are discussed for simulated and clinical data.

### Results for Simulated Data

**I(a)** From (Figure 7.13), performance of the M-H algorithm over the run cycles appears to be heterogeneous for the two sets of data with respect to the parameter space regions predominantly explored. For the case of intact

immune function, the majority of M-H samples is concentrated around mean values larger than  $\sim 800$ , (Figure 7.13 a). However, for the case of impaired immune function, the region with most samples appears to cluster around lower mean values (Figure 7.13 b), with mean values larger than 1200 explored to a lesser extent. These first results demonstrate the power of the key characteristic of the M-H algorithm and highlight potential areas with high scores as evidenced by sample predominance.

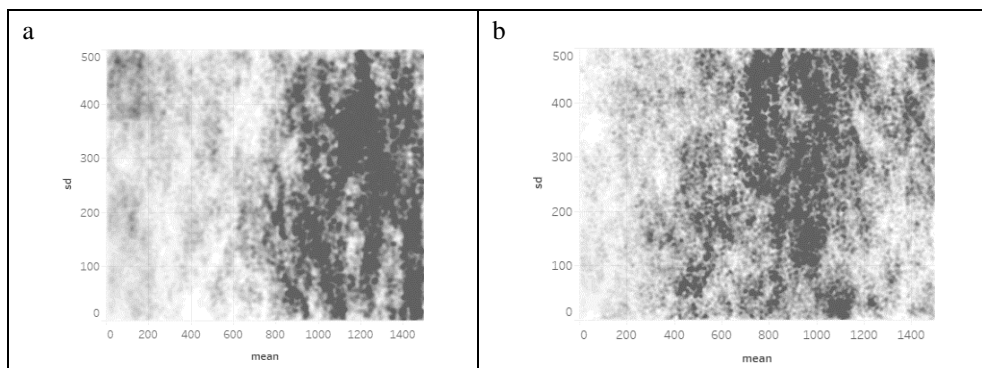


Figure 7.13: **Density of inverse MC samples** (as obtained with the Metropolis-Hastings algorithm) with respect to  $\mu$  (mean) and  $\sigma$  (sd) after 100k sampling steps on simulated risk progression data sets for (a) preserved/intact and (b) impaired immune functions. Shading is set to correlate with MC sample density.

**I(b)** The impact of the Metropolis algorithm behaviour becomes evident when examining the results of the above MC runs with respect to parameter combinations of  $\mu$  and  $\sigma$ . In this regard, I analyse the 1000 points with highest score  $S$  from both simulation results. The scatter plots in Figure 7.14 show the locations of those high scoring simulation results with respect to  $\mu$  and  $\sigma$  for both virtual patient groups and their respective scores denoted by colour. It is evident that high scoring values for  $\mu$  and  $\sigma$  accumulate in distinct regions which are distinctly separate for each virtual patient group. Each of those regions also includes the respective ‘real’ distribution parameters used to generate the simulated risk progression data sets, (providing some validation

for the inverse model). In both cases, the ‘real’ values are located towards the lower end of the respective regions of high scoring results, highlighting distribution breadth (and also perhaps the tendency of the model to encompass ‘worse-case scenarios’, presumably because no censoring is considered).

However, shape and size of these regions differ markedly between the two groups, being larger and less well-defined for those with preserved immune function, (Figure 7.14 a), compared to the impaired set, (Figure 7.14 b). Hence, variance is larger in the former case with risk average in the range ~1100 to ~1450. In contrast for those patients with impaired immune function, Figure 7.14b indicates accumulation of high scoring samples collected in an almost spherical region in the range ~700 to ~900 for  $\mu$  with small variance, suggesting more commonality of outcome.

In summary these simulation results indicate the potential of the inverse method in deriving distribution parameters for patient groups from risk progression data by means of generation of regions of probable parameter combinations.

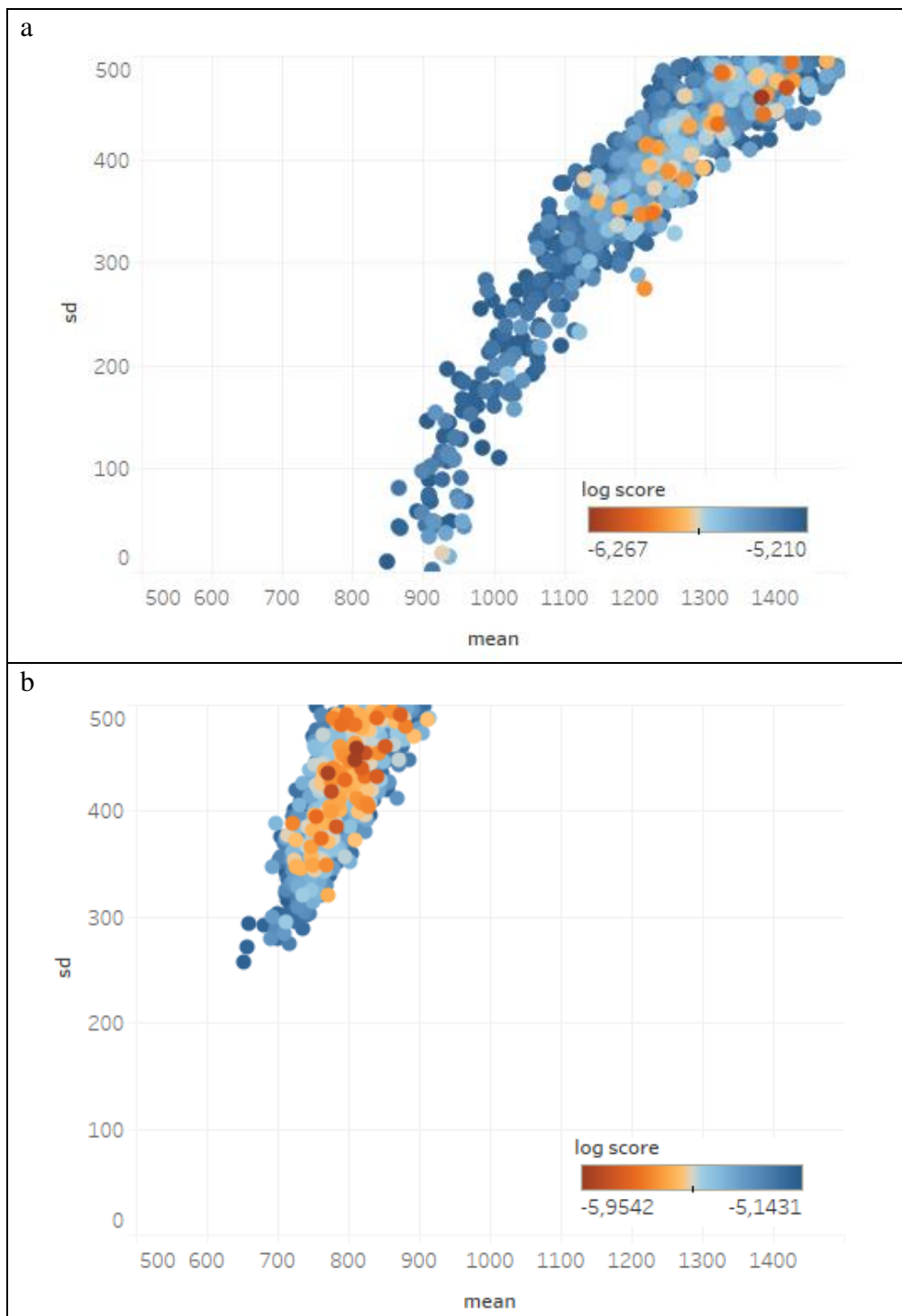


Figure 7.14: **Location of the respective 1000 MC samples with highest scores  $S$  in parameter space** ( $\mu$  -mean,  $\sigma$  -sd, x-axis truncated for visibility) for simulated datasets with immune function preserved/intact (a) and impaired (b). Colour gradient corresponds to negative  $S$  (= log score).

### Results for Clinical Data

Finally, I used risk progression data (opportunistic disease and death) from the SMART study to obtain immune system state distribution parameters, based on the same experimental set-up in terms of sample and simulation size as above with other model settings also left unchanged. Again, for analysis purposes, I considered the 1000 inverse MC samples with the highest values for score  $S$ .

**I(c)** Data points in Figure 7.15 show an aggregation of high scoring value combination for  $\mu$  and  $\sigma$  at a specified region as the simulated data sets. This region appears to be located between those from the former experiments (Figure 7.15, shaded regions I and P) and gives estimates for the mean ( $\mu$ ) of immune system function of between 800 and 1100. The results of the clinical data set appears to be close to those for the simulated data set with impaired immune function (shaded region I), which is not that evident from the comparison shown, (Figure 7.13).

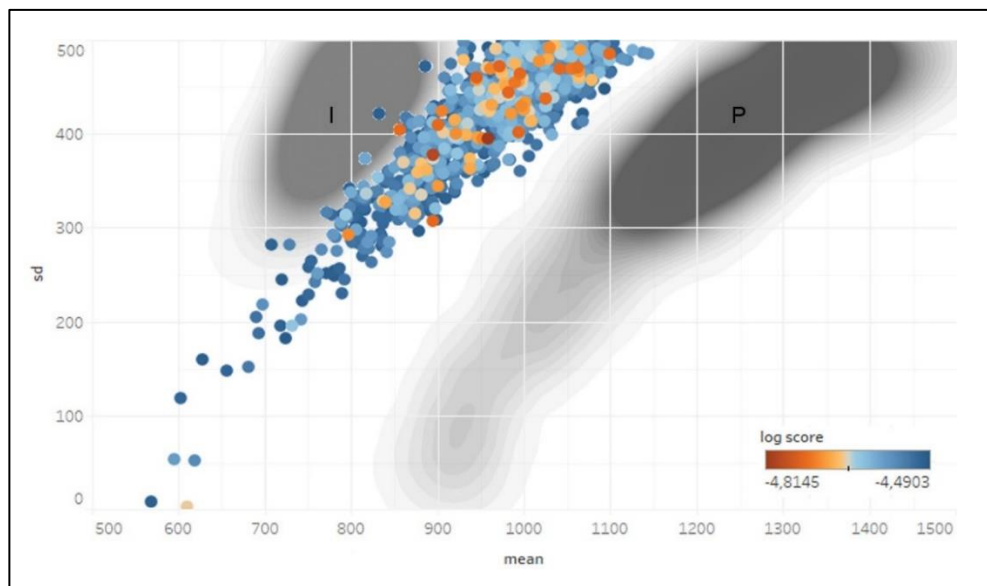


Figure 7.15: **Location of the 1000 MC samples with highest score  $S$  for clinical data from SMART study** (points) in parameter space ( $\mu$  -mean,  $\sigma$  -sd). Colour gradient corresponds to negative  $S$  ( $= \log \text{ score}$ ). Shaded areas show location of data for simulated data sets with immune function impaired (I) and intact/preserved (P).

This agreement of the results of the clinical data set to the simulated data with impaired immune function indicate that pre-existing immune system damage may indeed provide some explanation of observed study outcomes. However, the picture is complicated by large variance ( $\sigma^2$ ) in terms of predictive further analysis. It is noted, however, that the heavy lower tail for  $\mu$  also suggests that the immune function may have been seriously impaired for a sufficiently homogenous group of patients.

The utilisation of an inverse approach illustrates its potential application for analysis of historical data. Although high variability ( $\sigma$ ) does make inferring characteristics of the underlying but unknown patient population challenging. However, the identification of relatively homogeneous subsets in terms of immune system impairment does provide further support in this regard.

## **7.7 Performance Optimisation**

In the previous sections, I used the M-H algorithm to obtain an approximation for the inverse simulations. As stated in section 4.3.2, the algorithm has the advantage of avoiding being trapped in local minima. However, since it explores the parameter space sequentially, a large number of samples might be drawn from parameter space regions with low scores, leading to unnecessary computational cost. In contrast, algorithms such as the Particle Filter (PF, described in detail in section 4.3.2) explore multiple regions in parameter space in parallel (narrowing down to regions with high scores), hence utilisation of computational resources in this way has the potential to be superior. However, due to complexity of the parameter landscape, the performance gain using such a method needs to be weighed against validity of the results obtained. With this in mind, I used an implementation of the PF algorithm to determine parameters of known patient distributions using the same simulated data as in section 7.6.3. Computations were again performed

using the ICHEC resources, to track algorithm performance. Due to the fast convergence of the algorithm, I limited simulation size to 100 steps (for each particle, i.e. set of candidate parameters), corresponding to ~ 15 minutes (wall clock) time for the selected environment<sup>15</sup>. Further, I assessed the influence of the numbers of particles selected by either using 1 (40 particles) or 8 nodes (320 particles) of the cluster in parallel. Results of the inverse simulations for each of the two setups are summarised in Table 7.3 and compared to the ‘true’ values of the simulated data used.

**P(a)** Estimated population means are close to the real value with a less good fit for the data set with ‘preserved’ immune response. These observations are in line with the results of inverse simulations using the M-H algorithm, described in the previous section. Results obtained with the PF algorithm, however, contain less information, since they provide *averages* of the parameter distributions obtained with the M-H algorithm. However, computation costs are greatly reduced with 60 / 4,800 minutes CPU time (for 40 / 320 particles) compared to the M-H algorithm which took about ~29,000 CPU minutes to obtain parameter distributions in sufficient detail.

Table 7.3: Population parameters estimated from inverse simulations using the Particle Filter after 100 steps in comparison to the ‘real’ values used to prepare simulated data. Numbers in brackets denote standard deviations of particle values.

	<b>population</b>	<b>real value</b>	<b>40 particles</b>	<b>320 particles</b>
<b>impaired</b>	Mean	750	695 (23)	701 (28)
	SD	300	344 (29)	352 (34)
<b>preserved</b>	Mean	1200	1338 (29)	1336 (33)
	SD	300	475 (18)	474 (18)

**P(b)** Further, the results for 40 and 320 particles show marked similarity in both estimates for population mean and standard deviations, despite the

---

<sup>15</sup>Cluster ‘Kay’ with 335 nodes in total, each with 2 x 20-core 2.4 GHz Intel Xeon Gold 6148 (Skylake) processors, 192 GB of RAM, 100Gbit OmniPath network adaptor (1.9 Tflops per node).

large difference in computational costs. The diagrams in Figure 7.16 illustrate the distributions of particle clouds for the first 25 steps of the inverse simulations. These data suggest that estimates for the population means close to the final values are already obtained after about 10 simulation steps. The impact of the number of particles on this result appears to be less pronounced. However, the estimation of the population standard deviation appears to benefit more from a larger sample size, (as expected for statistical inference). For the smaller number of particles, the estimate converges to a final value after about 50 steps but is obtained after about 5 steps for the set-up with a higher number of particles.

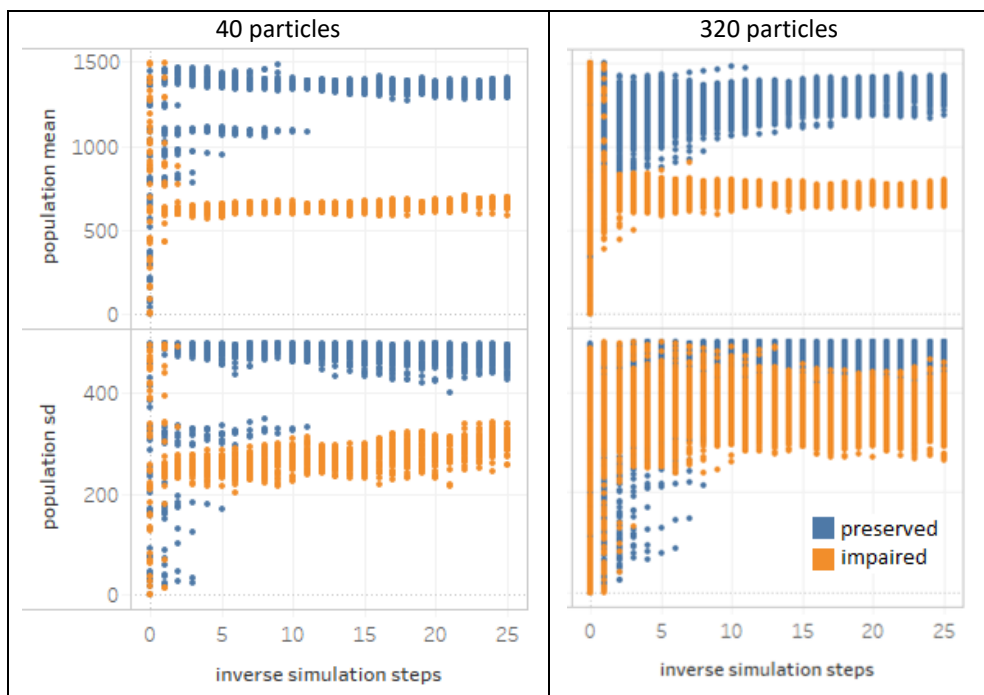


Figure 7.16: **First 25 steps of inverse simulations of Particle Filter algorithm for different particle numbers** with progression of estimates of population parameters for two sets of simulated data (preserved / impaired).

## 7.8 Summary

Clinical trial simulations based on the inverse Monte Carlo method have been shown to demonstrate potential for assessment of HIV structured treatment interruption studies. To this end, I constructed a mechanistic model describing decline and recovery of immune function (and CD4+ counts) under phases of treatment interruption, (where sensitivity analysis also emphasised importance of immune degradation). I have further shown the concept to be useful by comparing model results to clinical risk progression data, (results F(a,b)) and by deriving auxiliary data on immune system function from the SMART clinical trial on HIV structured treatment interruptions, (results I(c)). Validation of the approach is also discussed, (results I(a,b)) as well as practical considerations, such as efficient utilisation of parallel architectures (results P(a,b)).

Results obtained appear to provide some insight on the previously unknown state of immune system impairment for the patient group. While these experiments present a proof of concept model implementation only, inverse clinical trial simulation can be adapted to more complex model forms given suitable data availability.

Some limitations clearly apply: Parameterisation of the ‘inverse clinical trial model’ was obtained from the literature in the absence of other sources. Ideally, these parameters should be obtained via model training with sets of data from diverse clinical sources, which are yet lacking. The present framework may nevertheless be used to derive comparatively safe ranges of immune system degradation and interruption duration, which may stimulate further effort to reduce patient drug burden through structured treatment interruptions.

In methodological terms, population distributions for the ‘trial model’ are assumed Normal, while for STI studies, the Lognormal distribution or other choices appropriate to skewed values might usefully be investigated also.

Further, while the mechanistic model developed for this study is simplistic compared to other existing approaches (such as the LT-model), the present framework offers a valid compromise between realism and computational costs; the latter are non-trivial, given run times needed for coverage of the parameter space.

In summary, while further experimentation is clearly needed, this study has demonstrated the potential of the Inverse Monte Carlo approach for clinical trial simulation and offers a basis for examining the parameter space for clinical outcomes, under the restriction of sparse or incomplete data.

## 8 Conclusions and Further Work

### 8.1 Summary and Conclusions

In this thesis, I describe how computational models may be used to assess the potential harm of HIV treatment interruptions on multiple levels. First, I proposed a Cellular Automata-model to study localised collagen build-up effects in long-term progression of HIV infection in lymphatic tissues under antiretroviral treatment. To construct this novel model, I partly followed established approaches (e.g. (Zorzenon dos Santos and Coutinho, 2001)), incorporating infectivity in stochastic, rather than deterministic, terms and taking into account the neighbourhood of affected cells.

This SCA model permits an in-depth investigation of patterns of treatment interruptions. While preserving a simple rule structure, many effects observed during chronic HIV infection can be reproduced and (indirect) quantification of naïve T-cell populations achieved. For specifications corresponding variously to non-treatment, continuous treatment and interrupted treatment, the results from the model were found to be in line with those obtained from clinical observations.

Furthermore, using a modified version of the SCA model (CM model) which allows for a certain degree of cellular motility, I investigated the contribution of localised effects on the long-term progression of tissue collagenation. Findings indicate a marked contribution of the latter, giving direction to further clinical experiments. Further, the localised effects, observed in the numerical simulation experiments, suggest that infection affects lymphatic tissues through growth of infected cell clusters, (which act as a kind of ‘memory’ during phases of simulated treatment). This aspect of tissue damage acting as a permanent bias against immune recovery is especially interesting since clinical evidence suggests a high degree of inter-relation between tissue damage and immune system fitness, (Zeng et al.,

2012c). However, only limited evidence exists that this feature has been directly considered in mathematical and computational modelling to date, (Bogle and Dunbar, 2012; Donovan and Lythe, 2016).

In terms of the lymphatic tissue damage which is central to my research there have been recent attempts to delay harmful effects of HIV infection by employing a new class of medication in clinical settings. These drugs do not interfere with HIV directly but prevent the scarring of lymphatic tissues. The evidence from recent animal studies, (Estes et al., 2015), suggest that this approach could be a potential additional countermeasure in the arsenal against HIV, and one for which a detailed model could be useful for quantification.

Given controversial results from past clinical studies regarding structured treatment interruptions, I also developed a discrete computational model to analyse study outcomes at population level. Using Inverse Bayesian inference, it was possible to draw conclusions on pre-existing immune system impairment of the study population which was not considered in the original study.

Further clinical studies on the spatial distribution of HIV infection inside specific anatomic regions and tissues could provide valuable data to refine model parametrisation and enable model prediction. Samples obtained from lymphatic tissues originating in distinct parts of the body may provide a better basis for evaluating disease status and prognosis than the blood samples, which are typically used, (although such an invasive technique is an obvious disadvantage where samples are required on a repeated basis).

In terms of treatment initiation and interruption, results suggest that the timing of treatment initiation is crucial in terms of its impact on the tolerance to subsequent interruptions. With respect to these, my results reinforce the clinical view that pre-existing immune system damage needs to be considered more fully than has hitherto been the case, (Hirschel and Flanigan, 2009), in order to assess risk more precisely.

In general, my research shows that a model with simple rules and emphasis on spatial localisation can reproduce a wide range of clinical phenomena associated with HIV and antiretroviral therapy. Ideally, future emphasis in clinical research on these localised effects to provide e.g. better targeted drug delivery may improve therapy protocols and enable further empirical basis for model refinement and feedback.

## 8.2 Future Work

The stochastic model designed for this study can be used to study multiple effects associated with HIV treatment despite its simplicity. However, a model which has a solid foundation in the biology of lymphatic tissue, as exemplified, (Donovan and Lythe, 2016), is clearly desirable. One point to address in such extended studies may be that a Moore neighbourhood in a two-dimensional space allows only a limited view of the three-dimensional network of (real) lymphatic tissues. Moreover, recent clinical evidence employing 2-photon microscopy has shown that T-lymphocytes manifest a high degree of *motility* inside lymphatic tissues, (Mempel et al., 2004) and incorporation of this movement would facilitate more realistic representation. The computational requirements for these refinements would include utilisation of parallelisation methods on modern HPC architectures, for which some guidelines were given. Moreover, while the M-H algorithm is well-known and widely used, alternatives may also provide more efficient approximation, not least as patient drop-out is common in clinical studies. Hence there is a need for the ‘inverse clinical trial model’ to take data censoring more explicitly into account through implementation of more sophisticated algorithms and this is a focus of further experiments.

Further quantification of the dependence of *treatment interruption tolerance* on treatment initiation times is clearly necessary. As stated in the introduction, treatment interruptions are common and evaluation of their

influence in diverse patient populations is vital to deduce measures for healthcare agencies, as well as to support patient respite (so-called ‘drug holidays’). Short-term interruptions appear to have no lasting effects on the immune system capability, (Rothenberger et al., 2015). However, assessing the long-term effects of such breaks could be addressed by my model to determine a margin of error for missed doses, within which interruptions might still be considered as safe. Given that clinical data supporting investigation of this topic have been found to be sparse and largely outdated, (Hillmann et al., 2017a), stochastic generation of synthetic data should also be explored and its reliability evaluated. The potential of such synthetic data will ideally be pursued in future work.

## 9 Bibliography

- Abbas, I., Rovira, J., Casanovas, J., Greenfield, T., 2008. Optimal design of clinical trials with computer simulation based on results of earlier trials, illustrated with a lipodystrophy trial in HIV patients. *J. Biomed. Inform.* 41, 1053–1061. <https://doi.org/10.1016/j.jbi.2008.04.008>
- Acosta, E.P., Wu, H., Hammer, S.M., Yu, S., Kuritzkes, D.R., Walawander, A., Eron, J.J., Fichtenbaum, C.J., Pettinelli, C., Neath, D., Ferguson, E., Saah, A.J., Gerber, J.G., 2004. Comparison of Two Indinavir/Ritonavir Regimens in the Treatment of HIV-Infected Individuals. *JAIDS J. Acquir. Immune Defic. Syndr.* 37, 1358–1366. <https://doi.org/10.1097/00126334-200411010-00004>
- Adams, B.M., Banks, H.T., Kwon, H.-D., Tran, H.T., 2004. Dynamic multidrug therapies for hiv: optimal and sti control approaches. *Math. Biosci. Eng.* 1, 223–241. <https://doi.org/10.3934/mbe.2004.1.223>
- Ager, A., 2017. High Endothelial Venules and Other Blood Vessels: Critical Regulators of Lymphoid Organ Development and Function. *Front. Immunol.* 8, 1–16. <https://doi.org/10.3389/fimmu.2017.00045>
- Ager, A., May, M.J., 2015. Understanding high endothelial venules: Lessons for cancer immunology. *Oncoimmunology* 4, e1008791. <https://doi.org/10.1080/2162402X.2015.1008791>
- Agosto, L.M., Uchil, P.D., Mothes, W., 2015. HIV cell-to-cell transmission: effects on pathogenesis and antiretroviral therapy. *Trends Microbiol.* 23, 289–295. <https://doi.org/10.1016/j.tim.2015.02.003>
- AIDS.gov, 2010. CD4 Count [WWW Document]. URL <http://www.aids.gov/hiv-aids-basics/just-diagnosed-with-hiv-aids/understand-your-test-results/cd4-count/> (accessed 5.11.15).

- AIDS.gov, 2009. Overview of HIV Treatments [WWW Document]. AIDS.gov. URL <http://aids.gov/hiv-aids-basics/just-diagnosed-with-hiv-aids/treatment-options/overview-of-hiv-treatments/> (accessed 5.14.15).
- AIDSinfo, 2019. Clinical guidelines [WWW Document]. URL <https://aidsinfo.nih.gov/guidelines> (accessed 8.31.19).
- Aiuti, F., Mezzaroma, I., 2010. Failure to reconstitute CD4+ T-cells despite suppression of HIV replication under HAART. *AIDS Rev.* 8, 88–97.
- Albert, R., Wang, R.-S., 2009. Discrete dynamic modeling of cellular signaling networks. *Methods Enzymol.* 467, 281–306. [https://doi.org/10.1016/S0076-6879\(09\)67011-7](https://doi.org/10.1016/S0076-6879(09)67011-7)
- Ammassari, A., Murri, R., Pezzotti, P., Trotta, M.P., Ravasio, L., De Longis, P., Lo Caputo, S., Narciso, P., Pauluzzi, S., Carosi, G., Nappa, S., Piano, P., Izzo, C.M., Lichtner, M., Rezza, G., Monforte, A., Ippolito, G., d’Arminio Moroni, M., Wu, A.W., Antinori, A., Group, A.S., 2001. Self-reported symptoms and medication side effects influence adherence to highly active antiretroviral therapy in persons with HIV infection. *J. Acquir. Immune Defic. Syndr.* 28, 445–9.
- Ananworanich, J., Hirschel, B., 2007. Intermittent therapy for the treatment of chronic HIV infection. *AIDS* 21, 123–134. <https://doi.org/10.1097/01.aids.0000256414.91105.8e>
- Anderson, R.M., May, R.M., 1979. Population biology of infectious diseases: Part I. *Nature* 280, 361–367. <https://doi.org/10.1038/280361a0>
- Anderson, R.M., Medley, G.F., May, R.M., Johnson, a. M., 1986. A preliminary study of the transmission dynamics of the Human Immunodeficiency Virus (HIV), the causative agent of AIDS. *Math. Med. Biol.* 3, 229–263. <https://doi.org/10.1093/imammb/3.4.229>

- Appay, V., Sauce, D., 2017. Assessing immune aging in HIV-infected patients. *Virulence* 8, 529–538. <https://doi.org/10.1080/21505594.2016.1195536>
- Arts, E.J., Hazuda, D.J., 2012. HIV-1 Antiretroviral Drug Therapy. *Cold Spring Harb. Perspect. Med.* 2, a007161–a007161. <https://doi.org/10.1101/cshperspect.a007161>
- Attarian, A., Tran, H., 2017. An Optimal Control Approach to Structured Treatment Interruptions for HIV Patients: A Personalized Medicine Perspective. *Appl. Math.* 08, 934–955. <https://doi.org/10.4236/am.2017.87074>
- Bajaria, S.H., Webb, G., Kirschner, D.E., 2004. Predicting differential responses to structured treatment interruptions during HAART. *Bull. Math. Biol.* 66, 1093–1118. <https://doi.org/10.1016/j.bulm.2003.11.003>
- Baldazzi, V., Castiglione, F., Bernaschi, M., 2006. An enhanced agent based model of the immune system response. *Cell. Immunol.* 244, 77–79. <https://doi.org/10.1016/j.cellimm.2006.12.006>
- Barré-Sinoussi, F., Chermann, J.C., Rey, F., Nugeyre, M.T., Chamaret, S., Gruest, J., Dautet, C., Axler-Blin, C., Vézinet-Brun, F., Rouzioux, C., Rozenbaum, W., Montagnier, L., 1983. Isolation of a T-lymphotropic retrovirus from a patient at risk for acquired immune deficiency syndrome (AIDS). *Science* 220, 868–871. <https://doi.org/10.1126/science.6189183>
- Bauer, A.L., Beauchemin, C.A.A., Perelson, A.S., 2009. Agent-based modeling of host–pathogen systems: The successes and challenges. *Inf. Sci. (Ny)*. 179, 1379–1389. <https://doi.org/10.1016/j.ins.2008.11.012>
- Beauchemin, C., 2006. Probing the effects of the well-mixed assumption on viral infection dynamics. *J. Theor. Biol.* 242, 464–477.

<https://doi.org/10.1016/j.jtbi.2006.03.014>

Beltman, J.B., Marée, A.F.M., Lynch, J.N., Miller, M.J., de Boer, R.J., 2007. Lymph node topology dictates T cell migration behavior. *J. Exp. Med.* 204, 771–780. <https://doi.org/10.1084/jem.20061278>

Benson, C.A., 2006. Structured treatment interruptions--new findings. *Top. HIV Med.* 14, 107–11.

Benson, C.A., Vaida, F., Havlir, D. V., Downey, G.F., Lederman, M.M., Gulick, R.M., Glesby, M.J., Wantman, M., Bixby, C.J., Rinehart, A.R., Snyder, S., Wang, R., Patel, S., Mellors, J.W., 2006. A Randomized Trial of Treatment Interruption before Optimized Antiretroviral Therapy for Persons with Drug-Resistant HIV: 48-Week Virologic Results of ACTG A5086. *J. Infect. Dis.* 194, 1309–1318. <https://doi.org/10.1086/508289>

Berryman, A.A., 1992. The Orgins and Evolution of Predator-Prey Theory. *Ecology* 73, 1530–1535. <https://doi.org/10.2307/1940005>

Bianca, C., Pennisi, M., 2012. Immune System Modelling by Top-Down and Bottom-Up Approaches, in: *International Mathematical Forum*. pp. 109–128.

Bocharov, G., Novkovic, M., Onder, L., Kislitsyn, A., Savinkov, R., 2015. Modelling the FRC network of lymph node, in: *2015 International Workshop on Artificial Immune Systems (AIS)*. IEEE, Taormina, Italy, pp. 1–2. <https://doi.org/10.1109/AISW.2015.7469235>

Bogle, G., Dunbar, P.R., 2012. On-Lattice Simulation of T Cell Motility, Chemotaxis, and Trafficking in the Lymph Node Paracortex. *PLoS One* 7, e45258. <https://doi.org/10.1371/journal.pone.0045258>

Bonhoeffer, S., May, R.M., Shaw, G.M., Nowak, M.A., 1997. *Virus*

- dynamics and drug therapy. *Proc. Natl. Acad. Sci. U. S. A.* 94, 6971–6976. <https://doi.org/10.1073/pnas.94.13.6971>
- Braithwaite, R.S., Justice, A.C., Chang, C.-C.H., Fusco, J.S., Raffanti, S.R., Wong, J.B., Roberts, M.S., 2005. Estimating the proportion of patients infected with HIV who will die of comorbid diseases. *Am. J. Med.* 118, 890–898. <https://doi.org/10.1016/j.amjmed.2004.12.034>
- Braithwaite, R.S., Shechter, S., Chang, C.C.H., Schaefer, A., Roberts, M.S., 2007. Estimating the rate of accumulating drug resistance mutations in the HIV genome. *Value Heal.* 10, 204–213. <https://doi.org/10.1111/j.1524-4733.2007.00170.x>
- Breban, R., Blower, S., 2006. Role of parametric resonance in virological failure during HIV treatment interruption therapy. *Lancet* 367, 1285–1289. [https://doi.org/10.1016/S0140-6736\(06\)68543-7](https://doi.org/10.1016/S0140-6736(06)68543-7)
- Brenchley, J.M., Schacker, T.W., Ruff, L.E., Price, D.A., Taylor, J.H., Beilman, G.J., Nguyen, P.L., Khoruts, A., Larson, M., Haase, A.T., Douek, D.C., 2004. CD4+ T cell depletion during all stages of HIV disease occurs predominantly in the gastrointestinal tract. *J. Exp. Med.* 200, 749–59. <https://doi.org/10.1084/jem.20040874>
- Broder, S., 2010. The development of antiretroviral therapy and its impact on the HIV-1/AIDS pandemic. *Antiviral Res.* 85, 1–18. <https://doi.org/10.1016/j.antiviral.2009.10.002>
- Brown, F.D., Turley, S.J., 2015. Fibroblastic Reticular Cells: Organization and Regulation of the T Lymphocyte Life Cycle. *J. Immunol.* 194, 1389–1394. <https://doi.org/10.4049/jimmunol.1402520>
- Burns, J., Ruskin, H.J., 2004. Diversity emergence and dynamics during primary immune response: A shape space, physical space model. *Theory Biosci.* 123, 181–193. <https://doi.org/10.1016/j.thbio.2004.05.001>

- Butcher, J.C., 1996. A history of Runge-Kutta methods. *Appl. Numer. Math.* 20, 247–260. [https://doi.org/10.1016/0168-9274\(95\)00108-5](https://doi.org/10.1016/0168-9274(95)00108-5)
- Buzon, M.J., Martin-Gayo, E., Pereyra, F., Ouyang, Z., Sun, H., Li, J.Z., Piovoso, M., Shaw, A., Dalmau, J., Zangger, N., Martinez-Picado, J., Zurakowski, R., Yu, X.G., Telenti, A., Walker, B.D., Rosenberg, E.S., Lichterfeld, M., 2014. Long-term Antiretroviral Treatment Initiated in Primary HIV-1 Infection Affects the Size, Composition and Decay Kinetics of the Reservoir of HIV-1 Infected CD4 T Cells. *J. Virol.* 88, 10056–10065. <https://doi.org/10.1128/JVI.01046-14>
- Cambiano, V., Bertagnolio, S., Jordan, M.R., Lundgren, J.D., Phillips, A., 2013. Transmission of Drug Resistant HIV and Its Potential Impact on Mortality and Treatment Outcomes in Resource-Limited Settings. *J. Infect. Dis.* 207, S57–S62. <https://doi.org/10.1093/infdis/jit111>
- Cardner, M., 1971. Mathematical Games. *Sci. Am.* 224, 112–117. <https://doi.org/10.1038/scientificamerican0271-112>
- Carneiro, J., Stewart, J., 1994. Rethinking “Shape Space”: Evidence from Simulated Docking Suggests that Steric Shape Complementarity is not Limiting for Antibody--Antigen Recognition and Idiotypic Interactions. *J. Theor. Biol.* 169, 391–402. <https://doi.org/10.1006/jtbi.1994.1161>
- Castiglione, F., Celada, F., 2015. Immune System Modelling and Simulation, Immune System Modelling and Simulation. CRC Press. <https://doi.org/10.1201/b18274>
- Castiglione, F., Ghersi, D., Celada, F., 2019. Computer modeling of clonal dominance: Memory-anti-naïve and its curbing by attrition. *Front. Immunol.* 10, 1–12. <https://doi.org/10.3389/fimmu.2019.01513>
- Castiglione, F., Pappalardo, F., Bernaschi, M., Motta, S., 2007. Optimization of HAART with genetic algorithms and agent-based models of HIV

- infection. *Bioinformatics* 23, 3350–3355.  
<https://doi.org/10.1093/bioinformatics/btm408>
- Castiglione, F., Pappalardo, F., Bianca, C., Russo, G., Motta, S., 2014. Modeling Biology Spanning Different Scales: An Open Challenge. *Biomed Res. Int.* 2014, 1–9. <https://doi.org/10.1155/2014/902545>
- Castro, M., Lythe, G., Molina-París, C., Ribeiro, R.M., 2016. Mathematics in modern immunology. *Interface Focus* 6, 20150093. <https://doi.org/10.1098/rsfs.2015.0093>
- Cavert, W., Notermans, D.W., Staskus, K., Wietgreffe, S.W., Zupancic, M., Gebhard, K., Henry, K., Zhang, Z.Q., Mills, R., McDade, H., Schuwirth, C.M., Goudsmit, J., Danner, S.A., Haase, A.T., 1997. Kinetics of response in lymphoid tissues to antiretroviral therapy of HIV-1 infection. *Science* 276, 960–4. <https://doi.org/10.1126/science.276.5314.960>
- Celada, F., Seiden, P.E., 1992. A computer model of cellular interactions in the immune system. *Immunol. Today* 13, 56–62. [https://doi.org/10.1016/0167-5699\(92\)90135-T](https://doi.org/10.1016/0167-5699(92)90135-T)
- Chakrabarti, L., Guyader, M., Alizon, M., Daniel, M.D., Desrosiers, R.C., Tiollais, P., Sonigo, P., 1987. Sequence of simian immunodeficiency virus from macaque and its relationship to other human and simian retroviruses. *Nature* 328, 543–547. <https://doi.org/10.1038/328543a0>
- Chaouiya, C., 2007. Petri net modelling of biological networks. *Brief. Bioinform.* 8, 210–219. <https://doi.org/10.1093/bib/bbm029>
- Chevalier, M.F., Weiss, L., 2013. The split personality of regulatory T cells in HIV infection. *Blood* 121, 29–37. <https://doi.org/10.1182/blood-2012-07-409755>

- Chomont, N., El-Far, M., Ancuta, P., Trautmann, L., Procopio, F. a, Yassine-Diab, B., Boucher, G., Boulassel, M.-R., Ghattas, G., Brenchley, J.M., Schacker, T.W., Hill, B.J., Douek, D.C., Routy, J.-P., Haddad, E.K., Sékaly, R.-P., 2009. HIV reservoir size and persistence are driven by T cell survival and homeostatic proliferation. *Nat. Med.* 15, 893–900. <https://doi.org/10.1038/nm.1972>
- Cohen, J., 2014. HIV resurfaces in “Mississippi baby” many presumed cured [WWW Document]. *Sci. News.* URL <http://news.sciencemag.org/biology/2014/07/hiv-resurfaces-mississippi-baby-many-presumed-cured> (accessed 8.21.15).
- Cohen, J., 2011. Tissue Says Blood Is Misleading, Confusing HIV Cure Efforts. *Science* (80- ). 334, 1614–1614. <https://doi.org/10.1126/science.334.6063.1614>
- Conway, J.M., Perelson, A.S., 2015. Post-treatment control of HIV infection. *Proc. Natl. Acad. Sci.* 112, 5467–5472. <https://doi.org/10.1073/pnas.1419162112>
- Conway, J.M., Perelson, A.S., Li, J.Z., 2019. Predictions of time to HIV viral rebound following ART suspension that incorporate personal biomarkers. *PLOS Comput. Biol.* 15, e1007229. <https://doi.org/10.1371/journal.pcbi.1007229>
- Corbeau, P., Reynes, J., 2011. Immune reconstitution under antiretroviral therapy: the new challenge in HIV-1 infection. *Blood* 117, 5582–5590. <https://doi.org/10.1182/blood-2010-12-322453>
- Corne, D.W., Frisco, P., 2008. Dynamics of HIV infection studied with cellular automata and conformon-P systems. *BioSystems* 91, 531–544. <https://doi.org/10.1016/j.biosystems.2007.01.007>
- Cory, T.J., Schacker, T.W., Stevenson, M., Fletcher, C. V, 2013. Overcoming

- pharmacologic sanctuaries. *Curr. Opin. HIV AIDS* 8, 190–5. <https://doi.org/10.1097/COH.0b013e32835fc68a>
- Coutinho, R.A., 1998. The Amsterdam Cohort Studies on HIV Infection and AIDS. *J. Acquir. Immune Defic. Syndr. Hum. Retrovirology* 17, S4–S8. <https://doi.org/10.1097/00042560-199801001-00003>
- Cramer, J.S., 2002. The Origins of Logistic Regression, *SSRN Electronic Journal*. <https://doi.org/10.2139/ssrn.360300>
- Cuadros, D.F., Abu-Raddad, L.J., Awad, S.F., García-Ramos, G., 2014. Use of agent-based simulations to design and interpret HIV clinical trials. *Comput. Biol. Med.* 50, 1–8. <https://doi.org/10.1016/j.combiomed.2014.03.008>
- Dandekar, S., 2007. Pathogenesis of HIV in the gastrointestinal tract. *Curr. HIV/AIDS Rep.* 4, 10–15. <https://doi.org/10.1007/s11904-007-0002-0>
- Davey, R.T., Bhat, N., Yoder, C., Chun, T.W., Metcalf, J.A., Dewar, R., Natarajan, V., Lempicki, R.A., Adelsberger, J.W., Miller, K.D., Kovacs, J.A., Polis, M.A., Walker, R.E., Falloon, J., Masur, H., Gee, D., Baseler, M., Dimitrov, D.S., Fauci, A.S., Lane, H.C., 1999. HIV-1 and T cell dynamics after interruption of highly active antiretroviral therapy (HAART) in patients with a history of sustained viral suppression. *Proc. Natl. Acad. Sci. U. S. A.* 96, 15109–15114. <https://doi.org/10.1073/pnas.96.26.15109>
- Dayan, I., Stauffer, D., Havlin, S., 1988. Cellular automata generalisation of the Weisbuch-Atlan model for immune response. *J. Phys. A. Math. Gen.* 21, 2473–2476. <https://doi.org/10.1088/0305-4470/21/10/023>
- de Korte, a C.J., Brouwers, H.J.H., 2013. A cellular automata approach to chemical reactions : 1 reaction controlled systems. *Chem. Eng. J.* 228, 172–178. <https://doi.org/http://dx.doi.org/10.1016/j.cej.2013.04.084>

- Diaz, J., Muñoz-Caro, C., Niño, A., 2012. A survey of parallel programming models and tools in the multi and many-core era. *IEEE Trans. Parallel Distrib. Syst.* 23, 1369–1386. <https://doi.org/10.1109/TPDS.2011.308>
- Dimopoulos, Y., Moysi, E., Petrovas, C., 2017. The Lymph Node in HIV Pathogenesis. *Curr. HIV/AIDS Rep.* 14, 133–140. <https://doi.org/10.1007/s11904-017-0359-7>
- Dixit, N.M., Perelson, A.S., 2004. Complex patterns of viral load decay under antiretroviral therapy: Influence of pharmacokinetics and intracellular delay. *J. Theor. Biol.* 226, 95–109. <https://doi.org/10.1016/j.jtbi.2003.09.002>
- Doitsh, G., Galloway, N.L.K., Geng, X., Yang, Z., Monroe, K.M., Zepeda, O., Hunt, P.W., Hatano, H., Sowinski, S., Muñoz-Arias, I., Greene, W.C., 2013. Cell death by pyroptosis drives CD4 T-cell depletion in HIV-1 infection. *Nature* 505, 509–514. <https://doi.org/10.1038/nature12940>
- Donovan, G.M., Lythe, G., 2016. T cell and reticular network co-dependence in HIV infection. *J. Theor. Biol.* 395, 211–220. <https://doi.org/10.1016/j.jtbi.2016.01.040>
- Donovan, G.M., Lythe, G., 2012. T-cell movement on the reticular network. *J. Theor. Biol.* 295, 59–67. <https://doi.org/10.1016/j.jtbi.2011.11.001>
- Doucet, A., de Freitas, N., Gordon, N., 2001. An Introduction to Sequential Monte Carlo Methods, in: Doucet, A., Freitas, N., Gordon, N. (Eds.), *Sequential Monte Carlo Methods in Practice*. Springer New York, New York, NY, pp. 3–14. <https://doi.org/10.1007/978-1-4757-3437-9>
- Dubé, K., Evans, D., Dee, L., Sylla, L., Taylor, J., Skinner, A., Weiner, B.J., Greene, S.B., Rennie, S., Tucker, J.D., 2018. “We Need to Deploy Them Very Thoughtfully and Carefully”: Perceptions of Analytical Treatment

Interruptions in HIV Cure Research in the United States—A Qualitative Inquiry. *AIDS Res. Hum. Retroviruses* 34, 67–79. <https://doi.org/10.1089/aid.2017.0067>

Duprez, D.A., Neuhaus, J., Kuller, L.H., Tracy, R., Belloso, W., De Wit, S., Drummond, F., Lane, H.C., Ledergerber, B., Lundgren, J., Nixon, D., Paton, N.I., Prineas, R.J., 2012. Inflammation, Coagulation and Cardiovascular Disease in HIV-Infected Individuals. *PLoS One* 7, e44454. <https://doi.org/10.1371/journal.pone.0044454>

Dybul, M., Chun, T.W., Yoder, C., Hidalgo, B., Belson, M., Hertogs, K., Larder, B., Dewar, R.L., Fox, C.H., Hallahan, C.W., Justement, J.S., Migueles, S.A., Metcalf, J.A., Davey, R.T., Daucher, M., Pandya, P., Baseler, M., Ward, D.J., Fauci, A.S., 2001. Short-cycle structured intermittent treatment of chronic HIV infection with highly active antiretroviral therapy: effects on virologic, immunologic, and toxicity parameters. *Proc. Natl. Acad. Sci. U. S. A.* 98, 15161–6. <https://doi.org/10.1073/pnas.261568398>

Dybul, M., Nies-Kraske, E., Daucher, M., Hertogs, K., Hallahan, C.W., Csako, G., Yoder, C., Ehler, L., Sklar, P.A., Belson, M., Hidalgo, B., Metcalf, J.A., Davey, R.T., Rock Kress, D.M., Powers, A., Fauci, A.S., 2003. Long-cycle structured intermittent versus continuous highly active antiretroviral therapy for the treatment of chronic infection with human immunodeficiency virus: effects on drug toxicity and on immunologic and virologic parameters. *J. Infect. Dis.* 188, 388–96. <https://doi.org/10.1086/376535>

El-Sadr, W.M., Lundgren, J.D., Neaton, J.D., Gordin, F., Abrams, D., Arduino, R.C., Babiker, A., Burman, W., Clumeck, N., Cohen, C.J., Cohn, D., Cooper, D., Darbyshire, J., Emery, S., Fätkenheuer, G., Gazzard, B., Grund, B., Hoy, J., Klingman, K., Losso, M., Markowitz,

- N., Neuhaus, J., Phillips, A., Rappoport, C., 2006. CD4+ Count–Guided Interruption of Antiretroviral Treatment. *N. Engl. J. Med.* 355, 2283–2296. <https://doi.org/10.1056/NEJMoa062360>
- Emami, J., 2006. In vitro - in vivo correlation: from theory to applications. *J. Pharm. Pharm. Sci.* 9, 169–89.
- Ernst, D., Stan, G.-B., Goncalves, J., Wehenkel, L., 2006. Clinical data based optimal STI strategies for HIV: a reinforcement learning approach, in: *Proceedings of the 45th IEEE Conference on Decision and Control*. IEEE, San Diego, CA, USA, pp. 667–672. <https://doi.org/10.1109/CDC.2006.377527>
- Estes, J.D., 2013. Pathobiology of HIV/SIV-associated changes in secondary lymphoid tissues. *Immunol. Rev.* 254, 65–77. <https://doi.org/10.1111/imr.12070>
- Estes, J.D., Reilly, C., Trubey, C.M., Fletcher, C. V., Cory, T.J., Piatak, M., Russ, S., Anderson, J., Reimann, T.G., Star, R., Smith, A., Tracy, R.P., Berglund, A., Schmidt, T., Coalter, V., Chertova, E., Smedley, J., Haase, A.T., Lifson, J.D., Schacker, T.W., 2015. Antifibrotic Therapy in Simian Immunodeficiency Virus Infection Preserves CD4+ T-Cell Populations and Improves Immune Reconstitution With Antiretroviral Therapy. *J. Infect. Dis.* 211, 744–754. <https://doi.org/10.1093/infdis/jiu519>
- European AIDS Clinical Society, 2014. European Guidelines for treatment of HIV-infected adults in Europe [WWW Document]. Eacsociety.Org. URL [http://www.eacsociety.org/files/guidelines\\_english\\_71\\_141204.pdf](http://www.eacsociety.org/files/guidelines_english_71_141204.pdf) (accessed 1.19.15).
- Fackler, O.T., Murooka, T.T., Imle, A., Mempel, T.R., 2014. Adding new dimensions: towards an integrative understanding of HIV-1 spread. *Nat.*

Rev. Microbiol. 12, 563–574. <https://doi.org/10.1038/nrmicro3309>

Fagard, C., Oxenius, A., Günthard, H., Garcia, F., Le Braz, M., Mestre, G., Battegay, M., Furrer, H., Vernazza, P., Bernasconi, E., Telenti, A., Weber, R., Leduc, D., Yerly, S., Price, D., Dawson, S.J., Klimkait, T., Perneger, T. V, McLean, A., Clotet, B., Gatell, J.M., Perrin, L., Plana, M., Phillips, R., Hirschel, B., 2003. A prospective trial of structured treatment interruptions in human immunodeficiency virus infection. *Arch. Intern. Med.* 163, 1220–1226. <https://doi.org/10.1001/archinte.163.10.1220>

Fagiolo, G., Guerini, M., Lamperti, F., Moneta, A., Roventini, A., 2019. Validation of Agent-Based Models in Economics and Finance, in: Beisbart, C., Saam, N. (Eds.), *Computer Simulation Validation*. Springer Cham, pp. 763–787. [https://doi.org/10.1007/978-3-319-70766-2\\_31](https://doi.org/10.1007/978-3-319-70766-2_31)

Falster, K., Petoumenos, K., Chuah, J., Mijch, A., Mulhall, B., Kelly, M., Cooper, D.A., 2009. Poor Baseline Immune Function Predicts an Incomplete Immune Response to Combination Antiretroviral Treatment Despite Sustained Viral Suppression. *JAIDS J. Acquir. Immune Defic. Syndr.* 50, 307–313. <https://doi.org/10.1097/QAI.0b013e3181945ed4>

Fauci, A.S., Lane, H.C., 2020. Four Decades of HIV/AIDS — Much Accomplished, Much to Do. *N. Engl. J. Med.* 383, 1–4. <https://doi.org/10.1056/NEJMp1916753>

Fauci, A.S., Pantaleo, G., Stanley, S., Weissman, D., 1996. Immunopathogenic mechanisms of HIV infection. *Ann. Intern. Med.* 124, 654–663. [https://doi.org/10.1016/0090-1229\(89\)90122-0](https://doi.org/10.1016/0090-1229(89)90122-0)

FDA, 2013. Antiretroviral drugs used in the treatment of HIV infection [WWW Document]. [fda.gov. URL http://www.fda.gov/ForConsumers/ByAudience/ForPatientAdvocates/](http://www.fda.gov/ForConsumers/ByAudience/ForPatientAdvocates/)

HIVandAIDSActivities/ucm118915.htm (accessed 1.18.14).

Feng, C., Wang, H., Lu, N., Tu, X.M., 2013. Log transformation: application and interpretation in biomedical research. *Stat. Med.* 32, 230–239. <https://doi.org/10.1002/sim.5486>

Ferreira, J., Hernandez-Vargas, E. a., Middleton, R.H., 2011. Computer simulation of structured treatment interruption for HIV infection. *Comput. Methods Programs Biomed.* 104, 50–61. <https://doi.org/10.1016/j.cmpb.2011.07.011>

Fidler, S., Porter, K., Ewings, F., Frater, J., Ramjee, G., Cooper, D., Rees, H., Fisher, M., Schechter, M., Kaleebu, P., Tambussi, G., Kinloch, S., Miro, J.M., Kelleher, A., McClure, M., Kaye, S., Gabriel, M., Phillips, R., Weber, J., Babiker, A., Investigators, T.S.T., 2013. Short-Course Antiretroviral Therapy in Primary HIV Infection. *N. Engl. J. Med.* 368, 207–217. <https://doi.org/10.1056/NEJMoa1110039>

Fiebig, E.W., Wright, D.J., Rawal, B.D., Garrett, P.E., Schumacher, R.T., Peddada, L., Heldebrant, C., Smith, R., Conrad, A., Kleinman, S.H., Busch, M.P., 2003. Dynamics of HIV viremia and antibody seroconversion in plasma donors: implications for diagnosis and staging of primary HIV infection. *AIDS* 17, 1871–1879. <https://doi.org/10.1097/00002030-200309050-00005>

Fischer, M., Hafner, R., Schneider, C., Trkola, A., Joos, B., Joller, H., Hirschel, B., Weber, R., Günthard, H.F., 2003. HIV RNA in plasma rebounds within days during structured treatment interruptions. *Aids* 17, 195–199. <https://doi.org/10.1097/00002030-200301240-00009>

Fletcher, A.L., Acton, S.E., Knoblich, K., 2015. Lymph node fibroblastic reticular cells in health and disease. *Nat. Rev. Immunol.* 15, 350–361. <https://doi.org/10.1038/nri3846>

- Fletcher, C. V, Staskus, K., Wietgreffe, S.W., Rothenberger, M., Reilly, C., Chipman, J.G., Beilman, G.J., Khoruts, A., Thorkelson, A., Schmidt, T.E., Anderson, J., Perkey, K., Stevenson, M., Perelson, A.S., Douek, D.C., Haase, A.T., Schacker, T.W., 2014. Persistent HIV-1 replication is associated with lower antiretroviral drug concentrations in lymphatic tissues. *Proc. Natl. Acad. Sci. U. S. A.* 111, 2307–12. <https://doi.org/10.1073/pnas.1318249111>
- Frisco, P., 2004. The conformon-P system: A molecular and cell biology-inspired computability model. *Theor. Comput. Sci.* 312, 295–319. <https://doi.org/10.1016/j.tcs.2003.09.008>
- Gallo, R., Sarin, P., Gelmann, E., Robert-Guroff, M., Richardson, E., Kalyanaraman, V., Mann, D., Sidhu, G., Stahl, R., Zolla-Pazner, S., Leibowitch, J., Popovic, M., 1983. Isolation of human T-cell leukemia virus in acquired immune deficiency syndrome (AIDS). *Science* (80- ). 220, 865–867. <https://doi.org/10.1126/science.6601823>
- Ganeshalingam, S., Koh, D.-M., 2009. Nodal staging. *Cancer Imaging* 9, 104–111. <https://doi.org/10.1102/1470-7330.2009.0017>
- Ganusov, V. V., Auerbach, J., 2014. Mathematical Modeling Reveals Kinetics of Lymphocyte Recirculation in the Whole Organism. *PLoS Comput. Biol.* 10, e1003586. <https://doi.org/10.1371/journal.pcbi.1003586>
- García, F., Plana, M., Ortiz, G.M., Bonhoeffer, S., Soriano, A., Vidal, C., Cruceta, A., Arnedo, M., Gil, C., Pantaleo, G., Pumarola, T., Gallart, T., Nixon, D.F., Miró, J.M., Gatell, J.M., 2001. The virological and immunological consequences of structured treatment interruptions in chronic HIV-1 infection. *AIDS* 15, F29–F40. <https://doi.org/10.1097/00002030-200106150-00002>

- Germain, R.N., Robey, E.A., Cahalan, M.D., 2012. A Decade of Imaging Cellular Motility and Interaction Dynamics in the Immune System. *Science* (80- ). 336, 1676–1681. <https://doi.org/10.1126/science.1221063>
- Gillespie, D.T., 2007. Stochastic simulation of chemical kinetics. *Annu. Rev. Phys. Chem.* 58, 35–55. <https://doi.org/10.1146/annurev.physchem.58.032806.104637>
- Gillespie, D.T., 1976. A general method for numerically simulating the stochastic time evolution of coupled chemical reactions. *J. Comput. Phys.* 22, 403–434. [https://doi.org/10.1016/0021-9991\(76\)90041-3](https://doi.org/10.1016/0021-9991(76)90041-3)
- Glass, T.R., Battegay, M., Cavassini, M., De Geest, S., Furrer, H., Vernazza, P.L., Hirschel, B., Bernasconi, E., Rickenbach, M., Günthard, H.F., Bucher, H.C., 2010. Longitudinal Analysis of Patterns and Predictors of Changes in Self-Reported Adherence to Antiretroviral Therapy: Swiss HIV Cohort Study. *JAIDS J. Acquir. Immune Defic. Syndr.* 54, 197–203. <https://doi.org/10.1097/QAI.0b013e3181ca48bf>
- Glass, T.R., Cavassini, M., 2014. Asking about adherence - from flipping the coin to strong evidence. *Swiss Med. Wkly.* 144, w14016. <https://doi.org/10.4414/smw.2014.14016>
- González, R.E.R., Coutinho, S., Zorzenon dos Santos, R.M., de Figueirêdo, P.H., 2013a. Dynamics of the HIV infection under antiretroviral therapy: A cellular automata approach. *Phys. A Stat. Mech. its Appl.* 392, 4701–4716. <https://doi.org/10.1016/j.physa.2013.05.056>
- González, R.E.R., De Figueirêdo, P.H., Coutinho, S., 2013b. Cellular automata approach for the dynamics of HIV infection under antiretroviral therapies: The role of the virus diffusion. *Phys. A Stat. Mech. its Appl.* 392, 4717–4725.

<https://doi.org/10.1016/j.physa.2012.10.036>

Goujard, C., Emilie, D., Roussillon, C., Godot, V., Rouzioux, C., Venet, A., Colin, C., Pialoux, G., Girard, P.-M., Boilet, V., Chaix, M.-L., Galanaud, P., Chene, G., 2012. Continuous versus intermittent treatment strategies during primary HIV-1 infection. *AIDS* 26, 1895–1905. <https://doi.org/10.1097/QAD.0b013e32835844d9>

Graner, F., Glazier, J. a., 1992. Simulation of biological cell sorting using a two-dimensional extended Potts model. *Phys. Rev. Lett.* 69, 2013–2016. <https://doi.org/10.1103/PhysRevLett.69.2013>

Gratie, D.-E., Iancu, B., Petre, I., 2013. ODE Analysis of Biological Systems, in: Bernardo, M., de Vink, E., Di Pierro, A., Wiklicky, H. (Eds.), *Formal Methods for Dynamical Systems: 13th International School on Formal Methods for the Design of Computer, Communication, and Software Systems, SFM 2013, Bertinoro, Italy, June 17-22, 2013. Advanced Lectures*. Springer Berlin Heidelberg, Berlin, Heidelberg, pp. 29–62. [https://doi.org/10.1007/978-3-642-38874-3\\_2](https://doi.org/10.1007/978-3-642-38874-3_2)

Graw, F., Perelson, A.S., 2013. Spatial Aspects of HIV Infection, in: Ledzewicz, U., Schättler, H., Friedman, A., Kashdan, E. (Eds.), *Mathematical Methods and Models in Biomedicine, Lecture Notes on Mathematical Modelling in the Life Sciences*. Springer New York, New York, NY, pp. 3–31. [https://doi.org/10.1007/978-1-4614-4178-6\\_1](https://doi.org/10.1007/978-1-4614-4178-6_1)

Graw, F., Regoes, R.R., 2012. Influence of the Fibroblastic Reticular Network on Cell-Cell Interactions in Lymphoid Organs. *PLoS Comput. Biol.* 8, e1002436. <https://doi.org/10.1371/journal.pcbi.1002436>

Greenough, T.C., Brettler, D.B., Kirchhoff, F., Alexander, L., Desrosiers, R.C., O'Brien, S.J., Somasundaran, M., Luzuriaga, K., Sullivan, J.L., 1999. Long-Term Nonprogressive Infection with Human

- Immunodeficiency Virus Type 1 in a Hemophilia Cohort. *J. Infect. Dis.* 180, 1790–1802. <https://doi.org/10.1086/315128>
- Grijzen, M.L., Wit, F.W.N.M., Jurriaans, S., Kroon, F.P., Schippers, E.F., Koopmans, P., Gras, L., Lange, J.M. a, Prins, J.M., 2014. Temporary Treatment during Primary HIV Infection Does Not Affect Virologic Response to Subsequent Long-Term Treatment. *PLoS One* 9, e89639. <https://doi.org/10.1371/journal.pone.0089639>
- Grilo, A., Caetano, A., Rosa, A., 2002. Immune System Simulation through a Complex Adaptive System Model, in: *Soft Computing and Industry*. Springer London, London, pp. 675–698. [https://doi.org/10.1007/978-1-4471-0123-9\\_57](https://doi.org/10.1007/978-1-4471-0123-9_57)
- Gruenert, G., Ibrahim, B., Lenser, T., Lohel, M., Hinze, T., Dittrich, P., 2010. Rule-based spatial modeling with diffusing, geometrically constrained molecules. *BMC Bioinformatics* 11, 307. <https://doi.org/10.1186/1471-2105-11-307>
- Günthard, H.F., Aberg, J. a, Eron, J.J., Hoy, J.F., Telenti, A., Benson, C.A., Burger, D.M., Cahn, P., Gallant, J.E., Glesby, M.J., Reiss, P., Saag, M.S., Thomas, D.L., Jacobsen, D.M., Volberding, P. a, 2014. Antiretroviral Treatment of Adult HIV Infection. *JAMA* 312, 410. <https://doi.org/10.1001/jama.2014.8722>
- Haase, A.T., 1999. Population biology of HIV-1 infection: viral and CD4+ T cell demographics and dynamics in lymphatic tissues. *Annu. Rev. Immunol.* 17, 625–56. <https://doi.org/10.1146/annurev.immunol.17.1.625>
- Haase, A.T., Henry, K., Zupancic, M., Sedgewick, G., Faust, R.A., Melroe, H., Cavert, W., Gebhard, K., Staskus, K., Zhang, Z.Q., Dailey, P.J., Balfour, H.H., Erice, A., Perelson, A.S., 1996. Quantitative image

analysis of HIV-1 infection in lymphoid tissue. *Science* 274, 985–9.

Haines, R., Corne, D., 2006. Evolving Novel and Effective Treatment Plans in the context of Infection Dynamics Models: Illustrated with HIV and HAART Therapy, in: Runarsson, T.P., Beyer, H.-G., Burke, E., Merelo-Guervós, J.J., Whitley, L.D., Yao, X. (Eds.), *Parallel Problem Solving from Nature-PPSN IX, Lecture Notes in Computer Science*. Springer Berlin Heidelberg, Berlin, Heidelberg, pp. 413–422. <https://doi.org/10.1007/978-3-319-10762-2>

Halling-Brown, M., Pappalardo, F., Rapin, N., Zhang, P., Alemani, D., Emerson, A., Castiglione, F., Duroux, P., Pennisi, M., Miotto, O., Churchill, D., Rossi, E., Moss, D.S., Sansom, C.E., Bernaschi, M., Lefranc, M.-P., Brunak, S., Lund, O., Motta, S., Lollini, P.-L., Murgo, A., Palladini, A., Basford, K.E., Brusica, V., Shepherd, A.J., 2010. ImmunoGrid: towards agent-based simulations of the human immune system at a natural scale. *Philos. Trans. A. Math. Phys. Eng. Sci.* 368, 2799–2815. <https://doi.org/10.1098/rsta.2010.0067>

Hammer, S.M., Squires, K.E., Hughes, M.D., Grimes, J.M., Demeter, L.M., Currier, J.S., Eron, J.J., Feinberg, J.E., Balfour, H.H., Deyton, L.R., Chodakewitz, J.A., Fischl, M.A., Phair, J.P., Pedneault, L., Nguyen, B.-Y., Cook, J.C., 1997. A Controlled Trial of Two Nucleoside Analogues plus Indinavir in Persons with Human Immunodeficiency Virus Infection and CD4 Cell Counts of 200 per Cubic Millimeter or Less. *N. Engl. J. Med.* 337, 725–733. <https://doi.org/10.1056/NEJM199709113371101>

Hammer, S.M., Vaida, F., Bennett, K.K., Holohan, M.K., Sheiner, L., Eron, J.J., Wheat, L.J., Mitsuyasu, R.T., Gulick, R.M., Valentine, F.T., Aberg, J.A., Rogers, M.D., Karol, C.N., Saah, A.J., Lewis, R.H., Bessen, L.J., Brosgart, C., DeGruttola, V., Mellors, J.W., AIDS Clinical Trials Group

- 398 Study Team, 2002. Dual vs single protease inhibitor therapy following antiretroviral treatment failure: a randomized trial. *JAMA* 288, 169–80.
- Harel, D., 1988. On visual formalisms. *Commun. ACM* 31, 514–530. <https://doi.org/10.1145/42411.42414>
- Harel, D., 1987. Statecharts: a visual formalism for complex systems. *Sci. Comput. Program.* 8, 231–274. [https://doi.org/10.1016/0167-6423\(87\)90035-9](https://doi.org/10.1016/0167-6423(87)90035-9)
- Hasenkrug, K.J., Chougnat, C.A., Dittmer, U., 2018. Regulatory T cells in retroviral infections. *PLOS Pathog.* 14, e1006776. <https://doi.org/10.1371/journal.ppat.1006776>
- Hastings, W.K., 1970. Monte Carlo sampling methods using Markov chains and their applications. *Biometrika* 57, 97–109. <https://doi.org/10.1093/biomet/57.1.97>
- Hawkins, J., Molinek, D., 2015. Markov cellular automata models for chronic disease progression. *Int. J. Biomath.* 08, 1550085. <https://doi.org/10.1142/S1793524515500850>
- Hecquet, D., Ruskin, H.J., Crane, M., 2007. Optimisation and parallelisation strategies for Monte Carlo simulation of HIV infection. *Comput. Biol. Med.* 37, 691–699. <https://doi.org/10.1016/j.compbiomed.2006.06.010>
- Hernandez-Vargas, E.A., 2017. Modeling Kick-Kill Strategies toward HIV Cure. *Front. Immunol.* 8. <https://doi.org/10.3389/fimmu.2017.00995>
- Hershberg, U., Louzoun, Y., Atlan, H., Solomon, S., 2001. HIV time hierarchy: Winning the war while, loosing all the battles. *Phys. A Stat. Mech. its Appl.* 289, 178–190. [https://doi.org/10.1016/S0378-4371\(00\)00466-0](https://doi.org/10.1016/S0378-4371(00)00466-0)

- Hill, A.L., Rosenbloom, D.I.S., Goldstein, E., Hanhauser, E., Kuritzkes, D.R., Siliciano, R.F., Henrich, T.J., 2016. Real-Time Predictions of Reservoir Size and Rebound Time during Antiretroviral Therapy Interruption Trials for HIV. *PLOS Pathog.* 12, e1005535. <https://doi.org/10.1371/journal.ppat.1005535>
- Hillmann, A., Crane, M., Ruskin, H.J., 2020. Assessing the impact of HIV treatment interruptions using stochastic cellular Automata. *J. Theor. Biol.* 502, 110376. <https://doi.org/10.1016/j.jtbi.2020.110376>
- Hillmann, A., Crane, M., Ruskin, H.J., 2019. Efficient Computational Models for assessment of Spatial Infection Features, in: 2019 International Conference on High Performance Computing & Simulation (HPCS). IEEE, Dublin, pp. 948–952. <https://doi.org/10.1109/HPCS48598.2019.9188232>
- Hillmann, A., Crane, M., Ruskin, H.J., 2017a. HIV models for treatment interruption: Adaptation and comparison. *Phys. A Stat. Mech. its Appl.* 483, 44–56. <https://doi.org/10.1016/j.physa.2017.05.005>
- Hillmann, A., Crane, M., Ruskin, H.J., 2017b. A computational lymph tissue model for long term HIV infection progression and immune fitness, in: McAuley, J., McKeever, S. (Eds.), *Irish Conference on Artificial Intelligence and Cognitive Science 2017*. Dublin, Ireland.
- Hirschel, B., Flanigan, T., 2009. Is it smart to continue to study treatment interruptions? *AIDS* 23, 757–759. <https://doi.org/10.1097/QAD.0b013e328321b791>
- Ho, D.D., Neumann, A.U., Perelson, A.S., Chen, W., Leonard, J.M., Markowitz, M., 1995. Rapid turnover of plasma virions and CD4 lymphocytes in HIV-1 infection. *Nature* 373, 123–126. <https://doi.org/10.1038/373123a0>

- Hoffmann, G.W., 2007. Immune network theory [WWW Document]. URL [http://www.phas.ubc.ca/~hoffmann/book/Immune Network Theory.pdf](http://www.phas.ubc.ca/~hoffmann/book/Immune%20Network%20Theory.pdf) (accessed 4.3.15).
- Holford, N., Ma, S.C., Ploeger, B.A., 2010. Clinical Trial Simulation: A Review. *Clin. Pharmacol. Ther.* 88, 166–182. <https://doi.org/10.1038/clpt.2010.114>
- Howick, J., Glasziou, P., Aronson, J.K., 2010. Evidence-based mechanistic reasoning. *J. R. Soc. Med.* 103, 433–441. <https://doi.org/10.1258/jrsm.2010.100146>
- Hsue, P.Y., Hunt, P.W., Schnell, A., Kalapus, S.C., Hoh, R., Ganz, P., Martin, J.N., Deeks, S.G., 2009. Role of viral replication, antiretroviral therapy, and immunodeficiency in HIV-associated atherosclerosis. *AIDS* 23, 1059–1067. <https://doi.org/10.1097/QAD.0b013e32832b514b>
- Hundt, R., 2011. Loop Recognition in C ++ / Java / Go / Scala, in: *Proceedings of Scala Days 2011*. Stanford, USA.
- Hunt, P.W., Brenchley, J., Sinclair, E., McCune, J.M., Roland, M., Page-Shafer, K., Hsue, P., Emu, B., Krone, M., Lampiris, H., Douek, D., Martin, J.N., Deeks, S.G., 2008. Relationship between T Cell Activation and CD4 + T Cell Count in HIV-Seropositive Individuals with Undetectable Plasma HIV RNA Levels in the Absence of Therapy. *J. Infect. Dis.* 197, 126–133. <https://doi.org/10.1086/524143>
- Imaz, A., Olmo, M., Peñaranda, M., Gutiérrez, F., Romeu, J., Larrousse, M., Domingo, P., Oteo, J.A., Curto, J., Vilallonga, C., Masiá, M., López-Aldeguer, J., Iribarren, J.A., Podzamczar, D., STOPAR study team, 2013. Short-term and long-term clinical and immunological consequences of stopping antiretroviral therapy in HIV-infected patients with preserved immune function. *Antivir. Ther.* 18, 125–30.

<https://doi.org/10.3851/IMP2249>

Jafelice, R.M., Bechara, B.F.Z., Barros, L.C., Bassanezi, R.C., Gomide, F., 2009. Cellular automata with fuzzy parameters in microscopic study of positive HIV individuals. *Math. Comput. Model.* 50, 32–44. <https://doi.org/10.1016/j.mcm.2009.01.008>

Jaffe, H.W., Bregman, D.J., Selik, R.M., 1983. Acquired immune deficiency syndrome in the United States: the first 1,000 cases. *J. Infect. Dis.* 148, 339–345.

Jerne, N., 1974. Towards a network theory of the immune system. *Ann. Immunol. (Paris)*. 125C, 373–89.

Kam, N., Cohen, I.R., Harel, D., 2001. The immune system as a reactive system: modeling T cell activation with statecharts, in: *Proceedings IEEE Symposia on Human-Centric Computing Languages and Environments (Cat. No.01TH8587)*. IEEE, Stresa, Italy, pp. 15–22. <https://doi.org/10.1109/HCC.2001.995228>

Katz, I.T., Ryu, A.E., Onuegbu, A.G., Psaros, C., Weiser, S.D., Bangsberg, D.R., Tsai, A.C., 2013. Impact of HIV-related stigma on treatment adherence: systematic review and meta-synthesis. *J. Int. AIDS Soc.* 16, 18640. <https://doi.org/10.7448/IAS.16.3.18640>

Kauffman, S.A., 1969. Metabolic stability and epigenesis in randomly constructed genetic nets. *J. Theor. Biol.* 22, 437–467. [https://doi.org/10.1016/0022-5193\(69\)90015-0](https://doi.org/10.1016/0022-5193(69)90015-0)

Kaufman, M., Urbain, J., Thomas, R., 1985. Towards a logical analysis of the immune response. *J. Theor. Biol.* 114, 527–561. [https://doi.org/10.1016/S0022-5193\(85\)80042-4](https://doi.org/10.1016/S0022-5193(85)80042-4)

Keuschnigg, M., Lovsjö, N., Hedström, P., 2018. Analytical sociology and

- computational social science. *J. Comput. Soc. Sci.* 1, 3–14.  
<https://doi.org/10.1007/s42001-017-0006-5>
- Kinter, A., McNally, J., Riggin, L., Jackson, R., Roby, G., Fauci, A.S., 2007. Suppression of HIV-specific T cell activity by lymph node CD25+ regulatory T cells from HIV-infected individuals. *Proc. Natl. Acad. Sci.* 104, 3390–3395. <https://doi.org/10.1073/pnas.0611423104>
- Kish, L.B., 2002. End of Moore’s law: Thermal (noise) death of integration in micro and nano electronics. *Phys. Lett. Sect. A Gen. At. Solid State Phys.* 305, 144–149. [https://doi.org/10.1016/S0375-9601\(02\)01365-8](https://doi.org/10.1016/S0375-9601(02)01365-8)
- Kislitsyn, A., Savinkov, R., Novkovic, M., Onder, L., Bocharov, G., 2015. Computational Approach to 3D Modeling of the Lymph Node Geometry. *Computation* 3, 222–234. <https://doi.org/10.3390/computation3020222>
- Kleijnen, J.P.C., 2004. Design and Analysis of Monte Carlo Experiments. *Cent. Discuss. Pap. No. 2004-17*. <https://doi.org/10.2139/ssrn.557742>
- Kleinman, A.J., Sivanandham, R., Pandrea, I., Chougnet, C.A., Apetrei, C., 2018. Regulatory T Cells As Potential Targets for HIV Cure Research. *Front. Immunol.* 9, 1–16. <https://doi.org/10.3389/fimmu.2018.00734>
- Krakovska, O., Wahl, L.M., 2007. Drug-sparing regimens for HIV combination therapy: Benefits predicted for “drug coasting.” *Bull. Math. Biol.* 69, 2627–2647. <https://doi.org/10.1007/s11538-007-9234-9>
- Kranzer, K., Ford, N., 2011. Unstructured treatment interruption of antiretroviral therapy in clinical practice: a systematic review. *Trop. Med. Int. Heal.* 16, 1297–1313. <https://doi.org/10.1111/j.1365-3156.2011.02828.x>
- Kubiak, S., Lehr, H., Levy, R., Moeller, T., Parker, A., Swim, E., 2001.

Modeling Control of HIV Infection Through Structured Treatment Interruptions with Recommendations for Experimental Protocol, in: Gremaud, P.A., Li, Z., Smith, R.C., Tran, H.T. (Eds.), *Industrial Mathematics Modeling Workshop for Graduate Students*, July 23 - July 31, 2001. NC State University, Raleigh, pp. 67–86.

Kumar, V., Scandella, E., Danuser, R., Onder, L., Nitschke, M., Fukui, Y., Halin, C., Ludewig, B., Stein, J. V., 2010. Global lymphoid tissue remodeling during a viral infection is orchestrated by a B cell-lymphotoxin-dependent pathway. *Blood* 115, 4725–4733. <https://doi.org/10.1182/blood-2009-10-250118>

Kwon, H.D., 2007. Optimal treatment strategies derived from a HIV model with drug-resistant mutants. *Appl. Math. Comput.* 188, 1193–1204. <https://doi.org/10.1016/j.amc.2006.10.071>

Lau, J.S.Y., Smith, M.Z., Lewin, S.R., McMahon, J.H., 2019. Clinical trials of antiretroviral treatment interruption in HIV-infected individuals. *AIDS* 33, 773–791. <https://doi.org/10.1097/QAD.0000000000002113>

Lin, H., Shuai, J.W., 2010. A stochastic spatial model of HIV dynamics with an asymmetric battle between the virus and the immune system. *New J. Phys.* 12, 043051. <https://doi.org/10.1088/1367-2630/12/4/043051>

Lindsey, J.C., Ryan, L.M., 1998. Methods for interval-censored data. *Stat. Med.* 17, 219–238. [https://doi.org/10.1002/\(SICI\)1097-0258\(19980130\)17:2<219::AID-SIM735>3.0.CO;2-O](https://doi.org/10.1002/(SICI)1097-0258(19980130)17:2<219::AID-SIM735>3.0.CO;2-O)

Link, A., Vogt, T.K., Favre, S., Britschgi, M.R., Acha-Orbea, H., Hinz, B., Cyster, J.G., Luther, S.A., 2007. Fibroblastic reticular cells in lymph nodes regulate the homeostasis of naive T cells. *Nat. Immunol.* 8, 1255–1265. <https://doi.org/10.1038/ni1513>

Link, K., Gayvert, K., Canter, B., Broido, A., Joyner, M., Hu, S., Banks, H.T.,

2012. A comparison of computational efficiencies of stochastic algorithms in terms of two infection models. *Math. Biosci. Eng.* 9, 487–526. <https://doi.org/10.3934/mbe.2012.9.487>
- Louzoun, Y., 2007. The evolution of mathematical immunology. *Immunol. Rev.* 216, 9–20. <https://doi.org/10.1111/j.1600-065X.2006.00495.x>
- Lundgren, J.D., Babiker, A., Gordin, F., Emery, S., Grund, B., Sharma, S., Avihingsanon, A., Cooper, D.A., Fätkenheuer, G., Llibre, J.M., Molina, J.-M., Munderi, P., Schechter, M., Wood, R., Klingman, K.L., Collins, S., Lane, H.C., Phillips, A.N., Neaton, J.D., 2015. Initiation of Antiretroviral Therapy in Early Asymptomatic HIV Infection. *N. Engl. J. Med.* 373, 795–807. <https://doi.org/10.1056/NEJMoa1506816>
- Macal, C.M., North, M.J., 2010. Tutorial on agent-based modelling and simulation. *J. Simul.* 4, 151–162. <https://doi.org/10.1057/jos.2010.3>
- Madonia, A., Melchiorri, C., Bonamano, S., Marcelli, M., Bulfon, C., Castiglione, F., Galeotti, M., Volpatti, D., Mosca, F., Tiscar, P.-G., Romano, N., 2017. Computational modeling of immune system of the fish for a more effective vaccination in aquaculture. *Bioinformatics* 33, 3065–3071. <https://doi.org/10.1093/bioinformatics/btx341>
- Maggiolo, F., Airoldi, M., Callegaro, A., Martinelli, C., Dolara, A., Bini, T., Gregis, G., Quinzan, G., Ripamonti, D., Ravasio, V., Suter, F., 2009. CD4 cell-guided scheduled treatment interruptions in HIV-infected patients with sustained immunologic response to HAART. *AIDS* 27, 799–807. <https://doi.org/10.1097/QAD.0b013e328321b75e>
- Maggiolo, F., Ripamonti, D., Gregis, G., Quinzan, G., Callegaro, A., Suter, F., 2004. Effect of prolonged discontinuation of successful antiretroviral therapy on CD4 T cells. *AIDS* 18, 439–446. <https://doi.org/10.1097/00002030-200402200-00010>

- Maina, E.K., Abana, C.Z., Bukusi, E.A., Sedegah, M., Lartey, M., Ampofo, W.K., 2016. Plasma concentrations of transforming growth factor beta 1 in non-progressive HIV-1 infection correlates with markers of disease progression. *Cytokine* 81, 109–116. <https://doi.org/10.1016/j.cyto.2016.02.009>
- Malthus, T.R., 1798. *An essay on the principle of population*, J. Johnson. London.
- Mancini, E., Castiglione, F., Bernaschi, M., de Luca, A., Sloom, P.M.A., 2012. HIV Reservoirs and Immune Surveillance Evasion Cause the Failure of Structured Treatment Interruptions: A Computational Study. *PLoS One* 7, e36108. <https://doi.org/10.1371/journal.pone.0036108>
- Mann, M., Lurie, M.N., Kimaiyo, S., Kantor, R., 2013. Effects of political conflict-induced treatment interruptions on HIV drug resistance. *AIDS Rev.* 15, 15–24.
- Mannion, R., Ruskin, H.J., Pandey, R.B., 2002. Effects of Viral Mutation on Cellular Dynamics in a Monte Carlo Simulation of HIV Immune Response Model in Three Dimensions. *Theory Biosci.* 121, 237–245. <https://doi.org/10.1078/1431-7613-00058>
- Mannion, R., Ruskin, H.J., Pandey, R.B., 2000. Effect of Mutation on Helper T-Cells and Viral Population: A Computer Simulation Model for HIV. *Theory Biosci.* 119, 10–19. <https://doi.org/10.1078/1431-7613-00002>
- Margaris, K.N., Black, R.A., 2012. Modelling the lymphatic system: challenges and opportunities. *J R Soc Interface* 9, 601–612. <https://doi.org/10.1098/rsif.2011.0751>
- Marinho, E.B.S., Bacelar, F.S., Andrade, R.F.S., 2012. A model of partial differential equations for HIV propagation in lymph nodes. *Phys. A Stat. Mech. its Appl.* 391, 132–141.

<https://doi.org/10.1016/j.physa.2011.08.023>

MathWorks, 2015a. Ordinary Differential Equations - Matlab and Simulink [WWW Document]. Online Help. URL <http://de.mathworks.com/help/matlab/math/ordinary-differential-equations.html> (accessed 7.7.15).

MathWorks, 2015b. MATLAB [WWW Document]. URL [www.mathworks.com/products/matlab/](http://www.mathworks.com/products/matlab/) (accessed 5.15.15).

Matzinger, P., 1994. Tolerance, danger, and the extended family. *Annu. Rev. Immunol.* 12, 991–1045. <https://doi.org/10.1146/annurev.iy.12.040194.005015>

May, M.T., Vehreschild, J.-J., Trickey, A., Obel, N., Reiss, P., Bonnet, F., Mary-Krause, M., Samji, H., Cavassini, M., Gill, M.J., Shepherd, L.C., Crane, H.M., d'Arminio Monforte, A., Burkholder, G.A., Johnson, M.M., Sobrino-Vegas, P., Domingo, P., Zangerle, R., Justice, A.C., Sterling, T.R., Miró, J.M., Sterne, J.A.C., 2016. Mortality According to CD4 Count at Start of Combination Antiretroviral Therapy Among HIV-infected Patients Followed for up to 15 Years After Start of Treatment: Collaborative Cohort Study. *Clin. Infect. Dis.* 62, 1571–1577. <https://doi.org/10.1093/cid/ciw183>

McEwan, C., Hart, E., 2009. Representation in the (Artificial) Immune System. *J. Math. Model. Algorithms* 8, 125–149. <https://doi.org/10.1007/s10852-009-9104-6>

McGreevy, R.L., 2001. Reverse Monte Carlo modelling. *J. Phys. Condens. Matter* 13, R877–R913. <https://doi.org/10.1088/0953-8984/13/46/201>

McGuinness, E., 2012. Role of delay differential equations in modelling low level HIV viral load. Dublin City University.

- McMichael, A.J., Borrow, P., Tomaras, G.D., Goonetilleke, N., Haynes, B.F., 2010. The immune response during acute HIV-1 infection: clues for vaccine development. *Nat. Rev. Immunol.* 10, 11–23. <https://doi.org/10.1038/nri2674>
- Mellors, J.W., 1997. Plasma Viral Load and CD4+ Lymphocytes as Prognostic Markers of HIV-1 Infection. *Ann. Intern. Med.* 126, 946. <https://doi.org/10.7326/0003-4819-126-12-199706150-00003>
- Mempel, T.R., Henrickson, S.E., von Andrian, U.H., 2004. T-cell priming by dendritic cells in lymph nodes occurs in three distinct phases. *Nature* 427, 154–159. <https://doi.org/10.1038/nature02238>
- Miao, H., Xia, X., Perelson, A.S., Wu, H., 2011. On Identifiability of Nonlinear ODE Models and Applications in Viral Dynamics. *SIAM Rev.* 53, 3–39. <https://doi.org/10.1137/090757009>
- Michaelis, L., Menten, M.L., 1913. Die Kinetik der Invertinwirkung. *Biochem Z* 49, 333–369. <https://doi.org/10.1021/bi201284u>
- Mielke, A., Pandey, R., 1998. A computer simulation study of cell population in a fuzzy interaction model for mutating HIV. *Phys. A Stat. Mech. its Appl.* 251, 430–438. [https://doi.org/10.1016/S0378-4371\(97\)00576-1](https://doi.org/10.1016/S0378-4371(97)00576-1)
- Milanez-Almeida, P., Meyer-Hermann, M., Toker, A., Khailaie, S., Huehn, J., 2015. Foxp3 + regulatory T-cell homeostasis quantitatively differs in murine peripheral lymph nodes and spleen. *Eur. J. Immunol.* 45, 153–166. <https://doi.org/10.1002/eji.201444480>
- Miller, R., Parrow, J., Walker, D., 1992. A Calculus of Mobile Processes, I. *Inf. Comput.* 100, 1–40.
- Moir, S., Fauci, A.S., 2009. B cells in HIV infection and disease. *Nat. Rev. Immunol.* 9, 235–245. <https://doi.org/10.1038/nri2524>

- Moonchai, S., Lenbury, Y., Triampo, W., 2010. Cellular automata simulation modeling of HIV infection in Lymph Node and peripheral blood compartments. *Int. J. Math. Comput. Simul.* 4, 124–134.
- Moore, G.E., 1965. Cramming more components onto integrated circuits. *Electronics* 38, 114ff.
- Moore, R.D., Keruly, J.C., 2007. CD4+ Cell Count 6 Years after Commencement of Highly Active Antiretroviral Therapy in Persons with Sustained Virologic Suppression. *Clin. Infect. Dis.* 44, 441–446. <https://doi.org/10.1086/510746>
- Moreno-Gamez, S., Hill, A.L., Rosenbloom, D.I.S., Petrov, D. a, Nowak, M. a, Pennings, P.S., 2015. Imperfect drug penetration leads to spatial monotherapy and rapid evolution of multidrug resistance. *Proc. Natl. Acad. Sci.* 112, E2874–E2883. <https://doi.org/10.1073/pnas.1424184112>
- Mould, D.R., Upton, R.N., 2013. Basic Concepts in Population Modeling, Simulation, and Model-Based Drug Development—Part 2: Introduction to Pharmacokinetic Modeling Methods. *CPT Pharmacometrics Syst. Pharmacol.* 2, e38. <https://doi.org/10.1038/psp.2013.14>
- MPI Forum, 2019. Message Passing Interface [WWW Document]. URL [mpi-forum.org](http://mpi-forum.org) (accessed 3.24.20).
- MPICH Collaborators, 2019. MPICH [WWW Document]. URL <http://www.mpich.org/> (accessed 5.25.15).
- Mueller, S.N., Germain, R.N., 2010. Stromal cell contributions to the homeostasis and functionality of the immune system. *Nat. Rev. Immunol.* 9, 618–629. <https://doi.org/10.1038/nri2588>
- Murata, T., 1989. Petri nets: Properties, analysis and applications. *Proc. IEEE*

77, 541–580. <https://doi.org/10.1109/5.24143>

Murphy, D.B., Herzenberg, L.A., Okumura, K., Herzenberg, L.A., McDevitt, H.O., 1976. A new I subregion (I-J) marked by a locus (Ia-4) controlling surface determinants on suppressor T lymphocytes. *J. Exp. Med.* 144, 699–712. <https://doi.org/10.1084/jem.144.3.699>

Murray, L.K., Semrau, K., McCurley, E., Thea, D.M., Scott, N., Mwiya, M., Kankasa, C., Bass, J., Bolton, P., 2009. Barriers to acceptance and adherence of antiretroviral therapy in urban Zambian women: a qualitative study. *AIDS Care* 21, 78–86. <https://doi.org/10.1080/09540120802032643>

Nagy, Z.A., 2014. *A History of Modern Immunology, A History of Modern Immunology*. Elsevier. <https://doi.org/10.1016/C2013-0-00672-X>

Nansseu, J.R.N., Bigna, J.J.R., 2017. Antiretroviral therapy related adverse effects: Can sub-Saharan Africa cope with the new “test and treat” policy of the World Health Organization? *Infect. Dis. Poverty* 6, 24. <https://doi.org/10.1186/s40249-017-0240-3>

Neri, F., Toivanen, J., Mäkinen, R.A.E., 2007. An adaptive evolutionary algorithm with intelligent mutation local searchers for designing multidrug therapies for HIV. *Appl. Intell.* 27, 219–235. <https://doi.org/10.1007/s10489-007-0069-8>

Nikolai, C., Madey, G., 2009. Tools of the Trade: A Survey of Various Agent Based Modeling Platforms. *J. Artif. Soc. Soc. Simul.* 12, 2.

Nilsson, J., Boasso, A., Velilla, P.A., Zhang, R., Vaccari, M., Franchini, G., Shearer, G.M., Andersson, J., Chougnet, C., 2006. HIV-1-driven regulatory T-cell accumulation in lymphoid tissues is associated with disease progression in HIV/AIDS. *Blood* 108, 3808–3817. <https://doi.org/10.1182/blood-2006-05-021576>

- Nobrega, C., Horta, A., Coutinho-Teixeira, V., Martins-Ribeiro, A., Baldaia, A., Rb-Silva, R., Santos, C.L., Sarmiento-Castro, R., Correia-Neves, M., 2016. Longitudinal evaluation of regulatory T-cell dynamics on HIV-infected individuals during the first 2 years of therapy. *AIDS* 30, 1175–1185. <https://doi.org/10.1097/QAD.0000000000001074>
- Novkovic, M., Onder, L., Cheng, H.-W., Bocharov, G., Ludewig, B., 2018. Integrative Computational Modeling of the Lymph Node Stromal Cell Landscape. *Front. Immunol.* 9, 1–9. <https://doi.org/10.3389/fimmu.2018.02428>
- Novkovic, M., Onder, L., Cupovic, J., Abe, J., Bomze, D., Cremasco, V., Scandella, E., Stein, J. V., Bocharov, G., Turley, S.J., Ludewig, B., 2016. Topological Small-World Organization of the Fibroblastic Reticular Cell Network Determines Lymph Node Functionality. *PLOS Biol.* 14, e1002515. <https://doi.org/10.1371/journal.pbio.1002515>
- Nowak, M.A., Anderson, R.M., Boerlijst, M.C., Bonhoeffer, S., May, R.M., McMichael, A.J., 1996. HIV-1 evolution and disease progression. *Science* 274, 1008–11. <https://doi.org/10.1126/science.274.5289.1010>
- Nowak, M.A., Bangham, C.R., 1996. Population dynamics of immune responses to persistent viruses. *Science* 272, 74–79. <https://doi.org/10.1126/science.272.5258.74>
- Nozaki, I., Kuriyama, M., Manyepa, P., Zyambo, M.K., Kakimoto, K., Bärnighausen, T., 2013. False Beliefs About ART Effectiveness, Side Effects and the Consequences of Non-retention and Non-adherence Among ART Patients in Livingstone, Zambia. *AIDS Behav.* 17, 122–126. <https://doi.org/10.1007/s10461-012-0221-2>
- Ogenstad, S., 2018. A Statistical Approach to Clinical Trial Simulations, in: Peace, K.E., Chen, D.-G., Menon, S. (Eds.), *Biopharmaceutical Applied*

- Statistics Symposium, ICSA Book Series in Statistics. Springer Singapore, Singapore, pp. 1–18. [https://doi.org/10.1007/978-981-10-7829-3\\_1](https://doi.org/10.1007/978-981-10-7829-3_1)
- Okoye, A.A., Picker, L.J., 2013. CD4+ T-Cell Depletion In Hiv Infection: Mechanisms Of Immunological Failure. *Immunol. Rev.* 254, 54–64. <https://doi.org/10.1111/imr.12066>
- Olesen, J.S., Jespersen, S., da Silva, Z.J., Rodrigues, A., Erikstrup, C., Aaby, P., Wejse, C., Hønge, B.L., 2018. HIV-2 continues to decrease, whereas HIV-1 is stabilizing in Guinea-Bissau. *AIDS* 32, 1193–1198. <https://doi.org/10.1097/QAD.0000000000001827>
- Oña, L., Kouyos, R.D., Lachmann, M., Bonhoeffer, S., 2013. On the role of resonance in drug failure under HIV treatment interruption. *Theor. Biol. Med. Model.* 10, 1–17. <https://doi.org/10.1186/1742-4682-10-44>
- Open MPI Project, 2020. Open MPI: Open Source High Performance Computing [WWW Document]. URL <http://www.open-mpi.org> (accessed 3.25.20).
- OpenMP Architecture Review Board, 2019. OpenMP [WWW Document]. URL <http://openmp.org> (accessed 8.10.17).
- Osuji, F.N., Onyenekwe, C.C., Ahaneku, J.E., Ukibe, N.R., 2018. The effects of highly active antiretroviral therapy on the serum levels of pro-inflammatory and anti-inflammatory cytokines in HIV infected subjects. *J. Biomed. Sci.* 25, 88. <https://doi.org/10.1186/s12929-018-0490-9>
- Oxenius, A., Price, D.A., Gunthard, H.F., Dawson, S.J., Fagard, C., Perrin, L., Fischer, M., Weber, R., Plana, M., Garcia, F., Hirschel, B., McLean, A., Phillips, R.E., 2002. Stimulation of HIV-specific cellular immunity by structured treatment interruption fails to enhance viral control in chronic HIV infection. *Proc. Natl. Acad. Sci.* 99, 13747–13752.

<https://doi.org/10.1073/pnas.202372199>

- Paci, P., Carello, R., Bernaschi, M., D'Offizi, G., Castiglione, F., 2009. Immune control of HIV-1 infection after therapy interruption: immediate versus deferred antiretroviral therapy. *BMC Infect. Dis.* 9, 172. <https://doi.org/10.1186/1471-2334-9-172>
- Paci, P., Martini, F., Bernaschi, M., D'Offizi, G., Castiglione, F., 2011. Timely HAART initiation may pave the way for a better viral control. *BMC Infect. Dis.* 11, 56. <https://doi.org/10.1186/1471-2334-11-56>
- Palella, F.J., Baker, R.K., Moorman, A.C., Chmiel, J.S., Wood, K.C., Brooks, J.T., Holmberg, S.D., 2006. Mortality in the Highly Active Antiretroviral Therapy Era. *JAIDS J. Acquir. Immune Defic. Syndr.* 43, 27–34. <https://doi.org/10.1097/01.qai.0000233310.90484.16>
- Pandey, R.B., 1998. A Stochastic Cellular Automata Approach to Cellular Dynamics for HIV: effect of viral mutation. *Theory Biosci.* 117, 32–41.
- Pandey, R.B., 1991. Cellular automata approach to interacting cellular network models for the dynamics of cell population in an early HIV infection. *Phys. A Stat. Mech. its Appl.* 179, 442–470. [https://doi.org/10.1016/0378-4371\(91\)90088-T](https://doi.org/10.1016/0378-4371(91)90088-T)
- Pandey, R.B., Stauffer, D., 1989. Immune response via interacting three dimensional network of cellular automata. *J. Phys.* 50, 1–10. <https://doi.org/10.1051/jphys:019890050010100>
- Pannocchia, G., Laurino, M., Landi, A., 2010. A model predictive control strategy toward optimal structured treatment interruptions in anti-HIV therapy. *IEEE Trans. Biomed. Eng.* 57, 1040–1050. <https://doi.org/10.1109/TBME.2009.2039571>
- Pantaleo, G., Graziosi, C., Demarest, J.F., Butini, L., Montroni, M., Fox,

- C.H., Orenstein, J.M., Kotler, D.P., Fauci, A.S., 1993a. HIV infection is active and progressive in lymphoid tissue during the clinically latent stage of disease. *Nature* 362, 355–358. <https://doi.org/10.1038/362355a0>
- Pantaleo, G., Graziosi, C., Fauci, A.S., 1993b. New concepts in the immunopathogenesis of human immunodeficiency virus infection. *N. Engl. J. Med.* 328, 327–335. <https://doi.org/10.1056/NEJM199302043280508>
- Papa, A.R.R., Tsallis, C., 1996. A local-field-type model for immunological systems: time evolution in real and shape spaces. *Phys. A Stat. Mech. its Appl.* 233, 85–101. [https://doi.org/10.1016/S0378-4371\(96\)00186-0](https://doi.org/10.1016/S0378-4371(96)00186-0)
- Pappalardo, F., Russo, G., Tshinanu, F.M., Viceconti, M., 2018. In silico clinical trials: concepts and early adoptions. *Brief. Bioinform.* 1–10. <https://doi.org/10.1093/bib/bby043>
- Parham, P., 2009. Elements of the Immune System and their Roles in Defens, in: *The Immune System*. Garland Sciences, pp. 2-27p.
- Passaes, C.P., Sáez-Cirión, A., 2014. HIV cure research: Advances and prospects. *Virology* 454–455, 340–352. <https://doi.org/10.1016/j.virol.2014.02.021>
- Păun, G., 2000. Computing with Membranes. *J. Comput. Syst. Sci.* 61, 108–143. <https://doi.org/10.1006/jcss.1999.1693>
- Perelson, A.S., Kirschner, D.E., De Boer, R., 1993. Dynamics of HIV infection of CD4+ T cells. *Math. Biosci.* 114, 81–125. [https://doi.org/10.1016/0025-5564\(93\)90043-A](https://doi.org/10.1016/0025-5564(93)90043-A)
- Perelson, A.S., Nelson, P.W., 1999. Mathematical Analysis of HIV-1 Dynamics in Vivo. *SIAM Rev.* 41, 3–44.

<https://doi.org/10.1137/S0036144598335107>

Perelson, A.S., Oster, G.F., 1979. Theoretical studies of clonal selection: minimal antibody repertoire size and reliability of self-non-self discrimination. *J. Theor. Biol.* 81, 645–670. [https://doi.org/10.1016/0022-5193\(79\)90275-3](https://doi.org/10.1016/0022-5193(79)90275-3)

Perelson, A.S., Ribeiro, R.M., 2013. Modeling the within-host dynamics of HIV infection. *BMC Biol.* 11, 96. <https://doi.org/10.1186/1741-7007-11-96>

Perrin, D., Ruskin, H.J., Burns, J., Crane, M., 2006. An agent-based approach to immune modelling, in: Gavrilova, M., Gervasi, O., Kumar, V., Tan, C.J.K., Taniar, D., Laganá, A., Mun, Y., Choo, H. (Eds.), *Lecture Notes in Computer Science (Including Subseries Lecture Notes in Artificial Intelligence and Lecture Notes in Bioinformatics)*, Lecture Notes in Computer Science. Springer Berlin Heidelberg, Berlin, Heidelberg, pp. 612–621. [https://doi.org/10.1007/11751540\\_65](https://doi.org/10.1007/11751540_65)

Perrin, D., Ruskin, H.J., Crane, M., 2010. Model refinement through high-performance computing: An agent-based HIV example. *Immunome Res.* 6, 1–9. <https://doi.org/10.1186/1745-7580-6-S1-S3>

Persaud, D., Gay, H., Ziemniak, C., Chen, Y.H., Piatak Jr., M., Chun, T.W., Strain, M., Richman, D., Luzuriaga, K., 2013. Absence of detectable HIV-1 viremia after treatment cessation in an infant. *N Engl J Med* 369, 1828–1835. <https://doi.org/10.1056/NEJMoa1302976>

Petri, C.A., 1962. *Kommunikation mit Automaten*. Fak. für Math. und Phys. Universität Hamburg.

Pradeu, T., Cooper, E.L., 2012. The danger theory: 20 years later. *Front. Immunol.* 3, 1–9. <https://doi.org/10.3389/fimmu.2012.00287>

- Precharattana, M., 2016. Stochastic modeling for dynamics of HIV-1 infection using cellular automata: A review. *J. Bioinform. Comput. Biol.* 14, 1630001. <https://doi.org/10.1142/S021972001630001X>
- Precharattana, M., Nokkeaw, A., Triampo, W., Triampo, D., Lenbury, Y., 2011. Stochastic cellular automata model and Monte Carlo simulations of CD4+ T cell dynamics with a proposed alternative leukapheresis treatment for HIV/AIDS. *Comput. Biol. Med.* 41, 546–558. <https://doi.org/10.1016/j.compbiomed.2011.05.005>
- Precharattana, M., Triampo, W., 2014. Modeling dynamics of HIV infected cells using stochastic cellular automaton. *Phys. A Stat. Mech. its Appl.* 407, 303–311. <https://doi.org/10.1016/j.physa.2014.04.007>
- Presicce, P., Orsborn, K., King, E., Pratt, J., Fichtenbaum, C.J., Chougnet, C.A., 2011. Frequency of Circulating Regulatory T Cells Increases during Chronic HIV Infection and Is Largely Controlled by Highly Active Antiretroviral Therapy. *PLoS One* 6, e28118. <https://doi.org/10.1371/journal.pone.0028118>
- Rabenseifner, R., Hager, G., Jost, G., 2009. Hybrid MPI/OpenMP Parallel Programming on Clusters of Multi-Core SMP Nodes, in: 2009 17th Euromicro International Conference on Parallel, Distributed and Network-Based Processing. IEEE, Weimar, Germany, pp. 427–436. <https://doi.org/10.1109/PDP.2009.43>
- Rabi, S.A., Laird, G.M., Durand, C.M., Laskey, S., Shan, L., Bailey, J.R., Chioma, S., Moore, R.D., Siliciano, R.F., 2013. Multi-step inhibition explains HIV-1 protease inhibitor pharmacodynamics and resistance. *J. Clin. Invest.* 123, 3848–3860. <https://doi.org/10.1172/JCI67399>
- Radjai, F., Voivret, C., 2013. Periodic Boundary Conditions [WWW Document]. *cpg-gateway*. URL <http://www.cpg->

gateway.org/resources/Articles/PBC.pdf (accessed 8.10.20).

- Rana, E., Giabbanelli, P.J., Balabhadrapathruni, N.H., Li, X., Mago, V.K., 2015. Exploring the Relationship between Adherence to Treatment and Viral Load through a New Discrete Simulation Model of HIV Infectivity, in: Proceedings of the 3rd ACM Conference on SIGSIM-Principles of Advanced Discrete Simulation - SIGSIM-PADS '15. ACM Press, New York, New York, USA, pp. 145–156. <https://doi.org/10.1145/2769458.2769477>
- Reddy, V.N., Mavrovouniotis, M.L., Liebman, M.N., 1993. Petri net representations in metabolic pathways. *Proc. Int. Conf. Intell. Syst. Mol. Biol.* 1, 328–336. <https://doi.org/082/11>
- Ribeiro, R.M., Qin, L., Chavez, L.L., Li, D., Self, S.G., Perelson, A.S., 2010. Estimation of the Initial Viral Growth Rate and Basic Reproductive Number during Acute HIV-1 Infection. *J. Virol.* 84, 6096–6102. <https://doi.org/10.1128/JVI.00127-10>
- Robbins, G.K., Daniels, B., Zheng, H., Chueh, H., Meigs, J.B., Freedberg, K.A., 2007. Predictors of Antiretroviral Treatment Failure in an Urban HIV Clinic. *JAIDS J. Acquir. Immune Defic. Syndr.* 44, 30–37. <https://doi.org/10.1097/01.qai.0000248351.10383.b7>
- Romero-Campero, F.J., Twycross, J., Cámara, M., Bennett, M., Gheorghe, M., Krasnogor, N., 2009. Modular Assembly of Cell Systems Biology Models Using P Systems. *Int. J. Found. Comput. Sci.* 20, 427–442. <https://doi.org/10.1142/S0129054109006668>
- Rosenberg, E.S., Altfeld, M., Poon, S.H., Phillips, M.N., Wilkes, B.M., Eldridge, R.L., Robbins, G.K., D'Aquila, R.T., Goulder, P.J., Walker, B.D., 2000. Immune control of HIV-1 after early treatment of acute infection. *Nature* 407, 523–526. <https://doi.org/10.1038/35035103>

- Rosenbloom, D.I.S., Hill, A.L., Rabi, S.A., Siliciano, R.F., Nowak, M.A., 2012. Antiretroviral dynamics determines HIV evolution and predicts therapy outcome. *Nat. Med.* 18, 1378–1385. <https://doi.org/10.1038/nm.2892>
- Rothenberger, M.K., Keele, B.F., Wietgreffe, S.W., Fletcher, C. V, Beilman, G.J., Chipman, J.G., Khoruts, A., Estes, J.D., Anderson, J., Callisto, S.P., Schmidt, T.E., Thorkelson, A., Reilly, C., Perkey, K., Reimann, T.G., Uday, N.S., 2015. Large number of rebounding / founder HIV variants emerge from multifocal infection in lymphatic tissues after treatment interruption. *Proc. Natl. Acad. Sci.* 112, 1–9. <https://doi.org/10.1073/pnas.1414926112>
- Roux-Rouquié, M., Caritey, N., Gaubert, L., Rosenthal-Sabroux, C., 2004. Using the Unified Modelling Language (UML) to guide the systemic description of biological processes and systems. *Biosystems* 75, 3–14. <https://doi.org/10.1016/j.biosystems.2004.03.009>
- Ruffault, A., Michelet, C., Jacquelinet, C., Guist'hau, O., Genetet, N., Bariou, C., Colimon, R., Cartier, F., 1995. The prognostic value of plasma viremia in HIV-infected patients under AZT treatment: a two-year follow-up study. *J. Acquir. Immune Defic. Syndr. Hum. Retrovirol.* 9, 243–248. <https://doi.org/10.1097/00042560-199507000-00004>
- Ruggles, K. V., Patel, A.R., Schensul, S., Schensul, J., Nucifora, K., Zhou, Q., Bryant, K., Braithwaite, R.S., 2017. Betting on the fastest horse: Using computer simulation to design a combination HIV intervention for future projects in Maharashtra, India. *PLoS One* 12, e0184179. <https://doi.org/10.1371/journal.pone.0184179>
- Ruiz, L., Carcelain, G., Martínez-Picado, J., Frost, S., Marfil, S., Paredes, R., Romeu, J., Ferrer, E., Morales-Lopetegui, K., Autran, B., Clotet, B., 2001. HIV dynamics and T-cell immunity after three structured treatment

- interruptions in chronic HIV-1 infection. *AIDS* 15, F19–F27.  
<https://doi.org/10.1097/00002030-200106150-00001>
- Ruiz, L., Martinez-Picado, J., Romeu, J., Paredes, R., Zayat, M.K., Marfil, S., Negredo, E., Sirera, G., Tural, C., Clotet, B., 2000. Structured treatment interruption in chronically HIV-1 infected patients after long-term viral suppression. *AIDS* 14, 397–403.
- Sackett, D.L., 1997. Evidence-based medicine. *Semin. Perinatol.* 21, 3–5.  
[https://doi.org/10.1016/S0146-0005\(97\)80013-4](https://doi.org/10.1016/S0146-0005(97)80013-4)
- Sáez-Ciri3n, A., Bacchus, C., Hocqueloux, L., Avettand-Fenoel, V., Girault, I., Lecuroux, C., Potard, V., Versmisse, P., Melard, A., Prazuck, T., Descours, B., Guernon, J., Viard, J.P., Boufassa, F., Lambotte, O., Goujard, C., Meyer, L., Costagliola, D., Venet, A., Pancino, G., Autran, B., Rouzioux, C., 2013. Post-Treatment HIV-1 Controllers with a Long-Term Virological Remission after the Interruption of Early Initiated Antiretroviral Therapy ANRS VISCONTI Study. *PLoS Pathog.* 9, 1–12.  
<https://doi.org/10.1371/journal.ppat.1003211>
- Sampah, M.E.S., Shen, L., Jilek, B.L., Siliciano, R.F., 2011. Dose-response curve slope is a missing dimension in the analysis of HIV-1 drug resistance. *Proc. Natl. Acad. Sci. U. S. A.* 108, 7613–7618.  
<https://doi.org/10.1073/pnas.1018360108>
- Sanchez, J.L., Hunt, P.W., Reilly, C.S., Hatano, H., Beilman, G.J., Khoruts, A., Jasurda, J.S., Somsouk, M., Thorkelson, A., Russ, S., Anderson, J., Deeks, S.G., Schacker, T.W., 2015. Lymphoid Fibrosis Occurs in Long-Term Nonprogressors and Persists With Antiretroviral Therapy but May Be Reversible With Curative Interventions. *J. Infect. Dis.* 211, 1068–1075. <https://doi.org/10.1093/infdis/jiu586>
- Santiago, M.L., Range, F., Keele, B.F., Li, Y., Bailes, E., Bibollet-Ruche, F.,

- Fruteau, C., Noë, R., Peeters, M., Brookfield, J.F.Y., Shaw, G.M., Sharp, P.M., Hahn, B.H., 2005. Simian immunodeficiency virus infection in free-ranging sooty mangabeys (*Cercocebus atys atys*) from the Tai Forest, Côte d'Ivoire: implications for the origin of epidemic human immunodeficiency virus type 2. *J. Virol.* 79, 12515–27. <https://doi.org/10.1128/JVI.79.19.12515-12527.2005>
- Schacker, T.W., Nguyen, P.L., Beilman, G.J., Wolinsky, S., Larson, M., Reilly, C., Haase, A.T., 2002. Collagen deposition in HIV-1 infected lymphatic tissues and T cell homeostasis. *J. Clin. Invest.* 110, 1133–1139. <https://doi.org/10.1172/JCI200216413>
- Schacker, T.W., Reilly, C., Beilman, G.J., Taylor, J., Skarda, D., Krason, D., Larson, M., Haase, A.T., 2005. Amount of lymphatic tissue fibrosis in HIV infection predicts magnitude of HAART-associated change in peripheral CD4 cell count. *AIDS* 19, 2169–2171. <https://doi.org/10.1097/01.aids.0000194801.51422.03>
- Schuster-Böckler, B., Bateman, A., 2007. An introduction to hidden Markov models. *Curr. Protoc. Bioinforma.* Appendix 3, Appendix 3A. <https://doi.org/10.1002/0471250953.bia03as18>
- Seitz, R., 2016. Human Immunodeficiency Virus (HIV). *Transfus. Med. Hemotherapy* 43, 203–222. <https://doi.org/10.1159/000445852>
- Shaw, J.M., Hunt, P.W., Critchfield, J.W., McConnell, D.H., Garcia, J.C., Pollard, R.B., Somsouk, M., Deeks, S.G., Shacklett, B.L., 2012. Viremic Slow Progressors Maintain Low Regulatory T Cell Numbers in Rectal Mucosa but Exhibit High T Cell Activation. *AIDS Res. Hum. Retroviruses* 29, 121016061035002. <https://doi.org/10.1089/aid.2012.0268>
- Sheiner, L.B., Steimer, J.-L., 2000. Pharmacokinetic/Pharmacodynamic

- Modeling in Drug Development. *Annu. Rev. Pharmacol. Toxicol.* 40, 67–95. <https://doi.org/10.1146/annurev.pharmtox.40.1.67>
- Shen, H., Wang, X., Shao, Z., Liu, K., Xia, X.-Y., Zhang, H.-Z., Song, K., Song, Y., Shang, Z.-J., 2014. Alterations of high endothelial venules in primary and metastatic tumors are correlated with lymph node metastasis of oral and pharyngeal carcinoma. *Cancer Biol. Ther.* 15, 342–349. <https://doi.org/10.4161/cbt.27328>
- Shi, V., Tridane, A., Kuang, Y., 2008. A viral load-based cellular automata approach to modeling HIV dynamics and drug treatment. *J. Theor. Biol.* 253, 24–35. <https://doi.org/10.1016/j.jtbi.2007.11.005>
- Shinde, S.B., Kurhekar, M.P., 2018. Review of the systems biology of the immune system using agent-based models. *IET Syst. Biol.* 12, 83–92. <https://doi.org/10.1049/iet-syb.2017.0073>
- Siegel, L., El-Sadr, W., 2006. New perspectives in HIV treatment interruption: The SMART study, in: Braun, J., Pozo, M. (Eds.), *The PRN Notebook*. Physicians' Research Network, New York, NY, pp. 8–9.
- Silverberg, M.J., Neuhaus, J., Bower, M., Gey, D., Hatzakis, A., Henry, K., Hidalgo, J., Lourtou, L., Neaton, J.D., Tambussi, G., Abrams, D.I., 2007. Risk of cancers during interrupted antiretroviral therapy in the SMART study. *AIDS* 21, 1957–1963. <https://doi.org/10.1097/QAD.0b013e3282ed6338>
- Sloot, P.M.A., Chen, F., Boucher, C., 2002. Cellular Automata Model of Drug Therapy for HIV Infection, in: Sirakoulis, G.C., Bandini, S. (Eds.), *5th International Conference on Cellular Automata for Research and Industry, ACRI, Lecture Notes in Computer Science*. Springer Berlin Heidelberg, Geneva, Switzerland, pp. 282–293. [https://doi.org/10.1007/3-540-45830-1\\_27](https://doi.org/10.1007/3-540-45830-1_27)

- Solas, C., Lafeuillade, A., Halfon, P., Chadapaud, S., Hittinger, G., Lacarelle, B., 2003. Discrepancies between protease inhibitor concentrations and viral load in reservoirs and sanctuary sites in human immunodeficiency virus-infected patients. *Antimicrob. Agents Chemother.* 47, 238–243. <https://doi.org/10.1128/AAC.47.1.238-243.2003>
- Sornette, D., 2014. Physics and financial economics (1776–2014): puzzles, Ising and agent-based models. *Reports Prog. Phys.* 77, 062001. <https://doi.org/10.1088/0034-4885/77/6/062001>
- Spicher, A., Michel, O., Cieslak, M., Giavitto, J.L., Prusinkiewicz, P., 2008. Stochastic P systems and the simulation of biochemical processes with dynamic compartments. *BioSystems* 91, 458–472. <https://doi.org/10.1016/j.biosystems.2006.12.009>
- Spiegel, H., Herbst, H., Niedobitek, G., Foss, H.D., Stein, H., 1992. Follicular dendritic cells are a major reservoir for human immunodeficiency virus type 1 in lymphoid tissues facilitating infection of CD4+ T-helper cells. *Am. J. Pathol.* 140, 15–22.
- Stecher, M., Claßen, A., Klein, F., Lehmann, C., Gruell, H., Platten, M., Wyen, C., Behrens, G., Fätkenheuer, G., Vehreschild, J.J., 2020. Systematic Review and Meta-analysis of Treatment Interruptions in Human Immunodeficiency Virus (HIV) Type 1–infected Patients Receiving Antiretroviral Therapy: Implications for Future HIV Cure Trials. *Clin. Infect. Dis.* 70, 1406–1417. <https://doi.org/10.1093/cid/ciz417>
- Strain, M.C., Levine, H., 2002. Comment on “Dynamics of HIV infection: a cellular automata approach.” *Phys. Rev. Lett.* 89, 219805.
- Strain, M.C., Richman, D.D., Wong, J.K., Levine, H., 2002. Spatiotemporal dynamics of HIV propagation. *J. Theor. Biol.* 218, 85–96.

<https://doi.org/10.1006/yjtbi.3055>

Su, B., Zhou, W., Dorman, K.S., Jones, D.E., 2009. Mathematical Modelling of Immune Response in Tissues. *Comput. Math. Methods Med.* 10, 9–38. <https://doi.org/10.1080/17486700801982713>

Svicher, V., Ceccherini-Silberstein, F., Antinori, A., Aquaro, S., Perno, C.F., 2014. Understanding HIV compartments and reservoirs. *Curr. HIV/AIDS Rep.* 11, 186–194. <https://doi.org/10.1007/s11904-014-0207-y>

Swartz, M.A., 2001. The physiology of the lymphatic system. *Adv. Drug Deliv. Rev.* 50, 3–20. [https://doi.org/10.1016/S0169-409X\(01\)00150-8](https://doi.org/10.1016/S0169-409X(01)00150-8)

Tarantola, A., 2005. *Inverse Problem Theory and Methods for Model Parameter Estimation.* Society for Industrial and Applied Mathematics. <https://doi.org/10.1137/1.9780898717921>

Teklu, A.M., Yirdaw, K.D., 2017. Patients who restart antiretroviral medication after interruption remain at high risk of unfavorable outcomes in Ethiopia. *BMC Health Serv. Res.* 17, 247. <https://doi.org/10.1186/s12913-017-2172-9>

Theron, A.J., Anderson, R., Rossouw, T.M., Steel, H.C., 2017. The Role of Transforming Growth Factor Beta-1 in the Progression of HIV/AIDS and Development of Non-AIDS-Defining Fibrotic Disorders. *Front. Immunol.* 8, 1461. <https://doi.org/10.3389/fimmu.2017.01461>

Thiébaud, R., Pellegrin, I., Chêne, G., Viallard, J.F., Fleury, H., Moreau, J.F., Pellegrin, J.L., Blanco, P., 2005. Immunological markers after long-term treatment interruption in chronically HIV-1 infected patients with CD4 cell count above  $400 \times 10^6$  cells/l. *AIDS* 19, 53–61. <https://doi.org/10.1097/00002030-200501030-00006>

- Tuckwell, H.C., Le Corfec, E., 1998. A stochastic model for early HIV-1 population dynamics. *J. Theor. Biol.* 195, 451–463. <https://doi.org/10.1006/jtbi.1998.0806>
- U.S. Department of Health and Human Services, 2014. Guidelines for the use of antiretroviral agents in HIV-infected adults and adolescents. February 5, 2001. [WWW Document]. *HIV Clin. Trials*. <https://doi.org/10.1310/4R1B-8F60-B57H-0ECN>
- Ulam, S., 1962. On some mathematical problems connected with patterns of growth of figures, in: *Proceedings of Symposia in Applied Mathematics*. Am. Math. Soc. Vol. 14, Providence, pp. 215–224.
- UNAIDS, 2019. 2018 Global Hiv Statistics [WWW Document]. URL <https://www.unaids.org/en/resources/fact-sheet> (accessed 8.31.19).
- United States Food and Drug Administration, 2014. FDA-Approved HIV Medicines [WWW Document]. [aidsinfo.nih.gov](http://aidsinfo.nih.gov). URL <http://aidsinfo.nih.gov/education-materials/fact-sheets/21/58/fda-approved-hiv-medicines> (accessed 1.18.15).
- van den Brekel, M.W., Castelijns, J.A., Snow, G.B., 1998. The size of lymph nodes in the neck on sonograms as a radiologic criterion for metastasis: how reliable is it? *AJNR. Am. J. Neuroradiol.* 19, 695–700.
- Vella, S., Schwartländer, B., Sow, S.P., Eholie, S.P., Murphy, R.L., 2012. The history of antiretroviral therapy and of its implementation in resource-limited areas of the world. *AIDS* 26, 1231–1241. <https://doi.org/10.1097/QAD.0b013e32835521a3>
- von Andrian, U.H., Mempel, T.R., 2003. Homing and cellular traffic in lymph nodes. *Nat. Rev. Immunol.* 3, 867–78. <https://doi.org/10.1038/nri1222>
- von Neumann, J., 1969. Theory of self-reproducing automata. *Inf. Storage*

- Retr. 5, 151. [https://doi.org/10.1016/0020-0271\(69\)90026-6](https://doi.org/10.1016/0020-0271(69)90026-6)
- Wahl, L.M., Nowak, M.A., 2000. Adherence and drug resistance: predictions for therapy outcome. *Proc. Biol. Sci.* 267, 835–43. <https://doi.org/10.1098/rspb.2000.1079>
- Walker, D.C., Southgate, J., 2009. The virtual cell--a candidate co-ordinator for “middle-out” modelling of biological systems. *Brief. Bioinform.* 10, 450–461. <https://doi.org/10.1093/bib/bbp010>
- Wang, J., Zhang, R., Kuniya, T., 2015. Mathematical analysis for an age-structured hiv infection model with saturation infection rate. *Electron. J. Differ. Equations* 2015, 1–19.
- Ward, J.M., Cherian, S., Linden, M.A., 2018. Hematopoietic and Lymphoid Tissues, in: *Comparative Anatomy and Histology*. Elsevier, pp. 365–401. <https://doi.org/10.1016/B978-0-12-802900-8.00019-1>
- Weisbuch, G., Atlan, H., 1988. Control of the immune response. *J. Phys. A. Math. Gen.* 21, L189–L192. <https://doi.org/10.1088/0305-4470/21/3/013>
- Whitley, E., Ball, J., 2002. Statistics review 2: Samples and populations. *Crit. Care* 6, 143–148. <https://doi.org/10.1186/cc1473>
- WHO, 2013. Consolidated guidelines on the use of antiretroviral drugs for treating and preventing HIV infection [WWW Document]. URL <http://www.who.int/hiv/pub/guidelines/arv2013/download/en/> (accessed 10.28.14).
- WHO, 2010. Antiretroviral therapy for HIV infection in adults and adolescents: recommendations for a public health approach [WWW Document]. URL <http://apps.who.int/iris/handle/10665/44379> (accessed 10.28.14).

- Williams, J.P., Hurst, J., Stöhr, W., Robinson, N., Brown, H., Fisher, M., Kinloch, S., Cooper, D., Schechter, M., Tambussi, G., Fidler, S., Carrington, M., Babiker, A., Weber, J., Koelsch, K.K., Kelleher, A.D., Phillips, R.E., Frater, J., 2014. HIV-1 DNA predicts disease progression and post-treatment virological control. *Elife* 3, e03821. <https://doi.org/10.7554/eLife.03821>
- Wolfram, S., 2002. A New Kind of Science [WWW Document]. URL <http://www.wolframscience.com/nks/> (accessed 8.1.20).
- Wolfram, S., 1983. Statistical mechanics of cellular automata. *Rev. Mod. Phys.* 55, 601–644. <https://doi.org/10.1103/RevModPhys.55.601>
- Wooldridge, M., Jennings, N.R., 1995. Intelligent agents: theory and practice. *Knowl. Eng. Rev.* 10, 115–152. <https://doi.org/10.1017/S0269888900008122>
- Worobey, M., Gemmel, M., Teuwen, D.E., Haselkorn, T., Kunstman, K., Bunce, M., Muyembe, J.-J., Kabongo, J.-M.M., Kalengayi, R.M., Van Marck, E., Gilbert, M.T.P., Wolinsky, S.M., 2008. Direct evidence of extensive diversity of HIV-1 in Kinshasa by 1960. *Nature* 455, 661–664. <https://doi.org/10.1038/nature07390>
- Wu, H., 2005. Statistical methods for HIV dynamic studies in AIDS clinical trials. *Stat. Methods Med. Res.* 14, 171–192. <https://doi.org/10.1191/0962280205sm390oa>
- Wynn, T., 2008. Cellular and molecular mechanisms of fibrosis. *J. Pathol.* 214, 199–210. <https://doi.org/10.1002/path.2277>
- Xiao, Y., Miao, H., Tang, S., Wu, H., 2013. Modeling antiretroviral drug responses for HIV-1 infected patients using differential equation models. *Adv. Drug Deliv. Rev.* 65, 940–953. <https://doi.org/10.1016/j.addr.2013.04.005>

- Xu, S., Srinivasan, P.A., Armaou, A., 2014. Optimization of Interruptions in HIV treatment using a multiscale mechanistic model, in: 53rd IEEE Conference on Decision and Control. Los Angeles, California, USA, pp. 3029–3034.
- Yamaguchi, T., Wing, J.B., Sakaguchi, S., 2011. Two modes of immune suppression by Foxp3+ regulatory T cells under inflammatory or non-inflammatory conditions. *Semin. Immunol.* 23, 424–430. <https://doi.org/10.1016/j.smim.2011.10.002>
- Yang, X.-S., Yang, Y.Z.L., 2010. Cellular Automata Networks. *Proc. Unconv. Comput.* 2007 280–302.
- Yukl, S.A., Boritz, E., Busch, M., Bentsen, C., Chun, T.W., Douek, D., Eisele, E., Haase, A., Ho, Y.C., Hütter, G., Justement, J.S., Keating, S., Lee, T.H., Li, P., Murray, D., Palmer, S., Pilcher, C., Pillai, S., Price, R.W., Rothenberger, M., Schacker, T., Siliciano, J., Siliciano, R., Sinclair, E., Strain, M., Wong, J., Richman, D., Deeks, S.G., 2013. Challenges in Detecting HIV Persistence during Potentially Curative Interventions: A Study of the Berlin Patient. *PLoS Pathog.* 9, e1003347. <https://doi.org/10.1371/journal.ppat.1003347>
- Zeng, M., Haase, A.T., Schacker, T.W., 2012a. Lymphoid tissue structure and HIV-1 infection: Life or death for T cells. *Trends Immunol.* 33, 306–314. <https://doi.org/10.1016/j.it.2012.04.002>
- Zeng, M., Paiardini, M., Engram, J.C., Beilman, G.J., Chipman, J.G., Schacker, T.W., Silvestri, G., Haase, A.T., 2012b. Critical role of CD4 T cells in maintaining lymphoid tissue structure for immune cell homeostasis and reconstitution. *Blood* 120, 1856–1867. <https://doi.org/10.1182/blood-2012-03-418624>
- Zeng, M., Smith, A.J., Wietgreffe, S.W., Southern, P.J., Schacker, T.W.,

- Reilly, C.S., Estes, J.D., Burton, G.F., Silvestri, G., Lifson, J.D., Carlis, J. V, Haase, A.T., 2011. Cumulative mechanisms of lymphoid tissue fibrosis and T cell depletion in HIV-1 and SIV infections. *J. Clin. Invest.* 121, 998–1008. <https://doi.org/10.1172/JCI45157>
- Zeng, M., Southern, P.J., Reilly, C.S., Beilman, G.J., Chipman, J.G., Schacker, T.W., Haase, A.T., 2012c. Lymphoid Tissue Damage in HIV-1 Infection Depletes Naïve T Cells and Limits T Cell Reconstitution after Antiretroviral Therapy. *PLoS Pathog.* 8, e1002437. <https://doi.org/10.1371/journal.ppat.1002437>
- Zhang, S., Liu, J., 2005. A Massively Multi-agent System for Discovering HIV-Immune Interaction Dynamics, in: Ishida, T., Gasser, L., Nakashima, H. (Eds.), *Lect. Note. Artif. Intell., Lecture Notes in Computer Science*. Springer Berlin Heidelberg, Berlin, Heidelberg, pp. 161–173. [https://doi.org/10.1007/11512073\\_12](https://doi.org/10.1007/11512073_12)
- Zhong, P., Agosto, L.M., Ilinskaya, A., Dorjbal, B., Truong, R., Derse, D., Uchil, P.D., Heidecker, G., Mothes, W., 2013. Cell-to-Cell Transmission Can Overcome Multiple Donor and Target Cell Barriers Imposed on Cell-Free HIV. *PLoS One* 8. <https://doi.org/10.1371/journal.pone.0053138>
- Zorzenon dos Santos, R.M., Coutinho, S., 2001. Dynamics of HIV Infection: A Cellular Automata Approach. *Phys. Rev. Lett.* 87, 168102. <https://doi.org/10.1103/PhysRevLett.87.168102>
- Zuse, K., 1969. *Rechnender Raum (Calculating Space)*, in: *Schriften Zur Datenverarbeitung*. Springer Fachmedien Wiesbaden. <https://doi.org/10.1007/978-3-663-02723-2>

## Appendix A The Human Immune System

As a complex system involving a multitude of different components with emergent and adaptive properties, the immune system has been subject to extensive research, (Nagy, 2014) but is still not well understood in many parts. This section gives a brief overview on the principal components and their known properties. For more detailed explanation, the reader is referred to an appropriate textbook, e.g. (Parham, 2009).

Clearly the purpose of the immune system is to provide protection and defence of the organism against pathogens attacking either from outside (e.g. infections) or inside (such as cancers). Any factor foreign to the organism, which is recognised by the immune system is called an *Antigen* in immunology terminology. This term is mostly associated with a pathogen, such as virus particles or specific structures on the surface of a pathogenic cell but may also be connected to non-pathogenic substances, e.g. in case of allergies.

The passage of pathogens into critical parts of the organism is firstly impeded by multiple epithelial and mucosal barriers. Apart from these static preventive measures, defence is concentrated in certain mobile components, circulating in the body fluids. These are classified into *Cell-mediated* and *Humoral* (non-cellular) immunity. Alternatively, immune system components are classified by how they deal with infections, e.g. whether they act either in an immediate (within minutes) but *unspecific* manner or are *selective* to certain pathogens on a longer time scale (days), the former known as *innate*, the latter known as *adaptive* immunity. The components and the properties of these two classes are listed here, a description of their functionality is the focus of the next sections:

## **A.1 Innate Immunity**

The first layer of defence is provided by *mechanical and physiological barriers*. This layer aims to prevent intrusion of antigen into the organism. It covers the surface exposed to the environment, namely the skin, the mucous membranes, (which line the digestive and respiratory systems and the urogenital tract). These boundaries are populated by immune cells or substances but also by foreign microorganisms. These symbiotic organisms feed from by-products of the organism and displace potential pathogens.

Pathogens may pass these barriers through wounds or damaged mucosal tissue. This intrusion of antigen causes an early response by a protein class called cytokines which are released at the infection site by effector cells. Cytokines are considered the cause of *inflammation* symptoms e.g. local pain and swelling around the infection site, which facilitates the influx of immune cells and promotes immune response.

The *Complement System* is an effective part of the innate immune system, which consists of a set of proteins which bind to pathogens in an unspecific way. When discovered, this component was assumed to be ‘complementing’ the parts of the adaptive immune response. The binding to pathogen acts as a beacon, which attracts immune cells and promotes phagocytosis. The membrane-bound proteins also cause damage to bacterial membrane structure, leading to perforation and lysis of the pathogen. Apart from mechanical and soluble immune factors, the immune system consists of various types of *cellular components* (see Figure A.1) with both innate and adaptive effects.

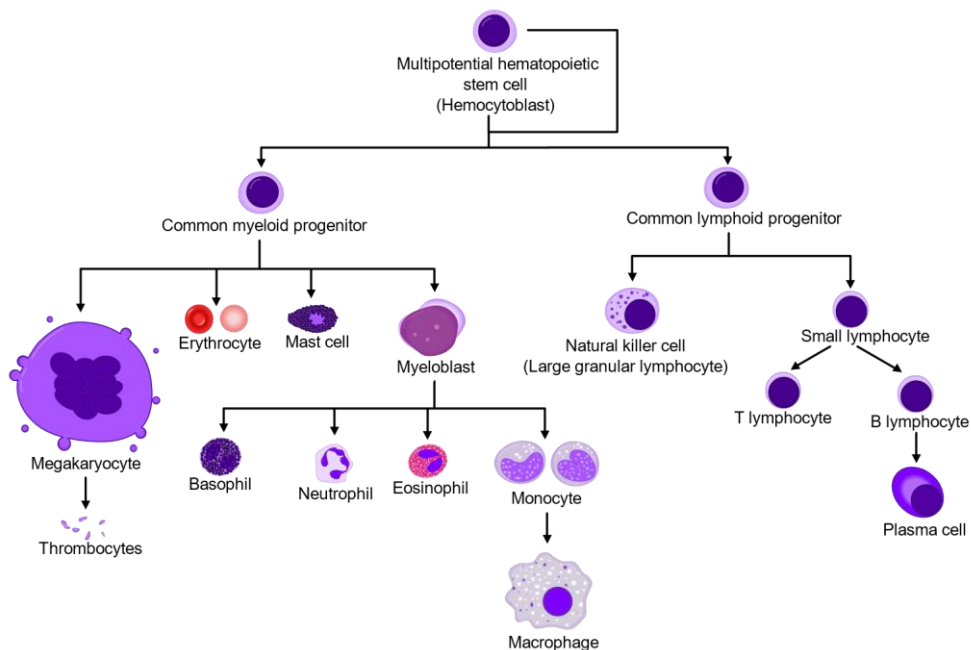


Figure A.1: **Cellular components of the immune system.** Figure shows differentiation paths from common multipotent stem cells, which propagate in the bone marrow. Myeloid (Greek ‘bone marrow’) precursor cells (left) form red blood cells and thrombocytes as well as cellular components of the innate immune system. Right path leads to lymphoid cells which need lymphoid organs for maturation and form the components of the adaptive immune system.

Image Source: Rad, A. and Häggström, M. (2009) *Simplified hematopoiesis*, Wikimedia Commons, the free media repository. Available at: [https://commons.wikimedia.org/wiki/File:Hematopoiesis\\_\(human\)\\_diagram.png](https://commons.wikimedia.org/wiki/File:Hematopoiesis_(human)_diagram.png) (Accessed: 27 May 2020). Use permitted under the Creative Commons Attribution License CC BY-SA (<http://creativecommons.org/licenses/by-sa/3.0/>)

*Phagocytes* are involved in direct attack on pathogens of foreign origin. Antigen is engulfed by the plasma membrane of the immune cells and digested inside. Cells in this category are *Macrophages*, which reside in tissues or *Monocytes*, equivalently, in blood. Another type of cells, *Dendritic Cells*, have a large surface area to collect Antigen from the environment and ‘present’ it to cells of the adaptive immune system. This capability is shared also by *Macrophages* and *B-Cells* from the adaptive immune system.

A type of *Phagocytes*, which does not target foreign antigen are *Natural Killer Cells*. These cytotoxic cells attack cellular components of the organism,

which lack certain recognised characteristics. This may be the case for cancerous or infected cells for which Natural Killer Cells induce apoptosis<sup>16</sup>.

*Granulocytes* contain inclusion bodies ('granules') consisting of cytotoxic substances, which are released near potential pathogen. Beside this function they also play a role in immune regulation and Antigen presentation. Cell types in this category are Basophils, Eonophils and Neutrophils.

*Mast Cells* act similar to the Granulocyte type of Basophils, but appear in outward tissue, such as skin and mucosa, rather than in blood. They are activated when exposed to the external environment e.g. due to a wound and release cytotoxic and inflammatory signals. Due to their exposure to external substances which may be potential antigens, they are also involved in allergic reactions, e.g. hay fever.

## **A.2 Adaptive Immunity**

The ability to adapt to infections of known pathogens and to improve response upon reinfection is central to the immune system. An important role in adaptive immune response is played by lymphocytes, commonly named 'white blood cells'. These mainly reside in the lymphatic organs after their formation in the blood marrow, hence their name. HIV infection has major implications for these cells. Commonly, there are two types of Lymphocytes, B and T (see Figure A.1). The letters indicate the place where the cells mature, bone marrow or thymus. The B-Lymphocytes are able to secrete a large number of immune globulins upon activation (as Plasma cells). These proteins, also termed 'antibodies' have high specificity to certain antigen. This binding enhances attraction of other parts of the immune system and

---

<sup>16</sup> Apoptosis stands for a variety molecular pathway cascades inside a cell, which lead to eventual destruction of the cell. Induction of apoptosis may originate from external factors like Killer cells, but can also be initiated by the cell, e.g. when vital components like DNA are critically damaged by pathogens.

phagocytosis. Activation of B-Lymphocytes and formation of secreting Plasma cells is a comparatively slow process, taking several days. However, immune response is effective and long-lived Plasma cells remain in the organisms after infection with much shorter re-activation time, forming a kind of 'immune memory'.

For T-Lymphocytes there are two types, which are most common, and which have different functions. T-helper cells play an essential role in immune response mediation between the innate and the adaptive system and for the immune memory. On their surface they have receptors<sup>17</sup> of certain types, which are important for their function. According to the receptor, these cells are called CD4 positive T-cells or CD4+.

The other type of T-Lymphocytes has a cytotoxic effect. The signalling receptor which is central to their functionality is named CD8 (hence CD8+ cells). These cells need activation through the CD4+ cells. Interdependencies of different components of the cellular immune system are described in the next section in greater detail.

---

<sup>17</sup> These receptors are typically proteins in conjunction with carbohydrates (glycoproteins) with a specific 3-dimensional structure allowing specific other macromolecules to dock, which may catalyse reactions inside the cells.

## A.2.1 Lymphatic System

The lymphatic system consists of a widespread network of ducts throughout the whole body (see Figure A.2). Unlike the blood stream, movement of fluid (the *lymph*) is not controlled by a central pumping organ, but through mechanical and osmotic processes of the single lymphatic organs, (Margaris and Black, 2012; Swartz, 2001).

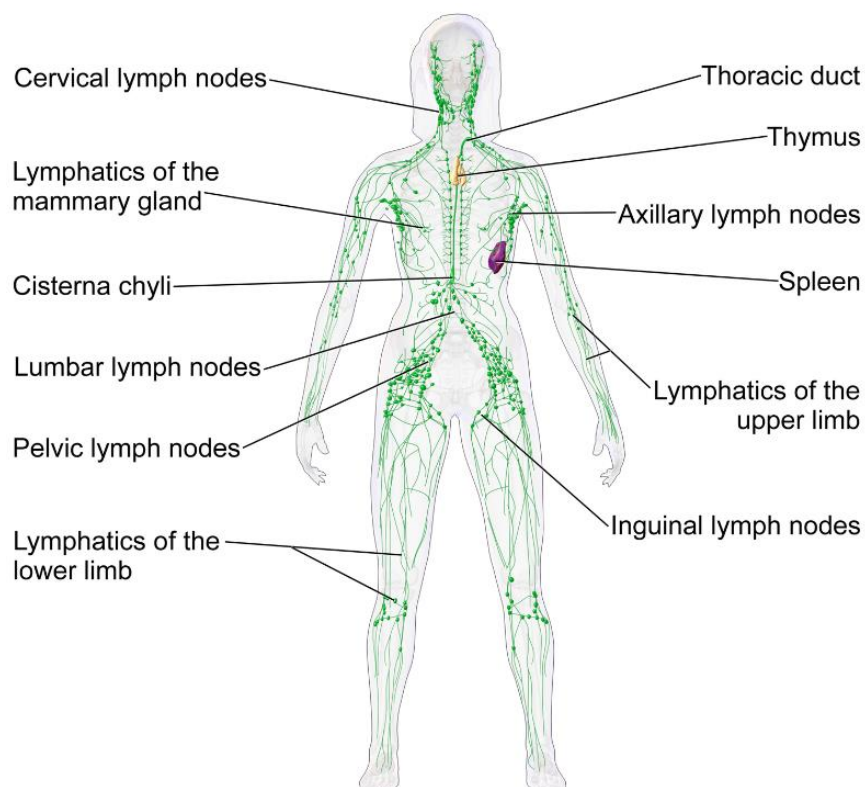


Figure A.2: **Lymphatic system (female) with principal organs.** Nodes and ducts forming the lymphatic network coloured green.

Image source: Blausen.com staff (2014) 'Medical gallery of Blausen Medical 2014', WikiJournal of Medicine, 1(2). doi: 10.15347/wjm/2014.010. Use permitted under the Creative Commons Attribution License CC BY (<https://creativecommons.org/licenses/by/4.0/>)

Physiologically, this system allows excess water in tissues to be collected and returned to the blood stream. Along with the lymph nodes it acts as a filter system through which the body fluid (*lymph*) is cleaned of antigens. The

lymph fluid enters a node through specific vessels and passes through the mesh structured tissue to leave the node through effluent vessels (see Figure A.3).

Lymph nodes enable a prolonged contact of the fluid with immune cells through a slow flow rate of the lymph which contrasts with fast-flowing blood circulation. The system does not act as a filter against toxins as this function is covered by the liver and kidneys. The spleen is also acting as a lymph node. In recent years technologies like two-photon microscopy have enabled a better insight into the movement of immune cells inside the lymph nodes (Germain et al., 2012).

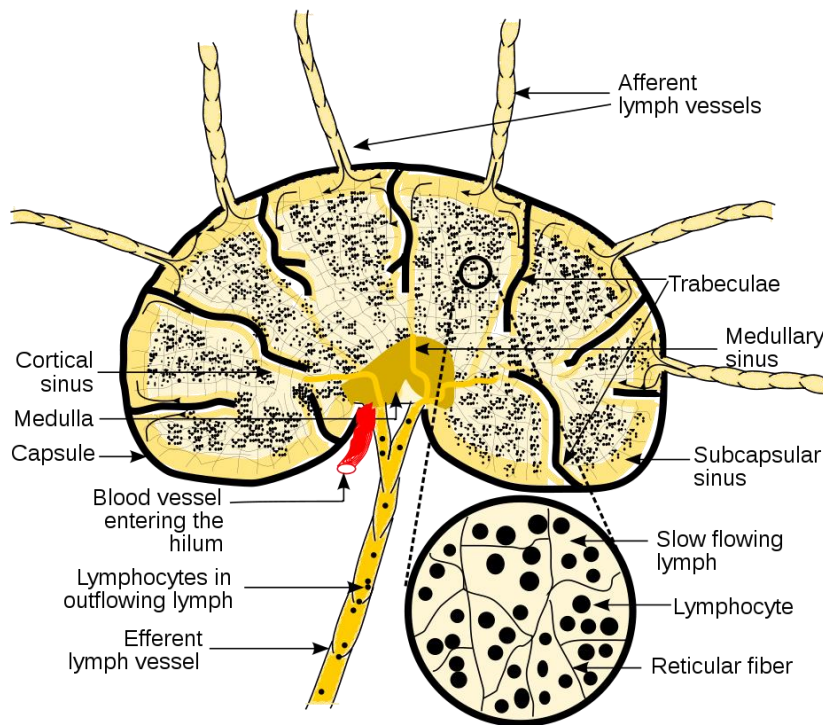


Figure A.3: **Schematic of a lymph node.** Lymph entering the node through afferent vessels flows slowly through the reticular network (enlarged portion), enabling lymphocyte contact with stromal cells before leaving the node through afferent vessels.

Image Source: KC Panchal (2008) *Schematic\_of\_lymph\_node\_showing\_lymph\_sinuses*, *Wikimedia Commons, the free media repository*. Available at: [https://commons.wikimedia.org/wiki/File:Schematic\\_of\\_lymph\\_node\\_showing\\_lymph\\_sinuses.svg](https://commons.wikimedia.org/wiki/File:Schematic_of_lymph_node_showing_lymph_sinuses.svg) (Accessed: 27 May 2020). Use permitted, public domain

## **A.2.2 Maturation of Immune Cells**

All immune cells are generated and continuously replenished from pluripotent stem cells in the bone marrow (see Figure 1). Depending on the type of immature immune cells their respective receptors (T-cell or B-cell) gain a random conformation. The immature cells undergo a process of positive and negative selection in the thymus (T-cell) or bone marrow (B-cells) through exposure to *self-antigens*<sup>18</sup>. Cells for which receptor bindings to those antigens are too weak or too strong are removed through apoptosis. The first process ensures that only cells with functional receptors remain (positive selection) where the second process prevents autoimmune reactions. This second process is called *self- non-self-discrimination*<sup>19</sup>.

## **A.2.3 Immune Activation**

Immature immune cells which undergo the selection process are typically resident in the lymph nodes. These become activated when encountering an antigen matching their respective receptor conformation (see Figure A.4 for a schematic). The receptor binds to the antigen non-covalent with weak van-der-Waals force maintaining a stable connection if the contact area is large enough. T-cell receptors do not bind to antigen in their environment but are ‘presented’ by other cells bound to specific macromolecules (Major Histocompatibility Complex MHC) on their surface. MHC can be differentiated into types 1 and 2. Type 1 occurs on the surface of every cell in the organism and presents fragments of proteins coming from inside the cell. These may be self-antigens from the cells own protein repertoire but also virus fragments in case the cell has been infected. MHC type 1 bound antigen

---

<sup>18</sup> These may be any part of the organism (e.g. proteins on the surface of cells) which is recognized as antigen by the immune system.

<sup>19</sup> The ability of the immune system to distinguish between foreign antigen and self-antigen.

is recognized by CD8 receptor of cytotoxic T-cells. When binding is strong enough, cells become activated.

MHC type 2 appear on the surface of specific antigen presenting cells APC. These may be *dendritic cells*, *macrophages* or *B-cells*. These types of cells typically obtain antigen from their neighbourhood, which is digested, and fragments are presented via MHC type 2. The cells do not distinguish between antigens coming from the organism itself or from infected cells. Macrophages and dendritic cells pick up antigens without specificity where B-cells are specific to antigens matching their receptor conformation.

The MHC type 2 are necessary for activation of T-helper cells and binds to their CD4 receptor. Activated T-helper cells may proliferate, attract other immune cells, become memory cells or activate B-cells in turn. Activated B-cells may proliferate and develop to plasma cells which disseminate antibodies. The binding sites of these antibodies are identical to the B-cell receptor of the respective cell.

Activated immune cells proliferate through cell division which leads to a progeny with identical genetic setup. Stimulation of B-cells becomes stronger the more receptors are bound to antigen. This process is called *cross linking*, it also suppresses stimulation if too many receptors are bound. Upon proliferation of activated B-cells, random mutations are introduced at specific sites encoding the shape of the receptor and antibody. These modifications may lead to a higher antigen binding affinity and stronger proliferation of these clonotypes in turn. Applying Darwinian principles, one can say these clonotypes are selected because of increased fitness to the environment.

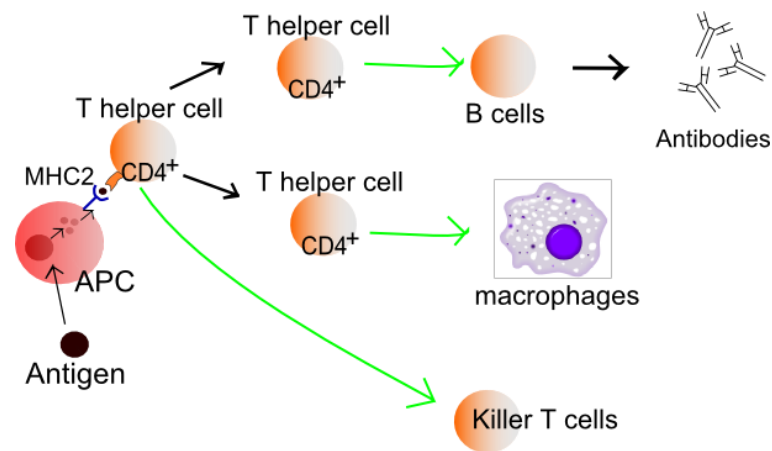


Figure A.4: **Immune cell activation** and parts of the cellular immune response; B-cell response (top), macrophage activation (middle) and T-cell / CD8+ response (bottom).

Image Source: Häggström, M. (2014) 'Medical gallery of Mikael Häggström 2014', *WikiJournal of Medicine*, 1(2). doi: 10.15347/wjm/2014.008. Use permitted, public domain.

## A.2.4 Immune Memory

Even after infection these clonotypes can persist through a process of self-renewal as memory T- and B-cells. Activation of these in the presence of antigens is faster than that of naïve cells which increases efficiency of the immune system in case of a re-infection. The total number of immune cells in the organism is limited. During the lifetime of an organism, the proportion of mature memory immune cells which are specific against certain epitopes is increasing against naïve cells. Self/non-self-discrimination is a central aspect in immune theory in explaining how autoimmune reactions are suppressed. There have been different approaches to explain this behaviour, one of them is Danger Theory, (Matzinger, 1994), which postulates that immune reactions are triggered exclusively through *danger signals* which are sent out by distressed cells in case of an infection. This would eliminate the need for self-non-self-discrimination. However, whether the theory describes all observable immune reactions in this context sufficiently, is still under discussion, (Pradeu and Cooper, 2012).

## Appendix B Antiretroviral Drug Regimen

Drugs are commonly mentioned with their abbreviations in the literature.

<b>NRTIs / NtRTIs</b>		<b>NNTRIs</b>		<b>PIs</b>	
<b>3TC</b>	lamivudine	<b>DLV</b>	delavirdine	<b>ATV</b>	atazanavir
<b>ABC</b>	abacavir	<b>EFV</b>	efavirenz	<b>DRV</b>	darunavir
<b>AZT</b>	or	<b>ZDV</b>	<b>ETR</b>	<b>FPV</b>	fosamprenavir
	zidovudine		<b>NVP</b>	<b>IDV</b>	indinavir
<b>d4T</b>	stavudine		<b>RVP</b>	<b>NFV</b>	nelfinavir
<b>ddL</b>	didanosine			<b>LPV/RTV</b>	ritonavir
<b>FTC</b>	emtricitabine			(only given in combination with other PI – denoted ‘r’)	
<b>TDF</b>	tenofovir			<b>SQV</b>	saquinavir
				<b>TPV</b>	tipanavir
<b>INSTIs</b>		<b>Entry / Fusion Inhibitors</b>		<b>Pharmacokinetic enhancer</b>	
<b>DTG</b>	dolutegravir	<b>MVC</b>	maraviroc	<b>COBI</b>	cobicistat
<b>EVG</b>	elvitegravir	<b>T-20</b>	enfuvirtide		
<b>RAL</b>	raltegravir				
<b>Primary recommendation:</b>			<b>Alternatives, if primary not available:</b>		
TDF + 3TC (or FTC) + EFV			AZT + 3TC + EFV		
			AZT + 3TC + NVP		
			TDF + 3TC (or FTC) + NVP		
<b>Primary recommendation:</b>			<b>Secondary recommendation:</b>		
AZT + 3TC + LPV/r			TDF + 3TC (or FTC) + ATV/r		
AZT + 3TC + ATV/r			TDF + 3TC (or FTC) + LPV/r		

## **Appendix C Alternative Model Formalisms**

### **C.1 P-Systems**

P-Systems were introduced by Gheorges Păun as a form of biological computing, (Păun, 2000) and are constructed similar to a biological cell with organelles, membranes arranged in a nested manner. This leads to the formation as a set of compartments which are arranged hierarchically. The membranes may contain objects, which are symbols or character sequences in the original concept and where membranes and objects form a super-cell. Objects can evolve according to a set of rules, which are assigned to the different compartments of the membranes. Rules apply only to the objects, which are currently in the respective compartment, i.e. for certain object configurations in the membrane compartment for which it is valid. Rules may cause objects to evolve (be changed) or to be moved into another membrane compartment, (parent or child) of the hierarchy. Modification of the membrane structure is also rules-based, where new membrane compartments can be created from a parent or existing membranes can be dissolved. In the latter case the contents of the dissolved membrane (objects and membranes) are now members of the parent membrane compartment.

In the original concept, the rules for the various compartment levels are executed in parallel with prioritisation to avoid conflicts. This approach has been criticized as not conforming to biological systems. To overcome this, rule execution directed by a Gillespie algorithm has been suggested, (Romero-Campero et al., 2009; Spicher et al., 2008), leading to stochastic P-systems. However, the original assumption for the Gillespie algorithm of a well-mixed compartment does not reflect interaction between the different organelles of a cell.

Objects were originally assumed to take the form of strings. The intention was to mimic the modification and mutation of DNA-fragments, (Păun, 2000). However, this approach makes modelling of quantities difficult, so conformon P-systems were introduced, (Frisco, 2004). Conformons represent name-value combinations and they make up the objects in the P-system. The P-system rules may modify the values of the conformons in the respective compartment and move them to different membranes depending on their names or values. This may be used to model quantities of biochemical substances inside a cell. Applications of conformon P-systems also include immune system simulation, (Corne and Frisco, 2008).

## C.2 State Charts

State Charts have been developed as a means to describe finite state machines, which are used for complex concurrent systems in an easily conceivable manner relating them to process algebras and petri nets. Introduced by Harel, (Harel, 1987), state charts presented an approach to develop and visualize complex technical systems like aircraft and automotive controls in a descriptive but formal manner. Subsequently state charts have been adapted to model immune system dynamics, (Kam et al., 2001). The state chart itself is not executable. To build a working model it has to be translated back into the corresponding finite state machine, which may then be implemented using a model formalism such as a system of ODEs. Their characteristics make state charts more of a *meta modelling* formalism, i.e. a way of visualizing another formalism.

Newer modelling approaches involve rule-based modelling, (Gruenert et al., 2010), where entities which obey relatively simple rules interact to produce emergent complex structures. Typically, these are used for protein interactions which self-organise to form macro structures.

### **C.3 Shape Space**

Network based theories were developed in the 1970s after initial discoveries on immune mechanisms and the complex interactions between the different elements. The idiotypic network theory was introduced by Niels Jerne, (Jerne, 1974), and aimed at answering questions on the way in which the immune system emerges from a naïve to mature state where certain ‘non self’ antigens cause immune reactions, (while others are tolerated) and what prevents the immune system from attacking parts of its own organism. The central idea was that the immune system basically does not distinguish between self and non-self and each component may react with each other, so everything is an antigen. An antigen region, which may be part of the immune system or the organism or some foreign substance, recognised by the immune system, is termed an idio type. Constant interaction occurs between elements of humoral and cellular immune defence and antigens, which causes either stimulation, suppression or death of both self- and non-self-antigen. The interaction is 2-way so the approach is also designated ‘symmetrical’ network theory.

The shape space concept, (Perelson and Oster, 1979), presents a way to describe this large number of idiotypes and their emergence. Each idio type is represented by a bit string of length  $N$ , therefore it has a location in a space of  $N$  dimensions. The closer two idiotypes are in shape space, the similar their basic shape. Interactions can be described by drawing a radius around a point in shape space in which other idiotypes have to be located in order to interact.

The overall concept has been applied to the wide range of immune reactions and was quite successful in describing autoimmune diseases, (Hoffmann, 2007), as well as the way which repeated infection with the same antigen changes immune response (secondary response). The shape-space model has also been applied to HIV infection, (Hershberg et al., 2001), and can be used to illustrate the high mutation rate of the virus with rapid shifts in shape space together with lagging and incomplete immune response.

The optimal length of  $N$  and therefore dimensionality of shape space or its validity for real biochemical reactions is not yet finally resolved, (Carneiro and Stewart, 1994; McEwan and Hart, 2009). Moreover, the immune network modes failed to describe all complex interactions occurring in the immune system, (Murphy et al., 1976), which led to some loss of popularity. Additionally spatial aspects, which have implications for immunological performance, (Graw and Perelson, 2013), are completely neglected. To deal with this aspect, hybrid models involving also physical space were also developed, (Burns and Ruskin, 2004; Papa and Tsallis, 1996).

## **C.4 Stochastic Simulations**

The Gillespie algorithm, (Gillespie, 2007), offers an interesting way of combining rate equations with stochastic discrete reaction events, instead of assuming reaction rates as for a deterministic set of ODEs. The algorithm was developed for chemical reaction kinetics in well mixed compartments, (Gillespie, 1976), and originates from thermodynamics. The model omits any other effects which may influence the reactants, such as collisions with the reaction vessel. A model run for a set of chemical reactions starts from an initial number of reactant molecules for which the next reaction occurring is randomly chosen. The probabilities for the reactions to occur depend on the state of the system and are updated at each step, together with the number of molecules, with time to the next reaction selected at random.

This algorithm approximates an ODE system while obtaining more information on system characteristics. In its basic form, the Gillespie algorithm is computationally expensive, but has been improved through optimisation algorithms like tau leaping, (Link et al., 2012). The algorithm has also gained popularity for use in hybrid models, (Romero-Campero et al., 2009; Spicher et al., 2008), and has been incorporated into immune system models to account for stochastic effects like movement or binding.

## C.5 Boolean Networks and Petri Nets

Boolean networks, (Albert and Wang, 2009; Kauffman, 1969), and Petri nets, (Chaouiya, 2007; Murata, 1989), are also a commonly used formalism originally intended to study genetic regulation networks. Both graph-based these can improve visualisation capability. Due to their simple rules they are easily accessible for non-computer scientists.

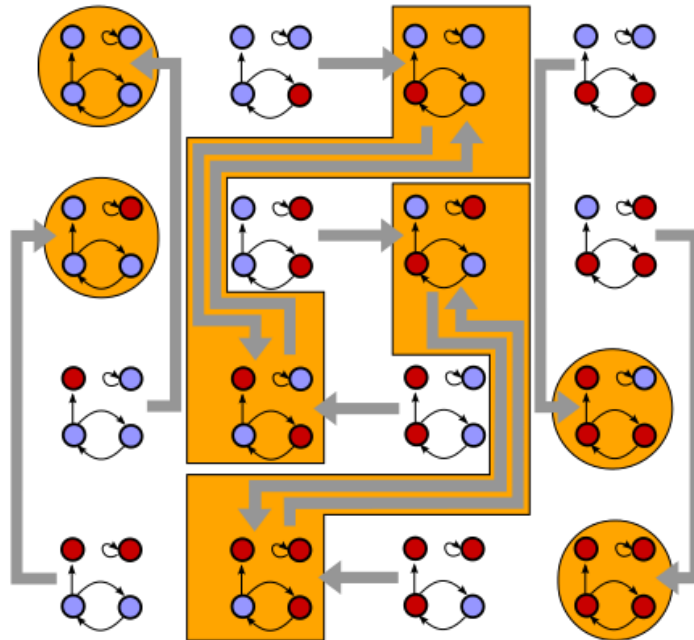


Figure C.1: **State space of a Boolean network** with  $N=4$  nodes and  $K=1$  links per node.

Image Source: Hou710 / (2014) Boolean Network, Wikimedia Commons, the free media repository. Available at: [https://commons.wikimedia.org/wiki/File:Hou710\\_BooleanNetwork.svg](https://commons.wikimedia.org/wiki/File:Hou710_BooleanNetwork.svg) (Accessed: 27 May 2020). Use permitted under the Creative Commons Attribution License CC BY-SA (<https://creativecommons.org/licenses/by-sa/4.0>)

The setup of a Boolean network consists of a graph with  $N$  Boolean variables which form the nodes, and which have  $K$  directed links each as edges. In the case of a Random Boolean Network, the links are arranged randomly. A node can also be linked to itself, i.e. the input node is equal to

the output node. Nodes are assigned with an initial state pattern and the model is run. At each discrete time step, the states of the Boolean variables are changed according to the input node connected by the link. The simulation is run until the network reaches a static or periodic final state. Obtaining the state space for all possible initial states gives tree-like structures which resemble biological reaction networks, (see Figure C.1). Despite the simple setup the state space can become very complex. Boolean networks are therefore related to cellular automata. They have been successfully applied to biochemical network modelling, (Albert and Wang, 2009).

Petri nets, (Petri, 1962), first suggested as a model for chemical reactions are related to the process algebras but feature two distinct node types, places and transitions. Places can only be connected via a transition and vice versa. These connections are typically directed (place – transitions – place) and have a certain weight assigned. In the original concept places may contain a number of ‘tokens’. If all places, which act as an input to a transition have equal or more tokens than the weight of their respective connection, the transitions ‘fires’. The number of tokens of the input places is then reduced by the weight of their connection. Correspondingly, the number of tokens of the places acting as output to the transition is decreased by the value of weights of the output connections (see Figure C.2 for an example). These elements allow building of complex networks. Evaluation of token number of places and firing of transitions occur at discrete time intervals and for the whole network in parallel. This concept has been used for biological networks, (Chaouiya, 2007; Reddy et al., 1993).

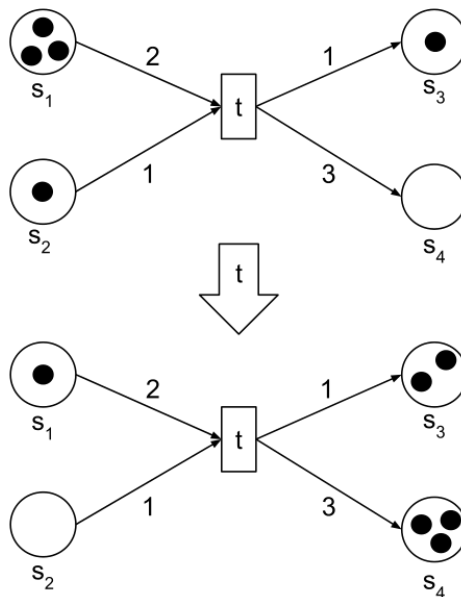


Figure C.2: **Petri net with 4 nodes and 1 transition** shown before and after transitions ‘fires’.

Image Source: Le blue (2014) *Petrinet\_transition\_example*, *Wikimedia Commons, the free media repository*. Available at: [https://commons.wikimedia.org/wiki/File:Petrinet\\_transition\\_example.svg](https://commons.wikimedia.org/wiki/File:Petrinet_transition_example.svg) (Accessed: 27 May 2020). Use permitted under the Creative Commons Attribution License CC BY-SA (<https://creativecommons.org/licenses/by-sa/4.0>)

## C.6 Cellular Potts

Cellular Potts had been introduced as a modification of the large-Q Potts models for simulation of aggregate formations on cells, (Graner and Glazier, 1992). The basic model is derived from thermodynamics where it is used to simulate ferromagnetism. Essentially these models are a special case of CA where an agent is not represented by a single cell but by continuous compartments on a lattice. These cell ‘shapes’ are allowed to change depending on their surface energy. This allows a better representation of biological reality than dealing with single lattice sites and cell –cell contacts can be examined more realistically. The concept has been applied to the motility of T-cells inside lymph nodes, (Beltman et al., 2007). However, computational costs are higher, which limits the size of simulations.

## Appendix D The ZdSC Model

The initial model followed a set of 4 rules in a square lattice with Moore neighborhood and periodic boundary conditions. Cells may have four states: healthy ( $H$ ), infected  $A1$ , infected  $A2$  and dead ( $D$ ).

The rules were therefore set as following:

**Rule 1:** Healthy cells  $H$  may become infected  $A1$

- With at least 1 infected  $A1$  cell in the neighborhood
- With at least  $r$  ( $2 < r < 8$ ) infected  $A2$  cells in the neighborhood

**Rule 2:** Infected  $A1$  becomes infected  $A2$  after  $\tau$  timesteps

**Rule 3:** Infected  $A2$  cells become dead cells  $D$

**Rule 4:** Dead cells  $D$  become  $H$  with probability  $P_{reg}$ , otherwise stay dead

- Regenerated cells become infected  $A2$  with probability  $P_{inf}$

In this setting, the state of a cell in the next step is determined by the states of its surrounding cells. There is no active influence of a cell on its neighbors. Therefore, the *sequence* of cell updates is not relevant and may occur synchronously. On a spatial level, the model shows a characteristic behavior of waves of infected cells progressing over the lattice during the simulated chronic phase of HIV, eventually covering it, which corresponds to the AIDS phase. Each discrete step (in which all cells are updated) corresponds to roughly a week in real time. With this set of model parameters it is possible to simulate the three phases of HIV infection on a qualitative basis, (see Figure D.1).

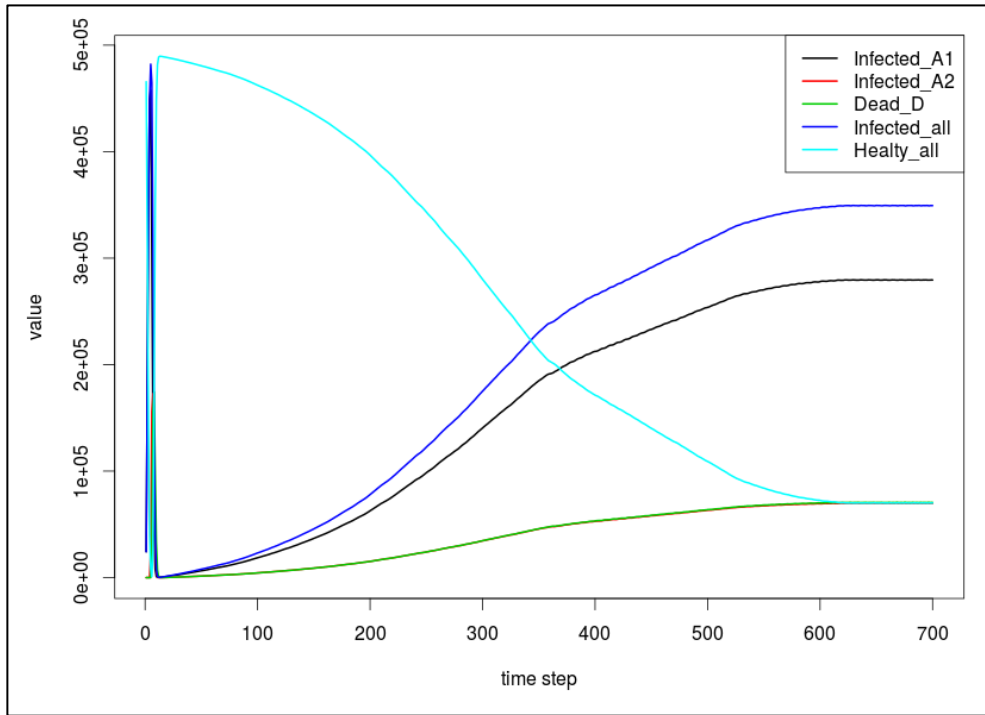


Figure D.1: **Simulation of the HIV time-course using the ZdSC model** (50 runs averaged).. Time step on x-axis corresponds to 1 week in real time, y-axis represents absolute values of cell states described in legend for a 700 x 700 square lattice.

## Appendix E STI Studies in chronological order

<b>Study name/ref</b>	(Davey et al., 1999)
<b>Start, end</b>	1999
<b>Type</b>	One interruption
<b>Aim</b>	Examine viral rebounds
<b>Size</b>	18 <b>treatment experienced</b> patients
<b>Conclusion</b>	Long term suppression does not lead to viral control
<b>Study name/ref</b>	(Rosenberg et al., 2000)
<b>Start, end</b>	2000
<b>Type</b>	One or more interruption
<b>Aim</b>	Examine difference of treatment initiation on immune control
<b>Size</b>	16 treated with <b>acute HIV</b> , 6 untreated control, 12 treated with chronic infection
<b>Conclusion</b>	Early treatment initiation improved viral control
<b>Study name/ref</b>	<b>Autovac</b> (Ruiz et al., 2001, 2000)
<b>Start, end</b>	2000
<b>Type</b>	Fixed cycle; three interruptions for 30 days (or until high rebound) with 90 days interval
<b>Aim</b>	Investigate immune response and potential immune boost of STIs
<b>Size</b>	12 patients with <b>undetectable viral load</b> , 14 control group
<b>Conclusion</b>	Increase of CD8 during interruption, no adverse effects
<b>Study name/ref</b>	(García et al., 2001)
<b>Start, end</b>	2001
<b>Type</b>	Viral load guided; starting point VL < 20 cp/ml, interruption until VL > 200 cp/ml, interruption until vl > 200 cp/ml lasted 4 weeks, no reintroduction
<b>Aim</b>	Analyse viral rebounds and investigate immune response
<b>Size</b>	10 <b>chronically infected</b> patients with VL < 20 cp/ml for at least 1 year
<b>Conclusion</b>	Approach is relatively safe in terms of recovery after reintroduction
<b>Study name/ref</b>	(Dybul et al., 2001)
<b>Start, end</b>	2001
<b>Type</b>	Fixed cycle; one week on – one week off for 52 weeks
<b>Aim</b>	Demonstrate proof of concept of feasibility of 50% reduction
<b>Size</b>	10 <b>treatment experienced</b> patients (initiation in chronic phase?)
<b>Conclusion</b>	Viral suppression could be maintained in blood and lymph tissue
<b>Study name/ref</b>	(Hammer et al., 2002)
<b>Start, end</b>	2002
<b>Type</b>	Salvage therapy
<b>Aim</b>	Assess efficacy of regimen modification (PI) after virological failure
<b>Size</b>	481 patients with VL > 1000 cp/ml and prior exposure to 3 PIs
<b>Conclusion</b>	Results comparable to other salvage therapy

<b>Study name/ref</b>	(Dybul et al., 2003)
<b>Start, end</b>	2003
<b>Type</b>	Fixed cycle; 4 weeks off – 8 weeks on for 48 weeks
<b>Aim</b>	Proof of immune boosting effect and reduction of toxicity for STI
<b>Size</b>	26 <b>treatment experienced</b> patients 26 control group
<b>Conclusion</b>	No hints for immune boost or reduction of toxicity. Resistance mutations in 5 patients on STI.

<b>Study name/ref</b>	(Fagard et al., 2003; Oxenius et al., 2002)
<b>Start, end</b>	2002
<b>Type</b>	Fixed cycle; 2 weeks off – 8 weeks on for 40 weeks
<b>Aim</b>	Proof of immune control
<b>Size</b>	133 <b>treatment experienced</b> patients
<b>Conclusion</b>	Correlation between patients peak viral load to pre- treatment loads, evidence of beneficial effect of therapy introduction during primary infection. No hints of immune stimulating effects. No adverse effects.

<b>Study name/ref</b>	<b>Swiss Spanish intermittent treatment trial</b> (Fischer et al., 2003)
<b>Start, end</b>	2003
<b>Type</b>	Fixed cycle; 1 week on 1 week off, longer period interruption after 5 <sup>th</sup> cycle
<b>Aim</b>	Verify Dybul's trial 1(Dybul et al., 2001)
<b>Size</b>	14 <b>treatment experienced</b> patients
<b>Conclusion</b>	Viral rebound significant at day 8, drug resistant mutations detected. Dybul's results not confirmed

<b>Study name/ref</b>	(Acosta et al., 2004)
<b>Start, end</b>	2002
<b>Type</b>	Pharmacokinetic comparison of two regimens
<b>Aim</b>	Determine pharmacokinetic parameters
<b>Size</b>	44 HIV-infected patients with VL between 500 and 100.000 cp/ml within 45 days of study entry.
<b>Conclusion</b>	Similar tolerability and response rates

<b>Study name/ref</b>	<b>Staccato</b> (Benson, 2006)
<b>Start, end</b>	2006
<b>Type</b>	CD4 guided 350/ul on, 350/ul off
<b>Aim</b>	
<b>Size</b>	Patients were <b>therapy naïve</b> and treated to suppression.284 CD4 guided, 146 control group for 96 weeks. + 1 week on 1 week off (discontinued due to virologic failure)
<b>Conclusion</b>	No adverse effects found

<b>Study name</b>	<b>Trivacan</b> (Benson, 2006)
<b>Start, end</b>	2006
<b>Type</b>	CD4 guided 250 on, 350 off (+ fixed cycle)
<b>Aim</b>	
<b>Size</b>	216 <b>Therapy naïve</b> patients treated to CD4 count of 350 and < 300 virus, (325 patients 4 months on 2 months off fixed cycle), 110 control group
<b>Conclusion</b>	<b>CD4 guided study terminated</b> due to more than 2-fold higher morbidity in STI group.

<b>Study name/ref</b>	<b>SMART</b> (El-Sadr et al., 2006)
<b>Start, end</b>	2006
<b>Type</b>	CD4 guided 250 on, 350 off
<b>Aim</b>	
<b>Size</b>	<b>5472 patients</b> (not clear how weighted, 1.1?) with CD4 counts of 350/ul and above (aim was 3000 + 3000 control) <b>immune functions already impaired, short follow up</b> , (Hirschel and Flanigan, 2009).
<b>Conclusion</b>	CD4 guided trial <b>terminated due to increased frequency of Aids and non-Aids related diseases in the STI group</b> <b>Biggest study so far, results widely accepted, lead to recommendations for continuous ART.</b>

<b>Study name/ref</b>	<b>Window</b> (Benson, 2006)
<b>Start, end</b>	2006
<b>Type</b>	Fixed cycle 8 weeks on 8 weeks off (for 96 weeks?)
<b>Aim</b>	
<b>Size</b>	200 patients with CD4 of 450 and above and virus RNA below 200 for STI, 203 control group
<b>Conclusion</b>	STI noninferior but lower CD4 counts in STI group no increased drug resistance.

<b>Study name/ref</b>	<b>ISS/Part</b> (Benson, 2006)
<b>Start, end</b>	2006
<b>Type</b>	Fixed cycle 1,1,2,2,3 months of interruption with alternating 3 months of therapy
<b>Aim</b>	
<b>Size</b>	136 STI, 137 control group
<b>Conclusion</b>	Higher CD4 count in control group after 24 months, increased rate of resistance mutations in STI group

<b>Study name/ref</b>	<b>LOTTI</b> (Maggiolo et al., 2009)
<b>Start, end</b>	
<b>Type</b>	CD4 guided, 700 ul and not detectable virus (<50) off, below 350 on
<b>Aim</b>	
<b>Size</b>	165 STI, 164 control group, patients <b>with preserved immune function</b>
<b>Conclusion</b>	<b>STI was not inferior</b> , recommendation to preserve immune function by keeping CD4 counts up, obtain safety limits – STI much less costly

<b>Study name/ref</b>	<b>SPARTAC</b> (Fidler et al., 2013)
<b>Start, end</b>	2003-2010
<b>Type</b>	Treatment removal after 48 weeks, 12 weeks or no treatment at all. Re- initiation when CD4 dropped below 350.
<b>Aim</b>	Also investigate HIV DNA, (Williams et al., 2014)
<b>Size</b>	123 patients with <b>primary HIV infection</b> with removal after 48 weeks, 120 after 12 weeks, 123 no treatment. Patients had not detectable virus for at least 6 months prior study.
<b>Conclusion</b>	No adverse effects of removal detected.

<b>Study name/ref</b>	<b>STOPAR</b> (Imaz et al., 2013)
<b>Start, end</b>	2004 - 2008
<b>Type</b>	CD4 guided, 500/ul and no detectable virus (for 3 months) off, below 350 on
<b>Aim</b>	
<b>Size</b>	56 treatment interruption 50 control patients with <b>preserved immune function</b> (85 per arm were planned but enrolment was <b>stopped due to outcomes of SMART study</b> )
<b>Conclusion</b>	Trend to higher frequency of Aids related illness and viral rebound but study size small.

## Appendix F SMART and LOTTI Comparison

	<b>SMART</b> (El-Sadr et al. 2006)	<b>LOTTI</b> (Maggiolo et al. 2009)
<b>Baseline CD4 – up limit [cells/ul]</b>	350	700
<b>Low limit [cells/ul]</b>	250	350
<b>Viral load up limit [RNA/ul]</b>		< 50
<b>CD4 Nadir [cells/ul]</b>		> 200
<b>CD4 limitation</b>		
<b>Follow-up times [months]</b>	1, 2, 4, 6, 8, 10, 12, 16, 20, ...	1, 2, 4, 8, 12, ...
<b>Avg. follow up [months]</b>	16	51
<b>Max follow up [months]</b>	44	>51
<b>Number of patients (STI/Control)</b>	2720 / 2752	165 / 164
<b>Clin end primary points</b>	death/opp. disease	Death/opp. disease/gen clin cond. Hosp.
<b>secondary</b>	Maj. cardiovasc., renal, hep disease	Sympt. disease not req. hosp./ grade 3,4 adv
<b>Hazard ratio</b>	2.6	1.05

## Appendix G Glossary

**Acquired Immunodeficiency Syndrome (AIDS):** General term for clinical symptoms indicating the terminal stage of HIV-infection.

**Adherence:** Measure on how well a patient adheres to a prescribed treatment.

**Antigen:** Molecular structure (usually on the surface of pathogens) which trigger an immune response.

**Antiretroviral therapy (ART):** General term for treatment of HIV infections. Current recommendation is Highly Active ART (HAART), a variant of combination ART (cART).

**CD4+ T-helper lymphocytes:** White blood cells with specific receptors (CD4) on their surface. Responsible for immune recognition of antigen and activation of effector cells. The CD4 receptor is also binding site for HIV, hence these cells are main target of the virus.

**CD8+ T-effector/cytotoxic lymphocytes:** White blood cells with CD8 receptors on their surface. These cells cause an immune response by killing pathogen or infected cells after being activated by CD4+ T-Lymphocytes.

**Collagen:** Protein fibres which form main component of connective tissues, do not have physiological function otherwise.

**Cytokines:** Proteins serving as chemical signalling between cells. Substances excreted by cells are bound by specific receptors on the surface of other cells, triggering certain biological processes.

**Deoxyribonucleic acid (DNA):** Macromolecule containing all genetic information of any living cell. Usually located in highly condensed form in the cellular nucleus.

**Fibroblastic Reticular Cell (FRC):** Specific cell type residing in lymph nodes on connective tissue. Crucial function for stability of the immune system has been identified only recently.

**Fibrosis:** Pathogenic alteration of tissue structure, where functional tissue is replaced by connectivity tissue mainly consisting of collagen fibres. Commonly occurring due to inflammation processes or injuries (e.g. scar tissue).

**High Endothelial Venules (HEVs):** Specialised blood vessels in lymphatic organs which serve as a connection to the blood circulation and enable entry of T-cells and antigen.

**Homeostasis:** Ability of the immune system to maintain stability, e.g. steady levels of immune cells in blood, and to provide effective immune response when challenged with pathogen.

**Human Immunodeficiency Virus (HIV):** Virus with unique properties able to evade the human immune system and causing a slowly progressing infection, ultimately causing lethal AIDS disease.

**Interleukin-7 (IL-7):** A cytokine, typically excreted by FRCs in response to Lymphotoxin-beta signalling.

**Lymph node:** Part of the lymphatic system, nodes occur at intersections of lymphatic ducts. Hosts the majority of Lymphocytes and has crucial function for immune maturation and activation but also HIV pathogenesis.

**Lymphatic system:** Widespread system of nodes and ducts and dedicated organs with multiple purposes of immune maturation and body fluid circulation.

**Lymphocytes:** White blood cells of diverse type, as part of the cellular immune system.

**Lymphotoxin beta (LT- $\beta$ ):** A cytokine, typically excreted by CD4+ cells, in response to Interleukin-7 signalling.

**Regulatory T-cells (Tregs):** Subset of CD4+ T-cells, assumed to dampen immune reactions in order to maintain immune system stability.

**Ribonucleic acid (RNA):** Macromolecule with similar structure to DNA with multiple purposes. Most importantly it is used to transcribe genetic information from the DNA and supply this to protein formation sites.

**Structured treatment interruptions (STIs):** Clinically prescribed interruptions of Antiretroviral Therapy with the aim of minimising patient risk and fostering benefits (e.g. recovery from drug side effects).

**Tissue growth factor beta 1 (TGF- $\beta$ 1):** A cytokine, typically excreted by regulatory T-cells, triggers the growth of connectivity tissue by elongation of protein fibres.

**Treatment Regimen:** A course of action to address a disease (e.g. drug dosages or surgery).

## Appendix H List of Publications

1. Hillmann, A., Crane, M. and Ruskin, H.J., Assessing the impact of HIV treatment interruptions using stochastic cellular Automata, *Journal of Theoretical Biology* 502, 110376, 2020.

URL: <https://doi.org/10.1016/j.jtbi.2020.110376>

**Abstract** Chronic HIV infection causes a progressive decrease in the ability to maintain homeostasis resulting, after some time, in eventual break down of immune functions. Recent clinical research has shed light on a significant contribution of the lymphatic tissues, where HIV causes accumulation of collagen, (fibrosis). Specifically, where tissue is populated by certain types of functional stromal cells designated Fibroblastic Reticular Cells (FRCs), these have been found to play a crucial role in balancing out apoptosis and regeneration of naïve T-cells through 2-way cellular signaling. Tissue fibrosis not only impedes this signaling, effectively reducing T-cell levels through increased apoptosis of cells of both T- and FRC type but has been found to be irreversible by current HIV standard treatment (cART). While the therapy aims to block the viral lifecycle, cART-associated increase of T-cell levels in blood appears to conceal existing FRC impairment through fibrosis. This hidden impairment can lead to adverse consequences if treatment is interrupted, e.g. due to poor adherence (missing doses) or through periods recovering from drug toxicities. Formal clinical studies on treatment interruption have indicated possible adverse effects, but quantification of those effects in relation to interruption protocol and patient predisposition remains unclear. Accordingly, the impact of treatment interruption on lymphatic tissue structure and T-cell levels is explored here by means of computer simulation. A novel Stochastic Cellular Automata model is proposed, which utilizes all sources of

clinical detail available to us (though sparse in part) for model parametrization. Sources are explicitly referenced and conflicting evidence from previous studies explored. The main focus is on (i) spatial aspects of collagen build up, together with (ii) collagen increase after repeated treatment interruptions to explore the dynamics of HIV-induced fibrosis and T-cell loss.

2. **Hillmann, A., Crane, M. and Ruskin, H.J., HIV models for treatment interruption: Adaptation and comparison. *Physica A Statistical Mechanics and its Applications* 483, 44–56, 2017.**

URL: <https://doi.org/10.1016/j.physa.2017.05.005>

**Abstract** In recent years, Antiretroviral Therapy (ART) has become commonplace for treating HIV infections, although a cure remains elusive, given reservoirs of replicating latently-infected cells, which are resistant to normal treatment regimes. Treatment interruptions, whether *ad hoc* or structured, are known to cause a rapid increase in viral production to detectable levels, but numerous clinical trials remain inconclusive on the dangers inherent in this resurgence. In consequence, interest in examining interruption strategies has recently been rekindled. This overview considers modelling approaches, which have been used to explore the issue of treatment interruption. We highlight their purpose and the formalisms employed and examine ways in which clinical data have been used. Implementation of selected models is demonstrated, illustrative examples provided and model performance compared for these cases. Possible extensions to bottom-up modelling techniques for treatment interruptions are briefly discussed.

- 3. Hillmann, A., Crane, M., Ruskin, H.J., 2019. Efficient Computational Models for assessment of Spatial Infection Features, in: 2019 International Conference on High Performance Computing & Simulation (HPCS). IEEE, Dublin, pp. 948–952.**

URL: <https://doi.org/10.1109/HPCS48598.2019.9188232>

**Abstract** Computational models can prove useful in investigation of numerous biological phenomena, including disease initiation and progression. Model experiments usually rely on simulation-based approaches, suitably formulated to maximize the utilization of available computing power. In this article, the approach is applied to spatial modelling of HIV infection and consequent damage to lymphatic tissue. With available clinical data, however sparse, a Bayesian sampling framework can be used to obtain estimates for key parameters. Our results indicate that HPC computing combined with efficient parallelization strategies, can provide detailed parameter estimates, potentially fostering the use of this kind of model in clinical practice.

- 4. Hillmann, A., Crane, M. and Ruskin, H.J., A computational lymph tissue model for long term HIV infection progression and immune fitness, in: McAuley, J., McKeever, S. (Eds.), Irish Conference on Artificial Intelligence and Cognitive Science 2017. Dublin, December 2017.**

URL: [http://ceur-ws.org/Vol-2086/AICS2017\\_paper\\_13.pdf](http://ceur-ws.org/Vol-2086/AICS2017_paper_13.pdf)

**Abstract** Given the complexity of biological systems, modelling the immune response to the spread of infectious disease is non-trivial and has been the subject of considerable computational efforts. HIV infection, if untreated, leads to a slow depletion of the immune system over many

years, resulting in terminal AIDS disease and death. Despite decades of research, the biological mechanisms underpinning the immune system response and implicit in its impairment remain a subject of discussion. Recent biological findings indicate the importance of functional lymphatic tissue in maintaining homeostasis of the immune system, which is vital for stability. HIV infection-related immune activation leads to chronic inflammation of this tissue and formation of non-functional scar tissue with detrimental effects on homeostasis. We propose a computational model based on the Cellular Automata formalism to quantify these effects in a simulated fraction of a lymphatic tissue. We also include effects of antiretroviral treatment and highlight implications for system representation through larger-scale simulations, as well as optimisations of treatment schedules.